Investigation of extracellular microRNAs and Serum Protein Biomarkers in dystrophic Muscle Disease

Anna Maria Lara Coenen-Stass

Department of Physiology, Anatomy and Genetics

St John's College, University of Oxford

Thesis submitted for the degree of

Doctor of Philosophy

Michaelmas Term 2016

Declaration

The work presented in this thesis was undertaken in Professor Matthew Wood's laboratory at the Department of Physiology, Anatomy and Genetics, University of Oxford, between 2013 and 2016. I, Anna Coenen-Stass, hereby declare that all work presented is my own with the following exceptions. The cardiotoxin injury experiment in chapter 3 was performed in collaboration with Jenny Morgan (University College London, UK). The peptide conjugates utilised in chapter 4 and 5 in this thesis were produced by Amer Saleh in the laboratory of Mike Gait at the MRC Laboratory of Molecular Biology in Cambridge. Clinical biochemistry assays (chapter 3 and 4) were performed at the clinical pathology laboratory, Medical Research Council Harwell (Oxford, UK). The serum proteomics profiling in chapter 5 was performed on the SOMAscan platform at SomaLogic, Inc. (Boulder, CO, USA). Furthermore in chapter 5, the -RT-qPCR and WB to quantify full-length dystrophin transcript and protein was performed in collaboration with other members of the Wood laboratory (Graham McClorey and Raquel Manzano). All patient samples were obtained from Newcastle biobank. This work has not been submitted for any other degree at this university or any other institute of learning. My thesis includes text excerpts and figures of my first-author articles published throughout my DPhil as listed in section 8.1. Where required, permission from individual journals was obtained.

Acknowledgements

Firstly, I would like to thank Professor Matthew Wood for the advice and support throughout the last years. He has given me the great opportunity to develop my own ideas as well as to plan and conduct my research independently and thereby mature into the scientist I am today. Especially, I would also like to thank Doctor Thomas Roberts for his day-to-day supervision and mentorship from across the ocean. I am truly grateful for his invaluable support and the countless skype meetings to discuss my research, sometimes even at the oddest times. His guidance has propelled many of my research projects forward and allowed me to successfully complete most of them. I would further like to thank the Medical Research Council and St John's College for their generous support of my DPhil scholarship.

In addition, I am most grateful for the help, guidance and friendship I received from all the members of the Wood laboratory and for the wonderful environment everyone has provided throughout my doctoral studies. In particular, I would like to thank Corinne Betts and Suzan Hammond for their help with regards to animal experiments. Imre Mager, Fiona Lee, Pieter Vader, Eduard Willims and Samir El Andaloussi provided much help and advice with experiments relating to extracellular vesicles. In addition, I am thankful to Graham McClorey and Caroline Godfrey for their general advice in various scientific aspects during the last few years. For the biomarker study in my last chapter, I must thank Professor Hanns Lochmüller and the clinicians and nurses involved in collecting the patient material; Andrew Douglas, Yoshitsugu Aoki, Misako Aoki, Volker Straub, Kate Bushby, Michela Guglieri and Ruth Wake, in addition to the Newcastle biobank technicians; Alison Blain, Mojgan Reza, Dan Cox and Kathleen Allinson.

Outside from work, I would like to express my gratitude to all the wonderful people I met during my time in Oxford, since their friendship and wonderful company made the last years truly enjoyable. Gianni, I am still missing our runs and your wonderful cheerful company. Leigh, during some periods, I spend more time with you then with anyone else, either during pentathlon training or in college. It has been an amazing journey with you and I am so glad we have met. During the last years I also

made wonderful friends at St John's: Rita, Andreas, Stefano, Lisa, Christos (almost a Johnsian) and Tim, how could I have survived without you. My time here would not have been the same without your friendship including our lunches, dinners, volleyball games and 'chair and skipping rope' parties. Anna and Kim, I am so glad you were here to share almost everything that there is to share. There is nothing more important than knowing that some people will always remain your friends, not matter what. This also includes many of my friends from home, who have been accompanying me all the way since school or undergraduate studies (Anni, Maria, Fidi, Henni, Luki, Anne, Lea F., Lea B., Joana, Lena und Selina).

Finally, I would like to thank my family for their love and support that has brought me to the end of this long path and enabled me to obtain the highest university degree possible. Siamak, you have been the most amazing partner to support me during my DPhil. I am so thankful for your wonderful ability to make me laugh, your excitement to discuss spontaneous ideas, your willingness to listen to literally anything I have to say, your support in any decision I make and most importantly, for the affection and love you have for me.

Abstract

Extracellular microRNAs (ex-miRNAs) and serum proteins are promising biomarkers for a variety of pathological conditions, including muscular dystrophies and, Duchenne Muscular Dystrophy (DMD) in particular. miR-1, miR-133 and miR-206 are muscle-specific miRNAs (myomiRs) that regulate myoblast proliferation and differentiation. These myomiRs are highly abundant in serum of DMD patients and dystrophic *mdx* mice and have therefore been investigated as biomarkers of dystrophic disease. The biological significance of miRNAs present in the extracellular space is currently not well understood. The work presented here demonstrates that ex-myomiRs are selectively released during periods of myogenic differentiation in cell culture and *in vivo.* Consequently, their release can be independent of dystrophic pathology, thus indicating that the presence of myomiRs in the serum may serve a physiological function in some contexts. In summary, serum myomiR abundance appears to be a function of the regenerative/degenerative status of the muscle, overall muscle mass, tissue expression levels and myomiR stability in serum. These findings have implications both for miRNA biology in normal muscle physiology as well as for the use of ex-myomiRs as biomarkers for DMD.

Secondly, size-exclusion chromatography was identified as a useful methodology to fractionate biofluids and thereby separate extracellular vesicles (EV) from protein complexes and lipoproteins. Using this tool, it was demonstrated that ex-myomiR carriers in cell culture supernatant and murine serum are predominantly non-vesicular, and furthermore, that their release is independent of ceramide-mediated vesicle secretion. In addition, it was found that EVs isolated from dystrophic mice are smaller and more numerous compared to EVs derived from wild-type mice, thereby indicating a role for dystrophic pathology in the regulation of vesicle biogenesis and/or secretion.

There is currently an urgent need for minimally invasive, therapy-monitoring DMD biomarkers for use in clinical trials. Serum protein biomarkers are desirable since they can typically be quantified by clinical biochemistry assays, which are technically facile and allow for rapid screening of large numbers of patients. Previously, identification of such biomarkers by mass spectrometry has been limited due to analytical challenges resulting from the massive complexity of the serum proteome. Here, an aptamer-based proteomics approach was utilised to profile 1,129 proteins in the serum of wild-type, *mdx* mice and, *mdx* mice treated with exon skipping therapy to restore dystrophin expression. A number of novel, therapy-responsive biomarkers were identified, and the leading candidate (ADAMTS5) was also found to be significantly elevated in DMD patient serum.

In conclusion, this work demonstrates that myomiR release accompanies myogenic differentiation and shows that serum myomiR levels are influenced by a number of physiological and pathological factors. Furthermore, multiple novel, therapy-responsive protein biomarkers were identified in the serum of the *mdx* mouse with potential utility in clinical trials for DMD.

List of Abbreviations

2OMe	2’-O-methyl RNA
6MWT	6 Minute Walk Test
AAV	Adeno-Associated Virus
AB	Antibody
ACTB	β-Actin
AGO1	Argonaute 1
AGO2	Argonaute 2
ALT	Alanine aminotransferase
ASO	Antisense Oligonucleotides
AST	Aspartate aminotransferase
ANOVA	Analysis Of Variance
BMD	Becker Muscular Dystrophy
BSA	Bovine Serum Albumin
bp	base pair
C	Control
cDNA	complementary DNA
Cas9	CRISPR associated protein 9
CD81	Cluster of Differentiation 81
CD9	Cluster of Differentiation 9
CK	Creatine Kinase
CPP	Cell-Penetrating Peptide
CRISPR	Clustered Regularly Interspaced Short Palindromic Repeats
CSF	Cerebrospinal Fluid
Cq	Quantification Cycle
d	days
DGC	Dystrophin Glycoprotein Complex
DM1	Myotonic Dystrophy Type 1
DMEM	Dulbecco’s Modified Eagle’s Media
DMSO	Dimethyl Sulfoxide
DMD	Duchenne Muscular Dystrophy
DNA	Deoxyribonucleic Acid
Dntp	Deoxynucleotide Triphosphate
DGCR8	DiGeorge Syndrome Critical Region 8
ELISA	Enzyme-linked immunosorbent assay
EDTA	Ethylenediaminetetraacetic Acid
ESCRT	Endosomal Sorting Complex Required For Transport
EV	Extracellular Vesicles
ex	extracellular
FPLC	Fast Protein Liquid Chromatography
FSHD	FacioScapuloHumeral Muscular Dystrophy
FBS	Fetal Bovine Serum
gDNA	genomic DNA
GM	Growth Medium
h	hours

HDAC	Histone Deacetylase
Hdl	High Density Lipoprotein
HMT	Histone Methyltransferase
HPLC	High Performance Liquid Chromatograph
IV	Intravenous
lncRNA	long non-coding RNA
kb	kilobase
LC	Liquid chromatography
LGMD	Limb Girdle Muscular Dystrophy
LDL	Low Density Lipoprotein
LDLR	Low Density Lipoprotein Receptor
LTR	Long Terminal Repeat
LNA	Locked Nucleic Acid
LOD	Limit Of Detection
LOQ	Limit Of Quantification
LPS	Lipopolysaccharide
Luc	Firefly Luciferase
MB	Myoblast
MHC	Myosin Heavy Chain
miRISC	miRNA -loadede RISC complex
miRNA	microRNA
miRNA*	miRNA minor species
MIQE	Minimum Information for publication of Quantitative real-time PCR Experiments
MLC	Myosin Light Chain
mRNA	messenger RNA
MS	Mass Spectrometry
MT	Myotube
Mw	molecular weight
ncRNA	non-coding RNA
nNOS	neuronal Nitric Oxide Synthase
NO	Nitric Oxide
ns	not significant
nSMase2	neutral SphingoMyelinase 2
nt	nucleotide
NTA	Nanoparticle Tracking Analysis
NTC	No Template Control
PAGE	Polyacrylamide Gel Electrophoresis
PAX3	Paired Box Protein 3
PAX7	Paired Box Protein 7
PBS	Phosphate Buffered Saline
PCR	Polymerase Chain Reaction
PI3K	Phosphoinositide-3-Kinase
PMO	Phosphorodiamidate Morpholino Oligonucleotide
PNA	Peptide Nucleic Acid
PPMO	Peptide-Phosphorodiamidate Morpholino Oligonucleotide
PVDF	Polyvinylidene fluoride
pre-miRNA	precursor-microRNA

pri-miRNA	primary-microRNA
PTEN	Phosphatase and Tensin homolog
PTGS	Post-Transcriptional Gene Silencing
RBP	RNA Binding Proteins
RISC	RNA Induced Silencing Complex
RIP	RNA Immunoprecipitation
RNA	Ribonucleic Acid
RNAi	RNA interference
RT	Reverse Transcription
RT-qPCR	Reverse Transcriptase-quantitative PCR
SD	Standard Deviation
SEC	Size Exclusion Chromatography
SEM	Standard Error of the Mean
siRNA	small interfering RNA
shRNA	short hairpin RNA
snRNA	small nuclear RNA
SOMAmer	Slow Off-rate Modified Aptamers
SRF	Serum Response Factor
TA	Tibialis Anterior
T_m	melting Temperature
TRBP	TAR RNA Binding Protein 2
TBS-T	Tris buffered saline with 0.1% Tween-20
UC	Ultracentrifugation
UF	Ultrafiltration
UTR	Untranslated Region
VLDL	Very Low Density Lipoprotein
WB	Western blotting

List of Figures I

List of Figures II

List of Tables

Table of Contents

1. Introduction

1.1 Neuromuscular and dystrophic muscle disease

Neuromuscular disorders encompass multiple genetic or acquired disorders that primarily affect structures in the neuromuscular unit, including skeletal muscle, motor neurons, peripheral nerves, and neuromuscular synapses. As such, they comprise a heterogeneous group of clinical entities, although they are united by the so-far largely unmet need for development of novel therapeutic approaches (reviewed in [1]).

Muscular dystrophies are a subset of neuromuscular diseases and comprise more than 30 different inherited diseases which are highly diverse with respect to cause, age of onset and severity (reviewed in [2]). However, they share muscle weakness and similar dystrophic changes in muscle biopsies. Typically, skeletal muscle wasting is progressive and in some variants, the condition has additional systemic effects on smooth and cardiac muscle or the central nervous system. Historically, muscular dystrophies were grouped according to the main clinical features and age of onset. Scientific advances in the last two decades have enabled the determination of the causative mutations in many cases, and allowed for the classification of muscular dystrophy variants using a more rational framework. The main classes of proteins affected in dystrophic conditions are: extracellular matrix and external membrane proteins, enzymes, sarcolemma-associated proteins, nuclear membrane proteins, sarcomeric proteins, and other proteins [2].

The most common and most severe form of childhood-onset muscular dystrophy is Duchenne Muscular Dystrophy (DMD). DMD, and the milder disease variant Becker Muscular Dystrophy (BMD) which occurs slightly less frequently, are commonly referred to as dystrophinopathies as they are caused by mutations in the *DMD* gene located on the X-chromosome which encodes the dystrophin protein [3]. This thesis focuses primarily on DMD as discussed in detail in the next section.

In adults, myotonic dystrophy (MD) is the most commonly inherited muscular dystrophy (prevalence ~1:10,000) [2]. The two distinct types of myotonic dystrophy are both inherited autosomal dominant and arise from micro-satellite repeat expansions in either the dystrophia myotonica protein kinase (DMPK) (MD type 1) or cellular nucleic acid-binding protein (CNBP) (MD type 2). If more than 50 repeat units are present in the non-coding microsatellite repeat regions of the mRNAs transcribed from these two distinct loci, toxic gain-of-function RNAs are generated [4]. Facioscapulohumeral muscular dystrophy (FSDH) is the second most common MD with a prevalence of ~1:30,000 [2]. FSHD is an inherited autosomal dominant disorder and patients develop progressive wasting of facial and shoulder girdle muscles. The genetic defect causing this disease is complex and a detailed understanding of FSHD molecular pathology is still lacking. The current consensus is that the condition is caused by mutations that result in inefficient epigenetic repression of the double homeobox 4 (*DUX4*) retrogene [5,6].

1.2 Duchenne Muscular Dystrophy

1.2.1 DMD disease progression

DMD is a severe X-chromosomal inherited disorder caused by the absence of dystrophin with a prevalence of 1:3,500 to 1:5,000 live male births [3,7]. Typically, the age of onset is between 3-5 years. Muscle wasting is accompanied by pseudo hypertrophy, especially of the lower leg muscles. In late childhood, progressive muscle degeneration, chronic inflammation and fibrosis lead to a severe decline of muscle function. In addition, abnormal bone development occurs, causing skeletal deformities of the spine and other areas. The majority of patients become non-ambulant at the age of 12. Continuous degeneration of both skeletal and cardiac muscle leads to a severe manifestation of the disease which eventually results in a premature death in the second or third decade of life, typically as a result of cardiac or respiratory failure [8]. Furthermore, some DMD patients show cognitive impairment, presumably caused by the absence of dystrophin isoforms in the brain, although the role of dystrophin within the CNS is not yet well understood [9]. The genetic cause of DMD has been known for decades, and despite extensive research effort, there are still no curative treatments available, thus emphasising the urgent need for therapy. Notably, two compounds which act to partially restore dystrophin have recently been the approved for treatment in a subset of patients (i.e. Ataluren and Eteplirsen) although the drug efficacy is still under investigation (section 1.2.6 and section 1.2.7).

1.2.2 DMD isoforms and mutations

The *DMD* locus encompasses 2.6 million base pairs and is the largest human gene known in terms of genomic space. The fully spliced mRNA is ~14 kb in length and contains 79 exons, although multiple isoforms have been identified. The full-length 427 kDa dystrophin isoform (Dp427) is the primary variant expressed in skeletal muscle [10]. Various mutation types have been described to cause DMD. Deletions account for about 60-65%, smaller mutations (including intronic deletions or exonic

insertions) for approximately 20-35% and duplications only for 5-15% [10]. These mutations can be transmitted either by carrier (maternal) or are spontaneous *de novo* mutations, probably owing to the enormous size of the gene [23]. Typically, a DMD causing mutation leads to the disruption of the reading frame and consequently, dystrophin mRNA is degraded by nonsense-mediated decay and not translated into dystrophin protein [11]. In-frame mutations in the DMD gene manifest as BMD, the milder allelic form of the condition. In the case of BMD, an internally truncated, but largely functional dystrophin protein is expressed. In BMD disease onset occurs later compared to DMD and patients usually remain ambulant until middle age or beyond [12].

1.2.3 The dystrophin-glycoprotein complex in muscle

In normal muscle, dystrophin protein is localised beneath the sarcolemma of the muscle fibres (Figure 1.1) [13] and associates with a number of functionally related proteins, known as the dystrophin-glycoprotein complex (DGC, also known as dystrophin-associated protein complex (DAPC)). The main function of dystrophin appears to be linking the cytoskeletal actin filaments with the extracellular matrix via the DGC, thereby providing stability to the sarcolemma and mediating force transmission during muscle contraction [14].

Dystrophin has a complex structure that can be divided into four distinct functional domains. The N-terminal region of dystrophin interacts with cytoplasmic actin filaments [15] and the central, rod-like domain consisting of 24 spectrin repeats, likewise contributes to this interaction but also provides a binding site for the enzyme neuronal nitric oxide synthase (nNOS) [16]. Additionally, four hinge regions serve to increase flexibility of the dystrophin protein and have been suggested to function as a shock absorber for stress induced by eccentric contractions [17]. The third region is the cysteine-rich domain that is associated with the sarcolemmal β-dystroglycan, which itself interacts with the transmembrane protein α-dystroglycan, which in turn interacts with the sarcoglycans [18]. Both dystroglycans and sarcoglycans are linked to other adaptor proteins including laminins which establish a link to the extracellular matrix (e.g. to collagen filaments) [14]. The C-terminus of

dystrophin binds to syntrophins [14]. In addition to providing mechanical stability, dystrophin is involved in numerous intracellular signalling pathways, mediated by its association to various adapter proteins. Most importantly, dystrophin (and the DGC) regulate the intracellular calcium concentration by interaction with Caveolin-3 and nitric oxide (NO) signalling via nNOS [19].

Absence of dystrophin results in an impairment in sarcolemma integrity and disruption of a variety of cellular pathways (briefly discussed in the next section). Notably, mutations which disrupt the various other members of the DGC are also associated with dystrophic pathology (e.g. mutation in genes encoding sarcoglycans can cause limb girdle muscular dystrophy, LGMD [17]). This finding underlines the fundamental importance of DGC has in normal muscle function.

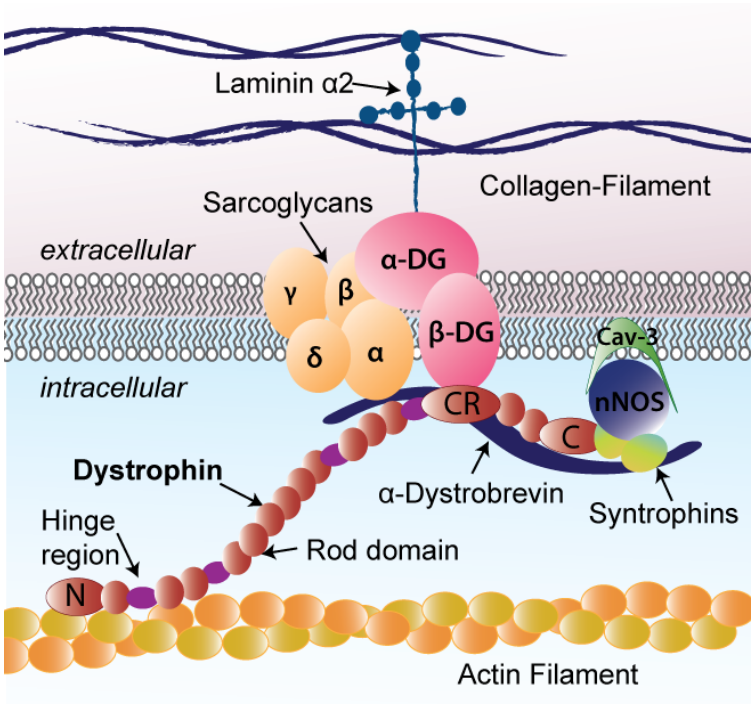

Figure 1.1 The dystrophin glycoprotein complex (DGC) in mammalian muscle.

The N-Terminus (N) of dystrophin interacts with the actin cytoskeleton whereas the cysteine rich (CR) domain binds to dystroglycans (DG) localised at the sarcolemma. Dystroglycans bind in turn to sarcoglycans and laminins which establish a link to the extracellular collagen filaments. The C-Terminus (C) of dystrophin has been described to interact with the neuronal nitric acid synthase (nNOS) and Caveolin-3 (Cav-3). All indicated proteins interact to form the DGC.

1.2.4 Molecular mechanism of DMD pathogenesis

Although the loss of dystrophin protein is unequivocally the cause of DMD, the link between the absence of dystrophin and the complex changes in myophysiology which result in profound muscular wasting and inflammation, are still under investigation (reviewed 2007 in [20]). The major characteristics of DMD pathophysiology observed in muscle tissue are high susceptibility to stretch-induced muscle damage, impaired calcium homeostasis, enhanced generation of reactive oxygen species (ROS) and increased sarcolemma permeability [21,22].

The cause of the increased membrane permeability observed in DMD remains a matter of debate. The two most widely accepted hypotheses are i) membrane lesions caused by contractile damage due to the absence of the DGC, and ii) increased intracellular calcium concentrations triggering a cascade of pathological changes that include enhanced receptor translocation from intracellular vesicles to the sarcolemma which thereby mediate enhanced membrane permeability [23]. Furthermore, the abnormalities in calcium homeostasis activate calcium-dependent proteases such as the calpains and trigger the release of pro-apoptotic factors by mitochondria [24].

The increased oxidative stress mediated by the formation of ROS has multiple consequences in dystrophic muscle, such as the activation of the pro-inflammatory transcription factor NF-κB, which induces several signalling pathways promoting chronic inflammation of the muscle [25]. Additional pathological changes arise from impaired signalling activities, primarily mediated by the mislocalisation of nNOS in the absence of the DGC [26].

These aberrant changes in sarcomere physiology result in increased myofibre necrosis, thus causing inflammation and necessitating the regeneration of the injured fibres. Muscle biopsies reveal necrotic fibres surrounded by macrophages and CD4+ lymphocytes, as well as small immature fibres with central nuclei, reflecting muscle regeneration mediated by the myogenic stem cells (the so-called satellite cells) [27]. Repeated cycles of degeneration and regeneration are thought to lead to depletion of the muscle stem cells (although to what extent satellite cells are exhausted in advanced

DMD pathology is a matter of debate [28,29]) and a reduction in regenerative potential of the muscle is observed. In the advanced disease stages, chronic inflammation and gradual replacement of myofibres with adipose and connective tissue occurs, thus leading to serve fibrosis and adipogenic degeneration of the muscle.

1.2.5 Animal models for DMD

Animal models of DMD include the *mdx* mouse and two dog models: the golden retriever muscular dystrophy (GRMD) dog and the canine X-linked muscular dystrophy animal model developed in Japan ($CXMD_J$) [30]. The dystrophic pathology in canine DMD models is more severe than that in *mdx* mice and therefore they are considered the better models, although due to the high cost and ethical considerations *mdx* mice remain the most widely used DMD animal model [31]. The *mdx* mouse was also utilised for all animal studies in this thesis.

The *mdx* mouse carries a single nucleotide polymorphism in exon 23 of the *Dmd* gene, resulting in a premature termination codon. As with DMD patients, dystrophin protein in these animals is truncated and not functional (although the specific *mdx* mutation is not typically observed in DMD patients). However, despite undergoing a phase of massive muscle necrosis followed by regeneration around 3-4 weeks of age, adult *mdx* mice develop only a mild phenotype. As such, the disease progression is slower than found in DMD patients, likely due to the large regenerative potential of murine muscle. Nevertheless, this mouse model is well-suited for proof-of concept studies for novel therapeutics. In addition, aged *mdx* mice exhibit advanced muscle wasting in addition to cardiac pathology and therefore resemble the pathological progression observed in patients better [32,33]. In recent years, a number of additional mouse model have been generated, including double-knock out mice that contain additional mutations in genes with relevance in DMD pathology (reviewed [31]).

1.2.6 Overview of therapeutic approaches for DMD

Until 2014, no approved drug was available that would specifically treat DMD. As a consequence, conventional therapies were and still are routinely applied. These are directed towards the improvement of the disease symptoms but not the cause itself. The current standard of care is corticosteroid treatment, (e.g. Prednison and Deflazacort) which aims to prolong ambulation and reduces the chance of patients developing scoliosis [34]. However, steroid treatment is associated with considerable negative side-effects such as weight gain, osteoporosis, hypertension and an increased likelihood to develop to diabetes [35].

A new pharmaceutical approach to restore dystrophin protein is to promote stop codon read-through. This therapy is applicable to about 10-15% of all DMD patients that have a nonsense mutation in the *DMD* gene leading to the formation of a premature stop codon [36]. The aminoglycoside antibiotic Gentamicin and the synthetic compound Ataluren (also known as PTC124) both enable continued translation through stop codons. The pharmaceutical company PTC Therapeutics recently received conditional approval for Ataluren (trade name Translarna) in Europe by the European Medicines Agency (EMA) in 2014 [37]. In contrast, the food and drug administration (FDA) has declined to review Ataluren for approval in the USA in the beginning of 2016. To this end, there had been uncertainty surrounding the efficacy of PTC126 and a study testing the compound in a range of *in vitro* assays found no evidence of consistent stop codon read-through activity of PTC126 [38]. As a consequence, despite the announced success of PTC's most recent phase 3 trial [39], the drug effectiveness remains unclear.

In the last two decades, major advances have been made in developing cell and gene therapies for DMD. In general, these therapies are intended to treat or manage a disease by the delivery of either cells (cell therapy) or nucleic acids (gene therapy). A variety of cell and gene therapeutic strategies have been investigated for DMD and an overview of the main approaches is given in Table 1.1.

Notably, all current approaches listed in Table 1.1 share the common bottlenecks of inefficient delivery of the therapeutic agent to muscle and the difficulties associated with inducing sustained dystrophin expression in the absence of vector-mediated or anti-transgene immunogenicity [40]. A major additional complication of gene replacement strategies is the large size of the dystrophin gene (2.4 Mb) and transcript (14 kB) which are too large to be accomodated by currently used gene therapy delivery vectors with good muscle tropism. However promising results have been obtained in animal models delivering an internally trunctated (similar to the BMD phenotype) pseudo-dystrophin protein by viral vectors, so-called mini or microdystrophin (Table 1.1, reviewed in [40]). The disadvantage of these approaches is that not all dystrophin isoforms will be restored and therefore, some tissue specific functions of dystrophin, e.g. in the brain or retina, cannot be rescued. Similary, cell therapies in principal allow delivering healthy myoblasts or muscle stem cells that express full length dystrophin and may thereby help repairing dystrophic muscle, but this approach also cannot restore dystrophin expression in other tissues. To this end, transplanted myoblasts have been shown to accumulate at the site of injection, thereby further limiting global dystrophin expression (reviewed in [41]). Autologous stem cell based therapies have at least the advantage of avoiding immune suppression and allowing systematic delivery of the cells.

Another possible treatment option is upregulation of the dystrophin homologue utrophin since these proteins share about 80% sequence identity. Utrophin expression in adult muscle is restricted to the neuromuscular and myotendinous junctions, however, it has been suggested that expression of utrophin could compensate for dystrophin loss since it was found to be up regulated in DMD patients and *mdx* mice [42]. Interestingly, a small molecule compound (SMT C1100, trade name Ezutromid) has been identified that transcriptionally upregulates utrophin gene expression which is now been studied in DMD patients in a phase 2 clinical trial [43]. In contrast to dystrophin, utrophin cannot mediate nNOS can relocalisation to the sarcolemma [44], although the importance of this is still under investigation [45].

Strategy	Action/Effect	Advantages	Disadvantages	Prospects
Myoblast transplantation/ Stem cell therapy	Transfer of dystrophin expressing muscle or stem cells.	Cells may express full-length dystrophin.	Poor survival of transplanted cells, immune suppression required unless autologous cell engineering is used.	Still in experimental stages, mostly autologous cells are utilised in proof of concept linical trials [41].
Gene replacement therapy	Delivery of full-length or mini-dystrophin (Adenoviral (AV) or Lentiviral (LV) vectors respectively).	Efficient transduction of skeletal muscle for AV. Expression of full length dystrophin in the case of LV.	Poor muscle transduction and immunogenic potential of AV. Tumorigenic potential of LV. Limited persistence of transgene expression.	Considerable safety risk associated with vectors, for a general review [46].
	Delivery mini and microdystrophin by recombinant Adenovirus-associated virus (rAAV)).	Efficient transduction of skeletal muscle, non immunogenic, non-pathogenic.	Inability to deliver full-length dystrophin, limited persistence of transgene expression.	Large number of animal studies conducted. First clinical trial conducted showed good safety but poor transgene expression [47].
Splice modulation of dystrophin mRNA by antisense oligonucleotides	Restoration of dystrophin reading-frame to generate internally truncated protein.	Synthetic drug, relatively safe, has the potential to restore all isoforms.	Inability to generate full-length dystrophin. Mutation specific, repeated administration of drug, poor cardiac delivery.	Limited efficacy in patients so far. FDA has granted accelerated approval for Eteplirsen by Sarepta [48], FDA declines approval for Drisapersen (BioMarin) [49].
Utrophin upregulation	Compensation for dystrophin loss by an autosomal homologue.	Small-molecule drug, oral administered, no immune response, relatively safe.	Currently low efficacy, utrophin cannot interact with nNOS.	Phase 2 proof of concept clinical trial by Summit Therapeutics, Compound SMT C1100 [43].

Table 1.1 Overview of cell and gene therapeutic treatment approaches for DMD (adapted from [40]).

Notably, with the recent discovery of CRISPR/Cas9 (Clustered Regularly Interspaced Short Palindromic Repeats/CRISPR associated protein 9) based genome editing [50], a tool has become available that allows to precisely delete genomic regions in the *DMD* gene to correct the mRNA reading frame and thereby permanently restore the expression of internally trunctated dystrophin. This approach could potentially be used to edit both autologous stem cells *ex vivo* or muscle stem cells *in vivo* [51–53]. Importantly, aspects regarding the safety of CRISPR/Cas9 based therapeutics especially for *in vivo* gene therapy require further investigations and are being widely discussed in the research community [54]. Despite efforts to generate high-fidelty Cas9 variants, off-target effects still comprises a major risk if Cas9 is expressed persistingly *in vivo* (e.g. if viral vectors are used for delivery) [55]. Consequently, transient delivery of Cas9 protein or Cas9 mRNA together with gRNAs may comprise a safer approach and is currently being investigated for both *in vitro* and *in vivo* application [56].

Currently, the most advanced gene therapeutic approach for the treatment of DMD is restoration of the translation reading frame by splice modifying antisense oligonucleotides (ASO), also commonly referred to as exon skipping (discussed in 1.2.7). In contrast to all above mentioned approaches with exception to CRISPR/Cas9, exon-skipping holds the great advantage that if systemic delivery of the ASO can be achieved, most, if not all isoforms of dystrophin can be restored and as result, tissue-specific gene regulation can be reinstated.

1.2.7 Exon skipping therapy for DMD

Exon skipping aims to convert an out-of-frame mRNA into an in-frame transcript by purposely splicing out exons from the pre-mRNA transcript. Consequently, exon skipping restores expression of an internally truncated pseudo-dystrophin, with the idea of transforming the DMD pathology into a BMD-like phenotype. Exon skipping can be induced by small antisense steric block oligonucleotides (ASOs) that specifically target intronic or exonic splicing signals. Masking recognition sites for the cellular splicing machinery results in the promotion of exon exclusion. ASOs were first developed in 1978 and the first ASO therapeutic was FDA approved 20 years later for the treatment of cytomegalovirus (CMV) retinitis [57,58]. A range of second and third generation backbone modified ASOs have since then been developed in order to reduce the bottlenecks of this approach which include: nuclease stability, targeted delivery and skipping efficiency. Most commonly used ASO chemistries are 2'-O-methyl-phosphorothioate RNA (2OMe), peptide nucleic acid (PNA), locked nucleic acid (LNA) and phosphodiamidate morpholino oligomers (PMO), all exhibiting favourable pharmacokinetic properties and all capable of effectively reaching the nucleus [59]. In addition to peptide conjugate delivery, virus assisted delivery of ASOs linked to U1 or U7 small nuclear RNAs (snRNAs) has also shown promise for inducing systemic exon skipping [60].

Currently, 2OMe and PMO are the most advanced chemistries for treatment of DMD. 2OMe has a negatively charged phosphorothioate backbone and 2'-O-methyl substitution of the ribose sugar. In contrast, PMO consists of a morpholine ring instead of riboses and has a neutrally charged backbone that allows for covalent conjugation to other components. The compound Eteplirsen (trade name Exondys 51, developed by Sarepta Therapeutics) is based on a PMO chemistry targeting exon 51 and has been granted accelerated approval in the USA by the FDA in September 2016 despite remaining concerns regarding its efficacy [48]. In contrast, the FDA declined to approve the application of the 2OMe based ASO Drisapersen (by BioMarin and previously also GSK and Prosensa Therapeutics, also targeting exon 51), after a phase 3 clinical trial failed to meet the primary endpoint of an

improvement in a 6 minute walk test (6MWT). It is noteworthy that the disappointing result from the Drisapersen trial was somewhat surprising given that the phase 2 trial demonstrated an improvement in the 6MWT compared to the placebo group, although a clear correlation with the amount of dystrophin restored could not be established [61]. These recent developments underline the current difficulties associated with designing clinical trials for DMD, which will be further discussed in section 1.5 and chapter 6.3.

In general, comared to 2OMe, PMOs have shown an improved ability to induce exon skipping in multiple studies in DMD animal models, as well as in studies in DMD patients [62,63]. In addition, PMO backbone-modified ASOs seem to be better tolerated than 2OMe chemistries and therefore have larger therapeutic windows (i.e. more flexibility with dosing). Drisapersen (2OMe chemistry) at high doses has been associated with kidney toxicity whereas no clear toxicity has so far been identified for the PMO-based ASO Eteplirsen [62]. As a result, Eteplirsen was could be dosed up to 50 mg/kg in clinical trials, which is more than eight times higher than Drisapersen. In summary, PPMO holds several advantages over the 2OMe chemistry. Nevertheless, it remains to be seen if Sarepta can demonstrate clear patient benefit of Eteplirsen in a further clinical trial.

Meanwhile future generation ASOs chemistries are being developed, aimed at improving on the limited efficacy of PMO and 2OMe. For example, the neutrally charged PMOs can be conjugated to positively charged peptides, so called cell penetrating peptide (CPPs), to improve cellular uptake. These conjugates are also commonly reffered to as peptide-PMO (PPMO). In particular, arginine-rich peptides have the intrinsic property of penetrating membranes by interaction with the negatively charged phospholipid head groups and additionally, PPMOs have been shown to sponatenously self-assemble into nanoparticles that can be taken up by scavenger receptors [64]. One of the first PPMOs was B-PMO (PMO conjugated to the so-called B-peptide), which showed efficient dystrophin restoration in animal studies [65]. In order to enhance tissue-specific delivery, a muscle targeting heptapetide (MSP) can be further combined with B-PMO to efficiently induce dystrophin expression

[66]. Another novel series of CPPs are the PNA or PMO internalisation peptides (Pips), which are based on the homeobox peptide of *Drosophila antennapedi* penetratin and have revealed a superior potential for dystrophin exon skipping compared to naked PMO, especially in heart tissue [67]. Recently, the novel ASO chemistry tricyclo-DNA (tc-DNA), has shown promise for inducing efficient exon skipping in cardiac and skeletal muscle and most importantly, also in the brain [68]. To this end, systemic treatment with tcDNA ASOs rescued tonic immobility in *mdx* mice and expression of dystrophin protein was found in the CNS, albeit at lower level than in muscle [68]. As yet, tcDNA is the only ASO chemistry that exhibit capacity to cross the blood brain barrier as naked ASO. This exciting finding offers not only the possibility to treat the neurocognitive impairment associated with DMD [9], but also holds great promise for treatment of other neuromuscular disorders, such as spinal muscular atrophy (SMA).

Furthermore, it is important to note that, exon skipping approaches are intrinsically mutation-specific and, due to the variety of DMD causing mutations, are only applicable to a subgroup of patients. For example, both Eteplirsen and Drisapersen target exon 51 which would be therapeutically effective for ~13% of all DMD patients [69]. A potential solution to this problem is a multi-exon skipping approach that would allow treatment of the majority of DMD patients with the same ASO therapy. Bioinformatic analysis has predicted that up to 63% of the patients could be treated with a drug that promotes exclusion of the exons 45-55 [70]. Successful multi-exon skipping was recently reported in the $CXMD_J$ model, although the cocktail of PMOs used exhibited toxicity, and so further optimisation of this strategy is needed [71].

In summary, efficient, safe and targeted delivery of the therapeutic agent remain bottlenecks for DMD gene therapy approaches, even for the most clinically advanced compounds. The limited efficacy in dystrophin restoration observed in patients, highlights the need to develop more reliable and accurate methodologies for dystrophin quantification. In addition, improving clinical outcome measures and developing biomarkers and surrogate endpoints is of utmost importance to

demonstrate treatment efficacy, and will be crucial for the future of DMD exon skipping therapies (discussed in section 1.5).

1.3 microRNAs in muscle biology and dystrophic pathology

1.3.1 microRNA biogenesis and mechanism of action

MicroRNAs (miRNAs) are a class of small (21-22 nt), non-coding RNAs which primarily regulate gene expression at the post-transcriptional level [72]. To this end, miRNAs are endogenous effectors of the RNA interference (RNAi) pathway. This pathway is defined as the mechanism that silences gene expression based on partial sequence complementarity of small RNAs to the targeted messenger RNA (mRNA) [73]. Other, non-endogenous, small RNAs capable of inducing RNAi in mammalian cells are short interfering RNAs (siRNAs) and short hairpin RNAs (shRNAs).

Ambros *et al.* first identified the 21 nt long lin-4 miRNA in *Caenorhabditis elegans (C. elegans)* in 1993 [74] and, in 2001, he and others described miRNAs as a large class of conserved small RNAs with potential regulatory functions [75–77] (Figure 1.3). In the following decade it was discovered that miRNAs typically bind in the 3' untranslated region (UTR) of the targeted messenger RNA (mRNA) and utilise a gene silencing pathway similar to that of RNAi. The majority of mammalian transcripts are regulated by miRNAs and ~45,000 target sites are conserved in the 3'UTRs of human protein coding genes (corresponding to more than 60% of human proteins [78]).

Typically, miRNAs are derived from larger precursor transcripts (primary miRNA, pri-miRNA) transcribed by RNA polymerase II (RNAPII) and form imperfect stem-loop structures [79]. The pri-miRNA is processed by the RNAse III endonuclease Drosha yielding a 60-70 nucleotide (nt) long stem loop intermediate called a precursor miRNA (pre-miRNA) (Figure 1.4). The Drosha (DROSHA)/ DiGeorge Syndrome critical Region 8 (DGCR8) complex cleaves the RNA duplex with a staggered cut close to the base of the initial stem-loop resulting in a 2 nt 3' hydroxyl overhang and a 5' terminal phosphate [80].

Next, the pre-miRNA is actively exported from the nucleus to the cytoplasm by interaction with the export receptor Exportin-5 (XPO5) using RanGTP as energy source [81]. Dicer (DICER1), a cytoplasmic

RNase III endonuclease, recognises the double-stranded portion of the pre-miRNA and cuts both strands approximately two helical turns away from the base of the stem loop to generate a short double stranded fragment by removal of the loop structure [82]. Subsequently, the strand with the most thermodynamically unstable 5' terminus (typically the guide strand) is incorporated into the RNA-induced silencing complex (RISC) as single stranded, mature miRNA [83,84]. The RISC itself is a ribonucleoprotein complex that contains a member of the Argonaute protein family as its core and recognises target transcripts based on either partial or perfect sequence homology guided by the loaded miRNA. There are four Argonaute proteins encoded in the human genome, although only Argonaute 2 (AGO2) exhibits endonucleolytic slicing activity to cleave mRNAs [85]. More recently, the RISC loading complex (RLC) was identified, comprising the proteins AGO2, Dicer and TRBP (human immunodeficiency virus transactivating response RNA-binding protein). TRBP has three double stranded (ds) RNA binding domains and is believed to mediate the interaction between Dicer and AGO2, thus facilitating the formation of an active RISC complex [86].

Post-transcriptional gene silencing can occur either by mRNA cleavage (mediate by the slicer activity of AGO2) if the homology is perfect, or by translational repression if the homology is incomplete [87]. Translational repression and mRNA destabilisation can be mediated by steric blockage of translation initiation or elongation and by deadenylation followed by mRNA decay [88]. Typically, endogenous miRNAs exhibit only partial sequence homology to their targets. Principally, sequence homology in the seed region, which is defined as the bases 2-8 from the 5' terminus of the guide strand, is sufficient to induce miRNA-mediated gene silencing [89]. Consequently, individual miRNAs can target multiple mRNA targets and in addition, each mRNA 3'UTR contains multiple potential miRNA binding sites. As a result, miRNAs can act as master regulators of gene expression by simultaneously controlling functionally related classes of transcripts.

As described above, the majority of mammalian mRNA transcripts are subjected to miRNA-mediated regulation, and as such, miRNAs are involved in the control of a wide variety of physiological

processes including development, proliferation, differentiation, apoptosis, and myogenesis [90,91]. Additionally, miRNAs have been implicated in various pathologies including viral infection, oncogenesis, cardiovascular disease, immunological disorders (reviewed in [92,93]) and muscular dystrophy (section 1.3.3). Consequently, miRNAs are potential pharmacological targets, and a number of therapeutic strategies to either antagonise miRNA activity or mimic their function are being developed (reviewed in [94]). Similarly, in 2001, it was discovered that RNAi in mammalian cells can be triggered by the introduction of exogenous short dsRNAs thus providing the basic principles for developing RNAi applications [95]. Notably, both synthetic siRNA and expressed shRNAs can function as analogues of intermediate products of the endogenous miRNA maturation. As such, they can enter the RNAi pathway at different stages to artificially regulate the expression of a gene of interest, thus providing a powerful platform for both research purposes and therapeutic gene regulation.

1.3.2 Regulation of myogenesis by microRNAs

Myogenesis describes both the process of embryonal muscle development and the regeneration of injured myofibres mediated by muscle satellite (stem) cells. In general, muscle is the largest organ of humans (comprising 40-50% of the whole body mass). Interestingly, despite being a largely terminally differentiated tissue, muscle tissues maintain a remarkable plasticity. Skeletal muscle originates from the paraxial mesoderm during embryonic development to form somites, then dermomyotome and finally the myotome [96]. Subsequently, myoblasts undergo proliferation and differentiation during which they fuse to form multinucleated myotubes. Importantly, a fraction of the muscle progenitor cells, the satellite cells, remain quiescent in postnatal muscle and reside underneath the basal lamina of adult myofibres. Upon muscle injury, (e.g. after intense exercise) satellite cells become activated and enter the cell cycle to generate myoblasts that mediate myofibre repair. Importantly, satellite cells are capable of asymmetric division and thereby replenish themselves, thus maintaining the regenerative capacity of muscle [97].

Myogenesis is a process that is regulated by a plethora of transcription factors as well as miRNAs (Figure 1.2). Muscle progenitor and satellite cells express the paired-box (Pax) 3 and Pax7 transcription factors that determine the myogenic lineage. Pax7 is essential for maintaining the myogenic potential of the satellite cells. Upon activation and commitment to the myogenic lineage, Pax7 is repressed whereas other myogenic regulatory factors (MRFs) are sequentially induced, giving rise to proliferative myoblasts. Early during myogenesis, Myf5 is highly expressed, followed by MyoD1. Once myoblasts have developed into myocytes, myogenin (MyoG) and MRF4 are induced and promote myocyte fusion to form adult myotubes which are organised into myofibres (myogenic transcription factors are reviewed in detail here [98]).

The importance of miRNAs in myogenesis is exemplified by the finding that Dicer has been shown to be indispensable for limb development [99]. Of key importance and first identified were miR-1, miR-133a/b and miR-206 which together correspond to more than 25% of all miRNAs in skeletal muscle

and their expression is dramatically increased during myogenic differentiation [100]. miR-1 and miR-133a are expressed in all muscle tissues whereas miR-206 is exclusive to skeletal muscle [101]. These miRNAs control muscle homeostasis by coordinating satellite cell and myoblast proliferation, as well as myotube differentiation [102,103]. Due to their tissue-specific expression and high abundance, miR-1, miR-133a/b and miR-206 are commonly referred to as myomiRs. They are expressed as bicistronic transcripts from three different loci in the human genome: miR-1-1/miR-133a-2 (20q13.33), miR-1-2/miR-133a-1 (18q11.2), and miR-206/miR-133b (6p12.1) [104,105].

Interestingly, the expression of miR-1, miR-133a/b and miR-206 are regulated by myogenic transcription factors (Figure 1.2). The myocyte enhancer factor 2 (MEF2) and MyoD activate miR-1/miR-133a expression whereas miR-206 transcription is induced by MyoD and myogenin [104,105]. Despite originating from the same transcript, miR-1 and miR-133a appear to have opposing effects on muscle homeostasis. miR-133a and miR-133b differ by only one nucleotide at the 3' end and therefore both repress the serum response factor (SRF) to enhance myoblast proliferation. SRF in turn induces miR-133 expression, thereby establishing a negative feedback loop. In addition, miR-133 also targets the splicing factor neuronal polypyrimidine tract-binding protein (nPTB) which alters the cellular splicing pattern to adopt a signature typical of myotubes, thus suggesting miR-133 also promotes differentiation [106].

miR-1 and miR-206 differ by only four nucleotides outside of the seed region and are therefore believed to regulate the same targets, although this has not yet been validated for all reported targets (only validated targets are indicated in Table 1.2). Notably, it has been shown that both miRNAs target histone deacetylase 4 (HDAC4), which epigenetically represses multiple genes that are essential for myogensis, the most important of which is MEF2. Consequently, myoblast proliferation is inhibited and myogenic differentiation is promoted [102,107]. miR-206 (and possibly also miR-1) was identified as a regulator of the DNA polymerase alpha (DNAPolα), thereby establishing a link to the suppression of DNA synthesis (and thereby also inhibiting proliferation) upon myogenic

differentiation [105] (Figure 1.2). Studies in C2C12 muscle cells have revealed a plethora of additional targets for these myomiRs (reviewed in [91] and an overview is given in Table 1.2).

In addition to miR-1, miR-133 and miR-206, another group of muscle-exclusive myomiRs are involved in controlling muscle fibre type: miR-208a/b and miR-499 are transcribed from introns of the myosin genes *MYH6, MYH7* and *MYH7b* (note that miR-208a is specific to cardiac muscle, whereas miR-208b and miR-499 are expressed in both heart and skeletal muscle) [108]. In addition, the muscle-enriched miR-486 is encoded within in the Ankyrin 1 gene *(ANK1)* and promotes differentiation by targeting Pax7 [109]. Furthermore, there are multiple other, ubiquitously expressed miRNAs that are either induced or repressed during myogenesis, and are involved in coordinating muscle cell growth and differentiation (summarised in Table 1.2). Consequently, the regulation of transcription during myogenesis is a highly complex process that is characterised by multiple feedback loops between miRNAs and their targets.

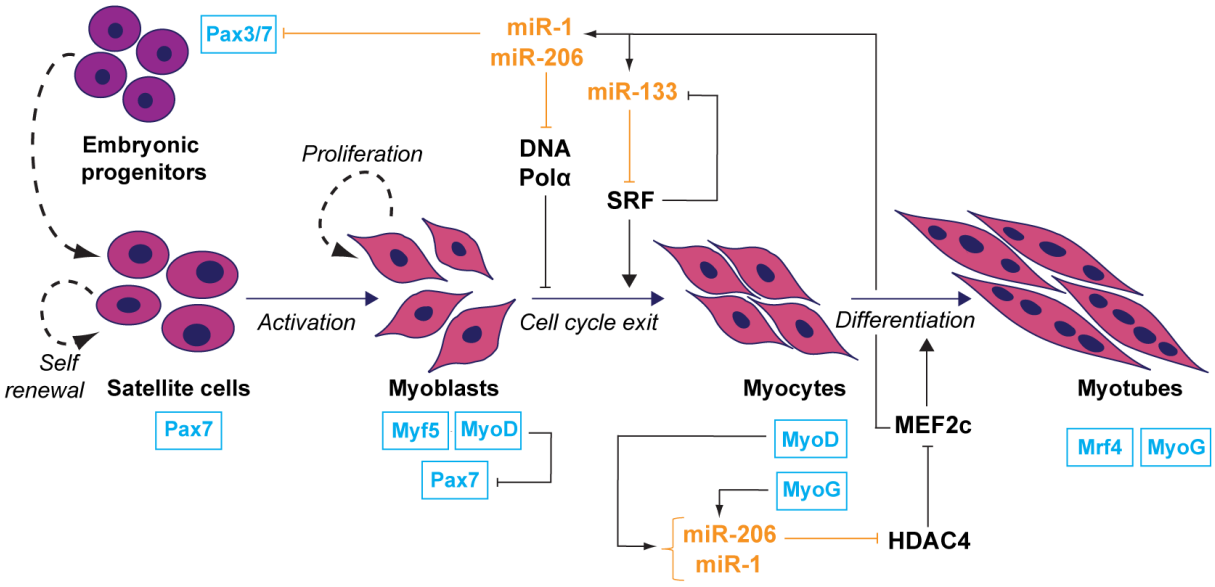

Figure 1.2 Regulation of myogenesis by microRNA and myogenic transcription factors.

Schematic depicting the myogenic transcription factors (blue boxes) and the myomiRs miR-1, miR-133 and miR-206 (in orange) that regulate activation and self-renewal of satellite cells, proliferation of myoblasts, and subsequent myogenic differentiation into myofibres. Expression of the individual components is modulated by a complex network consisting of multiple feedback loops that control myogenesis and muscle homeostasis. Paired box genes 3 and 7 (Pax3 and Pax7), serum response factor (SRF), DNA polymerase catalytic subunit (DNA polα), histone deacetylase 4 (HDAC4).

miRNA	Tissue		Expression and function in Myogenesis	Target(s)	Involvement in DMD*
miR-1	M	↑	Promotes differentiation, inhibits proliferation.	HDAC4, Cx43, Pax7, c-Met, G6PD [91]	Decreased in skeletal muscle of DMD patients and *mdx* mice.
miR-23a	U	↓	Inhibits differentiation.	Myh 1, 2, 4 [110]	Increased in *mdx* muscle, protective in atrophy.
miR-24	U	↑	Promotes differentiation.	Smad3 [111]	Increased in *mdx* muscle.
miR-26a	U	↑	Promotes differentiation.	Ezh2 [112,113] Smad 1 and Smad 3	N/A Induced during regeneration/hypertrophy.
miR-27a/b	U	↑	Promotes satellite cell activation and myoblast proliferation, but also differentiation.	Myostatin [114], Pax3 [115]	Increased in *mdx* muscle, Decreases myostatin and thereby increases muscle growth, downregulated in atrophy
miR-29b/c	U	↑	Promotes differentiation, inhibits proliferation, and fibrosis.	YY1, Akt3, HDAC4, COL1A1, ELN, Smad3, (reviewed in [116])	miR-29c is decreased in skeletal muscle of DMD patients and *mdx* mice, this reduction promotes fibrosis.
miR-31	U	↓	Maintenance of satellite cell quiescence.	Myf5 [117]	Strongly increased in skeletal muscle of DMD patients and *mdx* mice, inhibits dystrophin expression [118].
miR-125b	U	↓	Inhibits myoblast differentiation.	IGF-II [119]	N/A. May be part of the regulatory axis between myostatin signalling an IGF-1/ mTor pathway [119].
miR-133	M	↑	Promotes proliferation (and differentiation).	SRF [102], nPTB, UCP2, IGF-1	Decreased in skeletal muscle (DMD patients and *mdx* mice).
miR-146b	U	↑	Promotes differentiation.	Smad4, Hmga2, Notch1 [120]	Increased in skeletal muscle of DMD patients and patients with other dystrophies, strongly increased in *mdx* muscle.

miR-181	U	↑	Promotes terminal differentiation.	Hox-A11 [121]	Reduced in sarcopenia.
miR-186			Inhibits terminal differentiation.	Myogenin [122]	N/A
miR-206	Sk-M	↑	Promotes differentiation and inhibits proliferation. May promote regeneration.	Pax3, Pax7, Pola1,MyoR,], Id1-3, HDAC4, Utrn, TIMP3, c-Met, Cx43, PTB, Notch3, Igfbp5, Fstl1 (reviewed in [123])	Increased in skeletal muscle of DMD patients and *mdx* mice. Upregulated in regenerating fibres [124]. May regulate myotube size.
miR-208b **miR-499**	M	↑	Promote the slow-fibre type phenotype, activate slow and repressing fast myofibre gene program.	Sox6, Purβ, Sp3 , HP-1β [108]	Involved in determination myofibre type. Decreased in muscle of GRMD dog.
miR-221 **miR-222**	U	↓	Involved in regulation of differentiation.	p27 [125]	Increased in DMD patients and *mdx* muscle, Downregulates β1-syntropin [126].
miR-322 **miR-424**	U	↑	Promote differentiation.	Cdc25A [127]	N/A
miR-378	U	↑	Promotes differentiation.	MyoR [128]	Decreased in *mdx* muscle.
miR-486	M(U)	↑	Promotes differentiation.	Pax7, PTEN/FoxO1a [129]	Decreased in DMD patients and *mdx* muscle, influences cell cycle kinetics via PTEN/AKT [130].
miR-503	U	↑	Promotes differentiation.	Cdc25A [127]	N/A

Table 1.2 Overview of miRNAs modulating myogenesis and suggested to be involved in DMD pathology.

M: Muscle, Sk-M: Skeletal muscle, U: ubiquitously, ↑ induced during myogenesis, ↓ repressed during myogenesis, * expression changes and implication of diseases are summarised from multiple studies including [118,131,132] and reviews [133–137], unless otherwised referenced. N/A: no differential expression reported to the author's knowledge.

1.3.3 miRNAs implicated in dystrophic pathology

Given the importance of miRNAs in muscle homeostasis, it is unsurprising that impaired miRNA regulation is a common feature in pathologies of muscle such as DMD. A microarray profiling study by Eisenberg *et al.* (2007) found 185 miRNAs differently expressed in muscle tissue obtained from patients suffering from 10 primary muscular disorders including DMD and BMD [131]. Only 5 of these were commonly dysregulated in all 10 muscular dystrophies (miR-146b, miR-221, miR-155, miR-214, and miR-222). The five commonly differentially expressed miRNAs are typically expressed in immune cells and therefore their dysregulation is likely to arise from an inflammatory response [131]. A second study, undertaken by Greco *et al.* (2009) utilised TaqMan arrays to profile miRNA expression in muscle of *mdx* mice and DMD patients and found 36 miRNAs to be dysregulated [132]. In particular, miR-1, miR-29c, miR-135a, miR-486 were found to be downregulated whereas miR-34c, miR-124a, miR-206, miR-222, miR-223, miR-335, miR-449, miR-494 and especially miR-31 (by 70 fold) were found to be upregulated. Subsequently, Roberts *et al.* undertook miRNA microarray profiling in quadriceps, diaphragm and heart tissues of wild-type and *mdx* mice and identified 18 miRNAs that were differentially expressed in all three tissues, a number of which had not been described before [138]. In addition, there have been several other miRNA profiling studies in different muscles and also serum of DMD animal models and patients (key results summarised in (Table 1.2)).

Determining the miRNA signature of dystrophic tissue and serum is of interest for a number of reasons. Firstly, miRNAs, which show altered expression levels in dystrophic muscle or serum have potential as disease biomarkers. Secondly, DMD-associated differentially expressed miRNAs may act to regulate the molecular processes which contribute to DMD pathophysiology (e.g. aberrant nNOS signalling in the absence of dystrophin protein [139]). Thirdly, disease-associated miRNAs may constitute novel targets for therapy. To this end, miR-31 has been shown to keep satellite cells in a quiescent state by targeting Myf5 [117], but also directly downregulates dystrophin expression, thereby limiting the efficacy of dystrophin rescue by exon skipping therapy [118]. Interestingly, the

efficiency of exon skipping in DMD myoblasts has been shown to increase if miR-31 is inhibited, thereby underlining that combining these two strategies may improve treatment efficacy [118]. Furthermore, miR-486 modulates the cell cycle via the phosphatase and tensin homolog (PTEN)/AKT signalling pathways and overexpression has been shown to ameliorate muscular dystrophy–associated symptoms. In addition, miR-29c downregulation in dystrophic muscle has been shown to suppress myogenic differentiation and promote transdifferentiation of myoblasts into myofibroblast [140]. Consequently, miR-29c replacement therapy might ameliorate fibrosis and dystrophic pathology. Lastly, increased miR-21 expression has been shown to enhance fibrosis and consequently its inhibition in combination with miR-29c mimicking is an attractive therapeutic strategy to exploit miRNA-based therapeutics to reduce fibrosis in muscular dystrophy [141].

1.4 Extracellular microRNAs

1.4.1 Discovery of extracellular microRNAs

The discovery that small RNAs are stable in various in biofluids has caused excitement in the field of RNA research and may alter our current understanding of gene regulation and intercellular communication. As outlined in the following sections, extracellular microRNAs (ex-miRNAs) are considered to be a new class of promising biomarkers and potential therapeutic targets.

Until recently, research focused primarily on intracellular functions of miRNAs. Remarkably, the existence of nucleic acids in the circulation has been described as early as 1931, where they were found to be surprisingly resistant to degradation in this nuclease-rich environment [142,143]. Despite this early discovery of extracellular nucleic acids, the mechanisms of stabilisation and potential biological function largely remained unclear. Many years later in 2008, Chim *et al.* first made the observation that placenta-specific miRNAs were only present in the plasma of pregnant women and disappeared after childbirth [144]. This exciting finding indicates that some miRNAs in the extracellular space can carry information about the physiological status of an individual. At around the same time, ex- miRNAs were independently shown by several groups to act as disease signatures for certain cancer types [145–147]. Moreover, miRNAs were also found to exist in varying concentrations in almost all other body fluids including saliva, urine, breast milk, tears, cerebrospinal fluid, peritoneal fluid and pleural fluid [148].

The discovery of ex-miRNAs in plasma has had two major impacts on the miRNA field. Firstly, because blood is easily accessible, ex-miRNAs were suggested to be promising biomarkers for both diagnostic and prognostic purposes. Various pathological conditions have indeed been shown to be associated with altered profiles of circulating miRNAs, including cardiac damage [149], muscle injury [150], liver injury [151], diabetes [146] and various types of cancers [145]. Secondly, the fact that miRNAs might be selectively secreted and are stable in the extracellular space could indicate a

potential role in cell-to-cell communication *in vivo*. Furthermore, it ignited the hypothesis of a global, hormone-like functional mechanism of miRNAs that might allow regulation of gene expression across tissues at a distance. As such, paracrine or even endocrine communication via circulating miRNAs could be part of a previously unappreciated gene regulatory network that might have evolved to coordinate the activities of cells in multicellular organisms.

However, many questions remain to be answered in the emerging field of ex-miRNAs. Among these are: what are the sources of miRNA molecules in circulation and are there tissue/organ specific secretion patterns? Is the release of miRNAs passive, or are there specific release stimuli triggering miRNA packaging and export? How are miRNAs sorted for secretion and what are the mechanisms by which they enter into the blood circulation? By what means, and for how long are ex-miRNAs stabilised in blood or other biofluids? Can miRNAs in the circulation be targeted to specific locations in the body and if so, how are they recognised and internalised by recipient cells? Is the concentration of shuttled miRNAs high enough to induce biologically relevant effects in the target cell? While some of these questions have been addressed (at least to some extent) there is currently no consensus regarding the intrinsic biological function of ex-miRNAs. Several different modes of transport have been described, and it appears that the association of miRNAs with diverse carriers can have implications for their biological and pathological significance. As a result, ex-miRNAs may be categorised according to their mode of transport, highlighting that they are indeed not a homogeneous population.

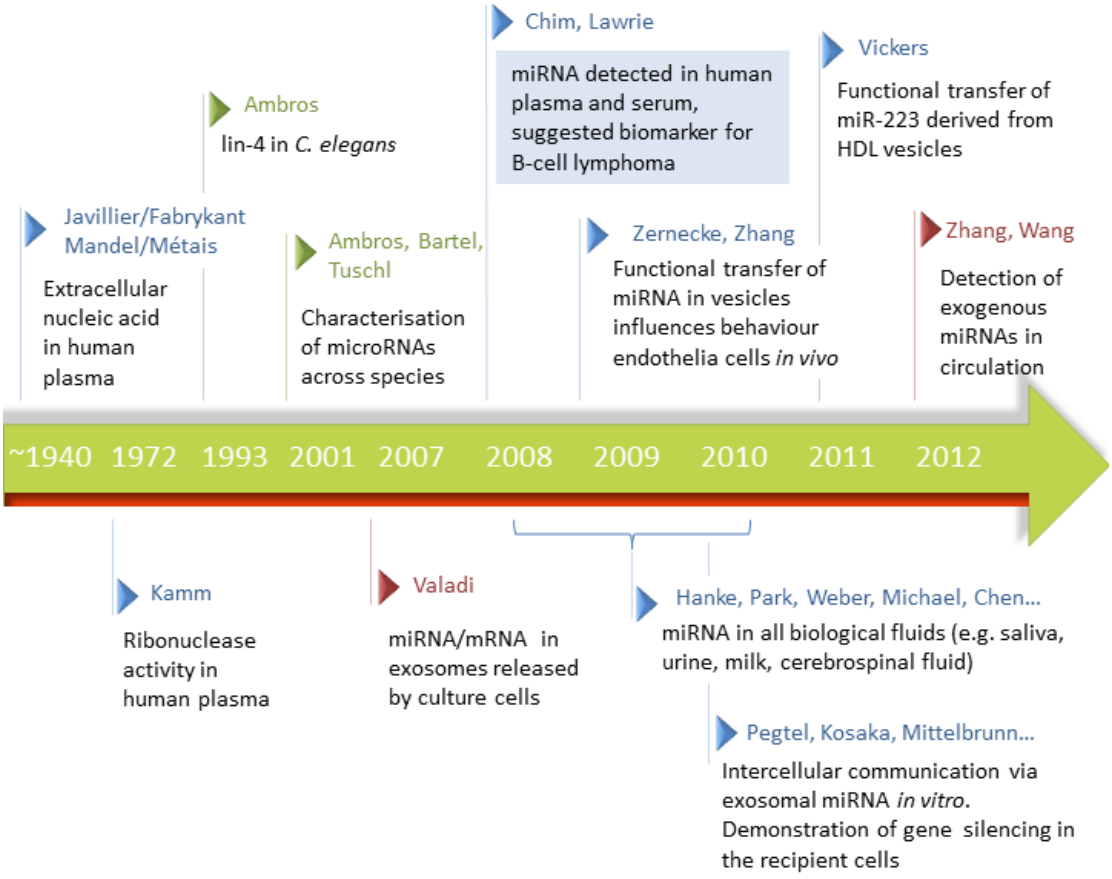

Figure 1.3 Milestones in extracellular miRNA discovery.

Overview of the landmark studies in ex-miRNA field. For convenience only the first authors of the respective studies are listed.

1.4.2 Modes of packaging for extracellular microRNAs

Currently, the cellular machinery that is involved in packaging and secreting small RNAs is not well understood, although multiple subclasses of ex-miRNA carriers have been identified (Figure 1.4). After the discovery of ex-miRNAs in biological fluids it had been assumed that they were most likely protected from nuclease degradation by encapsulation within lipid membranes [152]. Indeed, miRNAs were firstly found in extracellular vesicles (EV) isolated from cultured cells [153]. Subsequently in 2008, miRNAs were also found in exosomes and microvesicles isolated from human blood, thereby reinforcing the hypothesis of vesicle-encapsulation as the primary mode of stabilisation for ex-miRNAs [154].

However, in subsequent studies, the composition of blood plasma/serum and conditioned cell culture media was analysed more systematically using fractionation methods including ultracentrifugation, ultrafiltration and size-exclusion chromatography. Challenging the previous theory, Wang *et al.* demonstrated in 2011 that the large majority of small RNAs exported by mammalian cells are in fact vesicle-free and are associated with ribonucleoproteins [155]. Following this report, two independent studies confirmed that the vast majority (90-95%) of miRNAs in the circulation exist outside vesicles in complex with Argonaute proteins [156,157]. In addition to protein complexes and EVs, miRNAs were also found in apoptotic bodies [158]. To add further complexity, ex-miRNAs have also been demonstrated to associate with lipoproteins such as high density lipoprotein (HDL) complexes in the circulation [159,160].

These findings have implications for the potential biological relevance of ex-miRNAs as to date, functional uptake of miRNAs has only been shown for membrane-associated and lipoprotein carriers but not for miRNA-protein complexes. Generally, functional uptake is defined as the ability of the transferred miRNA to selectively influence gene expression in the recipient cell in a sequence-dependent manner (i.e. by repressing target gene expression). Important challenges are to differentiate these effects from other non-specific effects caused for example by treatment of the

cells with a high number of vesicles, and upregulation of endogenous miRNAs in the recipient cell. Indeed, some groups have dismissed ex-miRNA as a non-functional waste product that passively leaks into the circulation after cell death [152]. Consequently, one may hypothesise that each miRNA carrier is likely to have a distinct biological role. In addition, a carrier-specific ex-miRNA signature is a plausible scenario, although the extent of specificity of miRNA content might vary for different subpopulations, and some ex-miRNAs are likely to be shared among different carriers. Lastly, an exchange or transfer of ex-miRNAs between vehicles might be possible, as well as one may speculate that vesicle breakdown in circulation occurs.

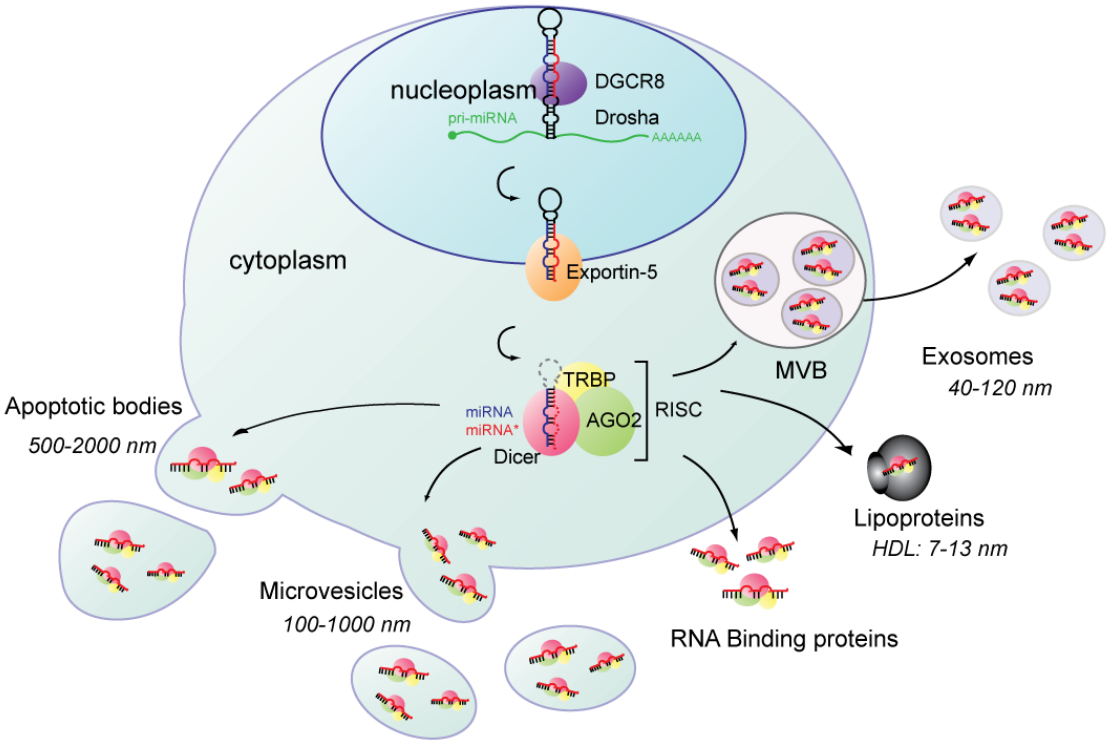

Figure 1.4 Overview of miRNA maturation and possible export pathways.

Primary miRNA transcripts are transcribed in the nucleus and progressively processed to generate the mature miRNA species. Firstly, a complex of Drosha and DGCR8 cleaves the pri-miRNA transcript to produce the precursor miRNA (pre-miRNA) in the nucleus. After being actively exported into the cytoplasm by exportin-5, the pre-miRNA is cleaved by Dicer, generating the mature double stranded miRNA. One strand of the duplex miRNA is loaded into RISC, consisting of Dicer, AGO2 and TRBP. Typically, miRNA loaded RISC is guided to a complementary target mRNA and induces translational repression or mRNA decay. However, since miRNAs have been demonstrated to exist in extracellular space, different export pathways are being investigated and multiple subclasses of ex-miRNA carrier have been identified in serum, including three types of membrane-derived vesicles: exosomes, microvesicles and apoptotic bodies. Additionally, lipoproteins such as high-density lipoproteins (HDL) and ribonucleoproteins such as AGO2 can incorporate miRNAs. MVB: multivesicular bodies.

1.4.3 Ex-miRNAs exported in microvesicles, exosomes and other membrane-encapsulated vesicles

As mentioned above, there is growing evidence that only a fraction of circulating miRNAs are found in association with extracellular vesicles (EVs) [155–157]. Generally, EVs are thought to partake in modulation of normal physiological processes, but are also likely involved in regulating disease progression by modulating the physiology of their target cells [161]. Notably, a subset of the mechanisms by which EVs contribute to the regulation of physiological processes is thought to be related to EV-associated ex-miRNAs. In the following paragraphs, an overview is given on EV subtypes, EV biogenesis and ex-miRNA sorting to EVs.

1.4.3.1 Biogenesis of microvesicles and exosomes

All membrane-encapsulated particles that are secreted or released by cells can collectively be called EVs. Further classification of these vesicles is based on either their cell type of origin, or their pathway of biogenesis. Both classification systems have their advantages and disadvantages. Firstly, the cellular origin of EVs can reflect their biological functions or cellular indentity. For example, ectosomes (originating from neutrophils or monocytes), microparticles (shed from platelets or endothelial cells), tolerosomes (extracted from antigen-fed mice), prostatosomes (isolated from seminal fluid), cardiosomes (secreted by cardiomyocytes) or vexosomes (related to adeno-associated virus infected cells) [162]. While some EV parent cell functions can be transferred to their vesicles, the molecular signature of EVs derived from different cell types is generally more similar to each other than that of EVs and their parent cells [153,163].

Secondly, with respect to their mode of biogenesis, there are three types of EVs – exosomes, microvesicles and apoptotic bodies. Exosomes originate from the endolysosomal pathway when multivesicular bodies (MVB) fuse with the plasma membrane to release the contained intraluminal vesicles to the extracellular environment (Figure 1.5) [161]. MVBs are formed during endosome maturation upon initiation of inward budding of endosomal membranes. This process either involves

the endosomal sorting complexes required for transport (ESCRT) or the lipid ceramide and neutral sphingomyelinase (converts sphingomyelin to ceramide) [162]. Once secreted, exosomes are generally 40–120 nm in diameter and contain numerous proteins that co-localise to their budding sites or are related to their biogenesis, such as tetraspanins, ESCRT components, programmed cell death 6 interacting protein (PDCD6IP) also referred to as ALIX, Tumor susceptibility gene 101 (TSG101), Flotillin 1 (FLOT1), Milk fat globule-EGF factor 8 protein (MFGE8), and others [162]. RNA constituents of exosomes include mRNA, miRNA, and many other species of non-coding RNA [164].

In contrast, microvesicles form directly on the plasma membrane by outward budding and subsequent fission (Figure 1.5). It is generally accepted that the transmembrane proteins of microvesicles resemble the cell surface more closely than those of the endolysosomal pathway derived exosomes due to intracellular protein sorting and trafficking. For example, integrins, selectins, CD40 ligand and cell surface receptors are preferentially associated with microvesicles. Microvesicular RNA consists similarly of both coding and non-coding RNA species, although it is often thought that RNA sorting to microvesicles might be less specific when compared to exosomes. However, this may partially appear to be the case as exosome cargo sorting mechanisms have been studied more extensivey than for microvesicles [165–168]. Even though microvesicles are on average larger, up to 1,000 nm, there is a considerable size overlap with exosomes (microvesicle size range from 100-1,000 nm). Therefore, it remains difficult to selectively purify exosomes from microvesicles, and vice versa. Owing to this pitfall, many studies which reportedly have focused on either exosomes or microvesicles have in reality been analysing a mixture of both types of vesicles. In the here presented work, isolated vesicles from serum or conditioned media are referred to as EVs, thus considering the fact that despite an isolation strategy that was designed to purify exosomes, there is no guarantee that smaller microvesicles were not co-purified.

Apoptotic bodies are the third type of EV that form during the process of programmed cell death which is characterised by large membrane disturbances and outward blebbing. These vesicles are

large in size (500–2000 nm) and as a hallmark contain very large amounts of exposed phosphatidyl serine, components of the nucleus and parts of various other subcellular organelles.

1.4.3.2 Mechanism for miRNA loading and secretion in EVs

Since the discovery that miRNAs are found in EVs, multiple studies have confirmed the finding that the neutral sphingomyelinase 2 (nSMase2) positively regulates miRNA export via EVs [169]. The enzyme is a critical regulator of exosome biogenesis, therefore it is unsurprising that inhibition of the nSMase2 generally reduces miRNA export in vesicles [163]. Consequently, it is likely that inhibition of other biogenesis regulators such as ALIX and TSG101 or the ESCRT machinery might have similar effects on reducing the export of vesicular miRNAs. It is further noteworthy that general mechanisms that lead to sorting of specific miRNAs into both exosomes and micorvesicles are often studied together due to the technical challenges associated with accurately separating them.

The evidence for specific targeting of miRNAs is related to the finding that EV-associated ex-miRNA and cellular miRNA levels seem largely uncorrelated, whereas the miRNA composition of EVs from different cell types may be similar [153,170]. Multiple studies have investigated selective sorting of miRNAs into EVs and identified a number of possible regulatory pathways which are described in the following paragraphs and illustrated in Figure 1.5.

Firstly, in several cell types, Dicer-independent miRNAs (i.e. which depend on AGO2 for their maturation [171]) such as miR-451, miR-150 and miR-134-3p among others seem to be preferentially sorted to EVs [172]. Furthermore, it was found that, at least in macrophages, higher intracellular levels of target transcripts of individual miRNAs can positively affect the extent to which these miRNAs are secreted from cells in association with vesicles [173]. Similarly, since EVs were found to contain increased amounts of 3'end mRNA fragments, it was hypothesised that miRNA binding sites in 3'UTR regions of these transcripts can regulate miRNA sorting too [174].

Some RNA molecules can be modified after being transcribed by addition of non-templated nucleotides. By studying miRNA secretion in B cells, it was recently found that when a miRNA 3'-end was uridylated, it was more likely to be found secreted with EVs, whereas 3'-adenylated miRNAs were preferentially retained in cells [175]. That study, importantly, draws attention to an idea that one of the active mechanisms that could determine which miRNAs can be secreted in EVs, may be an "intracellular signal motif" that restricts a miRNA from being sorted to EVs. Specific nucleotide motifs present in a given miRNA, could be recognised by particular RNA-binding proteins. Intracellular localisation of these proteins could then determine, at least to a certain extent, the localisation of the miRNA too and thereby affect sorting, retention and secretion.

One of these proteins was found to be heterogeneous nuclear ribonucleoprotein A2B1 (hnRNPA2B1). Once modified post-translationally by small ubiquitin-like modifier (SUMO) proteins, the sumoylated hnRNPA2B1 binds a subset of miRNAs bearing a GGAG motif in their 3'-region, leading to their sorting to EVs. Other similar motifs were also found overrepresented in EV-associated miRNAs and were collectively named "EXOmotifs" [176]. Interestingly, miRNAs bearing certain other nucleotide signatures were preferentially retained in cells, a similar finding to the earlier mentioned study where 3'-adenylated sequences were more likely found intracellular [175]. This suggests that miRNA secretion within EVs can be controlled by both of these principal mechanisms: guiding specific miRNAs for secretion and restricting other miRNAs from it. In line with this finding, it was reported that nearly 30% of miRNAs released in exosomes by malignant epithelial cells do not reflect the cellular profile, pointing towards specific release or retention mechanisms. Furthermore, different rates of release were measured for individual miRNAs [177].

However, while there is evidence that the secretion of at least some miRNAs is specific, this is not necessarily the case for all miRNAs, thus pointing towards a complicated network regulating miRNA secretion with EVs. To this end, Zernecke *et al.* reported a strong enrichment of miR-126 in purified apoptotic bodies from human endothelial cells [158]. Notably, the protocols most commonly used in

ex-miRNA or EV research exclude apoptotic bodies as they are removed by low-spin centrifugation during sample preparation. More detailed studies are needed in the future to determine to what extent miRNAs in apoptotic bodies account for the overall amount of circulating miRNAs.

It is important to note that the mechanisms that are involved in miRNA sorting to EVs for secretion may be different in altered physiological or pathological conditions. This hypothesis is based on the concept that in various diseases the expression of many molecules change, including alterations in miRNA expression networks and in proteins involved in EV biogenesis. Recognising these changes can help to both understand disease biology and to find biomarkers that would enable diagnosis or monitoring of disease progression.

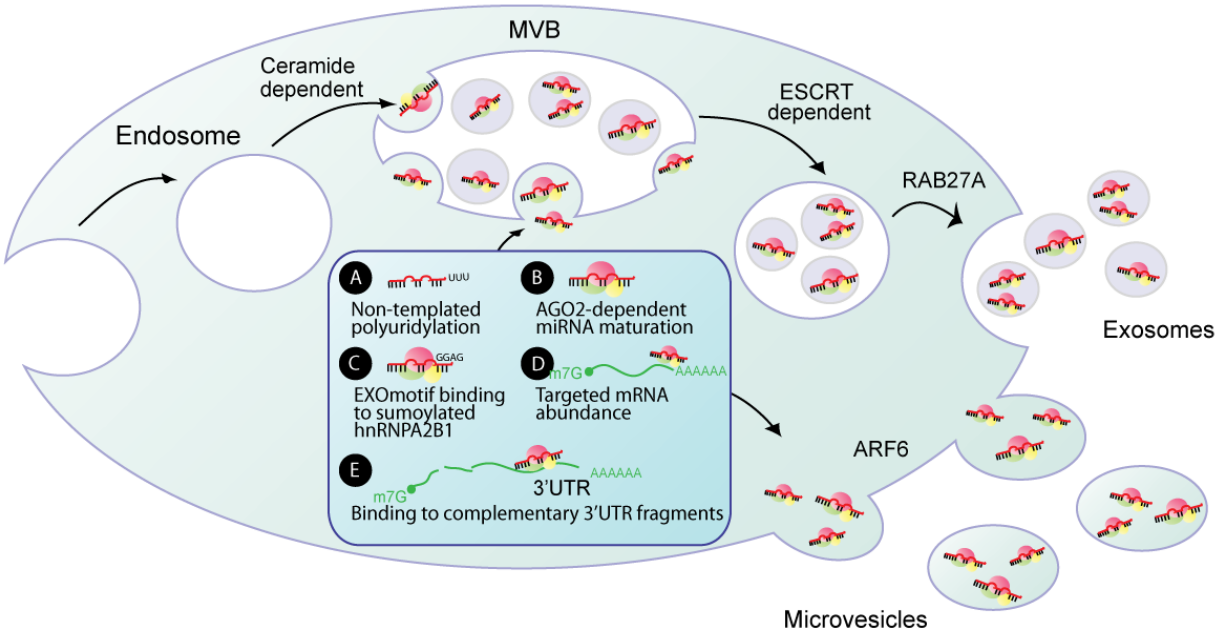

Figure 1.5 Pathways of EV biogenesis and miRNA sorting.

Exosomes and microvesicles have distinct biogenesis pathways. Exosomes are of endocytic origin and their biogenesis begins with the inward budding of the MVB membrane during the endosome maturation process. The budding and exosomal cargo sorting depends either ESCRT proteins or, alternatively, on the ceramide pathway. Exosomes are released to extracellular environment upon MVB fusion with the cell membrane, a process which is mediated by small GTPases, e.g. RAB27A. Microvesicles are considered more heterogeneous than exosomes and are formed by the outward budding of certain plasma membrane lipid domains and are regulated by proteins such as ADP-ribosylation factor 6 (ARF6). Selective miRNA secretion could be mediated by the following mechanisms of miRNAs sorting into EVs: (A) Non-templated nucleotide additions, e.g. polyuridylation leading to more efficient miRNA incorporation to EVs. (B) Several miRNAs whose maturation pathway depends on AGO2 are enriched in EVs. (C) Certain nucleotide motifs present in miRNAs lead to their binding to sumoylated hnRNPA2B1 protein and subsequent sorting to EVs. miRNA sorting to EVs can depend also on (D) the abundance of its target genes and (E) the presence of complementary 3'UTR mRNA fragments in EVs.

1.4.3.3 EV uptake and biological effects of miRNAs in recipient cells

In principle, EVs can be taken up by either endocytosis or membrane fusion [178–180]. If vesicles enter via the endocytotic pathway they can undergo transcytosis, be degraded by lysosomes or fuse with the endosomal membrane to release their cargo and exert functional effects in the target cell [179]. Currently, an understanding of EV internalisation is limited, although a variety of endocytic pathways are likely to be involved, including clathrin-dependent endocytosis, and clathrin-independent pathways such as caveolin-mediated uptake, macropinocytosis, phagocytosis, lipid raft-mediated internalisation and surfing on filopodia [180–184]. Notably, there might be multiple uptake mechanisms for a heterogeneous population of EVs, depending on surface protein and glycoprotein composition of both the vesicle and the target cell [185,186].

Multiple studies have demonstrated that vesicular miRNAs can be transferred to recipient cells and subsequently alter gene expression, thereby mediating functional effects (reviewed in [187,188]). The first direct example of a vesicular miRNA altering gene expression in target cells was described by Zernecke *et al.* in 2009. In this study the authors postulated that miR-126 enriched in apoptotic bodies can be transferred to alter the chemokine response of recipient vascular endothelial cells. In addition, a protective effect against development of artherosclerosis was observed *in vivo* [158]. Subsequently, Zhang *et al.* demonstrated functional transfer of EV-associated miR-150 to epithelial cells [170]. Thereafter, multiple studies confirmed the ability of vesicular miRNAs to repress gene expression and influence the phenotype of target cells. Notably, uptake and direct alteration of gene expression mediated by endogenous miRNAs has almost exclusively demonstrated in cell culture [189]. Furthermore, the effect is often specific for a donor and a recipient cell line combination and only occurs for some miRNAs. In addition, the quantities of EVs added to the recipient cells may be much higher than physiological concentrations. To this end, Sverdloc *et al.* calculated that the amount of applied exosomes per cell used in in ‘typical’ exosome studies is equivalent to the total number of exosomes in blood plasma [190]. On the other hand, EV concentration might be higher in local tissues compared to the bloodstream, highlighting the difficulty of determining what a

physiological exosome concentration is. As as a consequence, co-culture studies may be a more suitable experimental setting that allows studying miRNA transfer via EVs under more physiological conditions [191].

Evidently, further research is needed to provide insight into ex-miRNA internalisation mechanisms and most importantly into what amount can be delivered into the cytoplasm to exert a functional effect on target cell gene expression. A recent quantitative study of the miRNA content of exosomes suggested that most miRNAs are present at far less than one copy per exosome [192]. Assuming this stoichiometry is correct, a measurable effect on the gene expression could only be caused by transfer of miRNA-enriched exosome subpopulations or a rapid internalisation of numerous vesicles [193]. Other controversial aspects of EV-mediated miRNA transfer are whether miRNAs capable of repressing target mRNAs are required to be associated with AGO proteins prior to their uptake, or if they can be newly integrated into RISC complexes within the target cell. Furthermore, the extent to which immature miRNAs are secreted, and if they can undergo maturation and exert functional effects in the recipient cell, is currently unknown.

1.4.4 Lipoproteins function as ex-miRNA carriers

In addition to being encapsulated in phospholipid bilayer containing vesicles, nucleic acids can also associate with lipoproteins [194]. Notably, lipoproteins form a mono lipid layer with a hydrophobic core that can sequester water-insoluble molecules. Consequently, lipoproteins such as high-density lipoprotein (HDL) particles have frequently been exploited for the delivery of nucleic acids for gene therapy both *in vitro* and *in vivo* [195,196]. Classically, HDL particles are considered to be delivery vehicles that shuttle excess cholesterol, triglycerides and steroids between peripheral tissues and the liver/digestive system [197]. Remarkably, miRNAs were also found to co-purify with HDL from human blood thus revealing another constituent transported by HDL. In addition, low density lipoproteins (LDL) were also shown to carry ex-miRNAs, although to a much lesser extent than for HDL [159,160]. Furthermore, Vickers *et al.* discovered that the miRNA content of HDL particles can constitute a disease signature in the case of atherosclerosis and coronary artery disease (CAD), [159,160]. Additionally, it was shown that some miRNAs associate with HDL more efficiently than others. This finding either points to the existence of a cellular sorting system for HDL-bound miRNAs, but it could also be a non-specific passive phenomenon, caused by the varying affinity of RNA structures to phospholipids [194].

It has been shown that HDL particles are capable of delivering ex-miRNAs to hepatocytes, and their uptake was shown to be dependent on the presence of scavenger receptor class B type 1 (SR-B1) [159]. Upon uptake, miRNAs downregulated mRNA targets with putative target sites and many of the altered genes were associated with lipid metabolism, inflammation and atherosclerosis. This finding provides new insights into pathological pathways associated with these diseases which might be targeted by future therapeutics [159]. In contrast, another study reported that lipoprotein-bound ex-miRNAs were not efficiently transferred to endothelia, smooth muscle and peripheral blood cells [160]. Therefore, it is possible that uptake of HDL is restricted to cell-types that express SR-B1 and are naturally involved in HDL trafficking. Furthermore, Vickers *et al.* undertook an investigation of the

mechanism of miRNA export to HDL. The results indicated that HDL-miRNA export is negatively correlated with the expression of nSMAse2 and that upregulation of the ceramide pathway has a repressive effect on extracellular HDL-miRNA levels [159]. This is contrary to miRNA export in EVs which have been proven to be positively correlated with nSMAse2 activity, hence pointing towards distinct export mechanism of EVs and HDL [169,198]. However, it remains unclear how miRNAs are loaded into lipoprotein particles, and if they are simultaneously associated with miRNA binding ribonucleoproteins (RNPs).

Both Vickers *et al.* and Wagner *et al.* determined miR-223 to be the most abundant miRNA in HDL vesicles, although Wagner *et al*. measured a concentration of 10,000 copies per µg HDL which accounts for only 8% of total extracellular miR-223 when comparing to the total pool of miRNAs [160]. In summary, further investigation is needed to confirm that HDL mediates miRNA transfer to distal tissues *in vivo,* and so far this effect appears to be highly cell type-specific. Notably, even if not central to intercellular communication, HDL-miRNAs could still comprise a novel class of serum biomarkers that could be of clinical utility in the diagnosis and monitoring of diseases such as atherosclerosis.

1.4.5 Extracellular miRNA-ribonucleoprotein complexes

In 2011, three independent research groups systematically investigated the distribution of ex-miRNAs in fractionated blood and conditioned media, Extracellular vesicles were separated from protein complexes by using ultracentrifugation (UC), ultrafiltration (UF) or size- exclusion chromatography (SEC). Intriguingly, all reports concordantly revealed that the vast majority of ex-miRNAs were found in the non-vesicular fraction and that these protein-miRNA complexes were remarkably resistant to RNAse activity [155–157].

Turchinovich *et al.* estimated that 90% of ex-miRNAs are outside any known vesicular structure in blood plasma and conditioned media of cancer cell lines [157]. In accordance, Arroyo *et al.* described a similar trend and identified three different classes of ex-miRNAs: some of them were exclusively enriched in vesicles (let-7a, miR-142), while others were exclusively found in late-eluting SEC fractions containing small RNPs (miR-16, miR-122), and lastly some ex-miRNAs were present in all fractions (miR-150) [156]. Similarly, Wang *et al.* confirmed the existence of distinct ex-miRNA subpopulations using differential UC and undertook a mass spectrometry approach to identify protein-based ex-miRNA carriers. The most abundant protein was the 33 kD nucleophosmin 1 (NPM1), which was consequently shown to be capable of stabilising synthetic ex-miRNAs in the presence of RNaseA [155]. Additionally, two other reports demonstrated that a large amount of circulating miRNAs are associated with the 96 kD sized AGO2 and that, the SEC and UF pattern of AGO2 abundance closely matched ex-miRNA abundance [156,157]. Additionally, AGO1 has also been demonstrated to be associated with ex-miRNAs in human plasma [199].

Furthermore, Wang *et al.* observed striking differences in abundance levels of intracellular and extracellular miRNAs in cultured HepG2 cells, whereas Turchinovich *et al.* found that array analysis suggested that intracellular and ex-miRNA abundance are highly correlated in MCF7 cells. Controversially, Turchinovich *et al.* observed a proportional increase of secretion if a randomly selected miRNA is overexpressed, thus favouring the hypothesis of non-specific miRNA export [152].

Subsequently, the authors demonstrated that protein-associated ex-miRNAs are stable in the extracellular milieu for at least two months when stored at room temperature in serum containing media, pointing towards the possibility that these complexes are by-products of cellular activity accumulating over time [152]. In contrast, Wang *et al*. identified serum-deprivation as miRNA export stimulus and described a dynamic and energy-dependent secretion process, that is independent of cell death [155]. In agreement, Arroyo *et al.* described that the liver specific miR-122 is exclusively found outside of vesicles and thus hypothesised that hepatocytes might secrete this miRNAs via an undescribed particle carrier pathway [156].

In summary, while all groups agreed on the high stability of protein-bound ex-miRNAs, and that these account for the majority of ex-miRNAs, the results and conclusions drawn regarding the origin and possible biological functions are diverse across different reports. Notably, it is possible that both passive release via cell death or bulk exocytosis and specific export could occur in parallel, thus indicating that secreted miRNAs might comprise both a cellular waste disposal mechanism as well as contributing to intercellular communication in mammals. Nonetheless, it has yet to be convincingly demonstrated that non-vesicular ex-miRNA carriers can mediate functional miRNA transfer. So far, neither the export machinery nor specific receptors of recipient cells have been identified. However, protein based RNA carrier systems that allow cell-to-cell trafficking of small RNAs have been identified in lower organisms (e.g. in *C. elegans* and in plants [200,201]) and thus the existence of mammalian equivalents may be plausible.

1.4.6 Circulating miRNAs as prospective clinical biomarkers

While the significance of ex-miRNA function remains unclear, their potential as disease biomarkers is becoming increasingly well-established. A plethora of studies have identified specific ex-miRNA signatures in blood associated with various human pathologies including liver disease, cancer, cardiovascular disease, inflammatory disease and myopathies, and thereby have demonstrated the potential of this new class of biomarkers [202–207]. Circulating miRNAs are promising biomarkers since they are remarkably stable, can be specific to certain physiological and pathological conditions and are accessible to analysis through relatively non-invasive methods. In addition, ex-miRNAs can be measured reliably with high sensitivity. However, multiple pitfalls such as standardisation of sample preparation, quality control as well as data normalisation must be addressed and the established standard practices disseminated throughout the research community. In addition, improvements in downstream analytical technologies such as digital PCR and next-generation-sequencing (NGS) hold promise for advancing ex-miRNA research as they allow for more sensitive, accurate and informative quantification [208–211]. Furthermore, an important point to consider for any ex-miRNA biomarker study is the existence of different ex-miRNA populations defined by their origin, mechanism of export and the means by which they are stabilised in circulation. Therefore, the appropriate ex-miRNA purification strategy has to be considered if analysing ex-miRNAs segregated to specific complexes such as exosomes or lipoproteins.

Notably, ex-miRNA biomarkers can be grouped into two classes. Firstly, ex-miRNAs originating from tissue injury that are most probably passively released upon physical cell membrane damage and/or cell death. The tissue-specific release of miRNAs can be considered a signal of injury and may not contribute to pathology *per se.* The second class are ex-miRNAs that are selectively released during the development of pathology, possibly in an active and/or prolonged process that might have implications for disease progression.

For instance, miR-208, miR-133 and miR-499 which are highly abundant in heart muscle, have been shown to be released by the myocardium after acute cardiac infarct and are subsequently enriched in circulation [212,213]. Furthermore, in healthy individuals, muscle-associated miRNAs are only present at very low levels in the circulation. In contrast, levels of these miRNAs are highly enriched in the blood of DMD patients [214] (also discussed in detail in section 1.5.3). Similarly, miR-122 is highly expressed in hepatocytes and has been reported to be elevated in patients suffering from chronic hepatitis C or hypercholesterolemia [215]. In general, a correlation between tissue injury and subsequent enrichment of tissue-specific miRNAs in the circulation indicates for passive, non-selective release of miRNAs that is a consequence of the pathology but may not actively contribute to the disease pathophysiology.

In contrast, extracellular miR-126, miR-223 and miR-15a were measurably altered in patients with overt diabetes. Strikingly, this alteration was observed before disease manifestation, thus indicating that miRNAs might be causally involved in disease development. In particular miR-126, which has been described as biomarker for type 2 diabetes (T2D), is greatly enriched in the circulation of patients. However, it is not among the miRNAs that are most abundant in adipose tissue which is the key tissue involved in T2D pathogenesis [216]. These findings suggest that ex-miRNAs may contribute to disease progression and may provide novel insights into disease etiology. Another example are circulating miRNAs that are deregulated during carcinogenesis. There is an indication that these potential biomarkers modulate cancer progression and the probability of metastasis by signalling to endothelial and immune cells [145,217]. Cancer- associated miRNAs have been found in EVs and are reported to mediate tumor dormancy, angiogenesis, transfer of drug resistance, suppression of immune system and tumor metastasis [145,217,218]. As such these ex-miRNAs are not only prospective biomarkers but may also constitute novel therapeutic targets (further discussed in section 1.4.7).

1.4.7 Therapeutic potential of extracellular miRNAs

Aside from the potential predictive power of measuring extracellular miRNAs, their potential to contribute to physiological and pathological processes in a paracrine or endocrine manner suggest them as potential therapeutic targets. As discussed earlier, functional transfer of miRNAs to date has only been demonstrated for vesicle-encapsulated and HDL-associated miRNAs, and so current therapeutic applications have focused primarily on exploiting these as nucleic acid delivery strategies. In principle, three different possibilities for therapeutic intervention exploiting miRNA transported in EVs can be envisioned.

Firstly, the bioactive cargos of exosomes provide an opportunity for autologous therapeutic intervention that has been especially well-studied in driving tissue regeneration and modulation of the immune system. In the field of regenerative medicine, exosomes derived from mesenchymal stem cells (MCSs) exhibit a beneficial effect not only upon myocardial infarct but also in several other modes of tissue damage such as kidney or cardiac injury (reviewed in [219]). Notably, some of the protective effects were though to be mediated by transfer of both mRNA and miRNAs [220,221]. Furthermore, the immunosuppressive properties of certain EVs could be applied to the treatment of autoimmune diseases [222]. Mittelbrunn *et al.* described the unidirectional transfer of exosomal miRNAs derived from T-cells to antigen-presenting cells (APCs), therefore suggesting that ex-miRNAs contribute to immune modulation [163]. Finally, epithelial PNT-2 prostate cells have been shown to secrete a number of tumor-suppressive miRNAs, including miR-143, thus inhibiting the proliferation of metastatic PC-3M prostate cancer cells [223]. A significant bottleneck in the development of specific cell type-derived vesicles will be to develop large-scale production protocols. One possibility is liquid chromatography-based separation methods which allow for a higher yield of more intact vesicles than UC (discussed in chapter 4) [224].

Secondly, EVs have also been demonstrated to drive a variety of pathological functions such as tumor progression and establishment of a pre-metastatic niche, reviewed in [225,226]. Notably, Skog *et al.* reported stimulation of tumor growth and angiogenesis mediated by the transfer of mRNA and miRNAs via glioblastoma derived exosomes [217]. In addition, tumor-associated macrophages secrete exosomes enriched with miRNAs, especially miR-223, capable of promoting local invasion of breast cancer cells [227]. Beyond tumorigenesis, viral miRNAs were shown to be transferred to uninfected recipient cells upon infection of B cells with Epstein-Barr virus (EBV), thereby promoting viral pathogenesis and latency [191]. In addition, exosomes have been shown to release miRNAs that downregulate oncogenes such as let-7 targeting *RAS* and High-mobility group AT-hook 2 (*HMGA2)* suggesting another mechanism by which cancer cells maintain their tumorigenicity [228,229]. Alternatively, various cancer cells reportedly release miRNAs capable of downregulating tumour suppressor genes in recipient cells (e.g. miR-21 targeting *PTEN* [230]). More recently, ex-miRNAs have been reported to act as agonists of TLR7/8 both in immune and neuronal cells, thus inducing secretion of pro-metastatic inflammatory cytokines or neurodegeneration, respectively [231,232]. Given their pivotal role in disease, inhibition of these pathological EVs comprise a promising platform for therapeutic intervention. Possible approaches to decrease formation, release or uptake of exosomes include targeting Rab27a, components of the ESCRT pathway or nSMase2 via shRNAs or small molecule inhibitors (reviewed in [162,218]). The plethora of strategies to decrease the serum concentration of EVs in various diseases promises to have a large impact on future clinical studies, although it should be emphasised that risks of undesirable off-target effects must be carefully investigated. One attractive alternative is the removal of pathogenic EVs from blood using a combination of dialysis and subsequent affinity chromatography that captures the EVs based on lectins and antibodies on their surface [233].

Lastly, given the suggested ability of EV-associated miRNAs to participate in long-distance cell-to-cell communication, their potential as drug delivery vehicles is an emerging therapeutic opportunity that has been investigated in a range of studies. The use of EVs as a delivery platform of siRNA/miRNA therapeutics harbours several advantages, such as their resistance to plasma nucleases, low-immunogenicity (if they are derived from autologous cells) and the ability to traverse major biological barriers including the blood brain barrier [234–236]. A landmark study on the transfer of exogenous small RNAs was undertaken in 2007 by Wolfrum *et al.* demonstrating the successful delivery and subsequent target gene silencing mediated by siRNAs packaged into HDL particles *in vivo* [237]. Subsequently, Zhang *et al.* published in 2010 the first report using EVs to shuttle a miR-150 mimetic to recipient endothelial cells [170]. Remarkably, siRNA loaded into exosomes modified for neuron-specific targeting induced strong RNAi effects in the murine brain as reported by the Wood laboratory [234]. In this study exosomes derived from dendritic cells, transfected with a fusion protein consisting of the exosomal membrane protein lysosomal associated membrane protein 2 (LAMP2) and a neuron-specific peptide (rabies virus glycoprotein (RVG)-derived peptide) [234]. The remaining bottlenecks to this novel class of therapeutics are efficient loading of small RNAs into the vesicular carriers, efficacy of *in vivo* delivery and in particular, achieve cell-type or tissue-specific targeting. Strategies to overcome these key challenges are being extensively tested and are reviewed elsewhere [238,239]. In conclusion, modulating levels of EV-associated miRNAs or utilising EVs for delivery of miRNA therapeutics has potential for a variety of pathological conditions and some approaches, in particular for cancer treatment, are advancing towards clinical trials [240].

1.5 Serum biomarkers for DMD

1.5.1 The importance of defining biomarkers and outcome measurements

In recent years, the pace of developing experimental therapies to replace or restore dystrophin by either pharmaceutical drugs or gene therapy has rapidly accelerated. As a result, clinical trials were initiated, before it was completely clear, which parameters should be measured to determine success or failure of the therapeutic interventions. Furthermore, detailed knowledge on the natural history of disease progression and its connection to distinct mutations is limited. In addition, several disease modifier genes have been identified that have been shown to impact DMD severity and thus need to be carefully considered when assigning patients to clinical trial cohorts (reviewed [241]). These difficulties have since then been extensively evaluated and discussed among researchers and clinicians in order to establish functional scales that can describe DMD disease progression (reviewed in [242,243]). The following sections aim to provide an introduction to biomarkers and to provide an overview of current and novel biomarkers for DMD, with a focus on circulating miRNAs and protein biomarkers.

By definition, a biomarker is a "characteristic that is objectively measured and evaluated as an indicator of normal biological processes, pathogenic processes or pharmacological responses to a therapeutic intervention" [244]. This definition includes various types of biomarkers such as diagnostic biomarkers (identification of disease or classification of the disease stage), prognostic biomarkers (indicator of disease progression) and therapeutic monitoring biomarkers (allows for the monitoring and prediction of clinical responses to therapeutic interventions) [244].

Clinical outcomes are characteristics or variables that reflect the effect of a therapeutic intervention on the patients, and are utilised in clinical trials to assess the benefit and risk of experimental therapies. Establishing disease-appropriate endpoints has been a challenge for clinical trials in DMD and for neuromuscular diseases in general. A particular difficulty has been the identification of

specific and sensitive endpoints for trials conducted over short periods of time in small patient cohorts. Consequently, the use of biomarkers as surrogate endpoints in DMD clinical trials has been extensively discussed [245]. A surrogate endpoint is intended to substitute for a clinical endpoint and to predict clinical benefits based on epidemiologic, therapeutic, pathophysiologic, or other scientific evidence [244]. Notably, only very few biomarkers have the potential to constitute surrogate biomarkers and to date, there are no surrogate biomarkers for DMD, although the dystrophin protein itself has been discussed as a putative candidate (section 1.5.2).

An ideal biomarker or a panel of biomarkers for a given disease such as DMD should fulfil the following criteria: (a) be easily and repeatedly measureable while being minimally or non-invasive for the patient, (b) be able to diagnose the disease, (c) act as a pharmacodymanic marker to monitor safety and efficacy of the treatment, and (d) predict clinical benefit (surrogate biomarker) [246]. Additionally, biomarkers may provide further insight into DMD pathophysiology and thereby highlight new possibilities for therapeutic interventions.

1.5.2 Challenges of current clinical outcomes and biomarkers

Currently, the most accepted outcome measure used in DMD clinical trials is the 6 minute walk test (6MWT), in addition to measuring serum CK levels (discussed in section 1.5.3). The 6MWT assesses the distance a patient can cover in 6 minutes. More recently developed tests either quantify muscle strength directly or measure the muscle functions based on a number of physical exercises and observational tests (referred to as North Star Ambulatory assessment (NSAA) [247]). All of these tests have the disadvantages that they i) are subjected to high inter-patient variability, ii) are dependent on the compliance of the patients and iii) can only be assessed in ambulant patients. As a result, patients of a certain age group and those with the most severe disease manifestations are often excluded from trial testing. Furthermore, observing clinical benefit in a physical test might only be possible after prolonged treatment, thus requiring expensive and long-lasting clinical trials. It is further necessary to consider the natural disease history when evaluating these outcome measures.

In addition, there is a lack of consensus regarding what is a clinical meaningful improvement for these tests. In the case of the 6MWT, an improvement of 20-30 m compared to the placebo group or natural history disease progression data, has been suggested as the clinical range to manifest a therapeutic benefit of an experimental therapy in a trial lasting for 12 months [248].

Furthermore, Magnetic Resonance Imaging (MRI), T2 mapping and forced vital capacity (FCV) are alternative, non-invasive methods of monitoring pathology in DMD since they reveal the extent of muscle degeneration (e.g. muscle wasting, deposition of adipose tissue, fibrosis, assessment of cardiac function) [249], although these methods do not provide a direct read-out of muscle function *per se*. Additionally, this approach is subject to a number of limitations such as high cost, low throughput and a requirement for specialist personnel trained in interpreting the MRI data. These technologies are therefore less suitable for use in trials with large patient cohorts.

An obvious pharmacodynamic biomarker for experimental therapies that restore dystrophin is the dystrophin protein itself. Undoubtedly, measuring dystrophin expression is an essential factor in assessing drug efficacy. Nevertheless, accurately quantifying dystrophin with semi-quantitative methodologies such as Western blot or immunohistochemistry (IHC) analysis of muscle biopsies is associated with multiple difficulties (reviewed in [62,250]). To this end, some confusion was caused by the amount of dystrophin positive fibres reported in an earlier phase 1-2a Drisapersen trial as determined by IHC analysis. Variability in antibody affinity and highly unequal distribution of dystrophin positive and revertant fibres underline the importance of quantifying dystrophin by multiple approaches [251]. In the future, an alternative method for quantifying dystrophin in muscle biopsies in a more precise and reproducible manner may be by mass spectrometry, as developed Hathout by *et al.* [252]. However, a group of experts recently highlighted why dystrophin should not be used as surrogate endpoint biomarker at the present time [245]. They argued that restoring dystrophin cannot revert pathophysiological changes such as advanced fibrosis, and therefore in patients with advanced pathology, restoring dystrophin may not result in a therapeutic benefit.

Secondly, the link between absolute dystrophin levels and clinical outcomes like the 6MWT remains unclear [245]. To this end, initial efforts have been made in the *mdx* mice to relate dystrophin levels to improvements in muscle functions. A recent study revealed that restoration of 15% of wild-type dystrophin is sufficient to significantly increase muscle force and to protect against muscle injury caused eccentric contraction [253].

Recently, a number of studies have performed high-throughput ('omics' approaches) to profile differentially abundant proteins/peptides, nucleic acids, metabolites and lipids in skeletal and cardiac muscle in DMD patients and animal models (reviewed in [254]). These studies have provided new insights into disease mechanisms and identified a number of novel therapeutic targets or pathways driving DMD pathology, which could potentially be modulated by therapy. However, with respect to biomarkers, the usefulness of muscle biopsies is conceptually limited, given that only a tiny fraction of a single muscle is assayed, thus making the results highly variable and dependent on the region sampled by the biopsy. Muscle biopsy is also highly invasive and painful for patients, meaning that serial measurements are not ethically permissible or practical. Despite the imposed burden on the patients, biopsies are currently taken in most clinical trials [250], thus underlining the urgent need for less invasive biomarkers [245]. To this end, analysis of biomarkers in body fluids is minimally invasive or non-invasive and therefore allows for repeated sampling to assess drug efficacy throughout the course of a trial. As such, sampling serum or plasma has frequently been the first line of clinical investigation as it is simple, safe and provides insight into the physiology of the entire body. More recently, the proteome of urine samples from DMD patients has been profiled and titin was identified as the first prospective urinary DMD biomarker [255]. The following sections focus on two possible sources of biomarkers for DMD in blood: extracellular miRNAs (section 1.5.3) and circulating proteins (section 1.5.4). Additional classes of circulating biomarker include metabolic and lipid biomarkers (reviewed in [243]).

1.5.3 Extracellular microRNAs as biomarkers for DMD

As outlined in section 1.4, ex-miRNAs are promising biomarkers for numerous pathologies including muscular dystrophies. For DMD in particular, Caccheriarelli *et al.* in 2011 described elevated levels of the myomiRs miR-1, miR-133 and miR-206 in serum of 10 DMD patients and in *mdx* mice [256]. Interestingly, myomiR levels in BMD patients were only moderately elevated, suggesting a correlation between ex-myomiR levels and disease severity. Furthermore, ex-myomiR levels were reduced in *mdx* mice that were subjected to a virus-mediated exon skipping strategy [256]. Shortly after, these myomiRs were additionally shown to be elevated in $CXMD_J$ dogs [150]. Following on from these two discovery-targeted approaches, more systematic approaches have been performed that identified multiple other dysregulated miRNAs ([138,207,257], summarised in Table 1.3).

Importantly, a number of these studies have investigated the utility of these and additional ex-miRNAs (i.e. miR-31) as DMD biomarkers to monitor disease progression and response to exon skipping both in animal models and in human patients [138,207,214,256]. Whereas exon skipping therapy in mice restored serum myomiR levels towards wild-type levels, only a trend towards reducing ex-miRNA levels could be observed in 12 DMD patients treated with Eteplirsen [214]. However, this may be due to insufficient drug efficacy at the applied treatment regimen, or the relatively small sample size. To this end, it is noteworthy, that in all listed studies, in animal models and even more so in patients, ex-miRNA levels varied considerably. Consequently, in DMD patients, detecting changes in serum myomiR abundance following treatment with only minimal restoration of dystrophin protein might prove to be challenging.

With respect to monitoring disease progression, a study undertaken by Zaharieva *et al*. measured serum levels of miR-1, miR-133, miR-206 and miR-31 in a larger DMD cohort (44 patients), in order to determine if there was a correlation between miRNA levels and metrics of muscle function (i.e. lung function, NSAA score, ambulant status [214]). In contrast to the study by Cacchirelli *et al.*, the authors overall determined a negative correlation between serum myomiR levels and DMD disease

severity and patient age. Consequently, the authors hypothesised that ex-myomiRs may be utilised as biomarkers to assess the remaining muscle mass at least in patients older than 10 years [214]. This finding is reminiscent of the decreased abundance of serum CK in older DMD patients which likewise has been attributed to advanced muscle loss (further discussed in section 1.5.4). Notably, if this finding would be confirmed in larger follow-up studies, it would have important implications for the utility of serum miRNA biomarkers in patients with advanced pathology. Possible reasons for these conflicting findings may be the different age ranges in patient cohorts and as mentioned above, and the small number of patients included in the study by Cacchirelli *et al.* [214,256].

Despite some of these discrepancies, it is encouraging that miR-1, miR-133a and miR-206 are found to be consistently elevated across animal models and DMD patients. These myomiRs were also classified firstly as 'dystromiRs', underlining their differential expression in dystrophic pathology. To this end, it is important to note that some, or all, of these myomiRs are also elevated in serum of patients with a number of other muscular dystrophies (i.e. in various subtypes of LGMD and MD) [257,258]). These similarities indicate that an increase in serum abundance of these miRNAs is associated with the pathological changes occurring during muscle wasting in general. As a result, this set of miRNAs is unlikely to be suitable to effectively distinguish between specific muscular dystrophies with similar severity of muscle wasting. In contrast, it was shown that in muscular dystrophies with milder levels of muscle regeneration and degeneration, including Emery-Dreifuss muscular dystrophy (EDMD) and Ullrich congenital muscular dystrophy (UCMD), neither miR-1, miR-133 or miR-206 were found to be upregulated [214,257].

A further study utilising high-throughput ex-miRNA sequencing identified altered levels of miR-208a, miR-208b, miR-499 in serum of the GRMD dog and DMD patients [259]. The authors argue that elevation of these cardiac-enriched miRNAs may be attributed to the underlying cardiac pathology in DMD, although no correlation was found between the levels of these serum miRNAs and classical biomarkers of cardiac damage or cardiac functional parameters [259]. In parallel, another study by Li

et al. measured the serum levels of miR-1, miR-133a, miR-206, miR-208a, miR-208b and miR-499 in sera derived from DMD and BMD patients in relation to muscle fibre type composition [260]. Notably, the authors found that in patients aged 2-6, serum abundance of miR-206, miR-499, and miR-208b are positively correlated with age and type IIc fibres. In contrast, in patients older than 6 years, miR-499, and miR-208b are positively correlated with slow-twitch muscle fibres (type I) and negatively correlated with fast-twitch (type IIa and IIb). The authors further hypothesised that given their enrichment in slow-twitch myofibres, these serum miRNAs may be indicative of the remaining muscle mass in advanced DMD pathology [260].

Lastly, it is important to note, that multiple studies observed an asymmetry in the abundance of serum miRNA levels compared to their expression in tissue. The expression of miR-1 and miR-133 is decreased in skeletal muscle but increased in serum, whereas the opposite has been reported for miR-31 [138]. Furthermore, miR-206 levels are moderately elevated in muscle, possibly due to the increased presence of regenerating fibres [124], and very strongly elevated in serum [138]. Consequently, a number of groups have suggested that passive release from damaged and necrotic myofibres cannot account alone for the observed changes in ex-miRNA levels and hypothesised that individual miRNAs may be selectively secreted [207,214,260]. The investigation of this phenomenon is one of the main aims in this thesis.

Category	miRNA	Serum	Muscle	Pathological indications
miRNAs involved in myogenesis	miR-1	↑↑	↓	Damaged myofibres Muscle regeneration
	miR-133a/b	↑↑	↓	
	miR-206	↑↑	↑	
	miR-378/378*	↑	↑↓	
	miR-208a/b	(↑)	NS	Cardiac pathology? Muscle fibre type shift
	miR-499	(↑)	↓	
miRNAs related to tissue fibrosis and inflammation	miR-21	(↑)	↑	Muscle fibrosis
	miR-29c	↓	↑	Muscle fibrosis
	miR-31/31*	↑↓	↑↑	MPC proliferation
	miR-142	↑	↑	Inflammatory infiltration
	miR-223	NS	↑	Inflammatory infiltration
Others	miR-22	↑	NS	Unknown
	miR-30a	↑	↓	
	miR-122	↓	NS	
	miR-149-	↑	NS	
	miR-193b	↑	↓	
	miR-378	↑	↓	

Table 1.3 Overview of differentially abundant miRNAs in sera of DMD patients and animals models.

Findings summarised from [214,138,207,256,259,257,260] ↑↑ strongly elevated, ↑ elevated, (↑) elevation inconsistent across animal models and patients, ↑↓ conflicting finding, ↓ reduced abundance, NS unchanged. MPC: myogenic progenitor cells.

1.5.4 Serum protein biomarkers for DMD

The main advantage of circulating protein-based biomarkers is that once they are identified, they can typically be quantified by clinical biochemistry assays which are technical facile, can easily be incorporated into existing work-flows, and allows for rapid screening of large sample sizes. Traditionally, the metabolic enzyme creatine kinase (CK) and to a lesser extent also the pyruvate kinase have been used in as diagnostic biomarkers for neuromuscular disorders, and DMD in particular [261]. CK is a useful marker to screen for dystrophinopathy as it can be quantified conveniently and rapidly by enzymatic assays [262]. However, CK can vary substantially between individuals and is further influenced by age, races, pharmacological factors (e.g. statin use) and physical exercise. Furthermore, CK is a general marker of tissue pathology and not specific to muscle damage. As a result, CK is elevated in other medical conditions such as myocardial infarct and cerebral diseases as well as under stress conditions such as exercise [263,264]. Importantly, serum CK measurements do not always correlate with other read-outs of muscle function, such as MRI [265]. Furthermore, it has been shown that CK decreases with age in DMD patients in the natural history of DMD disease progression and also in most DMD animal models [255,266]. This observation is generally believed to be related to advanced muscle loss and inactivity due to loss of ambulance [267]. To date it remains unclear how exactly CK is released from dystrophic muscle. Historically, it was proposed that impairment of sarcolemma integrity due to the absence of the DGC (section 1.2) is the primary reason for passive release of CK (and other muscle derived molecules such as miRNAs) into the circulation. However, recently there has been some evidence that more complex mechanisms such as aberrant secretion from muscle tissues may contribute to the increased levels of muscle-derived proteins and nucleic acids [268].

Due to these limitations, CK is likely to be of only limited value for monitoring disease progression and the effectiveness of experimental therapies over longer periods of time. However, some utility of CK as secondary endpoint has been shown in the latest phase 3 drisapersen trial where a significant

decrease in CK levels was measured after 48 weeks of treatment, although the two preceding drisapersen trials did not show such an effect [245].

More recently, various other proteins were identified as differentially abundant in the sera of DMD patients and dystrophic animal models in a number of either proteomic profiling or targeted discovery studies (findings summarised in Table 5.3). Identified candidates mainly originated from muscle and included myofibrillar proteins (titin (TTN), myosin light chain (MYL) 1/3, myomesin 3 (MYOM3), filamin-C (FLNC)), metabolic enzymes (carbonic anhydrase III (CA3), lactate dehydrogenase B (LDHB), aldolase (ALDOA), phosphoglycerate mutase 2 (PGAM2), beta enolase 3 (ENO3), and glycogen phosphorylase (PYGM)), transport proteins (fatty acid binding protein-3 (FABP3), myoglobin (MB) and somatic cytochrome-C (CYCS)), extracellular matrix remodelling proteins (metalloproteinase-9 (MMP9), tissue inhibitors of metalloproteinase-1 (TIMP1), osteopontin (OPN)) and others (coagulation factor VIII (F13A1), malate dehydrogenase cytosolic (MDH1) and fibrinogen gamma(FGG)) [266,269–273].

These newly identified putative biomarkers need to be further assessed in longitudinal studies and most importantly linked to clinical outcome and patient benefit (discussed in 6.3). Notably, studying the serum proteome is still a major analytical challenge owing to the high complexity of this biofluid and the presence of a few highly abundant proteins that frequently mask the signal of the lower abundant proteins in profiling approaches utilising mass spectrometry. In this thesis, an aptamer-based approach was undertaken to identify differentially abundant circulating proteins in *mdx* mice sera that were restored towards wild-type levels after exon skipping therapy (chapter 5).

1.6 Thesis aims and hypotheses

This thesis addresses the following hypotheses and aims:

1.) I hypothesise that ex-myomiRs are released during periods of myogenic differentiation and thus, their release can be considered to be independent of dystrophic pathology in some contexts. Furthermore, I postulate that in dystrophic muscle disease, the abundance of circulating myomiRs is a complex function modulated by tissue expression levels, muscle regeneration, muscle fibre death, overall muscle mass as well as the stability of the individual miRNAs in the extracellular space. A further aim is to establish cell culture models suitable for the investigation of myomiR release *in vitro*.

2.) Based on previous findings of our group, I propose that ex-myomiRs are released by a common mechanism and that they are stabilised by similar miRNA carriers. To this end, an important aim is to establish an efficient methodology to reliably, separate vesicular and non-vesicular miRNA carriers in complex biofluids. Such methodology would additionally allow the characterisation of changes in vesicle secretion associated with dystrophic pathology, an as yet underappreciated area of DMD research.

3.) Utilising a novel approach for proteomic profiling of serum samples, my final aim is to identify therapy-responsive serum protein biomarkers in a mouse model of DMD.

2. General Materials and Methods

2.1 Animal Studies

Wild-type mice (C57/BL10, abbreviated in this work as C57) were obtained from Harlan Laboratories (Bicester, UK) and dystrophic C57/BL10ScSn-*Dmd*^{mdx}/J (*mdx*) mice from Jackson Laboratories. Animals were housed in the Biomedical Services Building, University of Oxford, and all experimental procedures were authorised and approved by the University of Oxford ethics committee and UK Home Office (project licence 30/2907) in accordance with the Animals (Scientific Procedures) Act 1986. All animals utilised in this study were male. For mice older than two weeks, mice were sacrificed by escalating CO_2 concentration and blood harvested from the jugular vein using Microvette CB300 serum collection tubes (Sarstedt, Leicester, UK). Whole blood was allowed to clot at room temperature for 30 minutes and then centrifuged at 10,000 *g* for 5 minutes. If tissue samples were required, these were removed after exsanguination, and snap-frozen in isopentane (pre-chilled on dry ice). Where tissue sectioning was necessary, dissected tissues were mounted on cork discs utilising optimal cutting compound (OCT) as a mounting matrix.

In order to restore dystrophin protein expression via exon skipping therapy (chapters 4 and 5), 12 week old male *mdx* mice were injected with a single dose of 12.5 mg/kg Pip6a-PMO (peptide-phosphorodiamidate morpholino oligonucleotide (PPMO)) conjugate (prepared in a sterile saline solution) via the tail vein. Pip6a-PMO consists of a PMO (5'-GGCCAAACCTCGGCTTACCTGAAAT) moiety chemically conjugated to an arginine-rich cell-penetrating peptide (Ac-RXRRBRRXR YQFLI RXRBRXRB-OH, where X is aminohexanoyl and B is β-alanine) and was synthesised and administered to the mice as described previously [274]. In short, the peptide was synthesised by standard Fmoc chemistry, purified by reverse-phase HPLC and conjugated to the 3' end of the PMO through an amide linage. Subsequently, the conjugate was purified by cation exchange HPLC, desalted and analysed by mass spectrometry. All animals were sacrificed two weeks post injection at 14 weeks of age.

2.2 RT-qPCR for mRNA quantification

RNA was extracted from cells or tissue cryo-sections by guanidinium thiocyantate-acid-phenol-chloroform extraction using TRIzol Reagent (Life Technologies, Paisley, UK) as per manufacturer's instructions. In the case of tissues, a Precellys tissue lyser (Bertin Technologies, Paris, France) was utilised to homogenize the samples prior to extraction. Following isopropanol precipitation, RNA pellets were re-suspended in a suitable amount of nuclease-free water (30-50 µl) (Life Technologies). Next, samples were quantified and purity-assed using a NanoDrop ND 1,000 spectrophotometer (Thermo Scientific, Loughborough, UK). Protein and phenol contamination of the sample can be assessed by the $\frac{A_{260}}{A_{280}}$ ratio since Tyrosine and Tryptophan absorb at 280 nm and phenol at 270 nm. This ratio is expected to be ~2 for pure RNA. Salt and organic contaminations are reflected in the $\frac{A_{260}}{A_{230}}$ ratio which is expected to be >1.8 for pure RNA. Samples that substantially failed to meet these criteria were re-extracted as described above.

500 ng - 1 µg of RNA was reverse transcribed using the High Capacity cDNA Kit (Life Technologies) according to manufacturer's instructions. The cDNA template was amplified on a StepOne Plus real-time PCR Thermocycler (Life Technologies) using TaqMan Gene Expression Master Mix (Life Technologies) and universal cycling conditions (95°C for 10 minutes (hotstart) and then 40 cycles of 95°C for 15 seconds, 60°C for 1 minute). Primer and probes used for qPCR were obtained from IDT or Life Technologies and sequences/assay IDs are listed in Table 2.1. Data were analysed using the StepOne Software v2.1 (Applied Biosystems). Individual transcripts were quantified using the relative standard curve method or Pfaffl method [275], and gene-of-interest expression was normalised to the expression of TATA Box Binding Protein *(Tbp)*. Tbp has been shown to be stably expressed in muscle even during muscular atrophy [276], and was therefore chosen as suitable reference (housekeeping) gene for this study. All Reverse Transcriptase quantitative Polymerase Chain Reaction (RT-qPCR) studies (mRNA and miRNA quantification) were designed to comply with the MIQE guidelines where possible.

ID	Sequence
Mmu_Myod1-FWD	GAC ACA GCC GCA CTC TT
Mmu_ Myod1-REV	GCT CTG ATG GCA TGA TGG AT
Mmu_ Myod1-PROBE	/56-FAM/ACG ACA CCG /ZEN/CCT ACT ACA GTG AGG /3IABkFQ/
Mmu_Myog-FWD	CGC GAG CAA ATG ATC TCC T
Mmu_ Myog-REV	CGA TCT CCG CTA CAG AGG
Mmu_ Myog-PROBE	/56-FAM/CCA GTG AAT /ZEN/GCA ACT CCC ACA GC/3IABkFQ/
Mmu_Tbp-FWD	AAG AAA GGG AGA ATC ATG GAC C
Mmu_ Tbp-REV	GAG TAA GTC CTG TGC CGT AAG
Mmu_ Tbp-PROBE	/56-FAM/CCT GAG CAT /ZEN/AAG GTG GAA GGC TGT T/3IABkFQ/
Hs_MYOD1-FWD	TGC TGG ACA GGC AGT CTA
Hs_MYOD1 -REV	CTC CGA CGG CAT GAT GG
Hs_MYOD1-PROBE	/56-FAM/TCG ACA CCG /ZEN/CCG CAC TCT TC/3IABkFQ/
Hs_MYOG-FWD	AGA AGT AGT GGC ATC TGT GG
Hs_MYOG-REV	GAC AGC ATC ACA GTG GAA GA
Hs_MYOG-PROBE	/56-FAM/ATG CCC GGC /ZEN/TTG GAA GAC AAT CT/3IABkFQ/
Hs_ BACT	Assay ID: Hs01060665_g1
Mmu-Pax7-FWD	GAA GAA GTC CCA GCA CAG C
Mmu-Pax7-REV	GCT ACC AGT ACA GCC AGT ATG
Mmu-Pax7-PROBE	/56-FAM/CCAAAAACG/ZEN/TGAGCCTGTCCACAC/3IABkFQ/
Mmu-Myh3-FWD	GAT CCT CTC CTT TTC CGA CTT G
Mmu-Myh3-REV	TCT GTC ACA GTC AGA GGT GT
Mmu-Myh3-PROBE	/56-FAM/ATGGAAGTG/ZEN/TTTGGCATAGCTGCAC/3IABkFQ/

Table 2.1 List of RT-qPCR primers used for mRNA expression analysis in this study.

2.3 microRNA analysis

The methods applied in this thesis for detection and quantification of ex-miRNAs in murine biofluids are described in detail in two publications from the Wood group [211,277]. In brief, RNA was extracted with TRIzol LS (for biofluid samples) or TRIzol reagent (for cell or tissue samples) (both Life Technologies) as per manufacturer's instructions. Aliquoted serum was stored at -80°C prior to analysis, as it has been shown that miRNAs are stable for at least 12 month under these conditions [278]. Furthermore, for serum samples, the volume used for extraction was kept constant within each study (10 µl for serial measurements in longitudinal animal studies, 25-50 µl for end point measurements). Similarly, when conditioned media was analysed, equal volumes (typically 300 µl) of cell culture supernatant were used for RNA isolation.

To monitor variation in extraction efficiencies for biofluid samples, 3 µl of a 5 µM synthetic miRNA oligonucleotide, cel-miR-39 (5'-UCACCGGGUGUAAAUCAGCUUG) (IDT, Leuven, Belgium), was added to each sample at the phenol extraction stage. During the isopropanol precipitation stage, RNase-free glycogen (Roche) was used as carrier to improve extraction efficiency. RNA was typically re-dissolved in 30 µl of nuclease-free water (Life Technologies). For miRNA quantification, either 5 µl of the RNA extracted from serum or culture media (or 10 ng of RNA if extracted from cells/tissue) was reversed transcribed using the MicroRNA Reverse Transcription Kit (Life Technologies) according to the manufacturer's instructions. Small RNA TaqMan assays (Life Technologies) employ miRNA-specific hairpin RT primer which hybridise to the 3' terminus of the miRNA (Figure 2.1). Once cDNA synthesis is accomplished, the resulting fragment is of sufficient length to be amplified by qPCR with a universal reverse primer and miRNA-specific probe and forward primer. In this study, qPCR was performed on a Step-One Plus Real-Time PCR instrument using the TaqMan Gene Expression Master Mix (all Life Technologies) according to the manufacturer's instructions. All small RNA assays used with exception of cel-miR-39 (no mammalian homologue) detect both the human and mouse miRNA sequences (assay IDs are listed in Table 2.2).

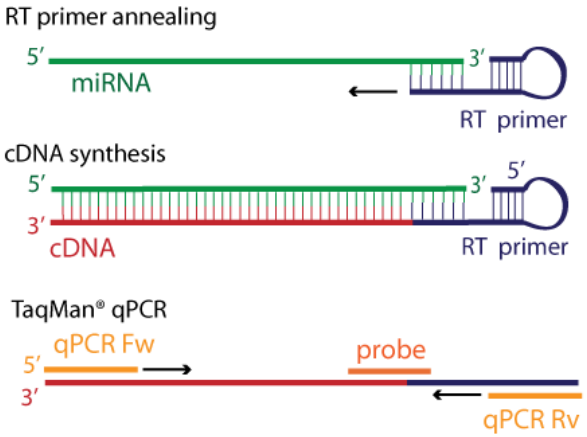

Figure 2.1 **Detection strategy of miRNA by small RNA TaqMan assays (Life Technologies).**

miRNA	Assay ID
miR-1	002222
miR-133a	002246
miR-206	000510
miR-16	000391
miR-31	000185
miR-223	002295
let-7a	000377
cel-miR-39	000200

Table 2.2 **List of small RNA RT-qPCR assays used in this study.**

For absolute quantification, sample miRNA quantities were compared to a 10 fold dilution series of synthetic miRNA oligonucleotides (IDT) spiked-in at the RT stage. Typical standard curves for all miRNAs are shown in Figure 2.2. Importantly, this technique enables the comparison of measurements between experiments, and also allows for direct comparison of miRNA copies between different miRNA assays. Where appropriate, relative quantification was performed using the Pfaffl equation (imputing PCR efficiency values determined empirically by amplification curve analysis using LinRegPCR) [275,279].

Suitable strategies to accurately quantify miRNAs in biofluids were discussed by the Wood group previously [211] and determined normalisation to an external spike-in control such as cel-miR-39 as

most reliable method. As a consequence, this method was chosen for normalisation of all biofluid samples analysed in this work [211].

In accordance with the MIQE guidelines, the limit of quantification (LOQ) in this study was defined as the highest value of the 10 fold dilution series (i.e. synthetic RNA standard curve) that was found not to be co-linear with the higher concentration standards [280]. For all miRNAs used the LOQ was determined at 1,5 copies/µl since at this dilution the standard curves reached a plateau and therefore accurate quantification became impossible (data not shown). Note that the LOQ is not equivalent to the limit of detection which typically has a higher cycle threshold value but falls outside the linear range of the assay.

To obtain serum miRNA concentrations (copy numbers per millilitre), the ratio of input volume used for extraction and RNA resuspension volume was calculated, and measured miRNA copy numbers scaled accordingly. Tissue sample quantities were normalised to miR-16 expression, as this miRNA has been shown to be relatively stable expressed [281], and was previously used as reference miRNA by the Wood group [138], and other groups [282,283].

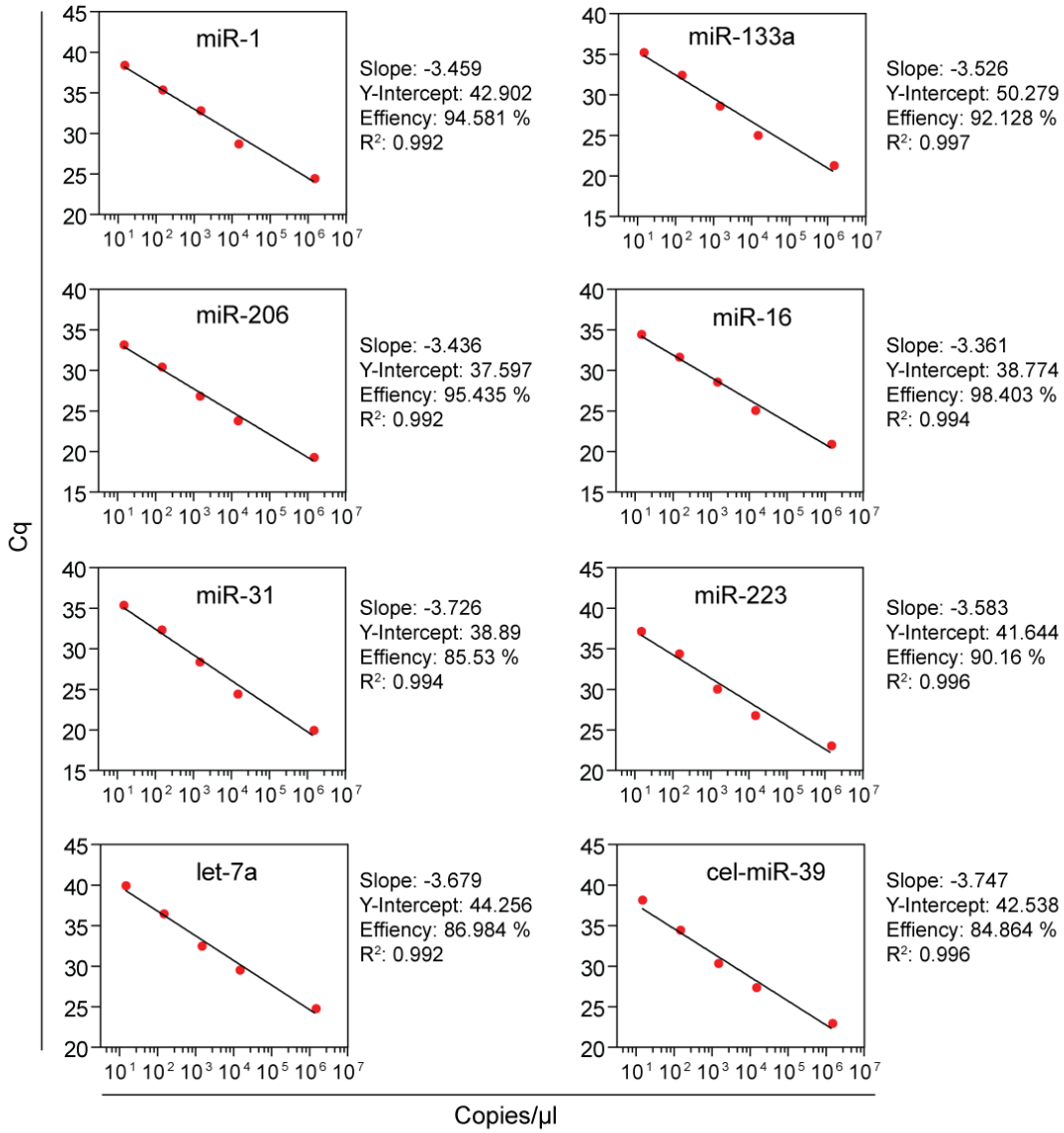

Figure 2.2 **Standard curves of synthetic RNA molecules used for absolute quantification of miRNA abundance by small RNA RT-qPCR.**

2.4 Maintenance and differentiation of muscle cells

C2C12 cells are a murine myoblast cell line originally generated from a thigh muscle of a C3H mouse after crush injury The cells were maintained in growth media; Dulbecco's Modified Eagle's Media (DMEM) supplemented with 10% fetal bovine serum (FBS) and 1% antibiotics/antimycotics (all Life Technologies) and cultured at 37˚C with 5% CO_2. C2C12 myoblasts were differentiated in DMEM containing 2% horse serum (HS) for 4-9 days to form multinucleated myotubes. Human primary myoblasts (a kind gift from Helene Fischer (Karolinska Institutet, Stockholm, Sweden)) were obtained from a healthy, 25 year old, Caucasian male donor with good physical fitness. Cells were cultured in DMEM-F12 (20% FBS, 1% antibiotics/antimycotics) until ~80% confluent. For induction of differentiation, serum concentrations were initially lowered to 2% HS and then increased after 3 days to 5% HS).

2.5 Isolation of extracellular vesicles

Extracellular vesicles (EVs) were isolated as outlined in Figure 2.3, either by ultracentrifugation (UC) or by a combinatorial approach of ultrafiltration and size-exclusion chromatography (UF-SEC) as further described in chapter 4. In both cases, if EVs were isolated from conditioned media, cells were cultured in pre-spun media which contains serum that has been pre-cleared of serum EVs (spun at 120,000 *g* for 70 minutes).

The workflow for EV isolation by UC was based on the protocol first reported by Théry e*t al*. in 2006 [284], with slight alterations as the protocol has been further optimised by members of the Wood group (300 *g* spin was omitted and 10,000 *g* spin replaced by filtering with 0.22 μm filters). These changes reduce hands-on time and were found not to influence quantity and quality of EVs purified [224]). In short, conditioned media was spun at 2,000 *g* for 10 minutes at 4˚C and filtered (0.22 μm). Subsequently, two steps of ultracentrifugation were performed (120,000 *g* for 70 minutes each) and pellets were washed with phosphate-buffered saline (PBS) between the two spins to minimise protein contamination. EV-pellets were re-suspended in a final volume of 50 μl in PBS. Isolated EVs were subsequently subjected to downstream analysis for characterisation as required (Figure 2.3)

In order to isolate EVs by UF-SEC, conditioned media or serum was spun at 2,000 *g* for 10 minutes at 4˚C and filtered (0.22 μm). The maximum injection volume for SEC is ~4 ml, therefore conditioned media was concentrated via ultrafiltration to ~3 ml utilising a 10 kDa cut-off Amicon Ultra-15 spin filter (EMD Millipore, Watford, UK) at 3,500 *g* for 15 minutes. In the case of serum, where a much lower input volume was typically used (150-1,000 μl), the sample volume was adjusted to 3 ml with sterile PBS prior to the 2,000 *g* spin. Next, the 0.22 μm filtrate was loaded onto a HiPrep 16/60 Sephacryl S-400 (GE Healthcare, Pollards Wood, UK) connected to an ÄKTA prime (GE Healthcare) equipped with a ultraviolet (UV) flow cell. After sample injection, separation was achieved by running 1.5 column volumes of PBS (180 ml) at a flow rate of 0.5 ml/min and collecting fixed volume fractions (2 ml). The temperature was kept at 4˚C. Based on UV 280 nm absorbance values (indicative of

protein content), the collected eluates were grouped into 4-6 new fractions. These fractions were pooled and re-concentrated via ultrafiltration using again 10 kDa cut-off filters to a final volume of ~200 µl and further analysed as outlined in Figure 2.3.

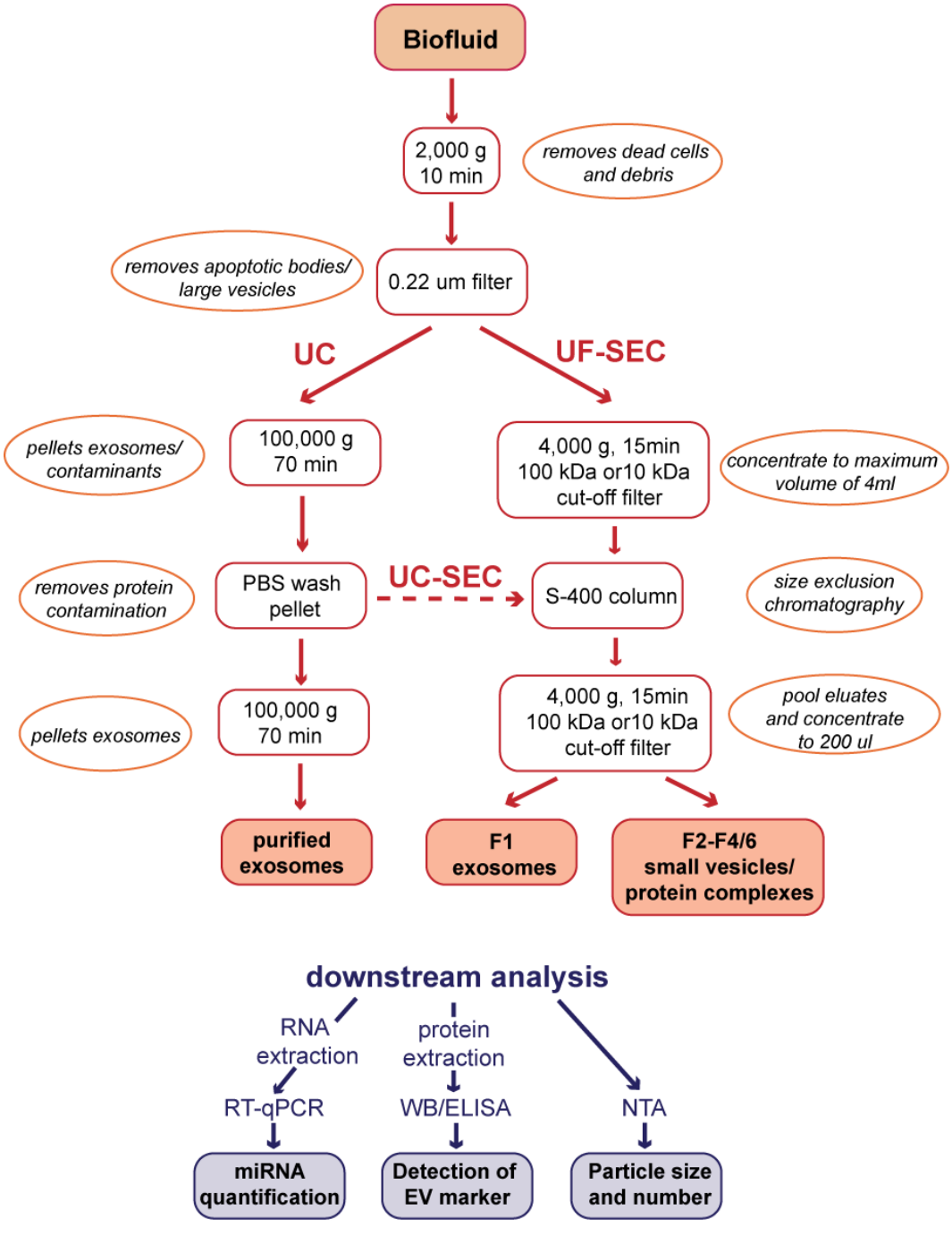

Figure 2.3 **Schematic outline of extracellular vesicle isolation and characterisation strategies.**

2.6 Characterisation of extracellular vesicles

2.6.1 Western blot

Western blotting for exosomal markers was performed on equal volumes of each sample (15 µl). First, samples were diluted 1:1 with 2x Laemmli sample buffer (Bio-Rad, Hemel Hempstead, UK) containing 5% β-mercaptoethanol (Sigma) and heated at 100°C for 10 minutes. Next, samples were then loaded in a 1.5 mm, 10% Tris/Glycine SDS-polyacrylamide gel and electrophoresis was performed at 170 V for 60-70 minutes in running buffer. Subsequently, proteins were transferred from the gel onto to a polyvinylidene fluoride (PVDF) membrane (Merck Millipore) via electroblotting at 100 V for 60-70 minutes in transfer buffer containing 20% methanol. To prevent non-specific antibody binding, membranes were then incubated in blocking buffer (5% fat-free milk in Tris buffered saline with 0.1% Tween-20 (TBS-T)) for 60 minutes at room temperature with gentle shaking. The membrane was then probed either overnight at 4°C or for 2 hours at room temperature (as required) with the following primary antibodies; anti-CD9 (ab92726), anti-PDC6I (ALIX) (ab117600) and anti-TSG101 (ab30871); all at 1:1,000 dilution (all Abcam). After three 10 minutes washing steps with TBST-T, the membrane was incubated for 1 hour at room temperature with secondary antibodies conjugated to infrared dyes (anti-mouse IgG IRDye800 (926-32210) for detection of ALIX (1:10,000); anti-rabbit IgG 680RD (926-68071) for detection of CD9 and TSG101 (1:10,000)) (all LI-COR, Cambridge, UK). Lastly, the membrane was washed again and visualised by scanning both 700 nm and 800 nm channels on the LI-COR Odyssey CLx infrared imaging system (LI-COR).

2.6.2 Enzyme-linked immunosorbent assay (ELISA)

CD63 ELISA (ABIN1572929, Antibodies Online, Aachen, Germany) was performed according to manufacturer's instructions. Each fraction was diluted to fall within the linear range of the assay. Sample concentrations were extrapolated with GraphPad Prism 5 (GraphPad Software Inc, La Jolla,

CA) using fourth-order polynomial data fit of the standard curves. CD63 quantities were normalised to total protein amounts as determined by micro BCA assay (Thermo Fisher Scientific).

2.6.3 Nanoparticle tracking analysis (NTA)

NTA was performed to determine particle count and size using a NanoSight NS500 instrument (Malvern Instruments Ltd, Worchestershire, UK) equipped with the NTA 2.3 analytical software. Samples were diluted in PBS to achieve a particle count of between 2 x 10^8 and 2 x 10^9 per ml (typically 1:500 to 1:10,000). For all recordings, a camera level of 13 or 15, and the automatic function was used for all post-acquisition settings: blur and minimum expected particle size, except in the case for detection threshold (where it was fixed it at a value of 5). Three 30 second videos for each sample were recorded using the script control function and measurements were then analysed using the batch process facility.

2.7 Statistical Analysis

Statistical analyses were carried out using GraphPad Prism 5. Comparisons between two groups were tested using a two-sided *t*-test. One-way analysis of variance (ANOVA) and Bonferroni correction *post hoc* test were performed for comparisons of one variable in more than two groups. All other statistical analyses are explained in the relevant chapter.

3. Results I

Characterisation of extracellular myomiRs in the context of dystrophic pathology and normal muscle biology

3.1 Introduction

The biological and clinical relevance of ex-miRNAs and muscle-specific ex-miRNAs (ex-myomiRs) in particular, is not currently well understood. Consequently, thorough studies addressing the key questions relating to their biology and involvement in regulatory processes such as myogenesis are of high interest. These aspects include ex-myomiR origin, secretion stimuli, release mechanisms, means of transportation/stability in the circulation, and potential communication with recipient cells (or other functions). In this section, some of these questions are addressed in the context of the muscular wasting disease Duchenne Muscular Dystrophy. As described in section 1.5.3, the Wood group [138,285], and others [150,286], have identified a set of miRNAs (miR-1, miR-133 and miR-206), also referred to as myomiRs, that are highly enriched in the circulation of dystrophic animal models (e.g. *mdx* mouse and CXMD$_J$ dog [138,150]) and DMD patients [214], compared to sera from unaffected controls.

Notably, muscle is an attractive model system in which to investigate ex-miRNA biology due to a combination of factors. Firstly, the tissue-specific expression of myomiRs limits their source tissues to cardiac, smooth and skeletal muscle. Notably, miR-206 is specific to skeletal muscle and enriched in regenerating fibres [124], thus, further narrowing its tissue of origin. In addition, myomiRs are not expressed in blood cells, thus measurement of ex-myomiRs is less likely to be influenced by hemolysis which is a common source of variation for the measurement of other circulating miRNAs [287]. Lastly, large changes in abundance are typically observed for ex-myomiRs in dystrophic serum [138], most likely owing to the fact that muscle comprises 40-50% of the body mass. Consequently,

myomiRs are likely to be more easily detected in the circulation compared to tumor-derived miRNAs, especially in the early phases of cancer where the tumor mass is small [288].

Previously, it has been suggested that miRNAs are released during tissue damage, for example, heart specific miRNAs are enriched in circulation after cardiac infarct and similar this has been shown to occur upon liver, muscle and brain injury [151,289]. In contrast, the Wood group [138], and others [260,286] have previously observed an asymmetry in myomiR expression patterns between musculature and the circulation. Despite increased levels in sera of the *mdx* mice compared to wild-type animals, miR-1 and miR-133a were downregulated in tibialis anterior (TA) muscle of *mdx* whereas miR-206 was upregulated in tissue but to a lesser extent than in serum [138]. This asymmetry highlights that the reason for the high abundance of circulating myomiRs cannot be explained by expression changes in muscle tissue alone. Alternatively, gross muscle breakdown and/or passive leakage due to dystrophic pathology-associated membrane defects (absence of DGC) may explain the presence of ex-myomiRs in the circulation. In both cases, elevated levels of ex-myomiRs would arise from passive release as consequence of dystrophic pathology, and the released myomiRs would be likely to be primarily by-products of muscle damage.

In contrast, in this chapter, it was investigated whether myomiRs can be released into the circulation in various physiological contexts including postnatal development, following physical exercise, and during cellular differentiation. Selective myomiR release in the absence of muscle pathology may suggest that their presence in the circulation does indeed serve a biological purpose, for example in controlling muscle homeostasis via cell-to-cell communication. To this end, it is important to note that a study undertaken in the Wood group by Roberts *et al.* showed that the large majority of ex-myomiRs is likely to be outside extracellular vesicles (EVs) [285]. This finding has implications regarding the potential functions of ex-myomiRs in intercellular communication since there is the caveat that functional miRNA transfer has so far only been described for membrane-associated and lipoprotein carriers, but not for miRNA- ribonucleoproteins (RNP) complexes (section 1.4).

In general, miRNAs-RNP complexes have been dismissed by some groups as a non-functional waste products that passively leak into the circulation after cell death [152]. However, other groups have found asymmetric abundance patterns when comparing intracellular and extracellular miRNA levels in cell culture and have described evidence for an active and selective export process [155]. The following two chapters aim to better understand the physiological and pathological release stimuli for myomiRs, to characterise myomiR carriers in greater detail and to study their export mechanism(s). Furthermore, cell culture models of ex-myomiR release will also be investigated. In combination, these studies aim to reveal new insights into the role of ex-miRNAs in muscle biology that may have additional implications for the use of ex-myomiRs as disease biomarkers for DMD.

3.2 Materials and methods

3.2.1 Animal work

Animal studies were conducted as described in section 2.1. For the exercise studies, mice were subjected to 20 minutes of treadmill exercise (Exer3/6, Columbus instruments, Columbus, OH, USA), running with either a downward incline of 15˚, or on a level surface as according to experimental requirements. Treadmill speed was initially set at 5 m/min and gradually increased to 20 m/min. If longitudinal blood measurements were required, ~25 µl blood was collected from the tail vein. For endpoint measurements animals were sacrificed by escalating CO_2 concentration and blood was harvested from the jugular vein as described in chapter 2.1. Animals younger than 14 days were decapitated and blood was harvested from the corpus.

For the cardiotoxin injury study, 12 week old male C57BL/10 mice (abbreviated as C57 in all figures) were anaesthetized with isoflurane, and 25 µl of 10 µM cardiotoxin (CTX) (Latoxan, Valence, France) was injected subcutaneously into the tibialis anterior (TA) muscles of the right and left hind-limbs. The muscles were removed 14 days after CTX injection, and 7 µm sections were stained with Hematoxylin and Eosin for histological analysis. Clinical biochemistry assays to determine the concentration of creatine kinase, alanine aminotransferase, aspartate aminotransferase and lactate dehydrogenase in serum samples were performed at the clinical pathology laboratory, Medical Research Council Harwell (Oxford, UK).

3.2.2 Collection of conditioned media and GW4869 treatment

Muscle cells were maintained and differentiated as described in section 2.4. Conditioned media was centrifuged at 2,000 *g* for 10 minutes at 4˚C and filtered (0.22 µm) to remove cellular debris and large apoptotic bodies prior to RNA extraction. To block exosome secretion, C2C12 muscles cells were differentiated for 4 days and then treated for 48 hours with GW4869 (Sigma-Aldrich, Dorset,

UK) at a final concentration of 10 µM. Subsequently, EVs were isolated from the supernatant by ultracentrifugation as described in chapter 2.5.

3.2.3 MHC Immunofluorescence

For detection of myosin heavy chain (MHC) in differentiated myotubes the cells were fixed in 4% Paraformaldehyde (Santa Cruz Biotechnology, Dallas, TX, USA) for 10 minutes, permeabilised in 0.25% Triton X-100 (Sigma-Aldrich) for 15 minutes and subsequently blocked in 5% bovine serum albumin (BSA) (Sigma Aldrich) for 30 minutes. Next, the cells were stained for 2 hours with anti-MHC antibody supernatant (MF 20) (1:10 in 5% BSA). MF 20 was deposited to the DSHB by Fischman, D.A. (DSHB Hybridoma). Afterwards, cells were incubated for 1 hour in secondary antibody Alexa Fluor 594 rabbit anti-mouse IgG (1:500 in 5% BSA) (Life Technologies) and Hoechst 33258 (1:5,000 in 5% BSA) (Life Technologies). All incubation times listed above were performed at room temperature. Representative microscopic images were taken at an appropriate magnification with an EVOS FL cell imaging system (Life Technologies).

3.2.4 Induction and detection of apoptosis of C2C12 myotubes

To chemically induce apoptosis, C2C12 cells were differentiated for 6 days and then treated with 1 µM Staurosporine (Abcam, Cambridge, UK) for 24 hours. Cell viability was determined by MTS assay using the CellTiter 96 AQueous One Solution Cell Proliferation Assay kit (Promega, Southampton, UK). For detection of apoptosis, the FITC Annexin V Apoptosis Detection Kit I (BD Pharmingen, Plymouth, UK) was used for fluorescence staining with minor alterations to the manufacturer's protocol. In brief, cells were washed in 1x Binding Buffer and then stained for 30 minutes with Propidium Iodide, Annexin V-FITC (both 1:30) and Hoechst (1:1,000). In addition, Trypan Blue was also used to assess cell viability by dye exclusion assay. In brief, cells were incubated with 0.4% Trypan Blue Solution (Sigma-Aldrich) for 2 minutes and analysed for dye uptake with the EVOS FL cell imaging system (Life Technologies).

3.2.5 Statistical analysis

Statistical analyses were carried out as described in section 2.7. If the influence of two independent variables on two different genotypes was tested, two-way ANOVA with Bonferroni post testing was applied (GraphPad Prism 5). In this statistical analysis, the interaction factor tests the null hypothesis that the effect of the genotype is the same at all time points. A non-significant interaction factor indicates that the effect of genotype is the same at all time points and in contrast, a significant interaction factor indicates that strain-specific differences are not equivalent between time points. Group factor and time factor are difficult to interpret if the interaction factor is significant and emphasis is therefore placed on the results of the Bonferroni post test. The two-way ANOVA group factor tests for difference in between two genotypes after combining all time points and the time factors analyses variances in the different time points after combining the wild-type and *mdx* mice. Differences were considered significant at *P*-values less than 0.05. Pearson correlation analysis was performed with GraphPad Prism 5.

Ex-miRNA stability curves were fitted using a one or two phase exponential decay model (GraphPad Prism 5). Whenever possible, curves were fitted using the one phase decay model, although for some serum samples, no appropriate curve fitting could be achieved. In this case, curves were fitted utilising two phase exponential modelling, which assumes that the measured outcome is the sum of a fast and a slow exponential decay.

3.3 Results

3.3.1 MyomiR release during neonatal muscle development and growth

During the first four weeks of life, murine muscle mass increases rapidly [290]. Notably, postnatal muscle development consists of a very active phase of initial satellite cell proliferation and myogenic differentiation [291,292], that is accompanied by upregulation of intracellular myomiRs (section 1.3.1). Hypothesising that this developmental process may also result in an altered serum myomiR signature, ex-myomiR abundance was measured in 7 day intervals during the first 28 postnatal days (PND) in wild-type (C57) and dystrophic *mdx* mice.

Importantly, the onset of dystrophic pathology in *mdx* mice occurs only at three weeks of age [293,294], and so up until 21 PND the *mdx* mice can be considered to be pre-symptomatic. To test for differences in ex-myomiR levels in *mdx* and wild-type sera during the perinatal and juvenile phase of life, two-way ANOVA analysis was performed. Beginning at three weeks of age, *mdx* mice undergo a so-called crisis where massive muscle fibre death followed by complete regeneration and stabilisation of the muscle tissue over the course of a few weeks can be observed [295]. An additional time point at 42 PND was also included in the study to assess ex-myomiR levels in dystrophic mice that have undergone this intensive period of remodelling. This time point was not included into the two-way ANOVA statistical analysis since the aim was to investigate changes in ex-myomiRs in early muscle development and compare these in dystrophic and healthy mice. At 42 PND, it is expected based on the disease progression, that wild-type and *mdx* mice would exhibit clear differences in ex-myomiR levels which are not related to perinatal muscle growth.

Interestingly, ex-myomiRs were highly enriched in the circulation at birth and throughout the first week of life in both genotypes before declining until PND 14 and then rising gradually for *mdx* mice from PND 21 onward (Figure 3.1A). According to two-way ANOVA (Table 3.1), the level of each individual released myomiR changed significantly with time (*P*-value of time factor $P<0.0001$ for all

myomiRs). Most importantly, miR-1, miR-133a and miR-206 abundance followed a similar pattern in both mouse strains (*P*-value of interaction factor $P>0.05$ for all myomiRs, i.e. not significant). The granulocyte-specific miR-223 was utilised as a non-myomiR control miRNA since it is stably abundant in murine serum (both wild-type and *mdx*) and has therefore previously been used as an endogenous control by the Wood group [211,285] and others [286,296]. Notably, serum abundance of miR-223 remained unchanged over the time period investigated (non-significant time factor). As expected, all myomiRs were upregulated in the circulation of 42 day old *mdx* sera compared to wild-type controls. Interestingly, the concentration of ex-myomiRs in dystrophic mice was higher at 42 PND than at 0 PND for miR-1 and miR-133a, but lower for miR-206. The latter might be due to increased levels of miR-206 in regenerating/developing fibres [124].

In parallel, clinical biochemistry markers of tissue damage that have been shown to be elevated in DMD were measured, including creatine kinase (CK), alanine aminotransferase (ALT), aspartate aminotransferase (AST) and lactate dehydrogenase (LDH) [297]. In contrast to CK and the myomiRs, analysis of LDH, ALT and AST showed a noticeable peak at PND 21 and levels remained elevated thereafter, consistent with the onset of dystrophic pathology in *mdx* mice at three weeks of age. (Figure 3.1B, Table 3.1). Interestingly, serum CK levels closely followed the pattern observed for myomiRs (Figure 3.1B). These findings are consistent with observations of elevated CK in healthy new-born humans due to birth trauma that return to normal within the first 10 days of life [298]. In line with the described *mdx* pathology and the ex-myomiR data, all markers of clinical pathology were elevated in 42 day old dystrophic mice.

In addition, *Pax7* transcript levels in the tibialis anterior (TA) muscles were monitored to confirm satellite cell proliferation (Figure 3.1C). In both genotypes, *Pax7* was highly abundant during the first week of life and expression subsequently dropped to a low baseline level at 21 PND. *mdx* mice exhibited a slight increase in *Pax7* expression at 4 weeks of age, possibly related to the high rate of

muscle turn-over caused by the onset of pathology. At 42 PND, *Pax7* levels were indistinguishable between *mdx* and wild-type mice.

In summary, the release of ex-myomiRs in wild-type and pre-symptomatic mice follows a similar pattern, with a large increase in abundance during the perinatal phase which occurred in the absence of elevated AST and ALT levels and independent of the onset of dystrophic pathology but concomitant with an increase in *Pax7* expression in muscle.

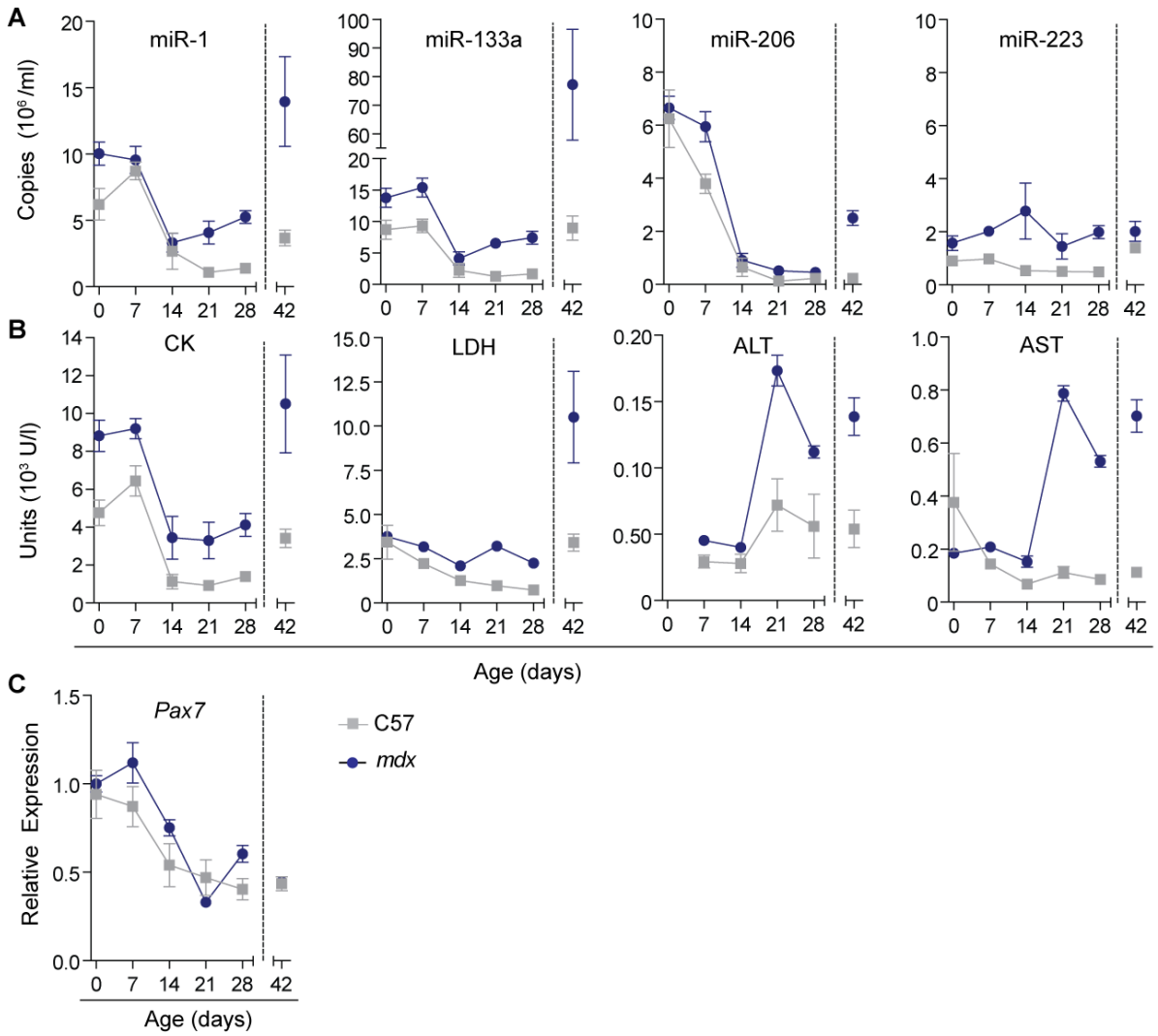

Figure 3.1 **Levels of ex-myomiRs are elevated in juvenile wild-type and pre-symptomatic *mdx* mice.**

Wild-type (C57) and *mdx* mice (*n*=4-8) were sacrificed at the indicated time points and blood was assayed for (A) ex-miRNA levels and (B) clinical biochemistry markers (CK, LDH, AST and ALT). Ex-myomiR and miR-223 levels were measured by RT-qPCR using synthetic RNA standards to determine absolute copy numbers. (C) *Pax7* transcript levels were determined in the TA muscle by RT-qPCR and normalised to TATA Box Binding Protein (*Tbp*) expression. Values are mean +/- SEM. Two-way ANOVA with Bonferroni post testing was performed for only the first 4 weeks of life of the animals (indicated by the dashed line) and *P*-values for interaction, group and time factors are listed in Table 3.1.

Juvenile *mdx* and C57 mice				
miRNA	**Interaction factor (*P*-value)**	**Group factor (*P*-value)**	**Time factor (*P*-value)**	**Results post test**
miR-1	0.220	**0.0051**	**<0.0001**	none
miR-133a	0.6232	**0.0013**	**<0.0001**	7d *
miR-206	0.3026	0.1110	**<0.0001**	7d *
miR-223	0.1732	**<0.0001**	0.3486	14d, 28d, **
CK	0.7750	**<0.0001**	<0.0001	0d**
AST	**<0.0001**	**<0.0001**	**<0.0001**	0d *; 21d, 28d ***
ALT	**0.0070**	**<0.0001**	**<0.0001**	21d ***; 28d *
LDH	0.0277	**<0.0001**	**<0.0001**	21d ***; 28d **
Pax7	0.1934	0.0498	**<0.0001**	none

Table 3.1 Results of two-way ANOVA of serum myomiR levels in juvenile mice 0-28 PND.

Juvenile wild-type (C57) and *mdx* mice (n=4-8) were sacrificed at the indicated time-points and blood was assayed for ex-miRNA levels and biochemistry markers as shown in Figure 3.1. Differences between groups were tested using two-way repeated measurement ANOVA statistical analysis with Bonferroni post testing and *P*-values were tabulated accordingly. *P*-values that were significant at the $P<0.05$ level are highlighted in bold. The group factors (comparing the two genotypes after combining all time points) and the time factors (analysing variances in the different time points after combining the wild-type and *mdx* mice) were significantly different for all myomiRs and clinical biochemistry markers (with the exception of the group factor for miR-206). *$P<0.05$, **$P<0.01$, ***$P<0.001$.

3.3.2 Exercise induces delayed myomiR release in dystrophic mice

Given the dynamic changes in ex-myomiR abundance during postnatal muscle development, it was of interest to further investigate a possible correlation between muscle regeneration in adult mice and ex-myomiR release. Therefore, the next experiments utilised physical exercise to induce regeneration through low-level, body-wide, muscle injury. Notably, adult muscle regeneration after injury is reminiscent of embryonic myogenesis and consists of two interdependent phases [299]. Initially, myofibre necrosis and inflammation is observed shortly after injury. This is followed by activation of satellite cells which initiate regeneration, remodeling and functional repair. Typically, satellite cells are activated 3 days after muscle injury, fuse with myotubes after 5 days and begin to close the injury lesion 7 days after the initial muscle damage [300].

In the following study, *mdx* and wild-type mice were subjected to 20 minutes of downhill exercise and blood samples were harvested repeatedly, every 2-4 days until 13 days after exercise in order to determine any changes in serum myomiR abundance that could result from either immediate muscle injury or a delayed regenerative response (Figure 3.2A). Repeated sampling via the tail vein and normalisation to day -1 bleeds for each individual mouse was employed in order to reduce noise caused by inter-animal variability. *mdx* mice were initially used as their serum is highly enriched for ex-myomiRs [138], and as a result, detecting changes in ex-myomiR detection is technically more facile than in wild-type animals. The mice were subjected to downhill exercise to further exacerbate exercise-mediated myoinjury, as eccentric contraction is known to cause more muscle damage than other types of contraction [301], and *mdx* mice have been shown to be highly susceptible to stretch-induced muscle damage [302].

Interestingly, in dystrophic mice all circulating myomiRs exhibited a dynamic abundance pattern with an immediate increase (day 0) and a second peak of smaller magnitude at day 7 after exercise (Figure 3.2B, upper panel). Importantly, this biphasic abundance pattern was highly similar in the exercised group for all ex-myomiRs. According to two-way ANOVA (Table 3.2), ex-myomiRs abundance changed

significantly with time (*P*-value of time factor $P<0.05$ for all myomiRs). Furthermore, the exercised and unexercised group behaved significantly different for miR-1 and miR-133a (*P*-value of group factor $P<0.05$). Similarly, *post hoc* analysis demonstrated a significant increase in miR-1 abundance immediately after exercise and a significant increase in miR-133a abundance 7 days after exercise. For all myomiRs, levels returned to the unexercised baseline within a few days following the second peak (~d9). Conversely, the non-myomiR control (miR-223) did not exhibit any significant changes throughout the duration of the experiment. The exercise experiment was repeated in wild-type mice although in this case no increase in ex-myomiRs were observed, possibly as a result of the reduced sensitivity of healthy muscles to contraction-induced damage relative to *mdx* [303,304] (Figure 3.2B, lower panel and Table 3.2).

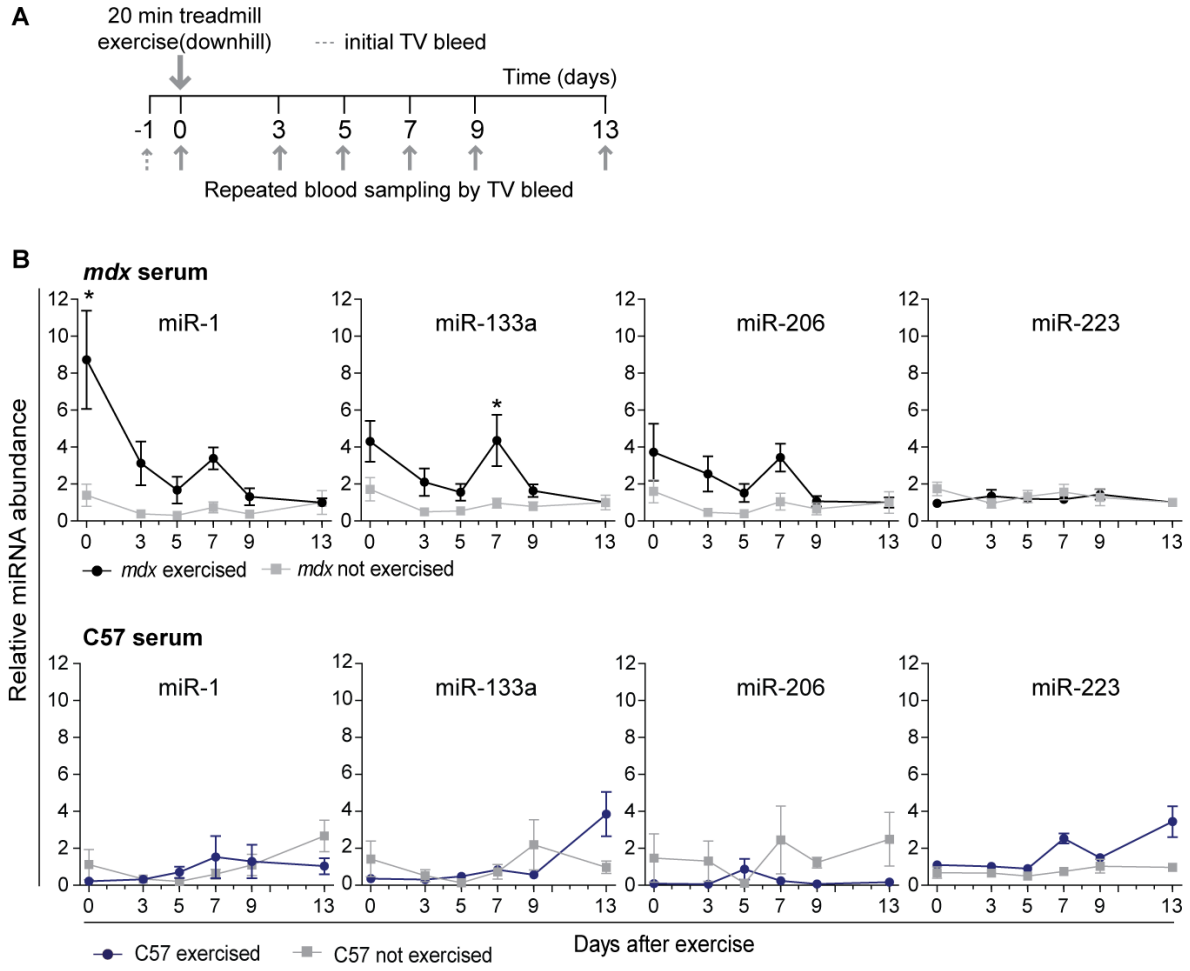

Figure 3.2 Acute eccentric exercise induces a biphasic abundance pattern of myomiR release in *mdx* mice.

(A) 12 week old male *mdx* (*n*=8) and wild-type (*n*=6) were exercised by running downhill for 20 minutes at increasing speed on a treadmill with a 15˚ incline and compared with unexercised controls (*n*=5 for *mdx* and *n*=4 for C57). Blood was collected at indicated time points by serially sampling from each mouse. (B) Levels of miRNAs in (upper panel) *mdx* and (lower panel) wild-type serum were determined by RT-qPCR. Expression of myomiRs was normalised to the day -1 bleed for each individual animal respectively to minimise noise due to inter-animal variability. All values are mean +/- SEM. **P*<0.05 (Two-way ANOVA, Bonferroni post test). *P*-values for interaction, group and time factors are listed in Table 3.2.

Longitudinal exercise study: *mdx* mice				
miRNA	**Interaction factor (*P*-value)**	**Group factor (*P*-value)**	**Time factor (*P*-value)**	**Results post test**
miR-1	0.0743	**0.0452**	**0.0176**	0d *
miR-133a	0.2406	**0.0377**	**0.0102**	7d *
miR-206	0.4127	0.1024	**0.0478**	none
miR-223	0.7919	0.7453	0.4579	none
Longitudinal exercise study: wild-type mice				
miRNA	**Interaction factor (*P*-value)**	**Group factor (*P*-value)**	**Time factor (*P*-value)**	**Results post test**
miR-1	0.3216	0.7443	0.1494	none
miR-133a	**0.0148**	0.8355	**0.0155**	none
miR-206	0.4319	0.1400	0.8070	none
miR-223	**0.0181**	**0.0009**	**0.0012**	none

Table 3.2 Results of two-way ANOVA of serum myomiR levels in exercised mice.

12 week old male *mdx* mice (*n*=8) and wild-type (*n*=6) were exercised and compared with unexercised controls (*n*=5 for *mdx* and *n*=6 for C57). Blood was harvested at the indicated time-points and assayed for ex-miRNA levels as shown in Figure 3.2. Differences between groups were tested using two-way ANOVA repeated measurements statistical analysis with Bonferroni post testing and *P*-values tabulated accordingly. *P*-values that were significant at the $P<0.05$ level are highlighted in bold. A significant interaction factor indicates that difference specific to the exercise-regimen are not equivalent between time points (eg miR-133a, miR-223 for C57 mice). For the *mdx*, the group and the time factors were significantly different for all myomiRs (with the exception of the group factor for miR-206). Conversely, group and time factors for all myomiRs in non-dystrophic mice with non-significant interaction factors were not significantly different.*$P<0.05$

Next, *mdx* and wild-type mice were exercised with a slightly altered exercise protocol without downhill incline with the aim of decreasing the severity of the initial myoinjury and observing whether the levels of myomiRs released immediately after exercise similarly decrease (Figure 3.3A). In addition, it was also of interest to see if the delayed increases in myomiR abundance could still be detected with this modified exercise protocol. For this experiment, end point measurements were performed to assess myomiR expression in skeletal muscle and to allow for sampling of larger volumes of serum (which enabled analysis of serum CK in parallel). CK was significantly elevated in the circulation of *mdx* mice compared to wild-type as reported previously [305] (Figure 3.3B, Table 3.3). However, CK levels after exercise varied considerably across animals, consistent with other studies [306]. Interestingly, no significant increases in ex-myomiR levels were observed immediately after treadmill running on a level surface (Figure 3.3C). Therefore, serum CK levels were more susceptible to exercise than ex-myomiR, which is in agreement with previous studies [150], although only if measured immediately after exercise activity. Importantly, miR-1 exhibited a similar increase in abundance 5 days after exercise as observed in the downhill exercise experiment (Figure 3.3B), possibly related to the regenerative phase. Likewise, miR-133a levels increased progressively following exercise and miR-206 exhibited a very similar pattern but failed to reach statistical significance at the $P<0.05$ level due to high inter-replicate variation. As with the previous downhill exercise study, no changes in ex-myomiR abundance in wild-type animals for either serum or skeletal muscle were detected (Figure 3.3B and 3.3C, only unexercised controls are shown for wild-type TA muscles for a general comparison with *mdx* muscle).

In contrast, analysis of miRNA levels *mdx* TA muscle sections harvested at the same time as the serum samples showed upregulation of miR-1 expression immediately after exercise, but downregulation at later time points (Figure 3.3D). miR-206 expression was increased in *mdx* TA muscle relative to wild-type animals, as described previously [138], but expression was not altered after exercise. No changes in miR-133a were observed in TA between wild-type and *mdx*, or following exercise thus highlighting that expression levels in tissue and abundance in serum do not

always correlate [138]. To confirm that physical exercised induced regeneration, transcript levels of the embryonic myosin heavy chain 3 (*Mhy3 or eMHC*) were measured in the TA muscle. Typically, *Mhy*3 is expressed during embryonic and fetal muscle development, but is also re-expressed in regenerating fibres after injury [307]. In *mdx* mice *Mhy3* was significantly increased 7 days after exercise (Figure 3.3C) whereas the transcript was undetectable in wild-type muscle, thus confirming that the exercise regimen was insufficient to induce regeneration in non-dystrophic mice. In summary, serum myomiRs in dystrophic *mdx* mice exhibit dynamic changes in abundance depending on the mode of exercise, possibly reflecting the degenerative and regenerative status of the muscle.

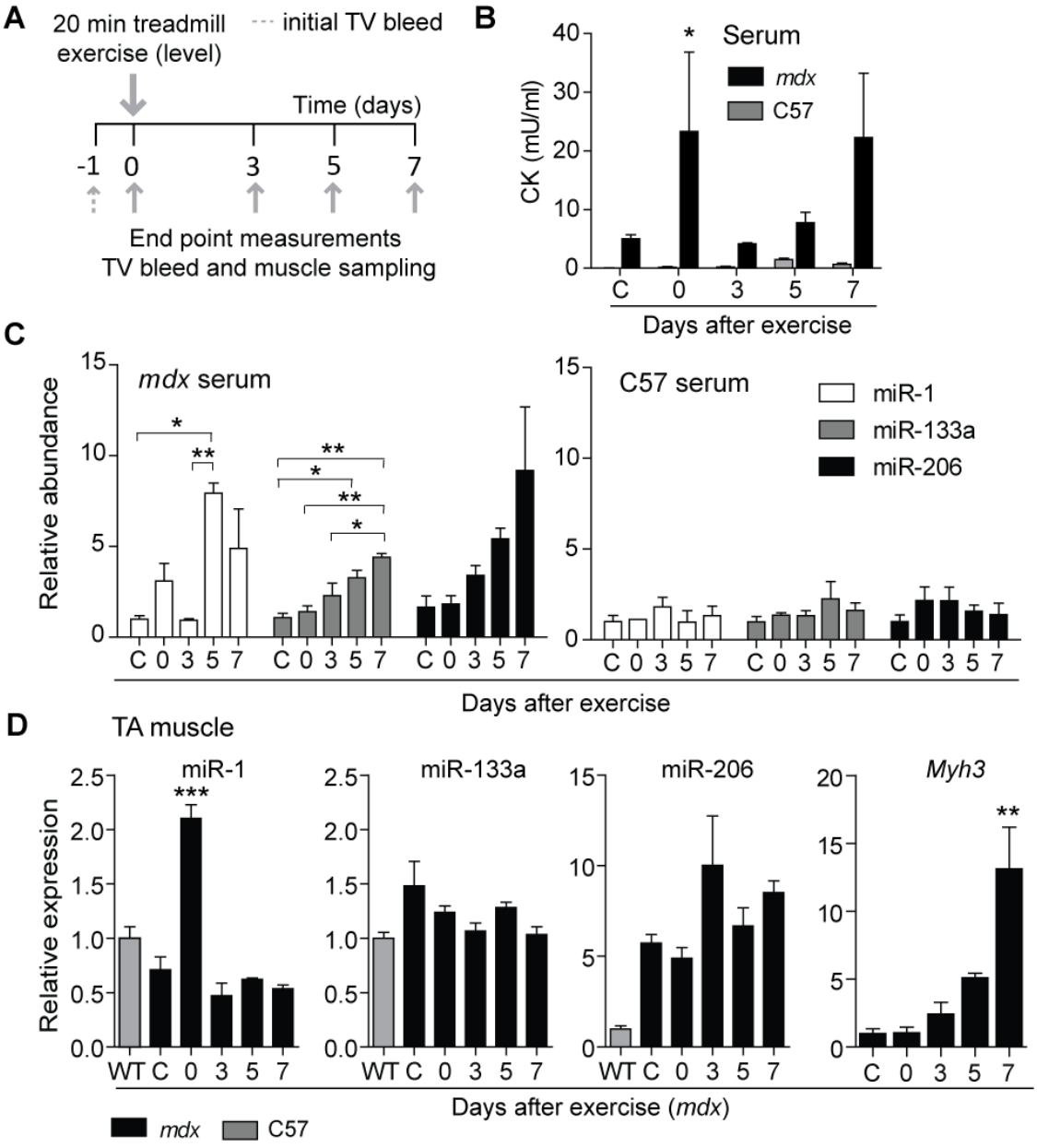

Figure 3.3 End point analysis of miRNAs and CK in serum and tissue after exercise.

(A) 12 week old male *mdx* and wild-type (C57) mice were exercised for 20 minutes by running on a level surface at increasing speed. Animals were sacrificed at the indicated end points (*n*=3) and tissue samples and serum harvested. (B) CK was measured in *mdx* and wild-type serum. Levels of miRNAs in (C) serum or (D) muscle of *mdx* and wild-type were determined by RT-qPCR. *Myh3* transcript levels were measured by RT-qPCR and normalised to TATA Box Binding Protein (*Tbp*) expression. *Myh3* was undetectable in wild-type mice and no changes in myomiR expression were measured (data not shown). CK= Creatine Kinase, WT= wild-type, C= not exercised control animals. All values are mean + SEM. **P*<0.05, ***P*<0.01, ****P*<0.001 (Two-way ANOVA with Bonferroni post test (B) (*P*-values in Table 3.3) and one-way ANOVA with Bonferroni post test (C,D).

End-point exercise study: *mdx* and wild-type mice				
	Interaction factor (*P*-value)	**Group factor (*P*-value)**	**Time factor (*P*-value)**	**Results post test**
CK-MM	0.2429	**0.0026**	0.2456	0d *

Table 3.3 Results of two-way ANOVA of serum CK levels in exercised mice.

12 week old male *mdx* and wild-type (C57) mice were exercised for 20 minutes at increasing speed on an even treadmill with no decline and serum was harvested as presented in Figure 3.3. Differences between groups were tested using two-way ANOVA statistical analysis with Bonferroni post testing and *P*-values tabulated accordingly. *P*-values that were significant at the $P<0.05$ level are highlighted in bold. A non-significant interaction factor indicates that the effect of genotype is the same at all time points. The group factor was highly significant whereas the time factor was not significant. *$P<0.05$.

Previously, Roberts *et al*. showed altered miRNA release in wild-type mice immediately after inducing localised myoinjury with cardiotoxin (CTX) in the TA muscle of wild-type mice [285]. In this chapter, this experiment was reproduced with the methodological improvements described above (i.e. day -1 normalisation and serial measurements taken over an extended time period) in order to monitor any delayed changes in ex-myomiR release due to muscle regeneration following the injury. Similar to the previously reported findings, CTX injury caused an increase in ex-myomiRs immediately after the treatment (Figure 3.4 and Table 3.4). However, no significant changes at later time points could be determined, possibly because injury followed by regeneration in a single muscle is insufficient to increase ex-myomiRs to a detectable level beyond the initial degenerative phase.

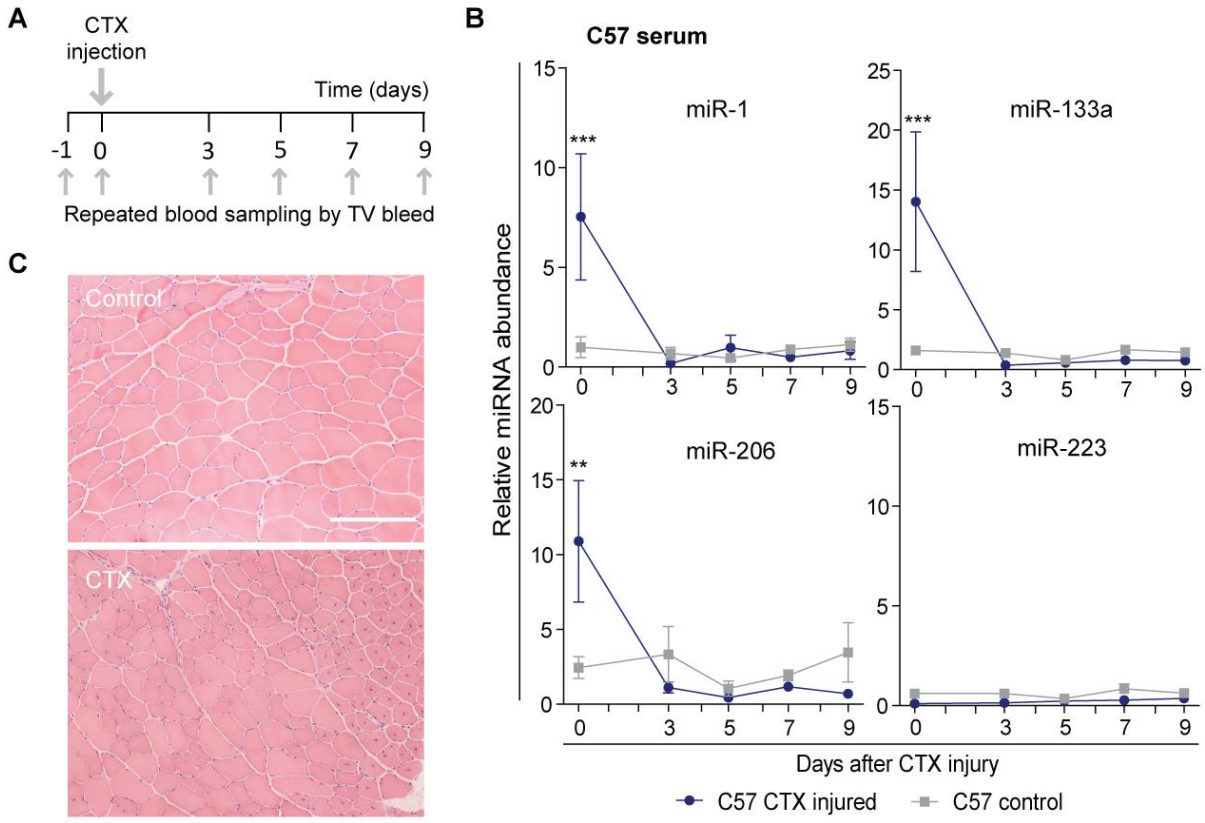

Figure 3.4 Cardiotoxin induces release of myomiRs immediately after injury.

12 week old male wild-type (C57) mice were injected with Cardiotoxin (CTX) in the TA and compared to untreated controls. (A) Blood was collected at indicated time-points post-injection via tail vein bleeds. (B) Serum myomiR levels were determined by RT-qPCR and all myomiRs were significantly increased after toxin injections but remained low afterwards. (C) After completion of the serial serum sampling, animals were sacrificed and Hematoxylin and Eosin staining of transverse sections through the mid-belly of the TA muscles was performed to confirm CTX injury. A large cluster of central nucleated fibres was observed around the injection site in CTX-injured muscle indicating the presence of regenerated fibres. All values are mean + SEM, *n* = 5 mice. Scale bars represent 100 µm. **P<0.01, ***P<0.001 (Two-way ANOVA, Bonferroni post test). *P*-values for interaction, group and time factors are listed in Table 3.4).

Wild-type cardiotoxin study				
miRNA	**Interaction factor (*P*-value)**	**Group factor (*P*-value)**	**Time factor (*P*-value)**	**Results post test**
miR-1	**0.0011**	**0.0390**	**0.0005**	0d ***
miR-133a	**0.0024**	**0.1110**	**0.0014**	0d ***
miR-206	**0.0086**	0.6500	**0.0073**	0d **
miR-223	0.7891	**0.0080**	0.6001	none

Table 3.4 Results of two-way ANOVA of serum myomiR levels in CTX treated mice.

12 week old male wild-type (C57) mice were injected with Cardiotoxin (CTX) in the TA whereas controls were untreated (Figure 3.4). Differences between groups were tested using two-way ANOVA repeated measurements statistical analysis with Bonferroni post testing and *P*-values tabulated accordingly. *P*-values that were significant at the $P<0.05$ level are highlighted in bold. A significant interaction factor indicates that strain-specific differences are not equivalent between time points (here for all myomiRs). Group factor and time factor are difficult to interpret if the interaction factor is significant and emphasis is therefore placed on the results of the Bonferroni post test. All myomiRs were significantly increased immediately after CTX injection. $^{**}P<0.01$, $^{***}P<0.001$

3.3.3 MyomiR release is reduced in aged *mdx* mice

The natural process of muscle loss during aging is exacerbated in *mdx* mice due to repeated cycles of degeneration and regeneration that follow as a consequence of dystrophin-deficiency [27]. In particular, at 72 weeks of age, the hind limb muscles of *mdx* mice were shown to decrease in muscle mass by more than 50% in TA, extensor digitorum longus, soleus, and plantaris. Furthermore, muscle mass decreased by up to 70% in quadriceps and gastrocnemius, compared to age-matched wild-type mice [32]. In this section, the aim was to determine whether chronic muscle-wasting in aged *mdx* mice is reflected in serum myomiR abundance. To this end, levels of myomiRs and clinical chemistry biomarkers were compared in the circulation of adult (14 weeks) and aged (88 weeks) *mdx* and wild-type animals.

Consistent with previous data, both ex-myomiR levels and clinical biochemistry markers of tissue injury were significantly increased in adult *mdx* compared to adult wild-type mice [138,297] (Figure 3.5 and Table 3.5). Ex-myomiRs exhibited larger fold changes at 14 weeks (ranging from 13-42 fold) than CK, LDH, ALT and AST (ranging from 2-9 fold). Conversely, neither the ex-myomiRs nor clinical biochemistry serum markers were significantly different between genotypes in aged mice. Ex-myomiR abundance was restored to near wild-type levels in the aged mice, likely as a result of aging-associated muscle loss and/or age-related changes in dystrophic pathology. In agreement, the body weight of aged *mdx* mice was significantly decreased compared to aged wild-type mice (Figure 3.5C). Furthermore, Hematoxylin and Eosin staining of the quadriceps femoris muscles demonstrated severely advanced pathology in aged dystrophic mice (Figure 3.5D).

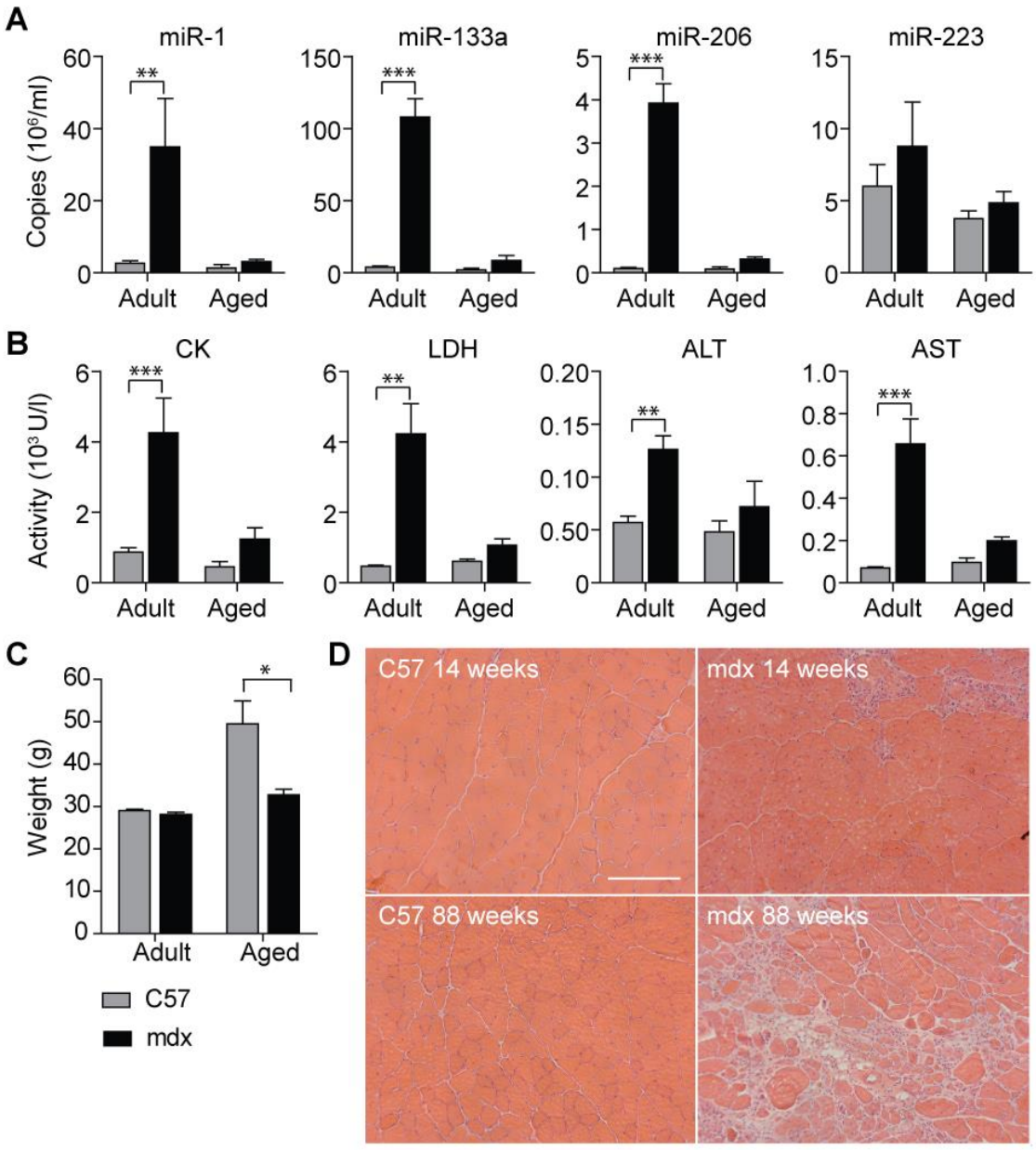

Figure 3.5 Serum myomiRs and clinical biochemistry markers are decreased in aged *mdx* mice. Blood from adult (14 week old) and aged (88 week old) wild-type (C57) and *mdx* mice (*n*=4-5) was harvested and assayed for (A) miRNA abundance and (B) clinical biochemistry parameters. (A) Serum myomiR levels were measured using RT-qPCR with synthetic RNA standards for absolute quantification. (B) In parallel, clinical biochemistry parameters were analysed using standard enzymatic assays and (C) body weights were measured. (D) Hematoxylin and Eosin staining of transverse sections through the mid-belly of the quadriceps femoris muscle were analysed by light microscopy and representative images are shown. Scale bar represent 100 µm. All values are mean + SEM. *P<0.05, **P<0.01, ***P<0.001, (Two-way ANOVA, Bonferroni post test in B) and unpaired *t*-test, 2 tailed in C). *P*-values for interaction, group and time factors are listed in Table 3.5.

Microscopic analysis showed that adult dystrophic mice displayed the characteristic histological changes associated with DMD pathology at 14 weeks of age, including variation in fibre size, immune infiltrate and muscle degeneration/regeneration (Figure 3.5D). In muscles of aged *mdx* mice extensive loss of myofibres and accumulation of connective and adipose tissue was observed. Several large hypertrophic fibres were observed in between the fibrotic material. In contrast, aged control mice maintained a uniform fibre size without evidence of muscle necrosis or fibrosis.

Similarly, serum myomiR levels in aged wild-type mice were not significantly altered compared to adult non-dystrophic animals. Notably, levels of the non-myomiR control miR-223 were unaffected by age or dystrophic pathology. Given their muscle-specific origin, these data suggest that serum myomiR abundance is also correlated to muscle mass in addition to reflecting the regenerative/degenerative status of muscle.

Adult and aged wild-type and *mdx* mice				
miRNA	**Interaction factor (*P*-value)**	**Group factor (*P*-value)**	**Time factor (*P*-value)**	**Results post test**
miR-1	**0.0318**	**0.0185**	**0.0214**	14wk **
miR-133a	**<0.0001**	**<0.0001**	**<0.0001**	14wk ***
miR-206	**<0.0001**	**<0.0001**	**<0.0001**	14wk ***
miR-223	0.6266	0.2734	0.0908	none
CK	**0.0152**	**0.0009**	**0.0033**	14wk ***
AST	**0.0004**	**<0.0001**	**0.0009**	14wk ***
ALT	0.1256	**0.0062**	**0.0414**	14wk **
LDH	**0.0006**	**<0.0001**	**0.0012**	14wk ***

Table 3.5 Results of two-way ANOVA of serum myomiR levels in adult and aged mice.

Two-way ANOVA statistical analysis with Bonferroni *post hoc* analysis of serum myomiRs and clinical biochemistry markers in 14 and 88 week old *mdx* and wild-type mice presented in Figure 3.4. *P*-values that were significant at the $P<0.05$ level are highlighted in bold. A significant interaction factor indicates that the effect of the genotypes is changed at the later time point. Group factor and time factor are difficult to interpret if the interaction factor is significant and emphasis is therefore placed on the results of the Bonferroni post test (here for all parameters apart from the control miR-223 and ALT). **$P<0.01$, ***$P<0.001$.

3.3.4 Progressive myomiR release during myogenic differentiation

Given that myogenic differentiation is accompanied by increased expression of cellular myomiRs (chapter 1.3.2), it was of interest to investigate whether intracellular myomiR induction in muscle cell cultures is correlated with an elevated release of muscle-specific miRNAs, reminiscent of the myomiR release observed *in vivo* during muscle development and regeneration. Firstly, primary human myoblasts were differentiated into multinucleated myotubes over the course of 9 days. RNA was isolated from cells and conditioned media collected every 3 days. To exclude the possibility that some miRNAs might be present in the cell culture media, RNA was extracted from fresh differentiation media and miRNA levels were measured RT-qPCR. Importantly, none of the miRNAs investigated in this study were detectable in fresh differentiation media (data not shown). During differentiation to myotubes, the medium was replaced at regular intervals so that each supernatant sample represents the quantity of released miRNAs over the 3 day period and not the accumulation of secreted miRNA over the entire duration of differentiation (Figure 3.6A). Myotube formation was confirmed by light microscopy and quantification of the transcripts levels of the myogenic regulatory factors *MYOD1* and *MYOG* by RT-qPCR (Figure 3.7A,C).

Cellular expression of myomiRs was strongly and progressively induced with a 100-1,000 fold increase in expression after 9 days of differentiation (Figure 3.6B). Absolute intracellular myomiR copy numbers after 9 days of differentiation reached similar levels of ~100 million copies/µg RNA with miR-206 and miR-1 being the most abundant species measured. Concurrently, myogenic differentiation was associated with a strong, progressive increase (up to ~100 fold) in the release of myomiRs, especially at the later stages of differentiation where multinucleated myotubes were visible (Figure 3.7C). Despite slightly differing patterns of release, after 9 days the absolute levels of ex-myomiRs in the media were similar for miR-206 (0.4 million copies/ml) and miR-133a (0.2 million copies/ml) and somewhat lower for miR-1 (0.04 million copies/ml). Notably, cellular miRNA and secreted ex-miRNA levels were positively correlated for all myomiRs (Pearson coefficients: 0.7809

(miR-1), 0.7515 (miR-133a), 0.8219 (miR-206); all *P*<0.01, Table 3.6). Three additional non-myomiR control miRNAs were measured in parallel: miR-16 (ubiquitously expressed, previously used for miRNA normalisation in tissues [138,282]), let-7a (ubiquitously expressed and highly abundant in muscle tissues [308]), miR-31 (involved in regulating muscle processes [117] and proposed as a reference miRNA in serum [257]). Notably, miR-223, the control miRNA utilised in *in vivo* experiments is undetectable in muscle cell culture media, most likely because of its granulocyte-specificity [309].

All of the three control miRNAs exhibited relatively stable expression in cells and stable abundance in cell culture supernatant over the course of the experiment (Figure 3.6B). Furthermore, there was no significant correlation between cellular and secreted miRNA levels for these three non-myomiR controls. Importantly, let-7a was highly abundant (1.5 billion copies/µg RNA) in muscle cells throughout the period of differentiation. Considering this high-intracellular abundance, let-7a was found at comparatively low levels in the supernatant (0.1 million copies/ml), thus highlighting the selectivity of myomiR release.

As primary muscle cells are of limited availability and are difficult to culture for extended periods of time, it was of interest to see if these findings could be recapitulated in an immortalised myoblast cell line (C2C12). Upon serum depletion, C2C12 cells differentiated to form multinucleated myotubes with a concomitant induction of cellular myomiR expression (Figure 3.6C). Myogenic differentiation was visualised by immunostaining for myosin heavy chain (MHC)-positive myotubes, which became apparent after three days of differentiation conditions, and continued to mature into larger myotubes (Figure 3.7D). Importantly, myogenic differentiation progressively induced myomiR release by up to ~100 fold after 9 days of differentiation. As with the primary human myoblasts, cellular and secreted levels of myomiRs in C2C12 cells were likewise strongly correlated (Pearson coefficients: 0.9291 (miR-1), 0.8878 (miR-133a), 0.8937 (miR-206); all *P*<0.0001, Table 3.6) whereas the non-myomiR controls were not correlated (miR-31 and let7-a) or had weak correlation coefficients (miR-

16). Notably, the absolute levels of myomiRs in the media were higher in C2C12 cells than in primary myoblast cells, probably due to higher cell density (~2.5 fold more nuclei per image section, data not shown) that these cells achieve in culture.

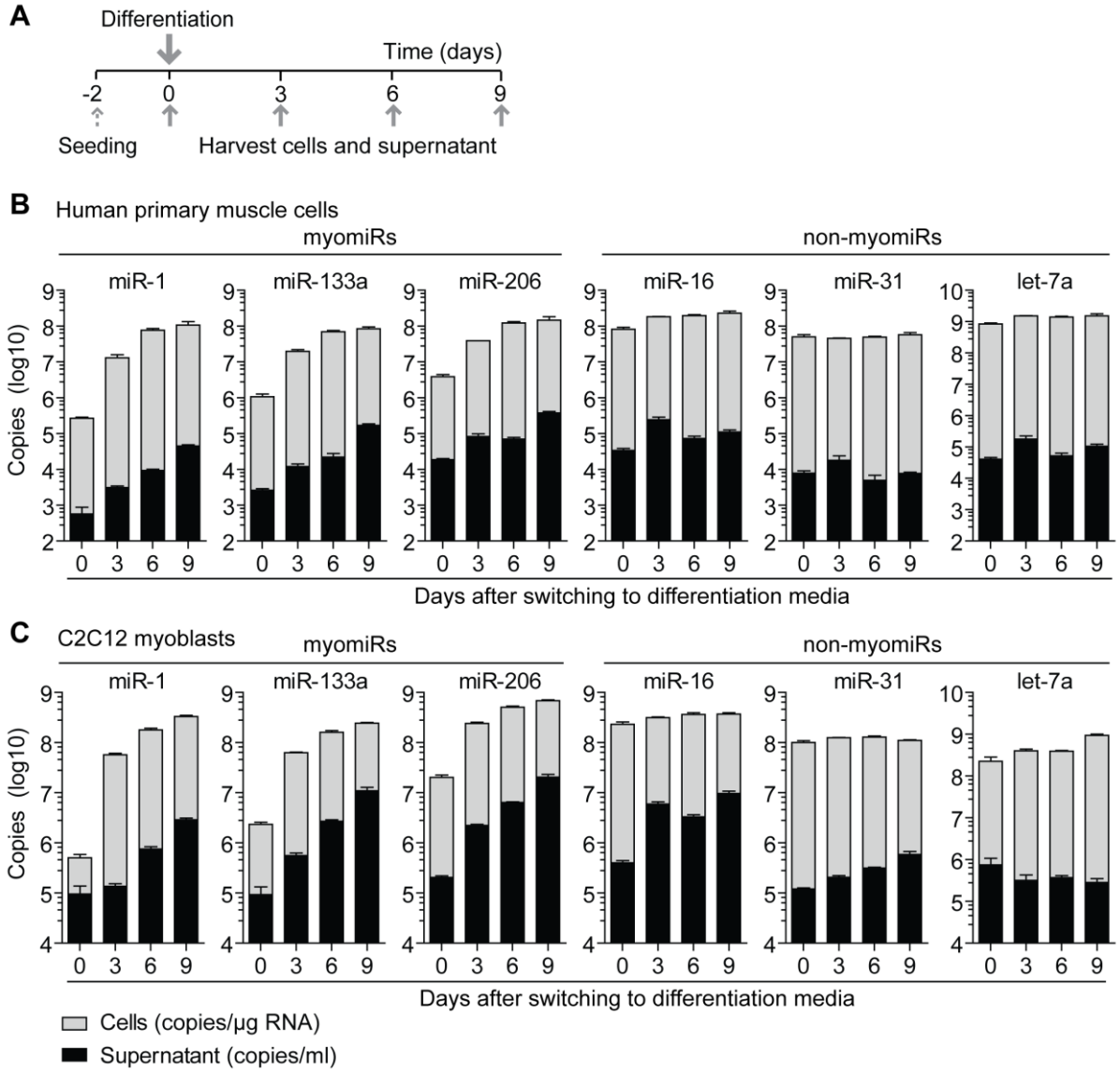

Figure 3.6 Progressive ex-myomiR release during myogenic differentiation in cell culture.
Human and murine myoblasts were differentiated for up to 9 days in reduced serum media. (A) Cells and conditioned media were sampled as indicated. Levels of myomiR and non-myomiR control miRNAs in (B) human primary muscle cells and (C) C2C12 cells were determined by RT-qPCR using synthetic RNA standards for absolute quantification. Expression of cellular miRNAs was normalised to total RNA content (copies/µg RNA). The cell supernatant was sampled over 3 days periods and miRNA abundance reported as copies/ml. Values are mean + SEM, *n*=3-4.

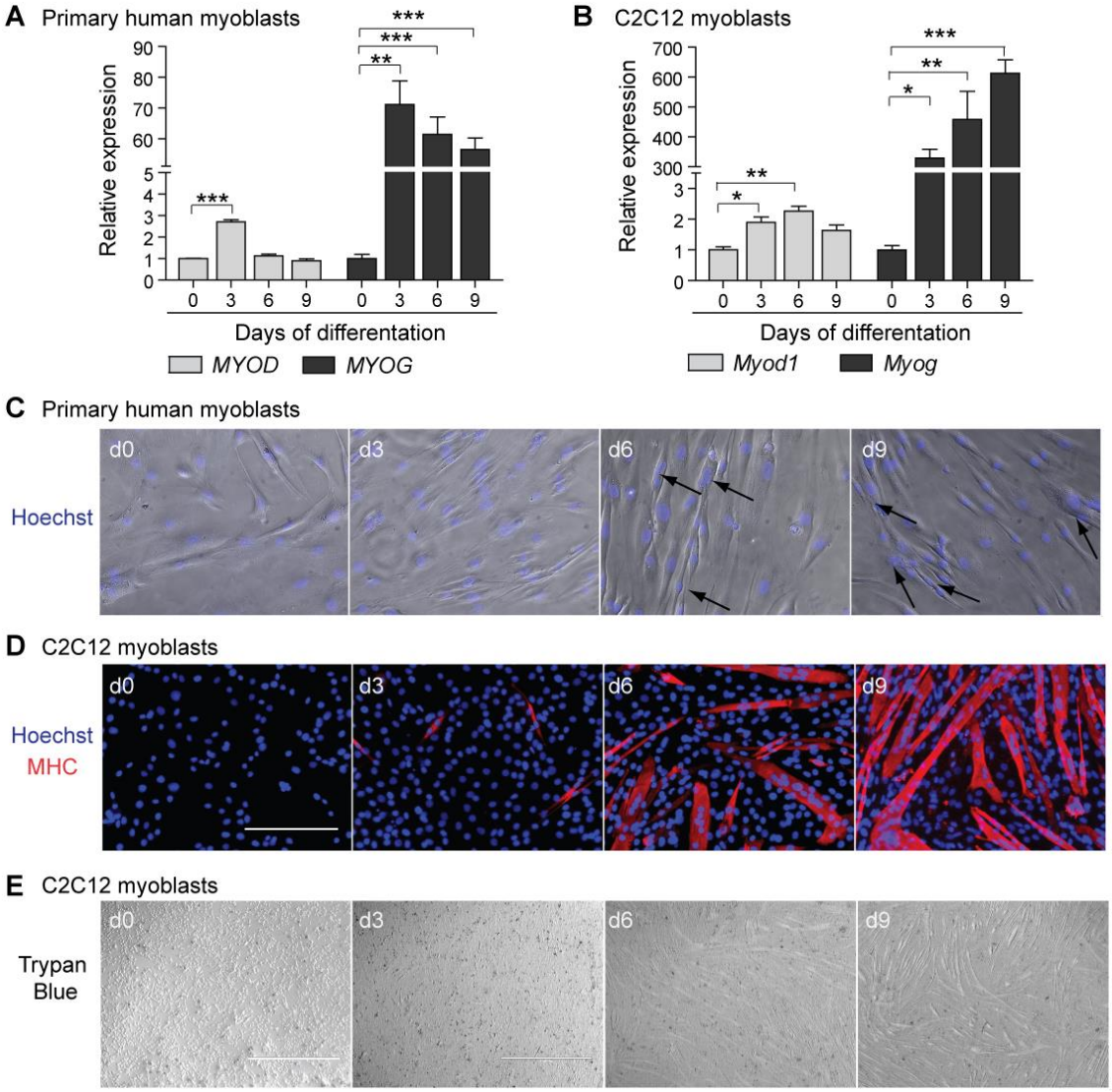

Figure 3.7 Primary human myoblasts and C2C12 cells differentiate into multinucleated myotubes expressing myogenin.

(A) Primary human myoblasts and (B) C2C12 cells were differentiated for 9 days and cells harvested for RNA extraction every three days. Transcript levels were determined by RT-qPCR and normalised to TATA Box Binding Protein (*Tbp*) (C2C12 cells) or β-Actin (*ACTB*) for human myoblasts. *MYOG*/*Myog* levels were progressively upregulated whereas *MYOD1/MyoD1* was transiently expressed in activated myoblasts that are committed to differentiation and subsequently downregulated. (C) Hoechst staining shows multinucleated myotubes for primary human myoblasts from day 6 onwards, as indicated by arrows. (D) MHC staining was performed in C2C12 cells to visualise matured myotubes. Nuclei were stained with Hoechst. Scale bar represents 200 µm (20x magnification). (E) Cell viability was monitored during C2C12 differentiation using a Trypan Blue dye exclusion assay. Scale bar represents 1 mm (4x magnification). All values are mean + SEM. *n*=3. **P*<0.05, ***P*<0.01, ****P*<0.001 (One-way ANOVA, Bonferroni post test).

miRNA	Human primary myoblasts		C2C12 cells	
	Pearson *r*	*P*-value	Pearson *r*	*P*-value
miR-1	0.7809	**0.0027**	0.9291	**0.0000**
miR-133a	0.7515	**0.0048**	0.8878	**0.0001**
miR-206	0.8219	**0.0010**	0.8937	**0.0001**
miR-16	0.3548	0.2577	0.6047	**0.0373**
miR-31	0.1054	0.7444	0.0331	0.9187
let-7a	0.5303	0.0762	-0.3137	0.3208

Table 3.6 Correlation analysis of cellular and secreted miRNA expression.

Pearson correlation coefficient and *P*-values are listed for each myomiR and non-myomiR control (data presented in Figure 3.6).

Apoptosis is known to accompany normal myogenic differentiation, especially during the first few days after serum withdrawal [310]. To ensure the above described progressive increase in ex-myomiRs was not due to passive release by apoptotic cells, cell viability was monitored throughout the course of differentiation using a Trypan Blue dye exclusion assay (Figure 3.7E). Inspection of culture wells revealed relatively few detached cells and only a minority of cells exhibited dye uptake.

In addition, apoptosis was induced in differentiated C2C12 myotubes by treatment with Staurosporine (SP) and miRNA release was measured after 24 hours. Both myomiRs and non-myomiRs were highly enriched (all $P<0.001$, with the exception of miR-31 ($P<0.05$)) in media from apoptotic cultures compared to vehicle (i.e. DMSO) treated cultures (Figure 3.8A). Release of myomiRs was increased by 10-25 fold in media after SP treatment. Non-myomiRs were similarly enriched in apoptotic media (5-25 fold), although miR-16 and let-7a were enriched to a lesser extent. Induction of widespread cell death was confirmed by MTS assay (Figure 3.8B) and fluorescence staining for Annexin V-FITC and propidium iodide (to label early-stage apoptosis and late-stage apoptosis/necrosis respectively) (Figure 3.8C). Given the dramatic increase in myomiR release during differentiation (100-1,000 fold relative to undifferentiated cells) it is unlikely that the non-selective release caused by apoptosis alone can account for ex-myomiR release in differentiating C2C12 culture media.

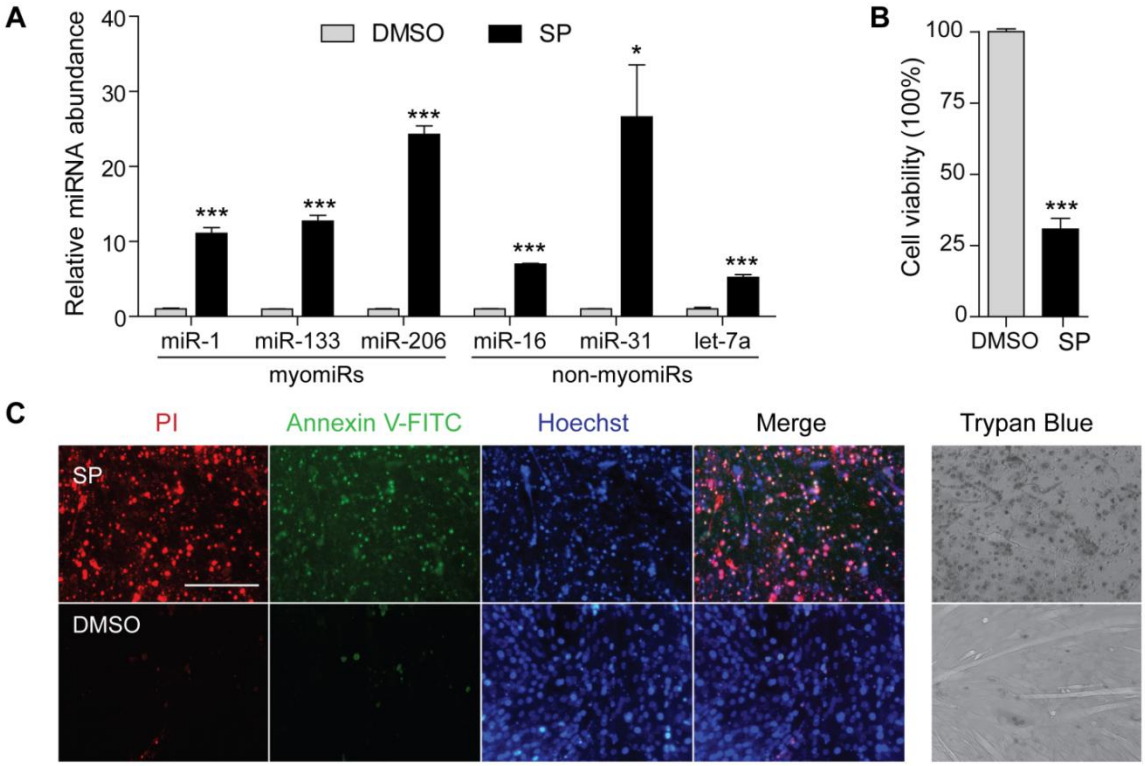

Figure 3.8 Induction of apoptosis in C2C12 myotubes induces indiscriminate ex-miRNA release.

C2C12 cells were differentiated for 6 days and then apoptosis was induced by incubation with 1 µM Staurosporine (SP) for 24 hours. (A) RNA was extracted from conditioned cell culture supernatants and miRNA levels were determined by RT-qPCR. Fold changes in miRNA abundance after SP treatment are shown relative to DMSO-treated control cultures. (B) Cell viability was determined by MTS assay and is reported as a percentage of the DMSO-treated control group. (C) Detection of apoptosis by Annexin V-FITC and Propodium Iodide (PI) fluorescence staining in Staurosporine treated (upper panel) and control cells (lower panel). Scale bar represents 200 µm (20x magnification). Apoptosis was further assessed using Trypan Blue staining to measure cell viability. All values are mean +SEM. **P*<0.05, ****P*<0.001 (unpaired *t*-test, 2 tailed, *n*=3).

In summary, both cell models demonstrate that elevated levels of ex-myomiRs follow myogenic differentiation in healthy, non-dystrophic myoblasts, thus supporting the idea that ex-myomiRs are released under physiological conditions. Additionally, the presented findings demonstrate that absolute expression is not necessarily linked to the amount of miRNA release (as in the case of let-7a), consistent with the hypothesis of a sequence-selective mechanism of miRNA secretion. Finally, the ability to model ex-myomiR release in C2C12 myoblast cultures (with a homogenous cell population with sufficient capacity for both proliferation and differentiation) will be useful for further mechanistic studies.

3.3.5 Kinetics of myomiR release from C2C12 myotubes

Given the specific and progressive increase of ex-myomiRs during cellular differentiation, the release kinetics of myomiRs and control miRNAs were investigated further with the aim to better understand their export stimulus and mechanism. In the preceding experiments, C2C12 myotubes were identified as a suitable and convenient model to monitor myomiR release and consequently they were utilised in the following studies. In order to monitor ex-miRNA export kinetics, differentiated myotubes were washed and then fresh media added. Subsequently, conditioned media was harvested at various time points over the course of three days to monitor ex-miRNA abundance.

Interestingly, a rapid release of miRNAs was observed immediately after replacement of the media (Figure 3.9). Notably, the time point zero (0 hours) refers to differentiation media that has been added to myotubes for a very short amount of time (~2 minutes, similar to a wash) and not fresh media which was shown not to contain any miRNAs related to the species measured (chapter 3.3.3). Nevertheless, the rapid release of such high amounts of miRNAs was unexpected and possible reasons for this phenomenon are discussed in chapter 3.4.3. Importantly, within the first 30 minutes, a continued bulk release was measured for both myomiRs and non-myomiRs which resulted in a further ~10 fold increase ex-myomiR abundance (slightly less for let-7a) compared to the initial measurement at 0 hours. Subsequently, ex-myomiR abundance remained stable for ~4 hours before eventually starting to decline. Importantly, the rate of this decline was different between miRNAs, with ex-miR-1 exhibiting the fastest rate of degradation. After 24 hours, ex-myomiR abundance gradually increased or was unchanged. Interestingly, miR-16 levels did not decline but gradually increased throughout the duration of the time course. In contrast, let-7a decreased immediately after the initial release but levels remained stable after 10 hours. The differences in the rate of decline in ex-miRNA abundance suggest that either some miRNAs are be released into the media at a basal rate whereas others are retained, thus indicating distinct export mechanisms, or miRNA-specific differences in stability. In addition, both of these hypotheses could be true.

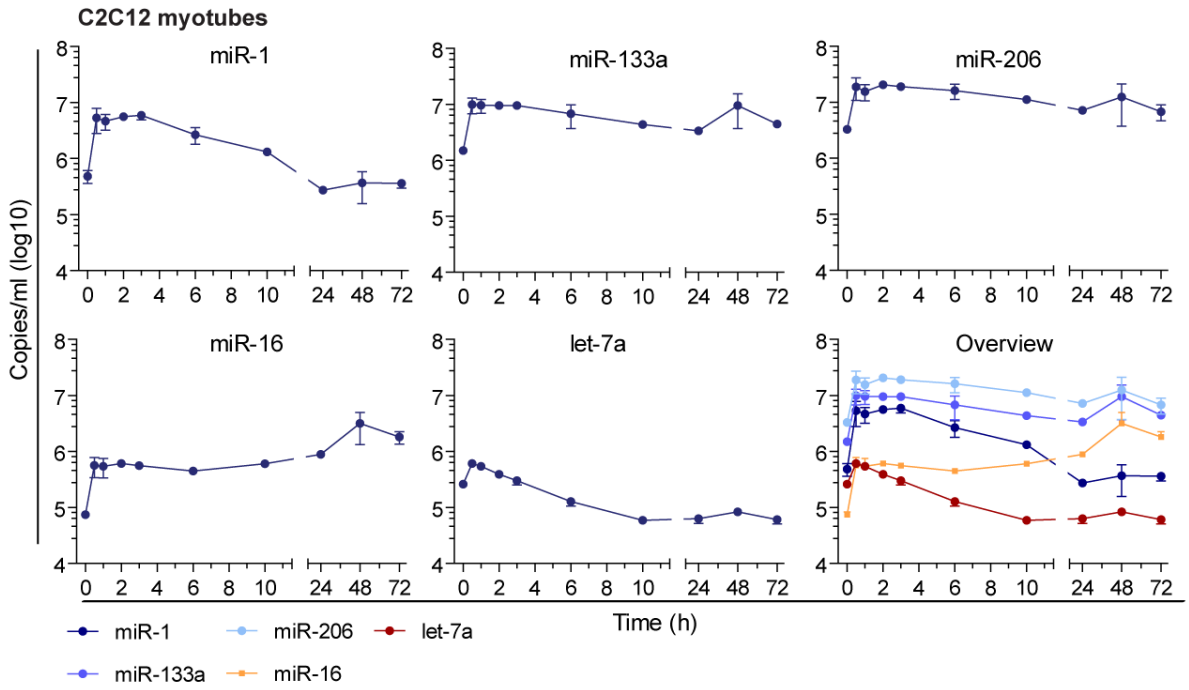

Figure 3.9 miRNAs are rapidly released after replacing the differentiation media.

Time course of miRNA released after replacement of differentiation media. C2C12 cells were differentiated into myotubes with regular changes of media. After 6 days the media was replaced again and cell culture supernatant was sampled at various time points. Ex-myomiR and control miRNA levels were measured by RT-qPCR utilising synthetic RNA standards for absolute quantification. *n*=3. All values are mean +/- SEM.

3.3.6 Stability of extracellular myomiRs in serum and conditioned media

Determining the stability of ex-miRNAs is of importance in order to assess the relation between intracellular and extracellular miRNA levels correctly. The kinetics of intracellular miRNA decay has been shown to be dependent on the 3' end of the miRNA where e.g. untemplated uracil residues are added that subsequently trigger miRNA degradation by exonucleases [311,312]. In contrast, there are currently relatively few studies which have investigated the stability of ex-miRNAs, and the majority of these have analysed RNA stability at room temperature or frozen during storage [156,278,313,314]. These studies are important for determining how best to store and handle biofluid samples for analysis of extracellular nucleic acids, and are relevant to the potential utility of miRNA biomarkers. However, they do not allow any conclusions to be made concerning ex-miRNA stability in the circulation of an organism or myoculture media. In the following section, the stability of ex-miRNAs in either conditioned media or serum was investigated at 37°C to simulate physiological conditions.

Conditioned media was harvested from myotubes and incubated at 37°C. 300 µl aliquots were taken at various time points and immediately stored frozen in TRIzol LS prior to assaying for ex-miRNA abundance (Figure 3.10A). Addition of TRIzol LS effectively inhibits the activity of RNases and proteases and therefore, no further miRNA degradation should occur after sample collection. Ex-miRNA levels were quantified in each sample and the degradation curves were fitted with an appropriate exponential decay model and the inferred ex-miRNA half-lifes were are listed in Table 3.7.

Interestingly, miR-1 was rapidly degraded during the first 10 hours of incubation as indicated by its short half-life (2.4 hours), before plateauing at a level close to the LOQ (discussed in section 2.3). In contrast, miR-133a was remarkable stable over the course of 72 hours with an extrapolated half-life of >18 hours. miR-206 exhibited an intermediate half-life compared to miR-1 and miR-133a and was relatively stable for the first 10 hours, although the concentration then decreased by 10 fold over the

course of 48 hours. The abundance of miR-16 declined over time at a linear rate whereas the concentration of let-7a rapidly decreased during the first 10 hours (similar half-life to miR-1).

In order to investigate the relevance of these findings in the *in vivo* setting, a similar stability time curve study was performed in *mdx* serum which comprises a more complex environment that is likely to better model ex-myomiR stability in the circulation of a whole organism (Figure 3.10B). Fresh serum was incubated at 37°C and 25 µl aliquots were taken at each time point and analysed for miRNA abundance. The miR-223 non-myomiR control miRNA was included for comparison (miR-223 is not secreted by myotubes in culture and there was not analysed in any cell culture studies).

Importantly, the degradation kinetics of all assayed miRNAs in murine serum were highly similar to the rates observed in conditioned media, albeit with different starting concentrations and a general trend towards shorter half-lifes (Figure 3.10C, Table 3.7). Notably, the degradation curves for most ex-miRNAs in serum could only be fitted assuming a two phase exponential decay that consists of a slow and a fast process (Table 3.7). The percentage of decay, that can be accounted for by the fast process is indicated as % fast and specifies the extent to which the fast decay process contributes to the overall observed ex-miRNA degradation (e.g. for miR-206, the slow decay process contributes more towards the overall decay).

In both cases miR-1 was degraded most rapidly and the concentration of this myomiR decreased by a large magnitude (almost 1,000 fold in *mdx* serum). In contrast, miR-133a was much more stable (half-life ~11 hours) and its overall abundance decreased by less than 10 fold during the first 72 hours. Furthermore the half-lifes of the non-myomiRs were likewise comparable to those measured in the cell culture experiment with miR-16 being relatively stable for the initial 8 hours. These observed similarities with the serum data provide further evidence that C2C12 cells are a suitable model to study ex-myomiR biology.

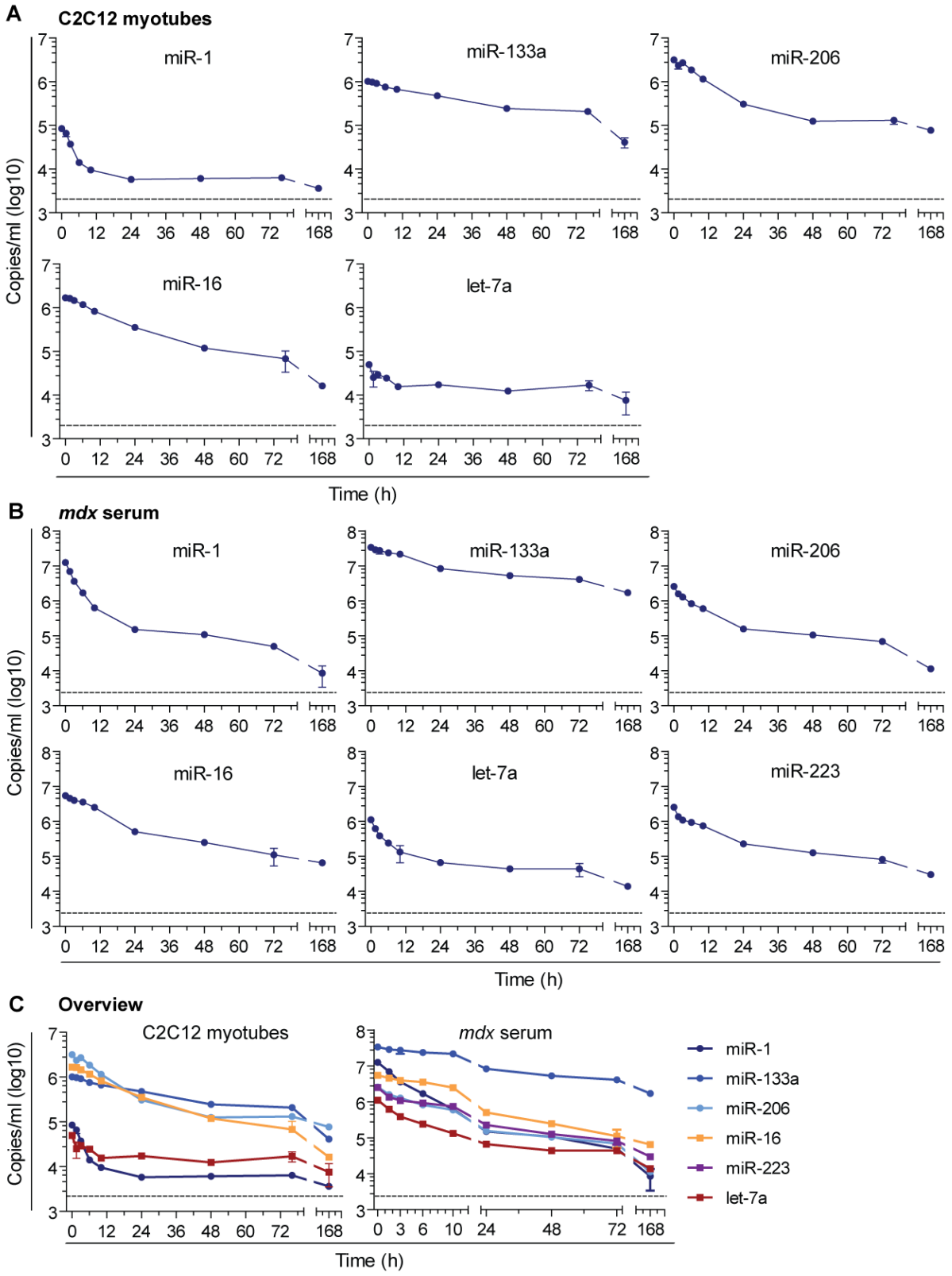
A
C2C12 myotubes
miR-1
miR-133a
miR-206
miR-16
let-7a
Copies/ml (log10)
Time (h)
B
mdx serum
miR-1
miR-133a
miR-206
miR-16
let-7a
miR-223
Copies/ml (log10)
Time (h)
C
Overview
C2C12 myotubes
mdx serum
Copies/ml (log10)
Time (h)
miR-1
miR-133a
miR-206
miR-16
miR-223
let-7a

Figure 3.10 Ex-MyomiRs in conditioned media and murine serum exhibit distinct stabilities.

Either (A) conditioned media obtained from 6 day differentiated myotubes or (B) *mdx* serum was stored at 37°C and aliquots were taken at the indicated time points. The harvested conditioned media was spun for 10 minutes at 2,000 *g* and filtered (0.22 µm) to remove cell debris and large apoptotic bodies that might gradually release miRNAs and thereby obscure the degradation rate (as described in 3.3.2). The abundance of ex-miRNAs was determined by RT-qPCR. (C) Comparison of ex-miRNA decay rates in conditioned media and serum. The limit of quantification (LOQ) is indicated by a dashed line. *n*=2. All values are mean +SEM.

ex-miRNA	C2C12 myotubes		*mdx* serum			
	Half-life (h)	R^2	Half-life (h)			R^2
			fast	slow	% fast	
miR-1	2.36	0.962	1.43	5.53	85.18	0.992
miR-133a	18.40	0.970		11.26		0.926
miR-206	7.23	0.96	0.59	5.60	33.68	0.984
miR-16	9.80	0.980		8.44		0.986
miR-223	N/A	N/A	0.44	9.43	46.72	0.973
let-7a	2.17	0.740	1.06	5.06	64.46	0.990

Table 3.7 Overview of miRNA half-lifes in conditioned media and serum.

The ex-miRNA degradation curves were fitted using either one-phase or two-phase decay model. For four ex-miRNAs in *mdx* serum, the one-phase decay model was insufficient to fit the ex-miRNA degradation curve, thus, an additional component was added to the model. The resulting two phase-decay assumes two different processes that contributes to the overall miRNA degradation, which is indicated by two half half-lifes (slow and fast). The column % fast indicates what percentage of the miRNA degradation can be explained by the fast process alone. h: hours.

In the case of ex-miRNAs present in conditioned media, the observed decline in miRNA abundance may be mediated by proteases (degradation of miRNA carriers) and RNases. In general, protease and RNases may either be secreted by the myotubes themselves or may already be present in the serum containing differentiation media. Typically, these enzymes are more active at the physiological temperature of 37°C than at room temperature. To also assess the influence of serum present in the differentiation media (2%HS), myotubes were this time incubated with serum-free minimal media (Opti-MEM) for 24 hours (maximum amount of time before myotube apoptosis is observed due to the absence of nutrients in the media). Subsequently, the conditioned media was harvested and then either incubated at room temperature or 37˚C and aliquots were collected at 4 different time points (Figure 3.11).

Overall, at 37°C, the abundance of miRNAs decreased during the 24 hour time course, although to a lesser extent than in the serum-containing differentiation media. Consistent with previous observations, miR-133a levels remained stable at both temperatures. Notably, after 24 hours, miR-1 was degraded at a faster rate at 37°C compared to room temperature (Figure 3.11 and Figure 3.10). Similar trends could be observed for miR-206, and miR-16, although the incubation time applied here was insufficient to measure a clear degradation curve for these miRNAs. Consequently these findings indicate that while protease/RNases present in the serum supplement of the differentiation media contribute to miRNA degradation, the most unstable miRNA (i.e. miR-1) is also degraded under serum-free conditions. The latter suggests that secreted protease/RNases are likewise involved in ex-miRNA decay. Notably, let-7a was degraded over time as observed previously, and in contrast to miR-1, temperature did not affect the degradation.

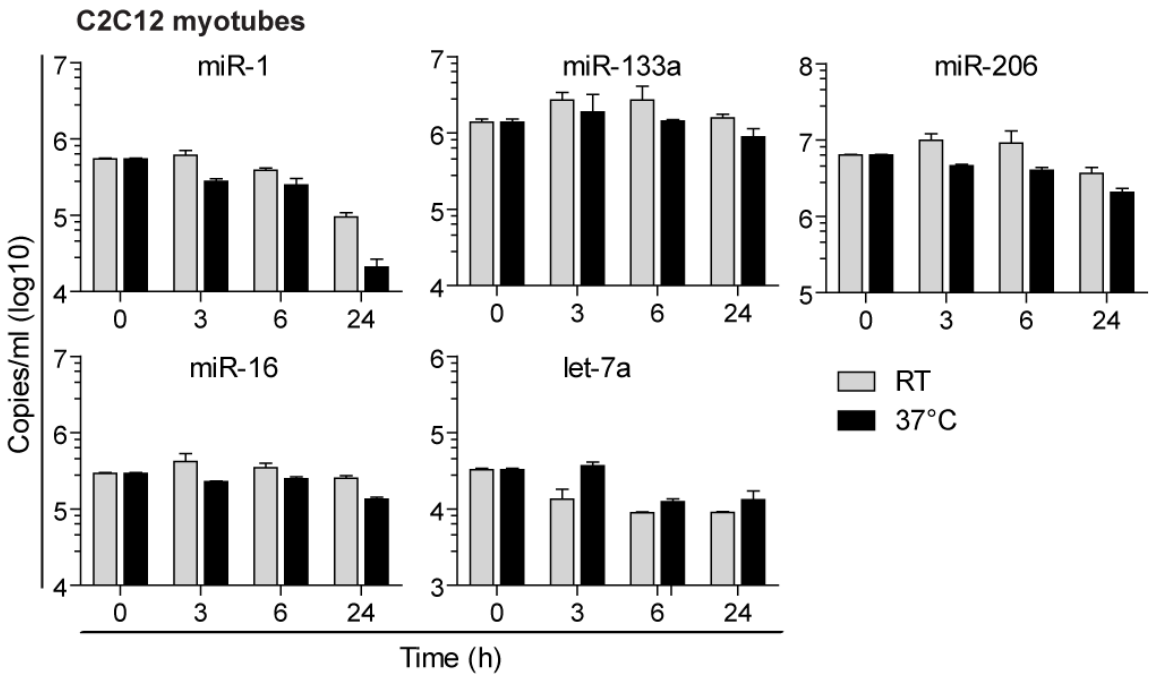

Figure 3.11 Ex-miRNA levels decay slower at room temperature and under serum free conditions.

6 day differentiated myotubes were incubated with serum free media Opti-MEM media for 24 hours. Conditioned media was then harvested and subsequently either stored at RT or 37˚C. 300 µl aliquots were collected throughout the course of 24 hours and assayed for miRNA abundance. All values are mean +SEM. *n*=2

3.3.7 Mechanisms of extracellular myomiR release

Given that the majority of ex-myomiRs are likely to be not associated with vesicular carriers, an unresolved issue is the mechanism(s) by which miRNA-protein complexes are exported from muscle cells. Currently, it is unclear how non-vesicular ex-miRNAs can cross the plasma membrane and be released into the extracellular space since a transmembrane export mechanism for non-lipid-based carriers has not yet been described (as discussed in section 1.4.5). One possibility is that protein-bound miRNAs are initially packaged into vesicles which are released into the extracellular space and are subsequently degraded to liberate their miRNA-protein cargos. To test this hypothesis, GW4869, an inhibitor of neutral sphingomyelinase 2 (nSMase2) was utilised to block exosomes secretion via the ceramide pathway (Figure 1.5) in differentiated C2C12 cells and the effect on myomiR release was monitored. Interestingly, no significant reduction in myomiR abundance was measured when analysing the supernatant of GW4869-treated cells compared with DMSO-treated or untreated cells (Figure 3.12A). Surprisingly, no reduction of let-7a was observed, even though this miRNA has been described to be enriched in EVs at least in human plasma [156]. In order to confirm that the GW4869 treatment successfully down-regulated exosome secretion, EVs from C2C12 myotube conditioned media were isolated via ultracentrifugation (UC). Notably, exosome marker proteins were decreased in the EV preparations isolated from GW4869-treated cells by 60-80% as demonstrated by Western blot (Figure 3.12B). Similarly, NTA showed a ~6 fold decrease in particle numbers after GW4869 treatment, thus confirming the successful inhibition of EV secretion (Figure 3.12C). Given that no reduction in myomiR release in unfractionated conditioned media was observed, ceramide-mediated exosome secretion is unlikely to be responsible for the majority of myomiR release.

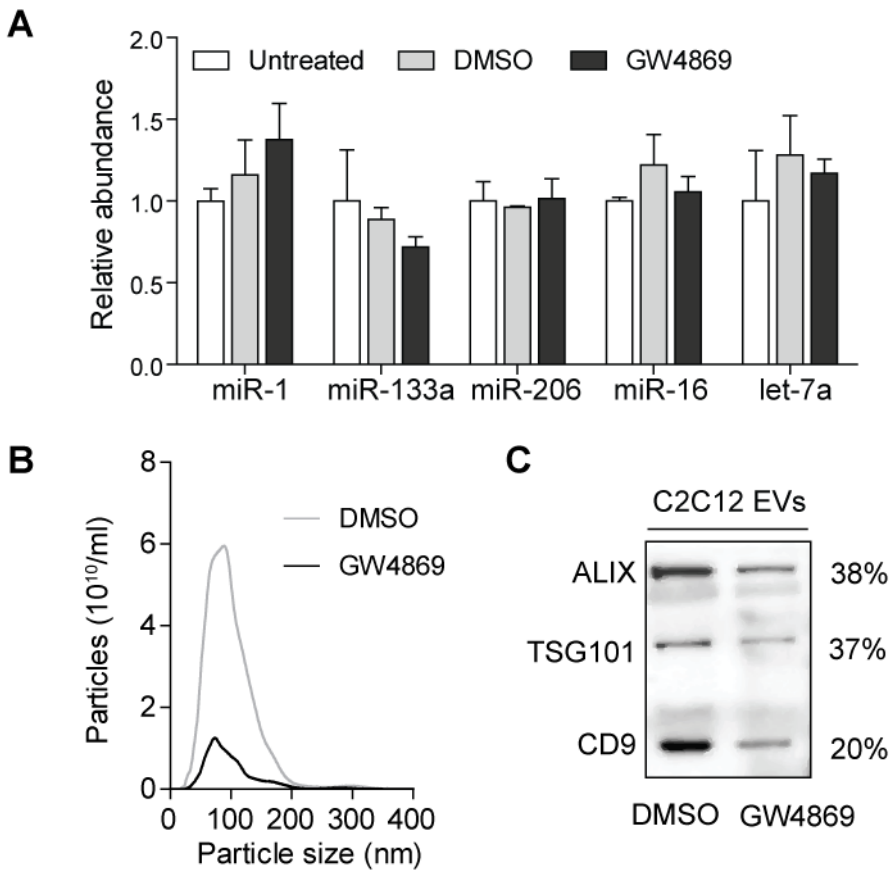

Figure 3.12 Reduction of EV secretion does not affect myomiR release from C2C12 myotubes.

C2C12 cells were differentiated for 4 days and treated with 10 µM GW4869 to block exosome secretion via the ceramide pathway. (A) RNA was harvested from C2C12 myotube culture supernatants and miRNA levels measured by RT-qPCR. Mean values for the untreated group were returned to 1 for each miRNA. To confirm successful decrease in exosome secretion by the small molecule inhibitor, EVs were isolated from drug- and vehicle (DMSO) treated cells. (B) Particle numbers were determined by NTA analysis in isolated EVs of GW4869 and DMSO-treated cells. The modal size was ~80 nm for both samples. (C) Western blot of the isolated EVs showed a decrease in exosomal marker proteins (ALIX, TSG101 and CD9) in GW4869 treated cells compared to vehicle treated cells (DMSO). Values are mean + SEM. *n*=3

3.4 Discussion

3.4.1 MyomiRs are released during periods of myogenic differentiation

While muscle pathology clearly contributes to an enrichment of muscle-specific miRNAs in the circulation, this chapter shows that the release process can also be dynamic and myomiR-specific in various physiological contexts, including during postnatal muscle development, after physical exercise, and as myoblasts differentiate in culture. Firstly, changes in ex-myomiR levels were monitored during postnatal muscle development, a highly coordinated myogenic differentiation process that occurs globally in all muscle groups. In murine muscle, growth during the perinatal phase is supported by rapid accretion of new nuclei from activated satellite cells [291]. Subsequently, the rate of nuclei addition decreases in combination with a reduction in satellite cell numbers per myofibre. After 21 days, the adult level for both the number of nuclei and satellite cells per myofibre is established, with further growth being solely mediated by an increase in the size of the myonuclear domain [291]. In agreement with these previous studies, transcript levels of the satellite cell marker *Pax7* were elevated in *mdx* and wild-type TA muscle during the first 7 days of life. Subsequently, transcript levels decreased in both genotypes and remained low from 21 PND onward. Strikingly, a strong enrichment of serum myomiRs was also found during the first week of life in wild-type and pre-symptomatic *mdx* mice (Figure 3.1), and thus concomitant with the highest rate of satellite activation and myonuclei fusion. In contrast, the period of myofibre growth mediated only by hypertrophy without addition of new nuclei after 21 PND [291], is not accompanied by elevated ex-myomiR levels in wild-type mice. Furthermore, previous studies in 14 day old wild-type and dystrophic mice found no evidence of increased membrane permeability [305], therefore arguing against the passive release of ex-myomiRs due to defects sarcolemma integrity at this age. In summary, elevation of serum myomiR levels occurs during periods of rapid myofibre growth and maturation, concomitant with high rates of myonuclear fusion, and most importantly, in the absence of dystrophic pathology.

Secondly, low level myoinjury caused by downhill exercise was found to induce a biphasic pattern of ex-myomiR release in *mdx* mice. This finding suggests that myomiRs are released both during the initial myofibre degeneration (immediately after exercise), and during subsequent regeneration (5-7 days post exercise). In the present study, miR-1 was the most strongly induced miRNA immediately after exercise in both serum and muscle (Figure 3.2 and 3.3). Previously, similar observations were made for miR-1 in human skeletal muscle after various types of exercise both immediately following exercise as well as up to 10 days later (depending on the mode of exercise and the training status of the individual) [315–317]. Interestingly, it has been shown that administration of exogenous miR-1, miR-133, and miR-206 oligonucleotides in rats accelerates muscle regeneration [318]. Furthermore, miR-206 is highly expressed in newly regenerated fibres [124], is upregulated in skeletal muscle 7 days after cardiotoxin injury, and miR-206 knockout mice exhibit delayed muscle regeneration [319]. Given the importance of myomiRs in regeneration, it is possible that their specific release during postnatal development and after exercise constitutes a regulatory signal which promotes myoblast proliferation and differentiation. Notably, no changes in ex-miRNA levels could be detected after exercise in wild-type mice or during the later days after cardiotoxin injury. Possible explanations for these negative findings are that the stimulus to induce myoblast proliferation followed by myogenic differentiation was insufficient (in the case of exercise) or too localised (only one muscle was affected by cardiotoxin injury) to cause a measurable effect in serum myomiR abundance. Furthermore, it is important to note that myomiR abundance in non-dystrophic mice is inherently low and close to the limit of detection, which complicates the measurement of relatively small changes in abundance compared to background levels. Consequently, it was not possible to clearly separate the effects of regeneration and degeneration/underlying dystrophic pathology on ex-myomiR abundance in this study. To this end, inducing ischemia in the hind-limbs of wild-type mice could be a more severe way to induce degeneration followed by global regeneration and it would be interesting to measure serum myomiR levels in this injury model.

Furthermore, a progressive release of myomiRs during terminal differentiation was observed in myogenic cultures, in line with the *in vivo* findings (i.e. myomiR release in perinatal mice). Differentiation of myoblasts to form multinuclear myotubes in culture has been widely applied as an *in vitro* model of myogenesis [136]. Notably, while regulation of differentiation by intracellular myomiRs has been extensively studied in this cell culture model, changes in ex-myomiRs during differentiation have not been reported previously (to the author's best knowledge). Importantly, both primary human myoblasts and C2C12 cultures exhibited a similar, dynamic pattern with a strong induction of myomiR expression and release, especially at the advanced stages of differentiation (Figure 3.6). The observed pattern of myomiR release coincides with the generation of multinucleated myocytes that express MHC as these begin to be formed after 3 days and mature continuously by fusing with neighbouring myotubes (Figure 3.7). Importantly, this release occurred with only minimal apoptosis and was specific to myomiRs. In contrast, chemical induction of apoptosis/necrotic in C2C12 myotubes (Figure 3.8) resulted in indiscriminate ex-miRNA release, therefore highlighting that although apoptotic cells may contribute to the pool of released miRNAs [157], the observed dramatic increases in ex-myomiR abundance are indictative of selective release [155].

3.4.2 Levels of ex-myomiRs are decreased in aged *mdx* mice

Furthermore, the abundance of serum myomiRs was monitored during aging (Figure 3.5) and a strong decrease in ex-myomiRs abundance was observed in *mdx* mice at 88 weeks of age compared with adult dystrophic mice, thus suggesting that their abundance in the circulation declines as muscle mass is progressively lost (as is the case with serum CK which also declines in DMD patients with advanced pathology [320]). Importantly, the well-described reduction in regenerative capacity of aged muscle [321], especially if mediated by changes in the satellite cell niche, could also be related to ex-myomiR levels. Nevertheless, these data highlight a potential complication for the utility of serum myomiRs as biomarkers of DMD disease progression and response to therapy. Previously,

myomiRs have been shown to be restored to wild-type levels by exon skipping therapy [138,285,286,296]. However, the results presented in this chapter indicate that advanced muscle wasting could also result in a return of ex-myomiRs to wild-type levels on account of the decline in muscle mass, reduction of regenerative potential or age-related changes in dystrophic pathology. Similarly, serum myomiR abundance is also affected by exercise. Consequently, ex-myomiR levels in patient serum must be analysed in the context of other clinical information.

3.4.3 Ex-myomiRs have similar release kinetics but are differentially stable

Interestingly, despite reaching different absolute levels, both myomiRs and non-myomiRs are rapidly released by differentiated C2C12 myotubes within 30 minutes of replacing the culture media (Figure 3.9). These findings are similar to a previous study performed by Wang *et al*. where a sudden burst of miRNAs released by human cancer cells was observed after serum withdrawal [155]. The authors hypothesised that acute serum withdrawal provides a stimulus for miRNA export [155]. However, in the results presented here, the serum concentration in the differentiation media itself was not changed. In addition, a considerable amount of miRNAs was rapidly released into the media after it had only been added to the cells for a few minutes, thus suggesting an active, rapid export mechanism. Another possible explanation of this rapid release might be stress imposed on cells during the changing of media. In addition, some miRNA carrier complexes might be attached to the outside of the cell by weak interaction and may be freed upon adding new media. Independent of release stimuli, the rapid response to media replacement suggests that miRNAs are exported from a pre-existing intracellular pool rather than being newly synthesised. Wang *et al.* observed a reduction in intracellular miRNA concentration after serum depletion that occurred simultaneously with a large increase in ex-miRNAs, therefore supporting the idea that released miRNAs originate from a pre-synthesised pool [155].

Importantly, the observed similarities between the initial release kinetics of myomiR and non-myomiRs may argue against a specific release stimulus for myomiRs that is related to myogenic

differentiation. However, given that the absolute levels differed and do not always correlate with intracellular abundance (i.e. let-7a) it is likely the miRNA export is selective at least in some cases. A noteworthy limitation of this study is the caveat that culture media has to be refreshed before assessing miRNA release kinetics, which introduces an artificial stress situation that may differ from physiological situation of myomiR release *in vivo*. Ideally, release kinetics should be investigated in a steady-state system although this is currently difficult to achieve without a strategy that would allow for the biochemical tracking of specific newly exported miRNAs.

In contrast to the similarities in release kinetics, striking differences in stability between miRNAs in the extracellular space were observed. miR-1, and also let-7a were highly unstable (half-lifes less than 2.5 hours) whereas miR-133a and also, even though to a lesser extent, miR-16, remained stable for hours (half-lifes more than 8 hours) in both conditioned media and serum. The rapid decay of miR-1 and the pro-longed half-life of miR-16 are in line with the findings of Köberle *et al.* when measuring ex-miRNA abundance in human serum incubated at room temperature for 24 hours [314].

To this end, one may hypothesise that the identity of the ex-miRNA carrier is likely to influence the stability of the respective miRNA. However, in the here undertaken experiment, no clear relation was observed between the nature of miRNA carrier and stability. For example, let-7a (described to be enriched in EVs in human plasma [156]) showed a similar degradation rate to miR-1 (likely to be outside EVs). In order to establish such a relationship, it is necessary to better characterise/identify miRNA carriers and to establish the extent to which individual miRNAs are associated with them. These questions are addressed in the chapter 4, where an improved method for separating vesicular from non-vesicular miRNA carriers was investigated.

In general, factors that are likely to influence ex-miRNA stability are miRNA export mechanism, association/dissociation with miRNA carrier, miRNA editing and miRNA primary sequence. Notably, investigation of ex-miRNA stability is essential for understanding absolute serum miRNA levels. For example, miR-133a typically exhibited the highest abundance in adult *mdx* serum, followed by miR-1

and miR-206 (Figure 3.5). Given the low stability of miR-1 compared to miR-133a, one may hypothesise that miR-1 is exported at higher or similar rates as miR-133a, but persists in the circulation for a shorter amount of time. In addition, differential miRNA stability may account for some of the discrepancies observed in between intracellular and extracellular miRNA levels (e.g. [155]). This highlights an important pitfall, because if miRNA stability is not considered, these discrepancies may falsely be interpreted as evidence for selective secretion.

Lastly, a limitation of the current ex-miRNA stability study was that potential differences in ex-miRNA stability between wild-type and *mdx* sera were not assessed to date, which should be addressed in the future. However, given the similarities observed in ex-miRNA stability released by C2C12 myotubes and serum, it seems unlikely that large differences will be found. Furthermore, it is important to note that if miRNA degradation would occur via the 3' end, it would prevent miRNA detection by RT-qPCR due to the inability of the hairpin RT primer to hybridise with the 3' end of the miRNA in the RT step (see Figure 2.1). Consequently, miRNAs that are degraded by 1-2 nucleotides at the 3'end are effectively invisible to small RNA TaqMan RT-qPCR but may still be functionally active given that the seed region is located at the 5' terminus. Small RNA sequencing of serum sample is one solution to address this current limitation, as with this technique, all miRNA species present can be detected.

3.4.4 Ex-myomiR release is independent of ceramide mediated EV release

In this chapter, GW4869-mediated suppression of exosome secretion was applied to test the hypothesis that myomiRs might be initially exported in exosomes that are subsequently broken down in the circulation (Figure 3.12). However, the amount of secreted myomiRs remained constant despite successful downregulation of EV secretion, thus the protein-bound myomiRs are unlikely to be the result of EV turnover. Furthermore, this finding argues in favour of either a yet undescribed, miRNA export process, or direct budding of non-exosomal microvesicles from the cell membrane that is followed by subsequent degradation of these vesicles and liberation of protein-miRNA complexes

in the circulation. To this end, it will be important for future work to identify the export machinery for miRNA-protein complexes in addition to characterising ex-myomiR carriers more closely.

With respect to let-7a, it remains to be elucidated why no reduction in extracellular abundance was found, even though a reduction in EV release was confirmed. A possible explanation may be that let-7a is enriched in a certain subpopulations of EVs which are exported independently from the ceramide pathway. To this end, a recent study describes distinct EV subpopulations which can be separated from the main EV fraction by more a complex purification protocol including sucrose density gradient centrifugation. Consequently, the changes observed here in numbers of EVs purified by UC may not be reflective of changes in this subpopulation [322].

3.4.5 Conclusion

In summary, myomiR release accompanies periods of myogenic differentiation and therefore serum myomiR abundance is likely to be a function of muscle mass and growth, degenerative/regenerative status, and tissue expression levels. Furthermore, myomiRs are differentially stable both in conditioned media as well as in murine serum which is likely to have a significant effect on absolute ex-myomiR levels measured in at the steady-state.

In conclusion, specific increases in serum myomiR abundance during periods of muscle growth, after exercise-induced injury, and concomitant with myogenic differentiation suggests that myomiR release is not exclusively a consequence of leakage from damaged or dystrophic muscle undergoing apoptosis/necrosis. Therefore it is possible that under some circumstances the presence of myomiRs in the serum may serve a physiological function. Despite a plethora of studies investigating the role of miRNAs during stem cell proliferation and progenitor cell differentiation (reviewed in [323]), the influence of secreted miRNAs on these processes is currently not well understood. While this work was focused on circulating miRNAs relating to myogenesis/muscle regeneration, one may hypothesise that ex-miRNAs release could accompany alternative developmental processes and/or cellular differentiation in other lineages, thus comprising a general biological phenomenon that is not exclusive to muscle.

4. Results II

Separation of vesicular and non-vesicular extracellular miRNA carriers by size-exclusion chromatography

4.1 Introduction

One possible approach to better understand how ex-myomiR are stabilised in the blood circulation, is to separate vesicular and protein-based miRNA carriers from biofluid samples and measure the abundance of miRNA levels in each of these fractions. Currently, the most established protocol for EV purification is differential ultracentrifugation (UC), first described in 2006 by Théry *et al.* [284]. However, it has become increasingly evident that this methodology is relatively crude with significant limitations. Specifically, UC-based isolation methods often result in poor yields and may compromise vesicle integrity as centrifugation at high speed can cause EV aggregation, fusion and/or rupture [324]. Furthermore, UC has the disadvantage to at least partially co-pellet large protein complexes [324]. Alternative methods that have been developed in recent years include liquid chromatography (size-exclusion chromatography (SEC), high performance liquid chromatograph (HPLC), fast protein liquid chromatography (FPLC)) and immunoaffinity capture approaches (reviewed in [325]). In this chapter, an improved methodology for EV isolation that combines ultrafiltration and size-exclusion-chromatography (UF-SEC) was utilised to determine distribution profiles for ex-miRNAs in complex biofluids, such as conditioned media from myotube cultures and serum. This technique has been established for fractionation of conditioned media derived from a variety of cell types by the Wood group and enables isolation of intact EVs with high purity and yield [224]. Furthermore, the technique allows for large-scale isolation of vesicles which is of relevance for the development of EV-based therapeutics.

In brief, SEC separates analytes on the basis of their size, and given that size and mass are typically correlated, also their molecular weight. In this study, sephacryl was used as a gel filtration media, packed into a 120 ml column. Sepharcryl consists of an allyl dextran and N,N'-methylene bisacrylamide cross-linked matrix, and is available at different porosities as determined by the dextran content. Here, the S-400 model (GE Healthcare) was utilised, which has a fractionation range of 20–800 kD and is suitable for separation of vesicular structures and other macromolecules (e.g. serum proteins).

Despite the importance of efficient and pure EV isolation from blood for clinical and diagnostic applications, relatively few studies have so far utilised SEC for EV isolation from these extremely complex biofluids [224,326–329]. Consequently, the technique is still in its infancy and referenced reports vary with respect to column packing materials, vesicle purities and obtained yields.

In the following section, the aim was to utilise UF-SEC to separate EVs from non-vesicular components and to subsequently profile the distribution pattern of ex-miRNAs (both myomiRs and non-myomiR controls). Given the high complexity of serum, UF-SEC methodology was initially tested utilising conditioned media derived from myotubes. In addition to studying the myomiR distribution pattern, it was also of interest to compare EV characteristics, such as particle size and numbers with the aim to determine a possible impact of dystrophic pathology on the biological properties of circulating EVs. To this end, changes in the secretome of dystrophin-deficient muscle cells has been described [268], but *in vivo* validation of this concept is as yet lacking.

4.2 Materials and methods

4.2.1 Animal work and clinical biochemistry assays

Animal studies including PPMO injections were conducted as described in section 2.1. All animals utilised in this chapter were male, 8-12 week old *mdx* or C57BL/10 wild-type mice (abbreviated as C57). Clinical biochemistry assays to determine the concentration of free cholesterol, free fatty acids, HDL, LDL, triglycerides and glycerol in fractionated or crude serum samples were performed at the clinical pathology laboratory, Medical Research Council Harwell (Oxford, UK).

4.2.2 EV isolation by UC and UF-SEC

Condition media and sera samples were collected as described in chapter 2 and section 3.2.2. The general workflow for EV isolation by UF-SEC is outlined in section 2.5 and illustrated in detail in Figure 2.3. Alterations to this protocol with the aim of optimising separation for serum samples are highlighted in this results chapter for the respective experiment as appropriate. Notably, only cell culture supernatant requires UF to concentrate the sample prior to loading on the liquid chromatography column, since the volume of serum samples was less than the maximum volume that can be injected into the column. After fractionation, both conditioned media and serum samples were concentrated via UF on 10 kD filters (Figure 2.3). For reasons of convenience, both fractionation processes are commonly referred to as UF-SEC in this chapter.

Protein and RNA concentrations in the fractionated samples were measured using micro BCA Assay (Thermo Fischer) and Quant-iT RiboGreen RNA Assay Kit (Life Technologies), respectively.

4.3 Results

4.3.1 Ex-myomiR distributions in UF-SEC fractioned, myotube conditioned media

Given that differentiated C2C12 cells appear to be a suitable model for myomiR release, as shown in chapter 3, this cell line was also utilised here to gain further insight into the nature of ex-myomiR carriers. In addition, conditioned media from C2C12 myotubes can be obtained at a large quantity which allows using more input material and thus facilitates downstream detection of exosomal markers in the separated fractions.

Firstly, C2C12 cells were differentiated for four days and then conditioned media was harvested over a 48 hour time-period, processed as described in section 3.2.2 and concentrated via UF. During SEC, protein content was monitored by measuring the absorbance at 280 nm (Figure 4.1A). Based on the absorbance trace and extensive previous data from the Wood group, the individual 2 ml fractions obtained from the liquid chromatography were pooled into four new fractions (F1-4), concentrated via UF to ~200 µl and subjected to downstream analysis (Figure 2.3). EVs are large in size (~80-120 nm) and are therefore expected to elute early during SEC (shortly after the 30 ml void volume of the column) as they are not anticipated to interact with the porous material in the column. Consequently, EVs are typically contained in fraction 1 (F1) as shown previously for other cell lines by the Wood group [224]. In contrast, protein complexes are typically much smaller in size and elute later during the fractionation process as indicated by the prominent peak in 280 nm absorbance trace (Figure 4.1A). Nanoparticle tracking analysis (NTA) of F1 demonstrated a modal particle size of ~80 nm in this fraction (Figure 4.1B). In addition, exosome marker proteins ALIX (PDC6IP) and TSG101 [161] were highly enriched in F1 as determined by Western blot (Figure 4.1C). Together these findings confirm that EVs contained in F1 exhibit typical exosomal properties.

Next, RNA was extracted from each of the four concentrated fractions and miRNA abundance was assayed by RT-qPCR. Notably, the ex-myomiRs showed a similar pattern of abundance with ~80% of

each miRNA detected in F4 and ~20% in F3 (Figure 4.1D). Conversely, less than 1% could be detected in F1, thus demonstrating that ex-myomiRs are predominantly present in small protein complexes, while only small minority are associated with vesicles. In particular, let-7a was found to be most abundant in the vesicular fraction F1 (~40%), followed by F2.

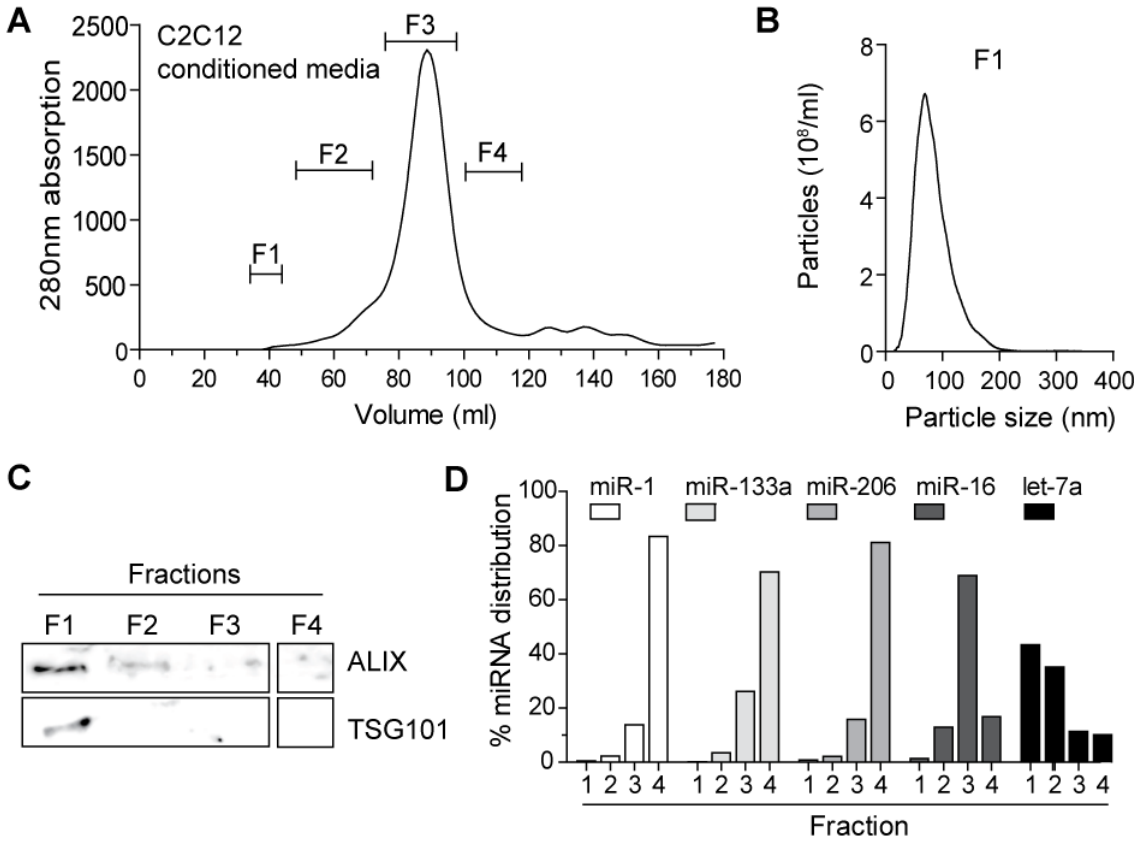

Figure 4.1 Ex-myomiRs in myotube-conditioned media are predominantly non-vesicular.
50 ml of conditioned media collected from differentiated C2C12 cells was fractionated via UF-SEC. (A) The protein content was monitored using the 280 nm absorbance and eluates were pooled into 4 new fractions as indicated. (B) NTA analysis shows a modal particle size of ~80 nm in F1. (C) Exosomal protein markers (ALIX and TSG101) were highly enriched in F1 as determined by Western blot analysis. (D) RNA was extracted from each pooled fraction and miRNA abundance measured by RT-qPCR. Values are depicted as the percentage distribution across all of the fractions.

4.3.2 Distribution profiling of ex-myomiRs in UF-SEC fractionated serum

Following the successful fractionation of myotube-derived conditioned media, it was of interest to establish the distribution profile vesicular and non-vesicular miRNAs for serum samples. One important question to address was how much serum material is required to generate sufficient EV yield for downstream analysis. In contrast to cell culture supernatant, the input material is of limited availability, in particular when blood of individual mice should be fractionated (as opposed to pooling serum samples from multiple mice). However, increasing the input material may facilitate downstream analysis, especially in terms of detecting exosomal markers, which is more challenging in serum than in conditioned media due to the aforementioned complex composition of serum. In addition, it is currently not entirely clear what the typical concentration of EVs in murine blood is, thus impeding estimations regarding an appropriate serum input volume. In contrast, if too much material is loaded onto the liquid chromatography column, filters might clog and the resolution of separation may decrease. Considering all these factors, 1 ml of pooled serum of three *mdx* mice was fractionated in the first instance (Figure 4.2).

The 280 nm absorption trace showed a clear protein peak that had two adjacent smaller peaks on either side. Furthermore, a peak of much smaller magnitude eluting at ~45 ml was visible. The eluate was subsequently pooled into 6 new fractions, based on the individual peaks observed in the 280 nm absorbance trace (Figure 4.2A). According to the early elution time, fraction 1 (F1) was predicted to comprise the vesicular fraction, whereas F3-F5 contain protein complexes and potentially very small vesicles such as HDL and LDL vesicles (section 4.3.4). F6 contains everything that elutes later than one whole column volume, e.g. small single proteins that interact with the column pores for an extended amount of time. F2 is likely to be an intermediate fraction, with very little protein content (according to the 280 nm absorbance) that may contain a mixture of both smaller vesicles and larger protein complexes (section 4.3.4).

NTA analysis demonstrated that vesicles in F1 had a modal size of ~65 nm (Figure 4.2B), thus, slightly smaller than EVs released from myotube cultures. Detection of specific bands for exosomal protein markers by Western blot failed in all fractions, possibly due to the complex composition of the sample. However, ELISA analysis determined that the CD63 antigen (a surface protein for exosomes [161]), was most abundant in F1 relative to total protein content (Figure 4.2C), thus confirming EV enrichment in this fraction.

Subsequently, myomiR abundance was measured in each fraction by RT-qPCR. Consistent with the cell culture findings, only 1% of ex-myomiRs were found in the early vesicular fraction F1 and the majority of ex-myomiRs were found to be highly abundant in the later eluting fractions with high protein content. This finding is in line with what Roberts *et al.* previously determined utilising cruder methods for EV isolation [207]. Furthermore, this data is consistent with an already earlier referenced study in human plasma which observed that let-7a is enriched in vesicles whereas miR-16 is predominantly non-vesicular [156]. These consistencies underline the robustness of the UF-SEC fractionation methodology. The observed similarities between the miRNA distribution pattern in myotube supernatant and that of serum provide further evidence that C2C12 cultures faithfully model *in vivo* myomiR release.

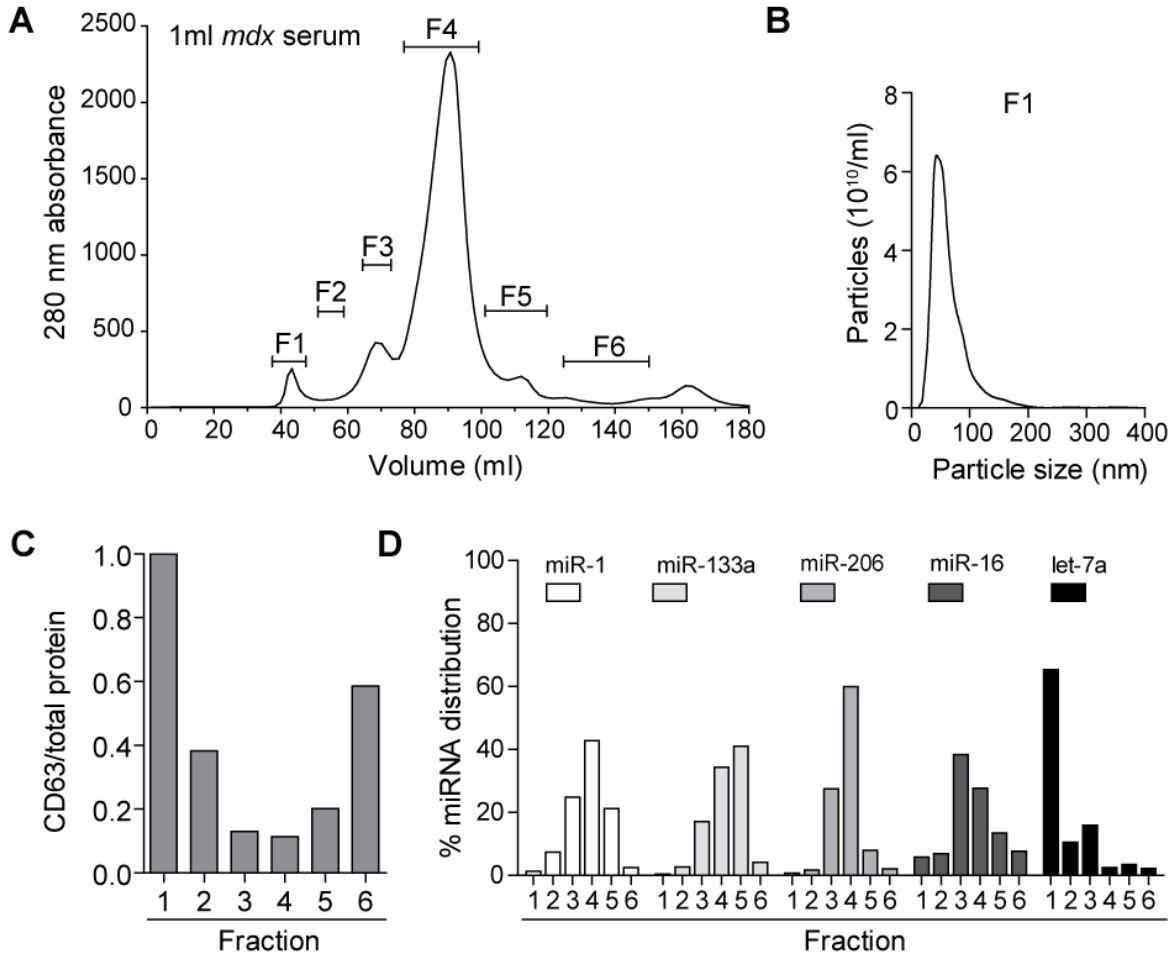

Figure 4.2 Ex-myomiRs in *mdx* serum predominantly co-elute with protein-rich fractions.

(A) 1 ml of pooled serum from 12-week old male *mdx* mice was fractionated by UF-SEC and the eluates were pooled into six new fractions as indicated in the 280 nm absorbance trace. (B) NTA analysis shows a modal vesicle size of ~65 nm in F1. (C) CD63 abundance was quantified using ELISA and normalised to total protein concentration to indicate fraction purity. (D) RNA was extracted from each fraction and miRNA abundance was quantified by RT-qPCR and normalised as described above.

4.3.3 UC-SEC fractionation of murine serum samples

Given that efficient isolation of pure EVs from serum is of importance for EV-based biomarker detection and also therapeutic exosome production, the SEC protocol was modified to determine if EV purity could be improved further. Even though in the preceding experiments it was found that ex-myomiRs are primarily non-vesicular, an improved methodology is still of high importance since there is a high interest for vesicle-based biomarkers for a variety of pathologic conditions including cancer and tissue injury (reviewed in [330]). To this end, reducing the complexity of the EV fraction further (i.e. isolating highly pure EVs) would facilitate profiling studies to identify new vesicle-based miRNA or protein biomarkers. Furthermore, differential abundance for putative EV-associated biomarkers may be more pronounced in fractionated serum compared to crude serum extract [331].

Given the high protein concentration of serum samples, a UC pre-spin preceding SEC (UC-SEC) might be advantageous to increase the purity of subsequently isolated EVs (Figure 2.3). To this end, the pre-spin may reduce the presence of lipoprotein complexes such as High-and Low-density-lipoproteins (HDL/LDL) which have been shown to also carry ex-miRNAs [159] and may contaminate the vesicle containing fraction(s) using the standard UF-SEC protocol. In contrast, HDL and LDL are not expected to pellet during the UC spin [332]. Similarly, soluble proteins and protein complexes are expected to largely remain in the supernatant. Consequently, the UC pre-spin is predicted to help eliminate protein and lipoprotein-associated miRNAs from the vesicular pellet.

To compare the performance of a pre-spin with the existent direct UF-SEC protocol, 300 µl of *mdx* serum was divided into 150 µl aliquots and fractionated either by UC-SEC or direct fractionation by SEC (Figure 4.3A). For the UC-SEC methodology, the serum was prepared as outlined in Figure 2.3 and subjected to one round of ultracentrifugation (70 minutes at 100,000 *g*). The obtained pellet (UC-P) was re-suspended in 5 ml PBS and the UC supernatant (UC-SN) was concentrated on a 10 kD cut-off filter. Particle size and number in the unfractionated crude serum sample, UC-SN and UC-P were determined via NTA (Figure 4.3B-C). Only ~1% of the particles in the original serum sample

were recovered in the UC-P and the large majority of many particles remained in the UC-SN. Although those were on average smaller particles (~50 nm) that are likely to comprise a heterogeneous particle population (not only EVs), this finding is suggestive of an overall poor EV recovery of the UC pre-spin.

Next, the resuspended UC-P was fractionated by SEC (Figure 4.3D). In line with the NTA findings, the 280 nm absorbance traces of the UC-SEC fractionated sample were difficult to interpret as the total protein content was very low. Nevertheless, the eluate was combined into 4 new fractions with F1 being the putative vesicular fraction based on elution time. The remaining eluate was concentrated into only 3 other fractions as the 280 nm trace had less peaks compared to the UF-SEC fractionated sample. Each of the new UC-SEC fractions was concentrated via UF and analysed by NTA (Figure 4.3E-F). Importantly, due to the poor efficiency of EV pelleting in the pre-UC spin, particle counts after UC-SEC were very low throughout all fractions. In addition, the NTA size distribution pattern of F1 indicated that vesicles were of very heterogeneous size and the vesicles were larger than that typically considered to be characteristic of EVs, therefore suggesting EV fusion might have occurred. Both poor EV yield as well as vesicle fusion have been described previously during UC-based EV isolation protocols [224].

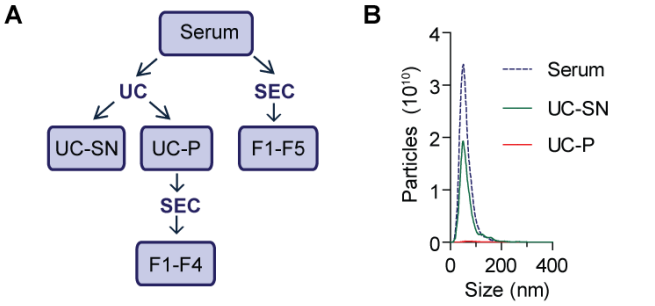

C

Sample	Particle				
	Mean (nm)	Mode (nm)	Conc. (10^{10}/ml)	Number (10^{10})	Recovery (%)
Serum	61.7	51.0	1165.3	151.5	100.00
UC-P	97.3	67.0	15.0	1.5	0.99
UC-SN	68.1	50.0	881.6	88.2	58.19

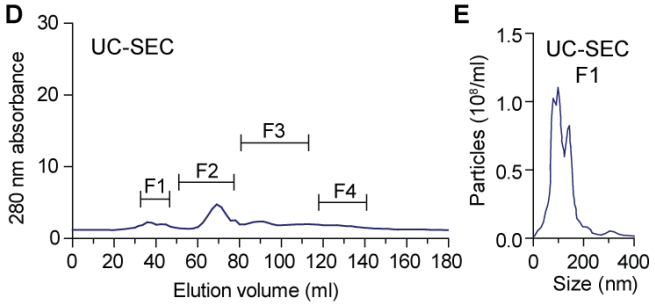

F

Sample	Particle				
	Mean (nm)	Mode (nm)	Conc. (10^{10}/ml)	Number (10^{10})	Recovery (%)
UC-P	97.3	67.0	15.0	1.5	100
F1	140.8	128	0.55	0.11	7.33
F2	111.2	81	2.28	0.46	30.67
F3	122.8	72	1.16	0.23	15.33
F4	142.5	100	0.21	0.04	2.67

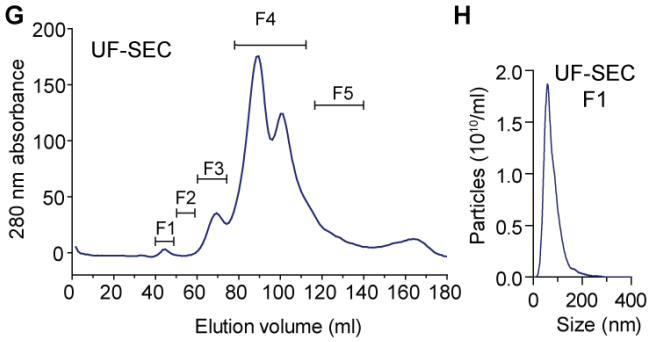

I

Sample	Particle				
	Mean (nm)	Mode (nm)	Conc. (10^{10}/ml)	Number (10^{10})	Recovery (%)
Serum	61.7	51.0	1165.3	151.5	100.0
F1	77.7	58.0	103.8	12.5	8.2
F2	79.9	56.0	38.8	4.7	3.1
F3	71.4	52.0	87.9	10.6	7.0
F4	58.2	45.0	187.1	22.5	14.8
F5	87.0	52.0	4.1	0.5	0.3

Figure 4.3 Comparison of UC-SEC and UF-SEC serum fractionation.

(A) Graphical outline of the workflow to compare efficiency of UC-SEC and UF-SEC. 300 µl of an 8 week old male *mdx* mouse was divided into two 150 µl aliquots and fractionated as indicated. (B) NTA size distribution profile of the original serum sample, the UC pellet (UC-P) and the UC supernatant (UC-SN). (C) Table indicating mean and mode particle size, particle concentration, total particle count and recovery rate of the UC-P and UC-SN as determined per NTA. 280 nm absorbance trace of (D) the re-suspended UC pellet and (G) serum sample. Eluates for both samples were pooled into 4/5 new fractions as indicated. NTA size distribution profile of F1 from either (E) the UC-SEC or (H) the UF-SEC fractionated sample. Table indicating mean and mode particle size, particle concentration, total particle count and recovery rate of the (F) UC-SEC and (I) UF-SEC fractionated sample as determined per NTA.

The second aliquot of the serum sample was fractionated via UF-SEC as described earlier in this chapter (with the slight alteration that the liquid chromatography eluate was pooled in only 5 fractions to match the elution range with the UC-SEC fractionated sample) and likewise analysed by NTA (Figure 4.3G-I). In contrast to the UC-SEC methodology, the 280 nm absorption trace showed a clear vesicular peak, suggesting a much higher vesicle recovery. In addition, more than 100 times more particles were detected in F1 of the UF-SEC fractionated sample. The NTA size distribution profile of F1 showed a well-defined particle peak with a modal size of 58 nm similar to the findings in section 4.3.2. Furthermore, 8% of all input particles were detected in F1 of the UF-SEC fractionated sample, indicating efficient EV isolation with this protocol (Figure 4.3I). Notably, F4 also contained many particles, although, due to their late elution time and small size, these are likely to be of non-vesicular nature (i.e. LDL particles). This hypothesis was subjected to further investigation as described in the next section (4.3.4).

Given the poor recovery of EVs in addition to their heterogeneous size distribution following the UC-pre spin, this modification to the UF-SEC methodology was deemed unsuitable for serum fractionation since the low yield would impede EV downstream analyses such as profiling of the EV proteome or miRNome. As such, further investigations using this alternative methodology were discontinued.

4.3.4 Distribution profiling of RNA, protein and lipid metabolites

Based on the difficulties associated with a pre-spin, the experiments in this section sought to further characterise the individual fractions of the UF-SEC fractionated sera in order to determine the RNA and protein distribution pattern, and to investigate to what extent lipoprotein complexes may be present in the vesicular fractions.

Three independent samples of 300 µl of *mdx* sera were fractionated via UF-SEC, the eluate pooled into six new fractions as described in section 4.3.2 and the RNA/protein content quantified in each individual fraction (Figure 4.4A). As indicated by the 280 nm trace, the majority (~70%) of the serum protein was found in F4, followed by F5. Less than 3% of the total protein and RNA was detected in F1. Interestingly, the RNA content was distributed across the fractions in a highly similar pattern to that of the protein content, indicating that it is likely that most of the extracellular RNA is associated with RNA binding proteins (RBPs). Protein and RNA content was also quantified in the input serum sample and the overall recovery rate after the UC-SEC was determined to be ~50% for protein and slightly higher for RNA (Figure 4.4B). Most likely the majority of material loss occurred during UF due to its association with the the filters.

In order to investigate the distribution of lipids and lipoproteins across the fractions, standard colorimetric assays were utilised to determine the concentration of free cholesterol, free fatty acids, HDL, LDL, triglycerides and glycerol in crude serum (Figure 4.4C) and UF-SEC fractionated samples (Figure 4.4D). Importantly, LDL and Cholesterol were exclusively detected in F4 for all samples. Similarly, HDL was highly enriched in F4 and a small amount was detected in F5 (<5%). The size of HDL ranges between 7-13 nm, whereas LDL is larger (18-23 nm), which explains the presence of HDL in F5 [333]. Likewise, free fatty acids were most abundant in F4 and F5 but could be detected in all fractions, albeit only at very low levels. Glycerol was found across all fractions whereas triglycerides were most frequently detected in F2 and F3 (30-40%). Notably, triglycerides are typically delivered to skeletal muscle, heart and adipose tissue by very low density lipoproteins (VLDL). With diameters

ranging from 23-35 nm and sometimes even up to 60 nm, VLDLs comprise the largest of all lipoproteins and are therefore also the most likely particles that may co-elute with the serum EVs [333]. A direct measurement of VLDL by a simple clinical chemistry assay is difficult (requiring pre-separation of the lipoproteins in the sample by repeated gradient density ultracentrifugation). Consequently, the concentration of VLDL is often inferred by the abundance of triglycerides as they are associated with each other in the circulation at a relatively constant ratio [334]. Since triglycerides were primarily enriched in F2 (40%), and to a lesser extent in F3 (~25%), it is likely that VLDL primarily elutes in fractions F2 and F3. Taken together, these results suggest that the UF-SEC methodology allows for separation of the vesicular fraction F1 from the majority of lipoproteins (some contamination of VLDL cannot be excluded) and serum proteins/RNAs. In contrast, the protein-and RNA-rich fraction F4 is co-elutes with the large majority of HDL and LDL particles.

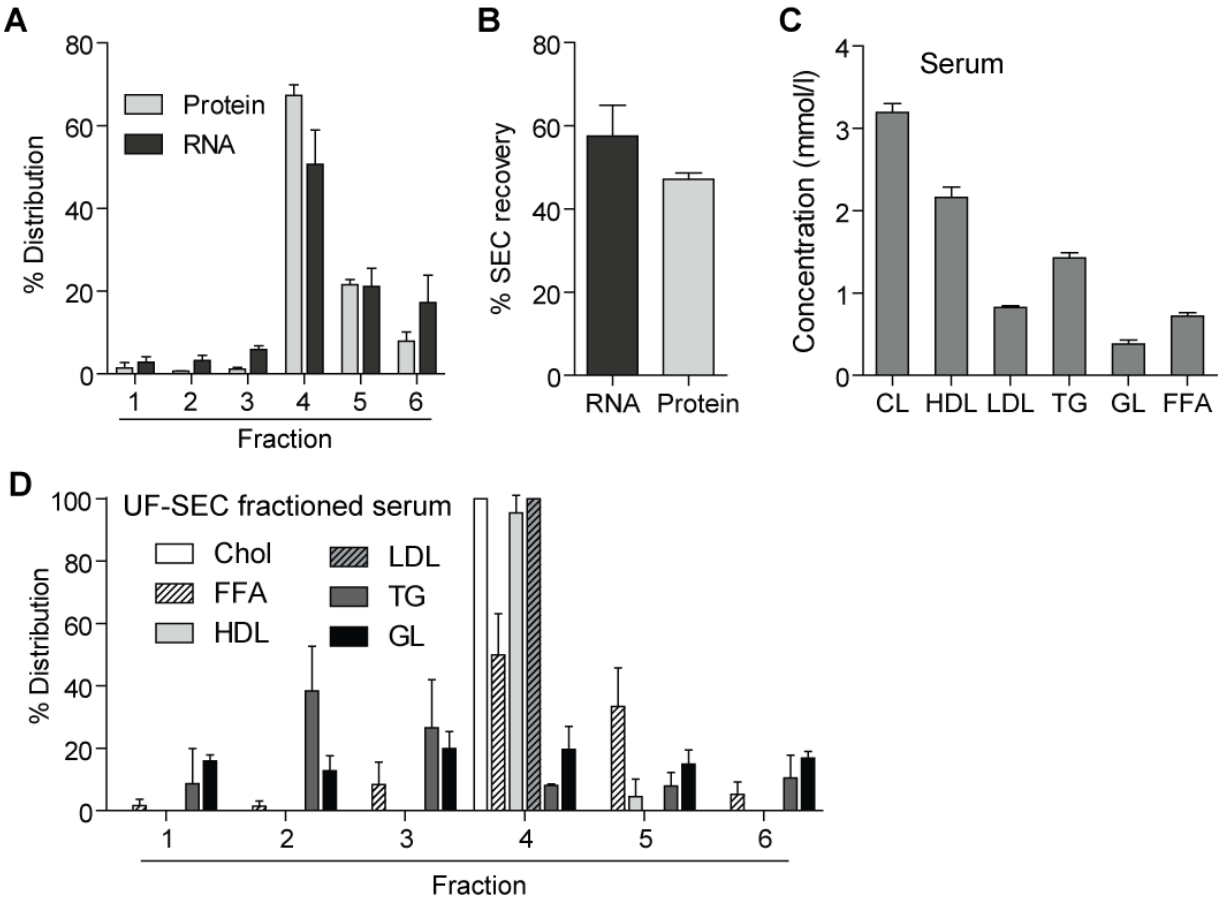

Figure 4.4 Distribution of RNA, protein and lipid derivative in UF-SEC fractionated *mdx* serum.

300 µl of serum from three independent male *mdx* mice was fractionated by UF-SEC and eluates were pooled into 6 new fractions as indicated in Figure 4.2. (A) The protein and RNA amount was quantified in each fraction and neat serum utilising micro BCA and RiboGreen assays respectively. Results are shown as the percentage distribution across all fractions, with the majority of protein and RNA being present in F4. (B) The SEC recovery was determined by calculating the total quantity of Protein/RNA in the SEC fractions as a percentage of the Protein/RNA content of undiluted serum. (C) Lipids and lipoproteins were quantified in neat (C) serum and (D) each fraction utilising with standard colorimetric assays. For fractionated samples, the values are depicted as the percentage distribution across all of the fractions. Free cholesterol (Chol), free fatty acids (FFA), high-density lipoprotein (HDL), low-density lipoprotein (LDL), triglycerides (TG) and glycerol (GL). All values are mean +SEM.

4.3.5 UF-SEC fractionation of wild-type, dystrophic and PPMO-treated murine serum

While multiple studies have investigated pathophysiological changes that occur in dystrophic muscle, the impact on vesicular trafficking and especially EV secretion is currently not well understood. A recent study by Duguez *et al.* observed increased vesicle secretion from dystrophin-deficient H2K myotubes. Vesicles were of diverse density and enriched in the Lysosomal-associated membrane protein 1 (LAMP1) [268]. The cell culture findings from this study suggested that dystrophin protein itself may be involved in the pathways that regulate EV biogenesis and so thorough characterisation of vesicles in dystrophic serum is warranted.

In order to investigate changes in the secretory profile *in vivo,* serum from *mdx* and wild-type mice (*n*=3 each, aged 10-14 weeks) was fractionated via UF-SEC. In line with the Wood group's previous findings, the 280 nm absorbance trace indicated a higher overall protein content in the dystrophic sera (Figure 4.5A) [211]. This is consistent with the cell culture studies where dystrophin-deficient cell secreted ~2.5 fold more protein than wild-type H2K cells [268]. Interestingly, an increase in total particle numbers in F1 was observed in dystrophic serum in combination with a decrease in modal EV size compared to healthy controls (Figure 4.5B-D) [268].

In addition, it was of interest to compare the distribution of ex-miRNAs between fractions in wild-type and dystrophic mice as changes in the ex-myomiR distribution pattern may point towards a dystrophic disease-specific modulation of myomiR release. Consequently, RNA was extracted from each fraction and the distribution of myomiRs and non-myomiR controls determined. In parallel, the non-muscle specific control miRNAs miR-16, miR-223 and let-7a were also profiled. Ex-miRNA abundance was depicted as percentage distribution across the six fractions (Figure 4.5D).

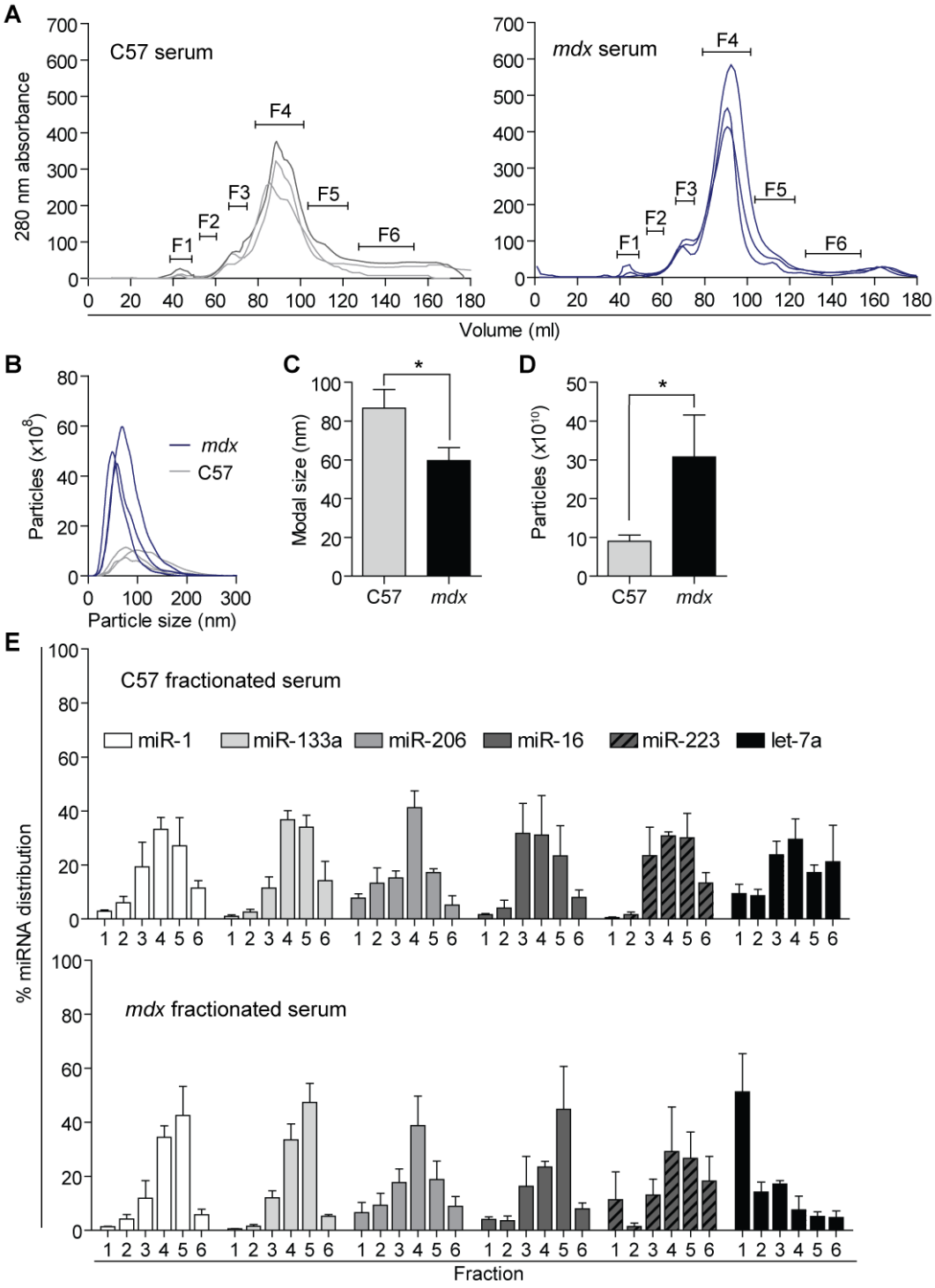

Figure 4.5 Comparison of UF-SEC fractionated wild-type (C57) and *mdx* sera.

(A) Three times 300 µl of wild-type and *mdx* sera was fractionated via UF-SEC (*n*=3) and the eluate was combined into six new fraction as indicated. (B-D) NTA size distribution profile and particle quantification in F1 fractions. (E) RNA was extracted from each fraction and quantified via RT-qPCR. The values are depicted as the percentage distribution across all of the fractions. All values are mean +SEM. **P*<0.05, (unpaired *t*-test, *n*=3).

In general, miRNA distribution patterns were similar in wild-type and *mdx* serum and, as demonstrated earlier in this chapter, most myomiRs co-elute with the protein-rich fractions F3-F5. Consequently, when comparing the shape of the myomiR distribution pattern, especially for miR-1 and miR-133a, a shift towards the right is visible, indicating that the increase in ex-myomiRs is much stronger in the later eluting fractions (F4 and F5). Notably, a similar shift in the distribution shape was observed for miR-16, possibly indicating an overall enrichment of ex-miRNAs bound in small RBP complexes. Previously miR-223 has been described as being associated with HDL particles [159] and, consistent with this notion, miR-223 was most abundant in F4 and F5. Interestingly, in comparison to the cell culture supernatant and dystrophic serum, let-7a was less enriched in the vesicular fractions of wild-type sera. However, serum levels were typical low for let-7a (10-100 less copies/ml compared to the myomiR, Figure 4.6E). In addition, C_q levels were in the late thirties for fractionated samples, thus increasing variation of the data for this miRNA and thereby somewhat limiting the meaningfulness of this finding.

The subsequent experiment was intended to investigate if partial dystrophin restoration by PPMO treatment has an effect on the EV content of dystrophic serum. In addition, it was of interest to determine if ex-myomiR restoration occurs at a similar level in all fractions. Initially, 300 µl of wild-type, PPMO-treated (section 2.1) and *mdx* serum (*n*=1, 14 week old male mice) was UF-SEC fractionated (Figure 4.6). To minimise variation in the EV extraction workflow, all samples were separated and re-concentrated in the space of 48 hours. PPMO treatment has been extensively shown by the Wood group to induce exon skipping and dystrophin restoration at high levels in skeletal muscle and diaphragm, and at moderate levels in the heart [253,273,274,285] (e.g. also in TA muscle ~20-30% exon 23 skipping, Figure 5.1).

Interestingly, the intensity of the 280 nm absorbance trace of the PPMO treated sample was intermediate with respect to the protein peak between wild-type and *mdx* serum, thus suggesting a decrease of serum protein levels in the treated animal (Figure 4.6A). Strinkingly, the NTA size

distribution showed restoration of the EV profile in PPMO-treated serum towards the wild-type profile Figure 4.6B). Similarly, in F1, both the modal EV size as well as the particle counts were restored towards the values observed for wild-type EV (Figure 4.6B).

Ex-myomiR levels were measured in each individual fraction and absolute copy numbers per fraction were determined by comparison to synthetic RNA standards (Figure 4.6C). Notably, ex-myomiR restoration was in general visible across all fractions (with exception for miR-1 in F2 and for miR-133a in F1, although these findings will need to be confirmed in a larger study). However, the restoration was strongest in the fractions that showed a higher degree of initial differential abundance, such as F4 and F5. Based on this preliminary data it appears that F4 exhibits the strongest ex-myomiR fold change (wild-type vs *mdx*) and that the differential myomiR abundance in this fraction is larger than in non-fractionated serum. For comparison, ex-myomiR and control miRNA levels were additionally measured in non-fractionated serum (Figure 4.6E). All ex-myomiRs were elevated in non-fractionated dystrophic mice and restored towards wild-type levels after PPMO treatment as described previously [138,285]. In contrast, serum levels of the non-myomiR miRNAs were unchanged.

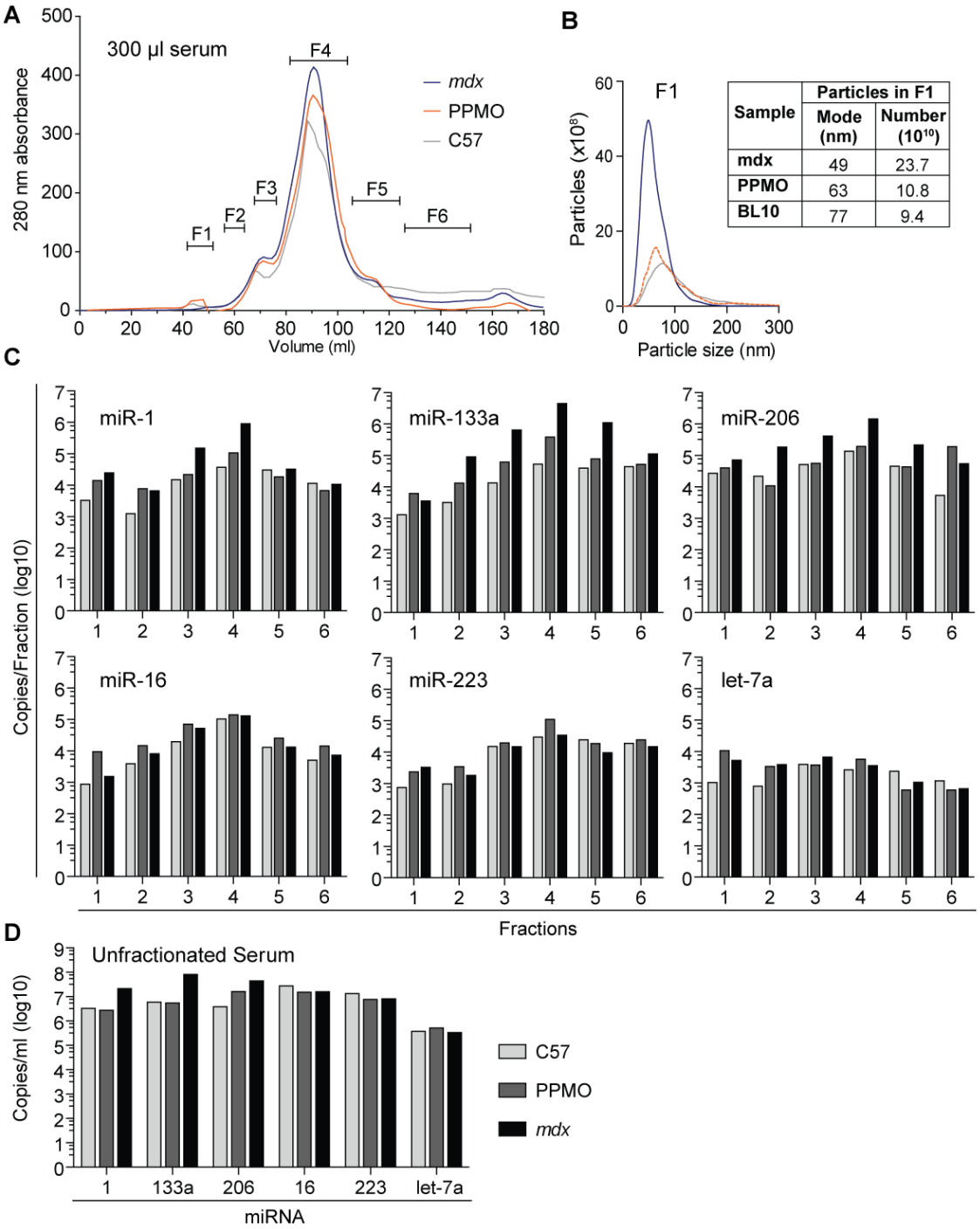

Figure 4.6 PPMO-mediated dystrophin restoration influences EV size and particle numbers.

Investigation of the effect of PPMO-mediated dystrophin restoration on EV size, EV number and ex-myomiR distribution. (A) 280 nm absorbance trace of UF-SEC fractionated wild-type, PPMO-treated and *mdx* serum (*n*=1, 300 µl, 14 week old male mice). (B) NTA size distribution profile of F1 from all samples and table listing modal size and total particle numbers for each sample. RNA was extracted from (C) all fractions and (D) unfractionated serum. The absolute copy number of ex-miRNAs per fraction or per ml biofluid was determined by RT-qPCR. *n*=1 per group.

4.4 Discussion

4.4.1 Ex-myomiRs co-elute with fractions enriched in proteins

Early experiments to fractionate serum with the purpose of separating distinct miRNA carrier classes were carried out by Arroyo *et al.* in 2011 utilising ultracentrifugation and size exclusion chromatography [156]. In an effort to separate EV-associated and vesicle-free miRNAs the authors demonstrated by microarray technology that most miRNAs are predominantly non-vesicular. Similarly, Vickers *et al*. used differential centrifugation to further characterise HDL-associated miRNAs [159]. As mentioned earlier, the Wood group has studied ex-myomiR abundance in UC isolated EVs in comparison to their abundance in the non-pelleted supernatant and concluded that ~99% of myomiRs are present outside of EVs [285]. However, as outlined in section 5.1, this technique is relatively crude and has only low resolution (discriminating between only EV and non-EV fractions). Consequently, it was of interest to confirm the previous findings using a more robust fractionation technique. In addition, it was desirable to establish a methodology that allows for separation of biofluids at a higher resolution compared to UC. To this end, any desirable number of fractions separated according to size can be via SEC fractionation, although in this work typically 4-6 pooled fractions were analysed.

In this chapter, it was demonstrated that a combination of ultrafiltration and size exclusion chromatography is suitable to efficiently separate EVs from lipoproteins and other protein complexes/RBPs in biofluids. In contrast, a UC spin prior to SEC fractionation decreased the vesicle recovery by at least 10 fold and was therefore not integrated into the fractionation protocol. Utilising the UF-SEC technique, it was possible to study ex-myomiR distribution across the different miRNA carriers in a greater detail than it has previously been undertaken. In summary, both in wild-type and dystrophic serum, ex-myomiRs predominantly reside outside EVs, and they co-elute with the protein-rich fractions. Consistent with previous findings, 99% of the ex-myomiRs were found in the fractions eluting later than the EV enriched fraction 1 (Figure 4.1 and 4.2) [285]. Furthermore, the distribution

of all tested ex-miRNAs was similar in conditioned media derived from myotube cultures and murine serum (Figure 4.1D and 4.2D), with the only difference being that ex-myomiRs in cell culture media eluted slightly after the main protein peak. To this end, it seems likely that, in serum, lipoprotein proteins may function as ex-miRNA carrier and that protein-bound miRNAs in the circulation may aggregate to form larger complexes which elute earlier.

An important limitation of the current fractionation methodology is that HDL and LDL particles could not be separated from other protein complexes (Figure 4.4). Importantly, the Wood group has previously shown that serum myomiRs are associated with AGO2, but also with APOA1, the major protein constituting HDL [285], underlining that serum myomiRs are indeed associated with at least with this type of lipoproteins. As a consequence, it would be of interest in the future to quantify the extent to which these smaller lipoprotein complexes may associate with myomiRs in greater detail. Selective depletion of lipoproteins by immunocapture or differential centrifugation may be a possibility to investigate ex-myomiR association with VLDL, HDL and LDL.

Given the highly similar ex-myomiRs distribution profiles observed in SEC fractionated serum/conditioned media samples, and their conserved patterns of secretion during myogenic differentiation (chapter 3), it is tempting to speculate that these three myomiRs are released and stabilised in the extracellular environment by similar means. However, the striking differences in ex-myomiR stability observed in section 3.3.6 present a challenge for this hypothesis. A possible explanation may be a differential degree of association of ex-myomiRs to APOA1 and AGO2 and/or other RBPs which in turn exhibit differential stability in serum. However, considering that miR-1 was also rapidly degraded in myotube cell culture supernatant, this may not be the primary reason. Given that HDL originates in hepatocytes and consequently, the only lipoproteins that are expected to be present in the supernatant would be derived from the horse serum component of the differentiation media. Another potential factor influencing ex-myomiR stability is miRNA unloading from AGO2, which has been described to occur in a sequence and target dependent manner [335]. The rate of

AGO2unloading can be tested biochemically [335] and in the future, it would be interesting to determine if it indeed differs between myomiRs, thus explaining the rapid degradation of miR-1 in the extracellular environment.

4.4.2 Dystrophic serum contains more EVs of smaller particle size

By comparing the biophysical properties of EVs isolated by SEC from dystrophic and wild-type sera it was observed that *mdx* serum contains more EVs, and that those EVs are of smaller modal size (Figure 4.5). These findings raise the questions if there are distinct populations of vesicles in dystrophic serum. If the latter would be true, it would be of interest to determine whether the absence of small vesicles in wild-type serum causes the observed shift in the NTA size distribution pattern (Figure 4.5B-D and Figure 4.6B). As a result, it would be useful in the future to analyse the compositions of the vesicular fraction of fractioned serum from *mdx* and wild-type mice by mass spectrometry based proteomics. Since this fraction is largely depleted of highly abundant serum proteins which confound this analysis, proteomic profiling should be significantly less technically challenging than in complete serum, and may reveal interesting changes in the EV protein composition in dystrophic mice and DMD patients. This technique would also allow for testing for enrichment of other exosomal markers (in addition to CD63) in the EV fractions, given that Western blot analysis lacks the required sensitivity. Another interesting approach would be to further separate vesicles contained in F1 to identify potential EV sub-populations (e.g. via SEC utilising a higher resolution column or by sucrose-gradient centrifugation [322]). In addition, imaging by electron microscopy would allow the assessment of vesicle shape and size.

Furthermore, an initial study undertaken in this chapter suggests that the observed dystrophy-associated phenotype in vesicle trafficking may be reversible by restoring dystrophin via exon skipping therapy (Figure 4.6). Therapeutic rescue of the EV phenotype will need to be further confirmed by repeating the PPMO study with more replicates. Notably, all three *in vivo* findings (decreased EV size, increase in EV particles and rescue by exon skipping therapy) are in line with a

previously undertaken cell culture study investigating the secretome of dystrophin-deficient and wild-type H2K myotubes [268]. Consequently, one may hypothesise that the absence of dystrophin perturbs vesicle biogenesis and/or secretion. Interestingly, dystrophin has been detected in lysosomal membranes in the context of other myopathies (i.e. [336]). Further studies will be needed to confirm how dystrophin absence influences vesicle trafficking, and if the observed disturbance in EV secretion may account fully or partially for the increase in secreted protein.

4.4.3 Utility of UF-SEC for ex-miRNA biomarker discovery

A possible application of biofluid fractionation is to identify differential abundances of miRNAs that occur only in particular carriers (e.g. only in the vesicular fraction). A recent study showed that EVs separated from serum via asymmetrical flow field fractionation showed that the fold change in miRNA abundance was enlarged in certain fractions compared to the difference observed in miRNA level in unfractionated serum [331].

In this study, the finding that the largest fold changes in ex-myomiR abundance (*mdx* vs. wild-type) were detected in fraction 4 (Figure 4.5-4.6) indicates that fractionation may facilitate detection of relevant changes if ex-myomiRs were to be used as disease biomarkers. Future work will further investigate this hypothesis, although it is important to note that fractionation greatly increases the workload (and therefore 'hands on' time) required to analyse a single serum sample. With the current protocol, every SEC run takes ~8 hours to complete and several hours to concentrate the pooled fractions afterwards, which would not be manageable in a clinical setting unless the protocol can be optimised for efficiency in speed and labour.

In general, it would be good to improve the resolution of SEC fractionation in complex biofluids further, (e.g. separate the vesicle peak more clearly from the protein peak and resolve the protein/lipoprotein peak in more detail). Careful optimisation of column material (other groups have used Sepharose as gel material [337]), pore size and column length may be one option to improve

the protocol. However, while longer columns increase fraction separation, it has to be considered, that they require an even longer run time, which is undesirable for usage in a clinical setting. Consequently, while SEC fractionation of biofluids may be useful for the discovery of circulating miRNA biomarkers, in its current form it is unlikely to be suitable for routine clinical diagnostics.

4.4.4 Conclusion

To conclude, UF-SEC is a powerful tool to separate complex biofluids although several challenges still need to be addressed, (i.e. improving the overall resolution and separating smaller lipoprotein particles from other protein complexes). Utilising UF-SEC to fractionate murine serum and conditioned media derived from C2C12 myotubes, it was confirmed that ex-myomiRs are predominantly present in protein complexes. Given that ex-miRNA transfer has only been demonstrated for vesicular miRNAs to date, future studies are required to understand the extent to which non-vesicular ex-myomiRs may participate in intercellular communication in normal physiology (discussed further in chapter 6.2).

Furthermore, it was observed that serum from *mdx* mice contains more EVs of smaller particle size, thus suggesting an increase in a distinct subpopulation of EVs and/or impairment in vesicular secretion as a feature of dystrophic pathology. The latter is a so far relatively unexplored area of research that is also of interest for the development of circulating biomarkers, since changes in the secretome may account for some of the observed increases in serum abundance of muscle-derived miRNAs and proteins.

5. Results III

Discovery of therapy-responsive protein biomarkers in DMD by aptamer-based serum proteomics

5.1 Introduction

Given the limitations of the outcome measures currently utilised for clinical trials as outlined in section 1.5, there is an urgent need for minimally invasive biomarkers that can be used to monitor the therapeutic efficacy of experimental therapies for Duchenne muscular dystrophy (DMD) in clinical trials. Serum protein biomarkers are ideal as sample collection is simple, minimally invasive and their measurement is technically facile since standard clinical biochemistry workflows can be applied for quantification (e.g. ELISA). The search for novel protein biomarkers entails the application of proteomics techniques to biofluids such as serum or plasma to identify differentially abundant proteins. Mass spectrometry techniques are by far the most commonly used methods of whole proteome analysis, and recent technical developments have enabled the simultaneous measurement of over 10,000 proteins from cell culture lysates [338] and over 3,000 proteins in dystrophic mouse muscle [339]. However, proteomic analysis of the serum/plasma proteome is complicated by the immense complexity of these biofluids. In principle, the circulation contains every possible protein in the body as it consists of both secreted proteins which exercise their functions in the extracellular space, and proteins derived from tissues that leak into the bloodstream following injury or stress. Furthermore, the composition of the circulating proteome is highly uneven, with a group of about 20 highly abundant proteins (concentration range in ~mg/ml) comprising ~90% of the total protein (e.g. serum albumin, α2-macroglobulin, immunoglobulins, fibrinogen etc.). Consequently, the majority of circulating proteins (including potential biomarkers) are typically much less abundant (in the ng/ml or even pg/ml range). Extracellular proteins span a concentration range of ~10 logs, meaning that

detection of lowly abundant potential biomarker proteins is frequently masked by peptides derived from the more massively abundant proteins [340]. As a result of these difficulties, mass spectrometric methods generally perform poorly on complex protein mixtures such as biofluids [341].

Multiple protein enrichment strategies have been applied in the past to deplete highly abundant serum proteins prior to mass spectrometry (reviewed in [254]). These include immune-depletion, typically utilising antibodies against albumin, immunoglobins, transferrin, fibrinogen and haptoglobin (i.e. the Multiple Antibody Removal System from Agilent Technologies). Similarly, pre-fractionation with hexapeptide libraries such as ProteoMiner (Bio-Rad), remove hyper abundant proteins by acting as 'baits'. Consequently, both techniques enable the 'compression' of the dynamic range of serum/plasma and thereby improve resolution for biomarker discovery experiments. However, it is debatable if this improvement is sufficient to improve detection of very lowly abundant biomarkers. In addition, there are some drawbacks of these approaches (e.g. co-depletion of low-abundance proteins due to protein-protein interactions in the case of immunodepletion [342]).

To overcome these challenges, an aptamer-based purification methodology (SOMAscan) was employed here to profile the abundance of more than 1,000 proteins in murine serum [343]. By definition, aptamers are short synthetic single-stranded oligonucleotides that specifically bind to various molecular targets including proteins. Routinely, aptamers are selected by a biospanning method referred to as SELEX (Systematic Evolution of Ligands by Exponential enrichment) [344,345]. The SOMAscan platform, consists of 1,129 aptamers, so-called SOMAmers (Slow Off-rate Modified Aptamers) and is designed to bind to human serum proteins. However, the majority of SOMAmers exhibit cross-reactivity, or predicted cross-reactivity based on homology, to their murine homologues. This new technology, developed by SomaLogic Inc., is predicted to allow for the determination of protein concentrations of a specific set of targets in a manner that is unaffected by the concentrations of the highly abundant serum proteins. As part of the methodology, SOMAmer-

protein complexes are precipitated and protein concentration are inferred by hybridising the SOMAmers to DNA micorarrays, thereby converting the protein signal to a nucleic acid-based signal [343].

In this chapter, the SOMAscan platform was utilised to compare the serum proteome of wild-type and dystrophic *mdx* mice to identify differentially abundant proteins. Additionally, animals that underwent systemic treatment with a peptide-antisense oligonucleotide conjugate designed to induce *Dmd* exon skipping and recover dystrophin protein expression were included in the study with the aim of discovering therapy-responsive biomarkers.

5.2 Materials and methods

5.2.1 Animal samples

14 week old male C57BL/10 wild-type (abbreviated as C57) and *mdx* mice (*n* = 8) were sacrificed and blood was collected from the jugular vein as described in section 2.1. 12 week old male *mdx* mice (*n* = 8) were injected with a single dose of 12.5 mg/kg Pip6a-PMO (PPMO) as described in section 2.1. The mice were sacrificed at 14 weeks of age and 75 µl of serum were analysed by SOMAscan proteomic profiling.

5.2.2 Human samples

Collection of samples from patients and their use in research has been ethically approved by the National Research Ethics Service (NRES) Committee North East – Newcastle and North Tyneside 1 in accordance with the Helsinki Declaration. Informed consent was obtained from all subjects. Serum samples from DMD, Becker Muscular Dystrophy (BMD) and facioscapulohumeral muscular Dystrophy (FSHD) patients were obtained from Newcastle University through the MRC Centre for Neuromuscular Diseases Biobank. The serum samples from healthy individuals were obtained from Newcastle University (as above, *n* = 5) or collected from volunteers at the University of Oxford (*n* = 13). Patients and healthy donors were all male individuals and the samples were collected according to standard operating procedures and were stored at -80°C prior to analysis.

5.2.3 Quantification of exon skipping by RT-qPCR and WB

Quadriceps femoris muscles were macrodissected and snap frozen in liquid nitrogen-cooled isopentane. RNA was extracted and reverse transcribed as described in chapter 2.2. Levels of *Dmd* exon 23 skipping were determined by probe based RT-qPCR using a FAM-assay spanning the exon 20-21 boundary and a HEX-assay spanning the exon 23-24 boundary (Assay IDs: Mm.PT.47.9564450 and Mm.PT.47.7668824 respectively, Integrated DNA Technologies, Leuven, Belgium). The percentage of

Dmd transcripts lacking exon 23 was determined by normalising exon 23-24 amplification levels to exon 20-21 levels. To quantify dystrophin protein expression, 8 µm cryosections were prepared from the mid-belly of the muscle and samples lysed in buffer (75 mM Tris–HCl pH 6.5, 10% sodium dodecyl sulphate, 5% 2-mercaptoethanol and protease inhibitors) prior to centrifugation at 10,000 *g* for 10 minutes to pellet debris. Supernatants were collected and incubated at 100^{o}C for 3 minutes. Protein lysates were separated on a 3-8% Tris-Acetate gel (Life Technologies), electrotransferred to a PVDF membrane and probed with monoclonal anti-dystrophin (1:200, NCL-DYS1, Novocastra) and anti-vinculin (loading control, 1:100,000, hVIN-1, Sigma) primary antibodies as previously described [285]. Secondary antibody IRDye 800CW goat anti-mouse was used at a dilution of 1:20,000 (LiCOR). Fluorescence was detected and quantified using the Odyssey imaging system. Dystrophin expression was quantified using the dystrophin to vinculin ratio compared with C57/BL10 wild-type dystrophin expression standards on each gel.

5.2.4 SOMAscan serum proteomics

Serum proteomics profiling was performed on the SOMAscan platform at SomaLogic, Inc. (Boulder, CO, USA). This platform measures the abundance of 1,129 target proteins, each of which is targeted by a unique aptamer the SOMAmer reagent. The SOMAmers are selected utilising the human protein sequence, but the majority are predicted to cross-react with mouse proteins. Each SOMAmers consist of the protein binding aptamer component which is developed by SELEX, a photo-cleavable biotin moiety for the initial SOMAmer-protein complex capture step, and a Cyanine3 fluorophore for the purposes of detection and quantification (Figure 5.1). To increase the dynamic range of analyte detection, the SOMAscan methodology utilises three dilutions of serum samples (0.5%, 2% and 5% respectively [343]) that are each mixed with a unique set of SOMAmer reagents immobilised on streptavidin-coated beads to capture target proteins (Figure 5.1A). A subsequent washing step reduces the non-specific protein binding (Figure 5.1B) and proteins that remained captured on the SOMAmer-beads were biotinylated using NHS-PEO4-Biotin (Figure 5.1C). Next, biotinylated-protein-

SOMAmer complexes were released from the beads using UV light to cleave the photo-cleavable linker contained within the SOMAmer component (Figure 5.1D). Beads were then exposed to an anionic competitor solution that prevents non-specific interactions from reforming after they are disrupted [343] (Figure 5.1E). Eluates were incubated with another set of streptavidin-coated beads to precipitate biotinylated-protein-SOMAmer complexes and free SOMAmer reagents were removed by subsequent washing of the beads (Figure 5.1F-G). Finally, protein-SOMAmer complexes were dissociated using denaturing conditions and the nucleic acid (SOMAmer) component quantified by hybridisation to custom DNA microarrays (Figure 5.1H). The measured relative fluorescence units (RFU) are directly proportional to the concentration of the target protein in the biofluid sample which is inferred utilising individual standard curves for each protein-SOMAmer pair [343].

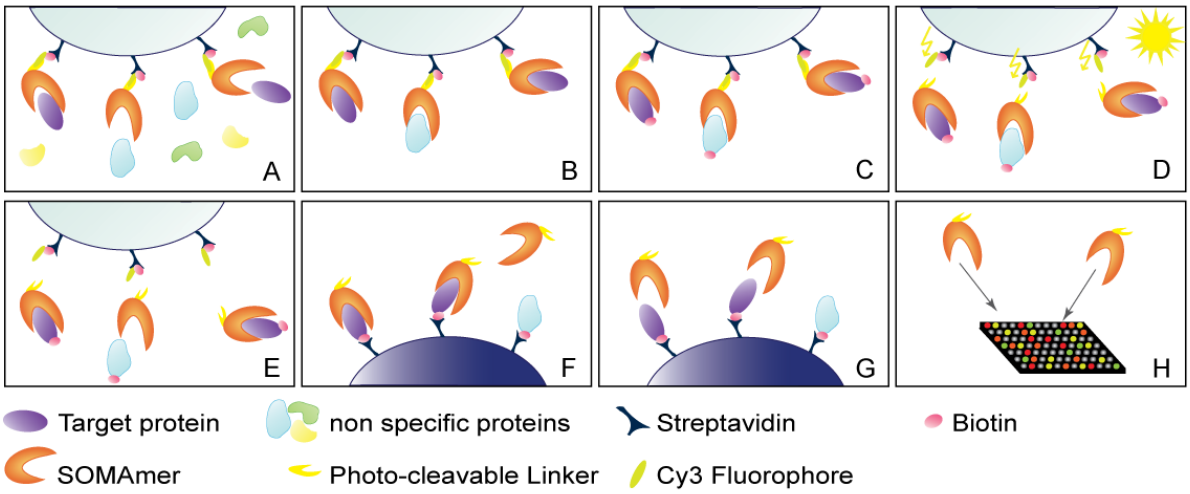

Figure 5.1 Workflow of SOMAscan proteomic profiling.

Three different sample dilutions were prepared and the concentration of target proteins was converted into a relative fluorescence signal utilising the SOMAscan platform. The SOMAmers were immobilised on streptavidin coated beads via a photo-cleavable biotin linker. Target proteins in the biological samples were captured by binding to the aptamer moiety of the SOMAmer (A) and non-specific proteins are removed by washing (B). Immobilised proteins are biotinylated (C) and subsequently the protein-SOMAmer complexes are removed by light-activated cleavage (D). A polyanionic competitor disrupts weakly bound, non-specific protein-SOMAmer complexes permanently (E). Biotinylated proteins were captured a second time on Streptavidin coated beads and unbound SOMAmers were removed by washing (F-G). Lastly, protein-SOMAmer complexes were dissociated and the SOMAmer oligonucleotides were quantified utilising microarray technology (H).

5.2.5 Enzyme-linked immunosorbent assay (ELISA)

The leading candidate proteins were validated using sandwich enzyme immunoassay. All ELISA kits were purchased from antibodies-online (Aachen, Germany) with assay IDs listed in Table 5.1. Whenever possible, sera from the animals used for the SOMAscan screen was used for validation. Due to limited sample volumes, additional age- and sex-matched animals were included in the validation stage, so that each group consisted of eight samples. The ELISAs were performed according to manufacturer's instructions and the serum was diluted to fall within the linear range of each respective assay (typically 3-10 fold dilutions). Sample concentrations were extrapolated with GraphPad Prism 5 using fourth-order polynomial data fit of the standard curves as indicated in Figure 5.2.

Species	Protein	Product code	Sensitivity	Comments
MOUSE	Capn1	ABIN424286	1.56-100ng/ml	Samples below detection limit
	Cycs	ABIN1569298	1.56-100ng/ml	
	Pgam1	ABIN820296	0.025-1.6 ng/ml	
	Tnni3	ABIN853281	0.0156-1.0 ng/ml	
	Adamts5	ABIN827175	0.625-40 ng/ml	
	Camk2b	ABIN811938	0.03125-2.0 ng/ml	
	CK-MM	ABIN1000121	0.156-10 mU/mL	
HUMAN	ADAMTS-5	ABIN649163	0.313-20 ng/mL	
	PGAM1	ABIN820295	28.12-1800 pg/mL	Samples below detection limit

Table 5.1 List of ELISA assays used in this study.

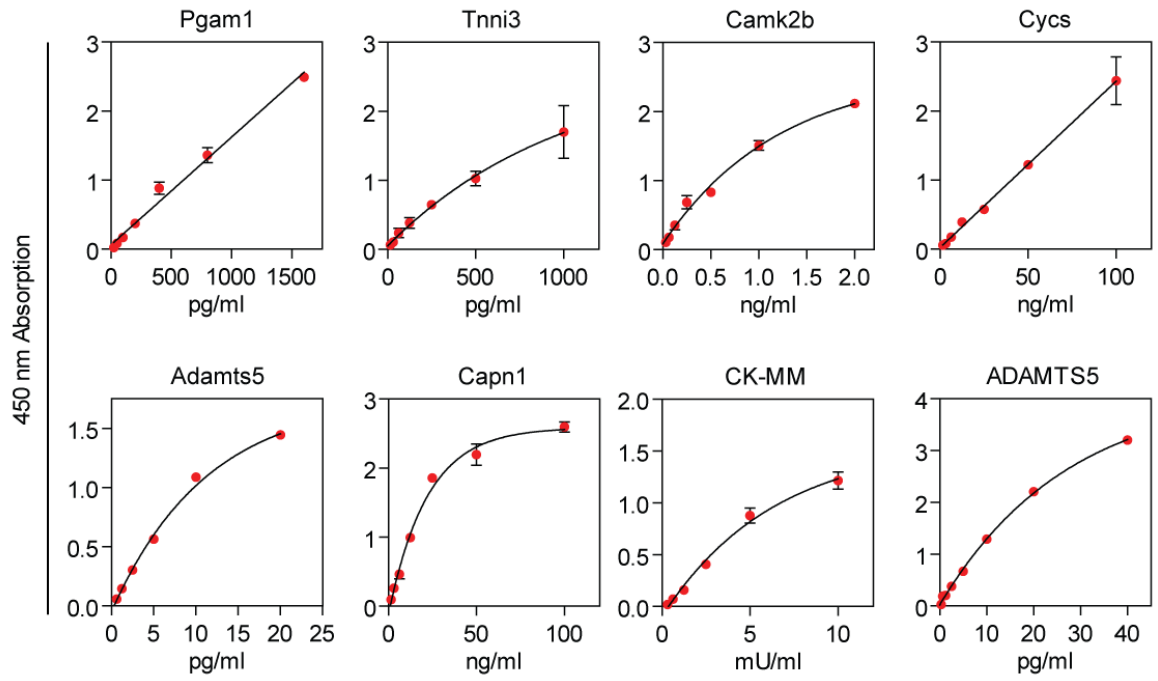

Figure 5.2 ELISA Standard curves.

Extrapolated standard curves for the ELISA assays. All values are mean +/- SEM.

5.2.6 Statistical analysis

The SOMAscan data were analysed using the SOMAsuite analysis software to perform Mann-Whitney U test (two-sided) and Kruskal-Wallis one-way ANOVA. Non-parametric tests were conducted as SOMAscan data were found not to be normally distributed as determined by the Shapiro-Wilk test (GraphPad Prism 5). MeV (Multiple Experiment Viewer (The Institute for Genomic Research, Rockville, MD, USA) was utilised for hierarchical clustering and heatmap visualisation [346]. Principal component analysis was performed in R version 3.2. Additional statistical functions were performed in GraphPad Prism 5: one-way ANOVA, Bonferroni post test, Pearson/Spearman correlation, linear regression and ROC curve analysis.

5.3 Results

5.3.1 Proteomic profiling of dystrophic serum by the aptamer screen SOMAscan

To identify novel protein biomarkers for DMD, serum from 14 week old C57, *mdx* and PPMO-treated *mdx* mice (*n*=8) was harvested. Dystrophin protein restoration in quadriceps femoris muscles of treated animals was confirmed by Western blot, and the amount of *Dmd* exon 23 skipping determined by RT-qPCR (Figure 5.3A,C). Similar to previous studies, median DMD protein expression in PPMO-treated animals was 39% with respect to wild-type controls [274,285]. Pearson's correlation analysis showed that dystrophin protein and mRNA expression were strongly correlated (Figure 5.3B).

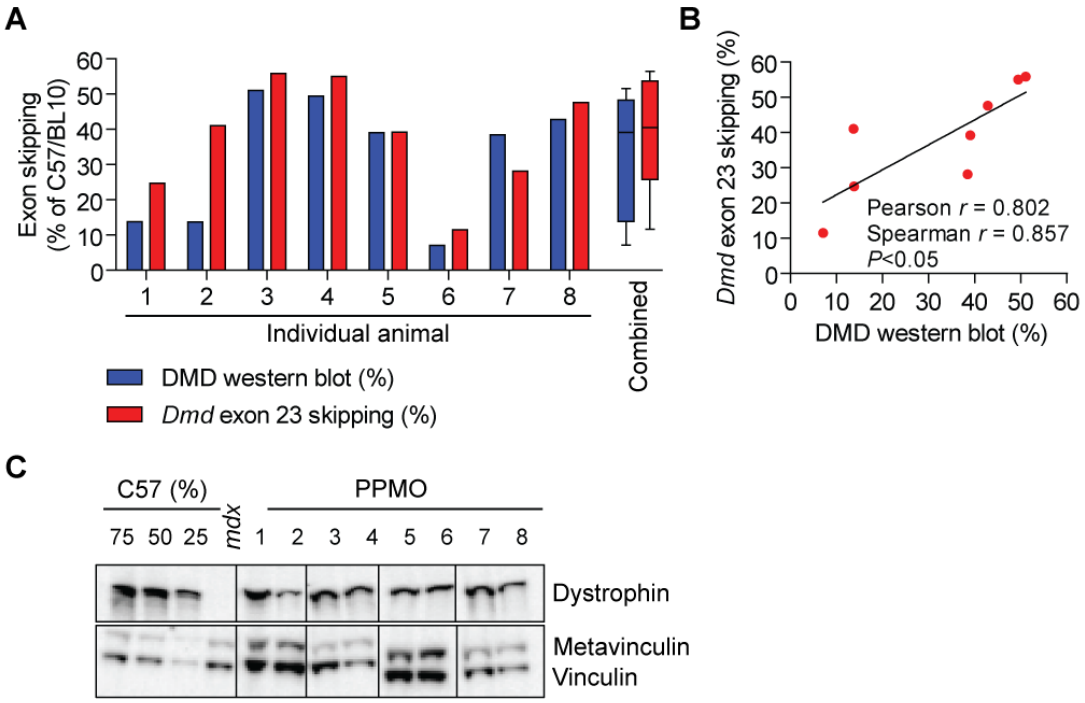

Figure 5.3 Quantification of PPMO therapeutic efficacy.

(A) Efficiency of PPMO therapy was assessed in quadriceps femoris muscles by Western blot to measure dystrophin protein and RT-qPCR to detect the degree of *Dmd* exon 23 skipping. Values for each individual animal are shown along with Tukey box plots of the combined data. (B) *Dmd* exon 23 skipping and dystrophin protein expression were positively correlated. (C) Images of Western blots. The standard curve from C57 tissue allows dystrophin quantification and vinculin serves as loading control.

Notably, all 1,129 SOMAmers were detected in all samples. The hybridisation normalisation and median normalisation (at all three dilutions) scale factors were calculated for all samples to normalise data across samples (Figure 5.4A). After these initial quality controls checks, one treated sample (T7) was excluded from the analysis as its median normalisation factor was outside the acceptable range (0.4-2.5) for all three dilutions. Importantly, hybridisation of the probe was equivalent between all samples (Figure 5.4B), although the median normalisation scale factors were slightly skewed in the *mdx* samples, suggesting an increase in total protein concentration in these samples (Figure 5.4C). This observation is similar to the increase in total RNA and total microRNA in dystrophic serum that has been reported previously [211].

Comparing only the C57 and *mdx* groups revealed 96 proteins with statistically significant changes in abundance (Mann-Whitney U test, FDR correction, $P<0.001$, $q<0.01$) of which 75 showed an increase and 21 a decrease in *mdx* sera. Highly differentially abundant proteins at each dilution level were visualised by scatter plot (Figure 5.5A). The majority of differentially abundant proteins were observed in the higher dilution samples (i.e. lower abundant proteins) with only LDHB (lactate dehydrogenase B) identified in the 0.5% dilution group (i.e. highly abundant proteins). Proteins that were both highly differentially expressed and highly statistically significant were identified by volcano plot (Figure 5.5B). When all three experimental groups were compared, 130 proteins were identified as statistically different (Kruskal-Wallis one-way ANOVA, $P<0.001$, $q<0.01$) of which 104 were restored towards wild-type levels after PPMO treatment (73 proteins were more, and 31 less abundant in *mdx* sera respectively). Experimental groups were well separated by hierarchical clustering of differentially expressed proteins (Figure 5.5C) and principal component analysis (Figure 5.5D). Importantly, a substantial overlap (72 proteins) was observed between the proteins found to be significant by Mann-Whitney U test and Kruskal-Wallis one-way ANOVA (Figure 5.5E).

A

Group	Sample	Hybridisation Normalisation Scale Factor	Median Normalisation Scale Factor		
			5%	2%	0.5%
C57	C1	0.938	0.938	0.913	0.953
	C2	0.913	1.081	1.092	1.1
	C3	0.962	1.002	0.997	0.878
	C4	0.94	1.024	1.01	1.081
	C5	0.94	0.927	0.935	0.956
	C6	0.929	1.09	1.093	1.099
	C7	0.917	1.076	1.101	1.004
	C8	0.966	1.041	1.077	1.022
mdx	M1	0.908	1.007	0.993	0.995
	M2	0.886	0.813	0.837	0.92
	M3	0.948	0.981	0.946	0.943
	M4	0.924	0.852	0.857	0.818
	M5	0.932	0.884	0.869	0.937
	M6	0.969	0.955	0.95	0.964
	M7	0.956	0.842	0.831	0.827
	M8	0.93	0.938	0.925	0.852
PPMO	T1	0.91	1.146	1.153	1.138
	T2	0.966	1.008	1.026	1.063
	T3	0.924	1.063	1.09	1.023
	T4	0.96	0.932	0.995	1.003
	T5	0.944	1.08	1.1	1.165
	T6	0.952	1.023	1.01	1.026
	T7	0.979	**6.105**	**7.026**	**3.869**
	T8	0.931	1.124	1.108	1.091

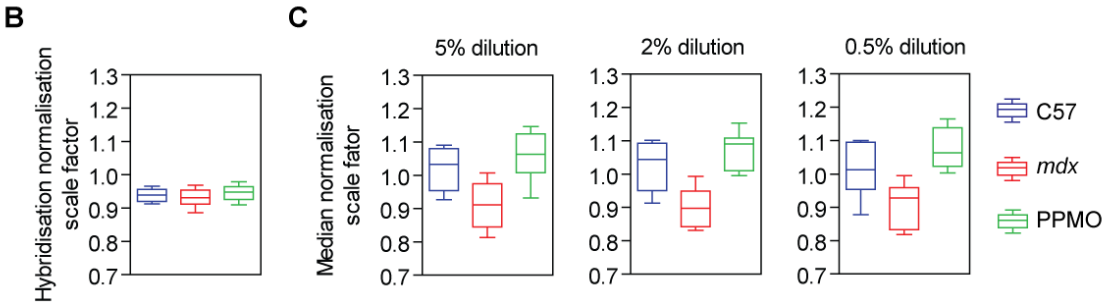

Figure 5.4 Quality control of SOMAscan data.

(A) Table of all hybridisation normalisation and median normalisation (at all three dilutions) scale factors. The acceptable range is 0.4-2.5. All scale factors were within the range and generally close to 1 (i.e. no scaling) with the exception of sample T7 (highlighted in red) – which was excluded from subsequent analyses. (B) Box plots of hybridisation normalisation scale factors separated by experimental group. (C) Box plots of median normalisation scale factors at all three dilution separated by experimental group. Scale factors were generally lower in *mdx* samples indicating a gross increase in protein content.

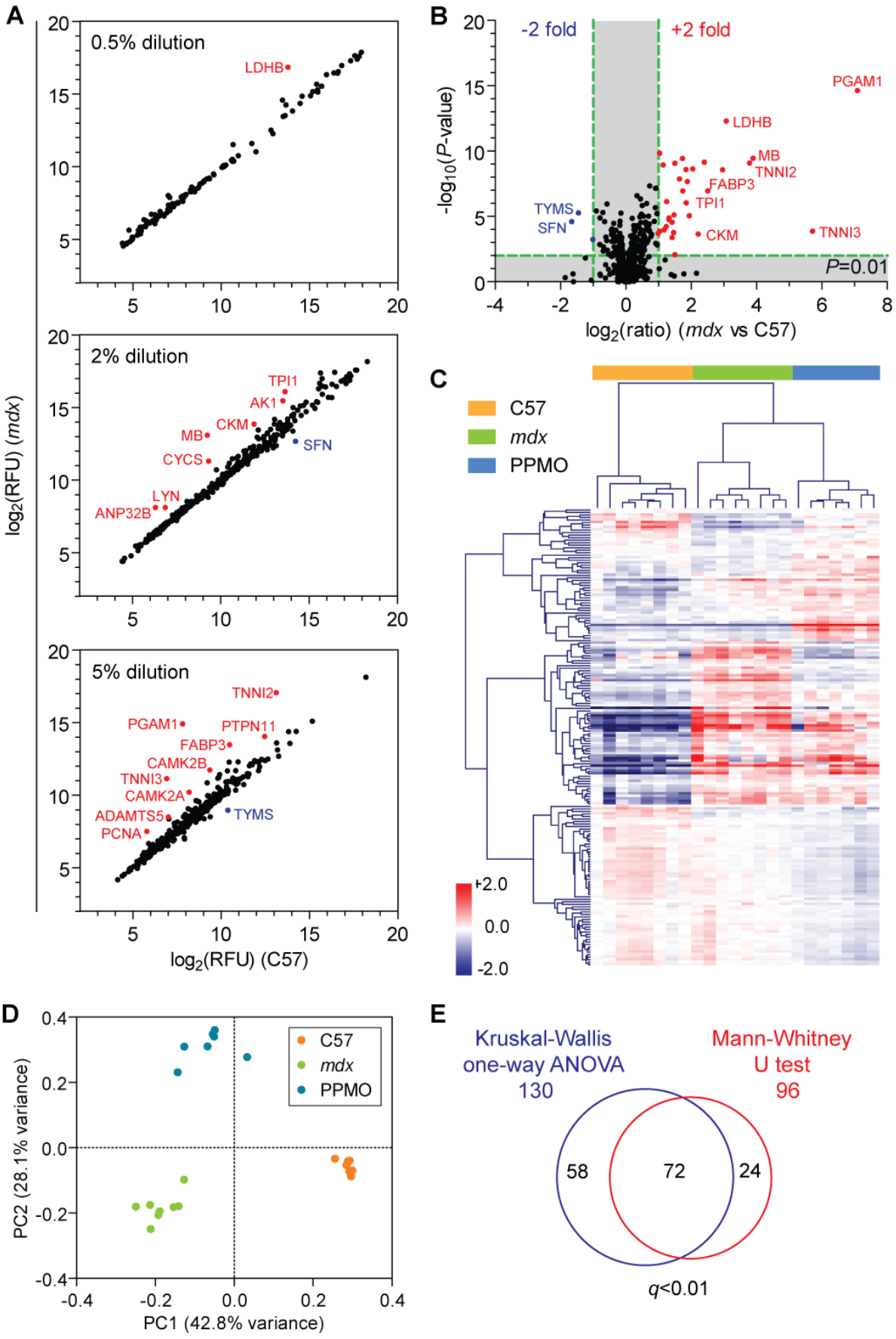
A
0.5% dilution
LDHB
2% dilution
TPI1
AK1
CKM
MB
SFN
CYCS
LYN
ANP32B
5% dilution
TNNI2
PGAM1
PTPN11
FABP3
CAMK2B
TNNI3
CAMK2A
ADAMTS5
PCNA
TYMS
log2(RFU) (mdx)
log2(RFU) (C57)
B
-2 fold
+2 fold
PGAM1
LDHB
MB
TNNI2
FABP3
TPI1
TYMS
SFN
CKM
TNNI3
P=0.01
-log10(P-value)
log2(ratio) (mdx vs C57)
C
C57
mdx
PPMO
+2.0
0.0
-2.0
D
C57
mdx
PPMO
PC2 (28.1% variance)
PC1 (42.8% variance)
E
Kruskal-Wallis
one-way ANOVA
130
Mann-Whitney
U test
96
58
72
24
q<0.01

Figure 5.5 Identification of novel DMD biomarkers and statistical analysis.

Serum samples from C57, *mdx* and PPPMO-treated *mdx* were analysed using the SOMAscan methodology. (A) Scatter plot of mean relative fluorescent units (RFU) for *mdx* vs C57 identifies differentially abundant proteins separated by dilution group. (B) Statistically significant (P<0.01) protein changes in *mdx* serum were determined by Mann-Whitney U test and visualised by volcano plot. (C) Proteins with statistically significant changes when comparing between all three experimental groups (Kruskal-Wallis one-way ANOVA P<0.001, q<0.01) were analysed by hierarchical clustering. Red indicates more abundant proteins and blue indicates less abundant proteins. The scale bar represents the row z-score. (D) Statistically significant (P<0.01) protein changes were visualised by principal component analysis (the first two components representing 71% of the data are shown). (E) A high degree of overlap was observed between statistically significant protein calls from both Mann-Whitney U test and Kruskal-Wallis one-way ANOVA analyses.

5.3.2 Identification of leading DMD biomarker candidates

A set of 21 proteins with increased, and 2 with reduced, serum abundance were identified as the most promising candidate DMD biomarkers based on the following criteria: (i) differentially abundant in *mdx* serum by >2 fold, (ii) statistically significant (P<0.01) as determined by both Kruskal-Wallis one-way ANOVA and Mann-Whitney U test, (iii) proteins which responded to treatment with PPMO were prioritised (Figure 5.6, Table 5.2, note that for convenience human Entrez gene identifiers are used to describe output from the SOMAscan analysis). Response to therapy was defined as a shift in the mean protein abundance towards wild-type levels. Some proteins showed complete restoration (i.e. CYCS, ADAMTS5, HTRA2 and CAPN1), whereas the majority of proteins showed more moderate restoration (i.e. MB, LDHB, FABP3, CAMK2B). In addition, two proteins (TNNI2 and TPI1) that displayed little or no response to therapy were included based on their potential as diagnostic biomarkers as they were among the most differentially abundant proteins in *mdx* sera. The resulting list of leading candidates contains a number of novel potential DMD biomarkers and some proteins which have been described previously as being elevated in dystrophic serum or as biomarkers of tissue damage in general (i.e. MB, LDHB, FABP3, CYCS, TPI1 and THBS4, respective references indicated in Table 5.2) [266,270,347,348]. Interestingly, many of these proteins are associated with known pathophysiological features of DMD including muscle function (MB, TNNI2, TNNI3), metabolic dysregulation (PGAM1, LDHB, TPI1, FABP3), calcium metabolism (CAMK2A, CAMK2B, CAMK2C, CAPN1), extracellular matrix remodelling/fibrogenesis (ADAMTS5, THBS4) and inflammation/NF-κB signalling (EDA2R) [349].

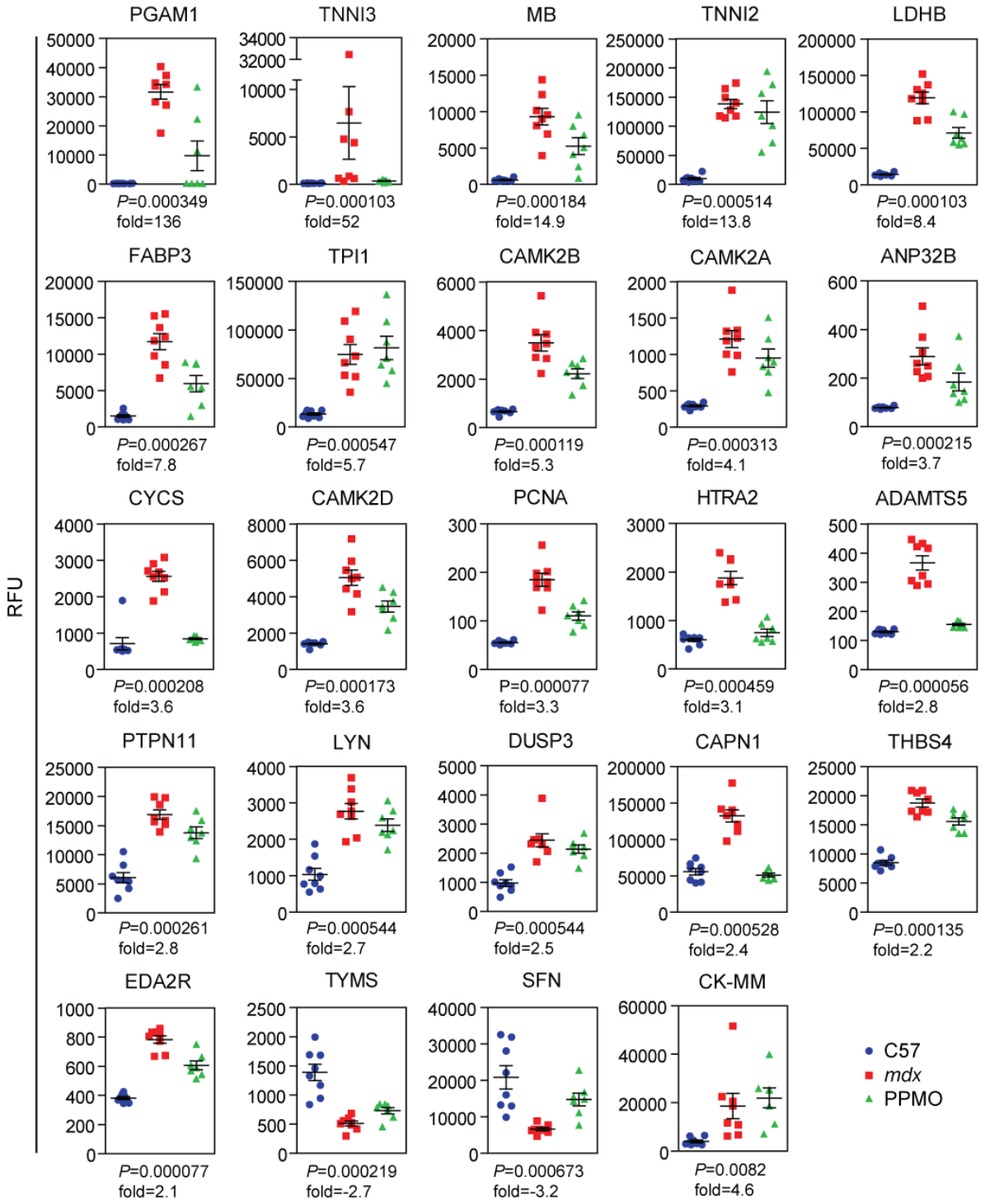

Figure 5.6 Top candidate disease biomarkers in dystrophic and exon skipping-treated serum.

RFU plots of protein abundance data showing each individual biological replicate for the top 23 ranked candidate biomarkers identified by SOMAscan. CK-MM was included based on its previous usage as diagnostic DMD biomarker. Error bars indicate mean +/- SEM. Kruskal-Wallis one-way ANOVA *P* values and *mdx* vs C57 fold changes are indicated for each protein. *q*=0.00822 for all proteins shown.

ENTREZ ID **Name**	**UniProt ID**	**Fold Change (*mdx* vs C57)**	**Dil. (%)**	**Restored by PPMO**	**Ref.**
PGAM1 **Phosphoglycerate mutase 1**	P18669	136	5	++	
TNNI3 **Troponin I, cardiac muscle**	P19429	53	5	+++	[266]
MB **Myoglobin**	P02144	15	2	++	[266,270,347]
TNNI2 **Troponin I, fast skeletal muscle**	P48788	14	5	+	[266]
LDHB **L-lactate dehydrogenase B chain**	P07195	8.4	0.5	++	[266,348]
FABP3 **Fatty acid-binding protein 3, heart**	P05413	7.8	5	++	[266,270]
TPI1 **Triosephosphate isomerase**	P60174	5.7	2	-	[270]
CAMK2B **Calcium/calmodulin-dependent protein kinase type II subunit beta**	Q13554	5.3	5	++	
CAMK2A **Calcium/calmodulin-dependent protein kinase type II subunit alpha**	Q9UQM7	4.1	5	++	[266]
ANP32B **Acidic leucine-rich nuclear phosphoprotein 32 family member B**	Q92688	3.7	2	++	[266]
CYCS **Cytochrome c**	P99999	3.6	2	+++	[270]
CAMK2D **Calcium/calmodulin-dependent protein kinase type II subunit delta**	Q13557	3.6	5	++	
PCNA **Proliferating cell nuclear antigen**	P12004	3.3	5	++	
HTRA2 **Serine protease HTRA2, mitochondrial**	O43464	3.1	5	+++	
ADAMTS5 **A disintegrin and metalloproteinase with thrombospondin motifs 5**	Q9UNA0	2.8	5	+++	
PTPN11 **Tyrosine-protein phosphatase non-receptor type 11**	Q06124	2.8	5	++	
LYN **Tyrosine-protein kinase Lyn**	P07948	2.7	5	++	
DUSP3 **Dual specificity protein phosphatase 3**	P51452	2.5	5	-	
CAPN1 **Calpain I**	P07384 P04632	2.4	2	+++	
THBS4 **Thrombospondin-4**	P35443	2.2	2	++	[270]
EDA2R **Tumor necrosis factor receptor superfamily member 27**	P35443	2.1	5	++	
TYMS **Thymidylate synthase**	P04818	-2.7	5	++	
SFN **14-3-3 protein sigma**	P31947	-3.2	2	++	

Table 5.2 Top candidate serum protein biomarkers for DMD identified by SOMAscan.
Candidate biomarkers were ranked according to the magnitude of the fold change, dilution group (Dil.), statistical significance and response to therapy. Reference publications (Ref.) are indicated whenever a candidate has been described in the context of dystrophic disease previously. +++ restored to wild-type levels, ++ restored towards wild-type levels, + inconsistent restoration towards wild-type levels between replicates, - not restored towards wild-type levels.

5.3.3 ELISA validation of leading candidates in murine serum

In order to further investigate the newly identified DMD biomarker candidates, a subset of proteins with no known previous association with DMD (Pgam1, Tnni3, Camk2b, Capn1 and Adamts5) and Cycs (which showed a strong response to therapy that has not been described before) was selected for validation by ELISA (Figure 5.7). In addition, murine CK-MM was included given its importance as an established DMD biomarker, although it ranked poorly relative to the top candidate proteins as determined by SOMAscan (Figure 5.6 and Figure 5.7).

Protein abundance was found to be significantly elevated in *mdx* serum ($P<0.0001$) for all candidates tested except for Camk2b ($P<0.06$). Pgam1, Tnni3 and Camk2b were enriched in *mdx* serum by 2.2-2.6 fold (relative to wild-type controls) but showed little or no restoration towards wild-type levels after PPMO treatment. In contrast, clear shifts in protein abundance towards wild-type levels were observed for Adamts5, Cycs and CK-MM following PPMO treatment. The concentration of Cycs in *mdx* serum was increased by 11 fold in *mdx* serum and reduced to a 7 fold increase after exon skipping treatment. Similarly, Adamts5 was enriched by 7.6 fold in *mdx* serum and restored to 2 fold after treatment. CK-MM levels were elevated by 4 fold in *mdx* serum and completely restored to wild-type mice levels following exon skipping therapy. In general, similar results were consistent with the findings from the SOMAscan array, although the degree of therapeutic restoration was less pronounced for Pgam1, Camk2b and Tinn3 when compared with the SOMAscan data. In contrast, for CK-MM therapeutic restoration was greater than in the ELISA data compared to the SOMAscan array. Note that Capn1 protein was undetectable in all samples by ELISA.

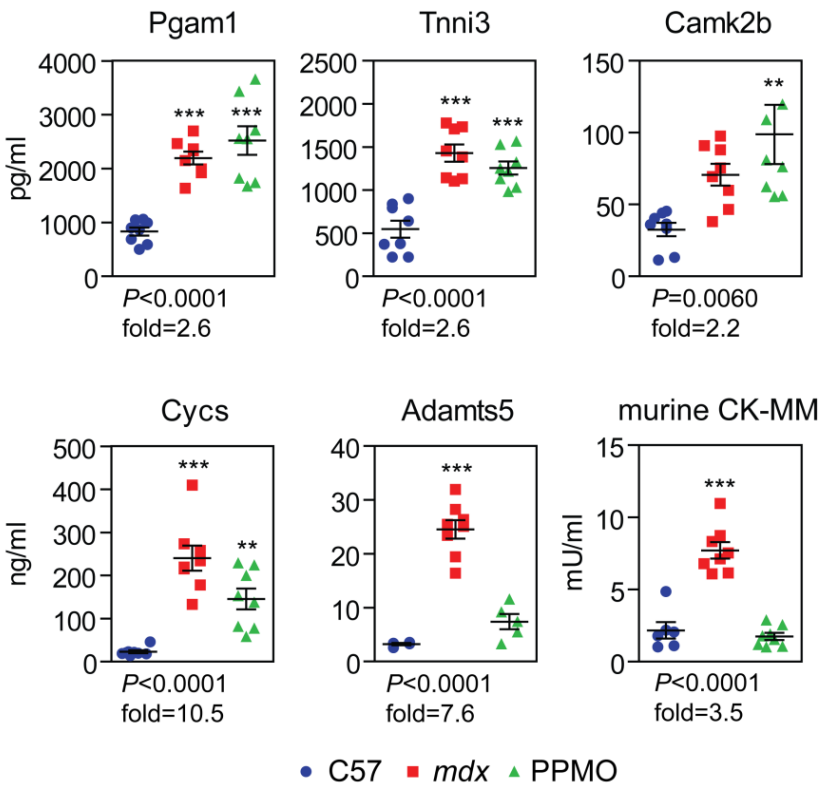

Figure 5.7 ELISA validation of candidate biomarkers.

Five of the top candidate biomarker proteins were selected for by ELISA validation using antibodies targeting the murine proteins. Murine CK-MM was included for comparison. Individual biological replicates are shown. Error bars indicate mean +/- SEM. One-way ANOVA *P* values and *mdx* vs C57 fold changes are indicated for each protein. Bonferroni *post hoc* test significance values are indicated by ***P*<0.01, ****P*<0.001.

5.3.4 Validation of top candidate biomarker in dystrophic patient sera

Based on the SOMAscan data and ELISA validation, ADAMTS5 and PGAM1 were selected as the best-performing biomarker candidates for further testing in human serum samples. ADAMTS5 was chosen as it exhibited the lowest *P* value in the SOMAscan screen (*P*=0.000056) and was profoundly restored after therapy. Similarly, the ELISA data showed good restoration after treatment, with low inter-sample variation, thereby suggesting that ADAMTS5 may be useful as a biomarker for monitoring the response to therapy in DMD patients. The second lead candidate, PGAM1, showed only a mixed response to therapy but was the most elevated protein (136 fold) in *mdx* serum as determined by SOMAscan array and so may consequently comprise a suitable diagnostic biomarker. Human-specific ELISAs for ADAMTS5 and PGAM1 were performed in DMD patient serum (*n*=30) and compared with healthy controls (*n*=18). Additionally, serum from patients with Becker Muscular Dystrophy (BMD) (*n*=30) and facioscapulohumeral muscular dystrophy (FSHD) (*n*=14) was also included. BMD is a dystrophinopathy with much milder symptoms than DMD [350,351]. In contrast to many other muscular dystrophies, FSHD is not associated with a defect of a structural protein. The disease is caused by deletions or hypomethylation in the D4Z4 macrosatellite repeat region leading to derepression *DUX4* retrogene, which encodes a double-homeobox transcription factor expressed in muscle cells [6]. Consequently, FSHD has a molecular pathogenesis that is in principle distinct from DMD and BMD, and it was thus of interest to investigate serum ADAMTS5 in this disease context.

Importantly, ADAMTS5 was significantly (*P*<0.01) elevated in the serum of DMD patients by 3.4 fold relative to healthy controls (Figure 5.8A). Similarly, ADAMTS5 was also elevated in BMD (*P*<0.05) and FSHD (*P*<0.01) patient serum. The mean of serum ADAMTS5 abundance was slightly lower in BMD patients relative to DMD although the median values were very similar. All experimental groups exhibited high variability, with the FSHD patient cohort being the most variable. Receiver operating characteristic (ROC) curve analysis showed that ADAMTS5 was similarly effective at distinguishing between healthy and dystrophic individuals from each patient group (AUC≥0.74, *P*<0.01 in all cases)

although the discrimination was marginally better for DMD (AUC=0.78) (Figure 5.8B). No correlations were observed between ADAMTS5 levels and age in the case of the DMD or FSHD cohorts, whereas a slight negative correlation (*P*=0.0082) was observed for BMD (Figure 5.8C). In addition, PGAM1 was tested in a small subset of DMD, BMD and control samples, although the human specific ELISA assay failed to detect PGAM1 in any samples (data not shown).

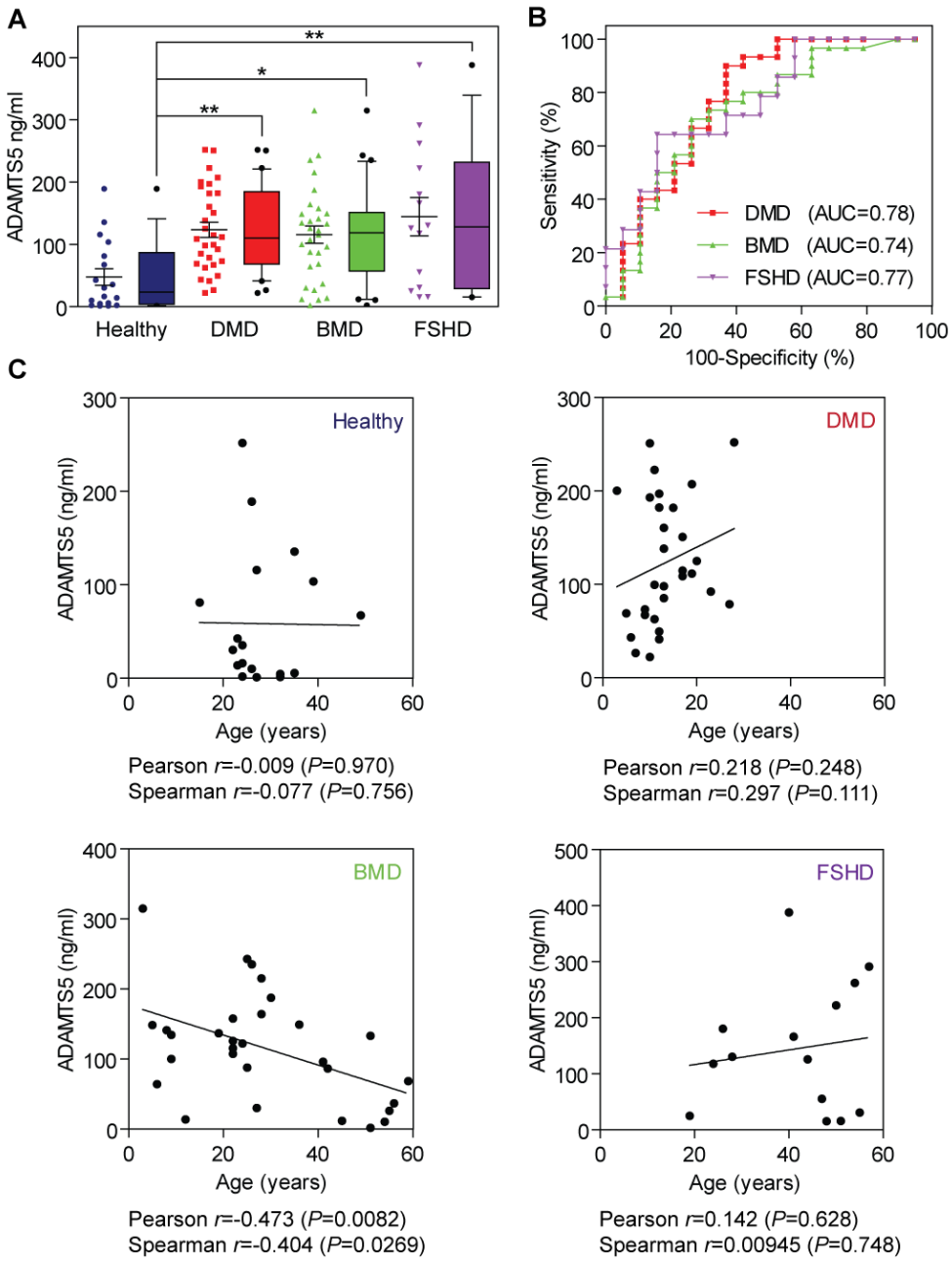

Figure 5.8 ADAMTS5 is elevated in DMD, BMD and FSHD patient serum.

(A) ADAMTS5 abundance was measured by ELISA in serum samples from healthy control individuals (*n*=18), DMD patients (*n*=30), BMD patients (*n*=30) and FSHD patients (*n*=14). Data are shown as scatter plots depicting individual replicates and box plots side-by-side. Error bars indicate mean +/- SEM. Box plots show median and interquartile range, whiskers represent the 10 to 90% range. Differences between groups were significant (*P*=0.0023) as determined by one-way ANOVA. Bonferroni *post hoc* test significance values are indicated as **$P<0.01$, *$P<0.05$. (B) ROC curves for DMD, BMD and FSHD patients. AUC, Area Under the Curve. (C) For each patient/healthy group, the ADAMTS5 ELISA results were compared with age and correlation analysis was performed.

5.4 Discussion

5.4.1 Summary of results

In this chapter, an aptamer-based proteomic screening approach was employed to identify a plethora of novel candidate biomarkers for DMD. The serum levels of 96 proteins were found to be significantly altered (P<0.001, q<0.01) in *mdx* mice. A number of these are consistent with previous studies, and well-described biomarkers of generic muscle tissue damage (CK-MM, MB, LDHB, and FABP3) [254,352,353] were successfully identified as being elevated in *mdx* sera (summarised in Table 5.2 and Table 5.3). Furthermore, CYCS, TPI1 and THBS4 were identified as being elevated in dystrophic serum, consistent with the findings of a mass spectrometry-based approach conducted by Hathout *et al.* [270] (Table 5.3). Importantly, here it was shown that all of these proteins were restored towards wild-type levels following exon-skipping mediated dystrophin restoration, supporting their putative usefulness for monitoring the effectiveness of therapeutic interventions in DMD patients.

In parallel with the SOMAscan profiling of murine sera presented here, a second study by Hathout *et al.* reported a SOMAscan study in DMD patient sera with many findings consistent with those presented here [266] (Table 5.2 and 5.3). In this study, serum samples from 93 DMD patients and 45 control individuals was analysed using the SOMAscan platform and 44 significantly changed proteins were identified. Among these, TNNI2, TINN3, FABP3, MB, LDHB, AN32B and CAMK2A were consistent with the murine study, thus underlining the robustness of the applied methodology despite the use of aptamers selected to bind to human proteins.

The proteins identified in the present study can be classified into a number of groups: (1) myofibrillar proteins (TNNI2, TNNI3), (2) metabolic enzymes (PGAM1, LDHB, TPI1, FABP, MB), (3) calcium metabolism (CAMK2A, CAMK2B, CAMK2C, CAPN1), (4) extracellular matrix remodelling/fibrogenesis (ADAMTS5, THBS4) and (5) others. Interestingly, two proteins (TYMS and SFN) were less abundant in

dystrophic serum relative to wild-type controls, which cannot be easily explained as the result of passive leakage from damaged muscle. The SOMAscan results for Pgam1, Tnni3, Camk2b, Cycs, Adamts5 and CK-MM were further assessed by ELISA. In the following paragraphs, these leading candidate biomarkers and some of the newly identified additional candidates are discussed in detail.

5.4.2 Discussion of novel and top candidate biomarkers

Myofibrillar proteins

In this study, both the skeletal muscle (fast twitch), and cardiac isoforms of Troponin I (TNNI2 and TNNI3 respectively) were highly elevated in *mdx* serum but only TNNI3 levels responded to dystrophin restoration, although to a lesser extent as measured by ELISA. Troponin I comprises the inhibitory subunit of troponin complex that provides calcium sensitivity to the actomyosin apparatus and is currently the most commonly used biomarker for myocardial infarction. However, it has also been previously identified as elevated in DMD patient sera as determined by antibody bead array [271]. Notably, a great number proteins belonging to the contractile actomyosin apparatus have been shown to be elevated in the circulation in the case of DMD, these include myosin light chain, myomesin, troponin and filamin-C (Table 5.3). To this end it is important to know that the SOMAscan array in its current format, has a poor coverage of these proteins (highlighted in red in Table 5.3). Interestingly, many proteins (including Troponin I) of the contractile apparatus that are elevated in dystrophic serum are unchanged or reduced in expression in muscle tissue itself [254].

Metabolic proteins

The glycolytic enzyme PGAM1 (phosphoglycerate mutase 1) was the most upregulated (136 fold) protein in *mdx* sera. However, the response of PGAM1 to exon skipping therapy was mixed, with some treated animals showing total restoration and others showing no response following treatment. Similarly, the ELISA assay showed only moderate restoration and the response between animals was mixed. Furthermore, PGAM1 could not be detected by ELISA in human samples,

suggesting that it may be absent, or present in circulation as peptide fragments. Interestingly, Hathout *et al.* identified the related protein PGAM2 (skeletal and cardiac specific isoform) as elevated in *mdx* and *mdx*-52 sera [270]. Given that PGAM1 and PGAM2 share 80% sequence homology [354], it is therefore possible that the PGAM1 SOMAmer cross-reacted with Pgam2 (which was not included in the SOMAscan analysis). An additional glycolytic enzyme, TPI1, was similarly upregulated in *mdx* sera but not further investigated in this study. Notably, a number of other glycolytic enzymes have previously been shown to be elevated in dystrophic serum but were not part of the aptamer panel (Table 5.3).

Furthermore, LDHB (the heart-specific subunit of lactate dehydrogenase, LDH), was also highly upregulated (8.4 fold) consistent with previous reports in DMD patients and in dystrophic animal models [243]. Elevated LDH is considered a non-specific marker of tissue damage and so its usefulness as a biomarker for DMD is limited. In general, the expression of glycolytic enzymes including LDHB and aldolase, are reduced in dystrophic muscle and there are numerous studies reporting evidence for perturbed energy metabolism in DMD [254,355].

Calcium-associated proteins

A number of calcium-metabolism-associated proteins were elevated in *mdx* serum. These include three protein subunits of the calcium/calmodulin-dependent protein Kinase type II; CAMK2A, CAMK2B and CAMK2D. (A fourth family member, CAMK2G, was not included in the SOMAscan panel). CAMK2 proteins are serine/threonine-specific protein kinases that are involved in a variety of Ca^{2+} signalling functions including metabolic processes, neurotransmitter synthesis/release, cytoskeleton organisation and intracellular calcium homeostasis [356]. In muscle, CAMK2 is a modulator of ryanodine receptor 2 (Ryr2) and inositol triphosphate receptor activity, thereby regulating Ca^{2+} release from the sarcoplasmic reticulum and coupling excitation to myocyte contraction [357,358]. Interestingly, inhibition of CAM2K phosphorylation of the Ryr2 in cardiac muscle has shown to prevent arrhythmias in *mdx* mice thereby suggesting that hyperactivity of

CAMK2 may be a pathological feature in dystrophic muscle [359]. Consequently, upregulation of CAMK2 subunits in the circulation of *mdx* mice is an important novel finding that may point towards a broader role for these proteins in dystrophic pathology.

Capn1 (calpain-1) was also elevated in *mdx* serum in the SOMAscan study. CAPN1 is a calcium-activated cysteine protease associated with a wide variety of cellular functions including apoptosis, myogenesis and sarcomeric remodelling [360]. Interestingly, calpain proteins are elevated in the muscles of both DMD patients and *mdx* mice, most likely due to an increase in intracellular calcium concentration [361,362]. Calpains are ubiquitously expressed, and more than a dozen isoforms have been identified. However, skeletal muscle contains only Capn1, Capn2 and the muscle-specific isoform Capn3 [363]. Given that Capn1 was undetectable by ELISA in mouse sera, it is possible that the CAPN1 SOMAmer cross-reacted with a different calpain isoform (i.e. Capn3) since no other calpain isoforms were assayed by the SOMAscan methodology.

Extracellular matrix/fibrosis-associated proteins

ADAMTS5 (ADAM metalloproteinase with thrombospondin type 1 motif 5) is a zinc metalloprotease that that is involved in proteoglycan (aggrecan) cleavage in cartilage [364–366]. Interestingly, *Adamts5* mRNA expression is upregulated in *mdx* muscle [367], which is likely a consequence of transcriptional activation mediated by the pro-inflammatory transcription factor NF-κB signalling [368]. Consistent with the SOMAscan and the ELISA validation in *mdx* serum, the concentration of ADAMTS5 was also found to be increased in DMD patient sera, supporting its use as a clinical biomarker. However, elevated ADAMTS5 was also observed in BMD and FSHD patients suggesting that it may be a non-specific marker of muscle pathology. To this end, it is worthwhile to mention that, despite having a different molecular pathogenesis, evidence for membrane impairment and sarcolemma reorganisation has also been described for FSHD [369]. Compromised membrane integrity may therefore explain the elevated serum ADAMTS5 levels in all three muscular dystrophies.

Consequently, ADAMTS5 may be useful for diagnosing general muscle pathology or monitoring the response to therapy in patients with established diagnoses, but is not capable of distinguishing between DMD, BMD and FSHD pathology. To this end, no clear correlation was observed between age and ADAMTS5 serum levels, although this may be due to the small size of each patient cohort.

It is noteworthy that expression of ADAMTS5 was previously shown to be elevated in the muscle of FSHD patients [370]. To this end, putative serum protein biomarkers for FSHD were recently identified in an antibody-based screen, although ADAMTS5 was not included in the panel of antibodies tested [371]. Conversely, ADAMTS5 was not identified as being increased in DMD patient serum in the Hathout *et al*. SOMAscan study [266]. This highlights a limitation of biomarker discovery studies in outbred patient populations where differences in genetic background may obscure important findings. To this end, the data presented in this chapter demonstrates that the use of genetically homogenous animal models is advantageous in some instances since inter-animal variation is low and as a result, the statistical power to detect differences is high (despite relatively small sample sizes).

Consistent with the findings of Hathout *et al*. [270], THBS4 (thrombospondin-4) was further identified as elevated in *mdx* serum. THBS4 is a secreted protein which regulates the production and organisation of extracellular matrix. THBS4 is upregulated in hypertrophic and failing hearts [372] and *Thbs4* knockout mice show increased fibrosis [373] suggesting that this protein acts to minimise fibrotic damage. To date, THBS4 has not been implicated in dystrophic pathology, although it may contribute to the adaptive response to fibrotic damage analogous to the situation in heart failure. As a consequence, THBS4 is an interesting candidate for further investigation.

5.4.3 Comparison of SOMAscan methodology with previous studies

Previous studies have investigated serum protein abundance in human DMD patients and dystrophic animal models using mass spectrometry [270,374,375], bead-based antibody arrays [271] or more focused approaches [272,376,377] (summarised in Table 5.3). As mentioned in section 5.4.2, a major limitation of this study is that only the predetermined 1,129 proteins (for which there are SOMAmer reagents available) could be measured. However, this is still a greater number of detected targets compare to the quantity of proteins currently detected by mass spectrometry (335 proteins detected) [270] or by antibody-based bead arrays (315 target proteins) [271]. In addition, only 75 µl of serum are necessary for the SOMAscan array and no pre-fractionation is required to quantify proteins across a large concentration range. Furthermore, the profiling can be automated, in contrast to labour-intensive and technically challenging mass spectrometric analyses.

Nevertheless it is important to note that there were no SOMAmer probes targeted against many putative biomarker proteins identified previously (e.g. XIRP1, F13A1, FN1, TIMP1, MMP9, TNNT3), and so these were invisible to this study. Another potential limitation of the approach used here is that the SOMAmer target capture reagents were developed to bind to recombinant human proteins, and so interspecies differences in protein sequence may obscure important disease-associated changes. Similarly, cross-reactivity of SOMAmer reagents with proteins that are closely homologous with the target analyte may explain the discordant ELISA results for PGAM1 and CAPN1 (in these cases, it is possible that the SOMAmers cross-reacted with Pgam2 (previously identified as elevated in dystrophic serum [270]) and the muscle-specific calpain isoform Capn3 respectively).

Coenen-Stass *et al.* [273]	Rouillon *et al.* [269]	Hathout *et al.* [270]	Ayoglu *et al.* [271]	Hathout *et al.* [266]	Alagaratnam *et al.* [377]
SOMAscan	**MS**	**MS**	**Ab array**	**SOMAscan**	**MS**
ADAMTS5	GOT1	ACTA1	CA3	ACY1	F13A1
ANP32B	**GPT**	ADIPOQ	CKM	ADAM9	
CAMK2A	ALDOA	ALDOA	COL6A1	**ANP32B**	
CAMK2B	**IGFALS**	CKM	ENO3	CA3	**Nadarajah *et al.* [272]**
CAMK2D	C4BPB	**CYCS**	ETFA	**CAMK2A**	**ELISA**
CAPN1	CADH5	ENO3	ETFB	CD55	
CYCS	**CA3**	**FABP3**	LCP1	CDH5	MMP9
DUSP3	CD109	FIBG	MDH2	CHL1	TIMP1
EDA2R	CETP	FLNC	MYL3	CKM	
FABP3	CHL1	GAPDH	PPM1F	CNTN5	
HTRA2	CNDP1	PKM	TNNT3	CXCL10	
LDHB	**COLEC11**	LDHA		**FABP3**	
LYN	CRAC1	LIFR		FAP	
MB	DPP4	LUM		FGA/FGB/FGG	
PCNA	**ENO3**	MDH1		GDF11	
PGAM1	FLNC	**MB**		GPI	
PTPN11	GPI	MYH4		GPT	
SFN	HBA1/2	MYL1		GSN	
THBS4	HBB	MYOM3		HDGFRP2	
TNNI2	HBD	PGAM2		HSPA1A	
TNNI3	HP	PLG		IBSP	
TPI1	**CKM**	PVALB		IL34	
TYMS	**PKM**	PYGM		JAG1	
	LBP	SAA2		**LDHB**	
	LDHA	TTN		MAPK12	
	LDHB	TPI1		**MB**	
	MB	**THBS4**		MDH1	
	MYH7			NOTCH3	
	MYOM2			OMD	
	MYOM3			PLA2G2A	
	GPLD1			PRKACA	
	PYGM			PSMA2	
	TTN			PSPN	
	TPI1			RELT	
	TPM2			RET	
	VASN			RPS7	
	VCL			SERPIND1	
				SET	
				SPINT1	
				TNNI2	
				TNNI3	
				UNC5C	
				WFIKKN1	
				WIF1	

Table 5.3 Comparison of key DMD serum biomarkers findings across seven studies.

Methodologies used in each study are indicated. Proteins for which there was no SOMAmer detection reagent (and were therefore invisible to the SOMAscan methodology) are highlighted in red. Protein biomarker candidates that were commonly detected with the present study are highlighted in bold. Ab: antibody. MS: Mass Spectrometry.

Additionally, some proteins may exist as processed fragments in the circulation [269], or may form protein complexes, meaning that their target epitopes are absent or concealed. Together, these factors may explain some of the minor discrepancies between the SOMAscan data and ELISA validation. The overall concordance with previous studies, and ELISA validation supports the effectiveness of this approach as a screening tool. Nevertheless, it appears that fold changes are higher in the SOMAscan assay compared to ELISA data, thus highlighting the necessity to further validate individual candidate biomarkers with alternative methods.

5.4.4 Conclusion

In conclusion, this chapter has identified multiple novel protein biomarkers in a murine model of DMD utilising the SOMAscan methodology and five of the leading candidate biomarkers identified (Pgam1, Tnni3, Camk2b, Cycs and Adamts5) were successfully validated by ELISA in mouse sera. Furthermore, ADAMTS5 was found to be significantly elevated in human DMD patient serum. Many of these putative biomarkers were restored towards wild-type levels following dystrophin exon skipping in the murine DMD model, suggesting that these may be useful for monitoring the response to experimental therapies in clinical trials. In addition, protein-based serum biomarkers have the advantage that they can be easily and cost-effectively measured with ELISA assays in an automated fashion, and are therefore suitable for screening large patient cohorts. Several of the identified proteins are involved in DMD-associated pathophysiological processes such as metabolic dysfunction, loss of calcium homeostasis and fibrosis, suggesting that they may have utility as biomarkers for these specific features of DMD pathology.

Given the limitations of the methods currently used to determine the relative success of therapeutic interventions in patients, there is an urgent need to identify DMD biomarkers with a high predictive power that can be correlated to clinical outcomes and therapeutic benefit. In order to investigate if ADAMTS5 might be such a suitable candidate, further work is required. For example, by measuring ADMATS5 in longitudinal studies with larger patient cohorts, and by analysing serum samples taken from patients treated with experimental therapies (e.g. exon skipping). In addition, the mechanisms leading to secretion or leakage of ADAMTS5, and other muscle-derived proteins, from dystrophic muscle remain to be elucidated.

6. Discussion and conclusion

6.1 Summary of results

This thesis has investigated two classes of blood-based biomarkers for DMD, namely ex-miRNAs and circulating proteins. Despite sharing a common purpose, the context in which these two classes were studied here was different. While a number of studies have explored the use of ex-myomiRs as promising biomarkers to monitor DMD disease severity and response to therapy, this work has focused on studying the biological relevance of ex-miRNAs both in the context of normal muscle physiology and in dystrophic pathology. In contrast, the development of serum protein biomarkers for therapeutic monitoring is still in its infancy. As result, the identification of novel, therapy-responsive candidate biomarkers was the main aim of the work undertaken in this area.

Chapter 3 demonstrated that myomiRs are selectively released during periods of myogenic differentiation in cell culture models and *in vivo.* Given that myomiRs can be released in absence of dystrophic pathology, their presence in the extracellular space cannot be explained by passive leakage after muscle damage alone, thus suggesting that they may serve a physiological function in some contexts. In summary, the presented findings suggest that serum myomiR abundance is a function of the regenerative/degenerative status of the muscle, overall muscle mass, tissue expression levels and miRNA stability in the extracellular space. Furthermore, myomiRs and other miRNAs are rapidly released from myotube cultures upon media change by an as yet unknown mechanism that was shown to be independent of ceramide-mediated EV secretion.

The fractionation studies in the chapter 4 of this thesis showed that ex-myomiRs are predominantly stabilised as part of protein and/or lipoprotein complexes and not in vesicles, as determined by size-exclusion chromatography. This technique allows for the isolation of EVs with improved purity and integrity relative to standard EV isolation protocols based on ultracentrifugation. Despite the observed parallels in myomiR release and distribution pattern after SEC fractionation, there are striking differences in the stability of individual ex-myomiRs at a physiologically relevant temperature

(37˚C). This observation may be explained by distinct ex-myomiR carriers. Alternatively, differing association/dissociation rates of the individual ex-miRNAs with their carriers may also explain these results. Together, these findings have important implications for both the biological relevance of ex-myomiRs in myogenesis (further discussed in 6.2) and the use of ex-myomiRs as biomarkers for DMD disease progression and monitoring response to therapy (further discussed in 6.3).

In the chapter 5, 1,129 pre-selected target proteins were screened in murine serum for their potential as therapy responsive DMD biomarkers. The identification of protein-based biomarkers in the circulation is complicated due to the massive complexity of the serum proteome and the typical low abundance of candidate biomarkers in comparison to highly abundant serum proteins such as albumin or immunoglobulins. To overcome these challenges, an aptamer-based proteomic methodology was applied in this work which is unaffected by the presence of high concentrations of serum proteins. This approach effectively converts measurements of protein concentrations into nucleic acid-based signals, which can be easily measured by DNA microarrays.

The serum levels of 96 proteins were found to be significantly altered in *mdx* mice and many of these were restored towards wild-type level after exon skipping therapy. Five top candidates were selected based on their potential as diagnostic or therapeutic monitoring biomarkers for DMD. These leading candidates (Pgam1, Tnni3, Camk2b, Cycs and Adamts5) were validated by ELISA in mouse serum. Furthermore, the best-performing candidate, ADAMTS5, was found to be significantly elevated in DMD patient serum and interestingly also in the serum of BMD and FSHD patients, thus indicating its potential utility either for diagnosing general muscle pathology or monitoring the response to therapy in patients with established diagnoses.

6.2 Physiological relevance of extracellular myomiRs

The discovery that miRNAs can be stable in various biofluids and display signatures of physiological/ pathophysiological states, holds great potential for future biomarker research, identification of therapeutic targets, and for furthering the understanding of molecular disease pathology. In general, the suggested functions of ex-miRNAs include waste disposal, signalling (endocrine or paracrine) via transfer to recipient cells and spread of viral infection/latency [378].

With respect to the muscle-specific miRNAs studied in this work (miR-1, miR-133a and miR-206), it remains unclear what their potential function in the extracellular space is. Based on the findings presented in this thesis it is likely that they are relevant to myogenic differentiation. However, it is worthwhile noting that this relevance may not necessarily entail functional transfer of these ex-myomiRs. Given the large increase of intracellular myomiRs upon induction of differentiation, release of myomiRs during myogenesis could help to regulated intracellular myomiR concentrations and may serve to facilitate shut-down myomiR functions once the necessary gene expression modulation has been achieved. To this end it will be interesting to investigate if secretion of tissue-specific miRNAs during organ development and cellular lineage differentiation comprises a general phenomenon of as yet unexplored biological relevance.

Furthermore, ex-miRNAs have been shown to be recognised by RNA-sensing receptors such as TLR7/8 which are expressed in muscle tissue [231,232,379]. As a result, one may speculate that cells are capable of ‘sensing’ ex-miRNAs levels and respond if these levels change (e.g. the rapid miRNA export observed after media change in section 3.3.5). Clearly more research is needed in this area to understand to what extent cells, and myocytes in particular, might be capable of sensing ex-miRNA concentrations and what the biological impact of this finding may be.

In contrast, assuming that ex-myomiRs could indeed contribute to intercellular communication, specific receptors on recipient cells recognising and internalising miRNA-RNP complexes would need to be identified, as it has yet to be demonstrated that non-lipid-encapsulated miRNAs can be taken

up by target cells and induce sequence-specific mRNA silencing [378]. Currently, there is some evidence that ex-miRNAs transported in EVs derived from myotubes or mesenchymal stem cells, can influence myogenesis [380,381]. Both studies, have the drawback that relatively crude methodologies were used for EV isolation (only a single UC step and no washing of the EV pellet), and further, high amounts of EVs were used (as discussed in section 1.4.3) thereby somehow limiting the usefulness of these findings. Furthermore, the experiments undertaken here, and previous work from the Wood group, have demonstrated that the large majority (~99%) of ex-myomiRs exists outside of EVs, therefore raising doubts as to which extent these myomiRs could be functionally transferred between cells. However, given that Roberts *et al.* demonstrated co-precipitation of ex-myomiRs with APOA1, the major lipoprotein complex of HDL vesicles, one may hypothesise that there is a possibility of 'loading' miRNAs into lipoproteins in the capillaries of muscular tissue. Once sequestered by HDL, ex-myomiRs may travel to distinct sites in the organism or simply circulate in the bloodstream until eventually degraded. Similarly, ex-miRNA associated to AGO2 may form ternary complexes with HDL in the circulation and can subsequently be transferred between cells via HDL uptake. Importantly, it remains to be investigated to what extent myomiRs associate with APOA1 and if miRNAs in HDL are also bound to AGO2.

Hypothesising further that myomiRs may participate in intercellular communication, it will be of pivotal importance to determine how many myomiR copies need to be transferred per recipient cell in order to cause a measurable effect on target gene expression. Therefore, this study aimed to generate more meaningful data by determining absolute copy numbers for both cellular and ex-miRNAs rather than by simply measuring fold changes. Previous reports state that at least 1,000 miRNA copies per cell are necessary to induce a measurable effect on target mRNA concentration, depending on individual mRNA turnover rate [382,383]. As a result, signalling between myofibres via ex-myomiR transfer is an unlikely scenario when considering the high levels of intracellular myomiRs already present in myotubes. However, myomiR levels are only induced during satellite cell activation and are therefore initially far less abundant in dormant satellite cells than in myotubes

[103,384]. Consequently, a plausible hypothesis may be that differentiating myotubes (expressing very high levels of myomiRs) secrete myomiRs locally and thereby signal to activate neighbouring satellite cells (much lower expression of myomiRs), thus serving to potentiate the regenerative response in a paracrine manner. Another possible scenario could be that released myomiRs might communicate with other cell types in the muscle niche, such as motor neurons or fibroadipogenic progenitors to influence synapse plasticity at the motor end plate or modulate the muscle extracellular milieu respectively. Indeed, communication between muscle and neuron has been demonstrated in mouse [385] and drosophila [386], although it is important to note that in both cases signalling was mediated by EV.

While there seem to be some correlation of intra- and extracellular levels of miRNAs expressed in muscle cells, it is noteworthy that not all muscle-enriched miRNAs are also highly abundant in the extracellular space or dystrophic serum. The example highlighted in this study is let-7a, which is very abundant in C2C12 myotubes and also in skeletal muscle [308], but only found at low levels in the culture supernatant. Even more importantly, let-7a is also only present at very low levels in serum and is unchanged in dystrophic serum [277]. This finding suggests that there is some selectivity in miRNAs release from muscle, indicating that some miRNAs may be sorted for export while others are retained. Consequently, one can speculate that this specificity is likely to be related to the intracellular locations of these miRNAs as well as by the nature of their carriers. Although the exact subcellular location of RNAi pathways is still being investigated, miRNA-AGO2 complexes have been shown to be almost exclusively associated with the rough endoplasmatic reticulum (rER) [387]. In contrast, miRNAs that are selectively loaded into EVs (chapter 1.4.3) must be in close proximity to MVBs, highlighting the possibility that individual miRNA-Argonaute complexes have distinct subcellular locations. Studying this phenomenon via miRNA fluorescence *in situ* hybridisation (FISH) and high resolution microscopy may provide exciting new insights into this under-appreciated area of miRNA biology. Additional examples of miRNAs which are enriched in skeletal muscle but not elevated during dystrophic pathology, could potentially be discovered by performing small RNA

sequencing in skeletal muscle and serum. In addition to their biological significance, understanding the causes and mechanisms of myomiR release from healthy and dystrophic muscle is of importance for the appropriate interpretation of serum myomiR levels in DMD patient serum (discussed further in 6.3).

6.3 Future prospects for circulating DMD biomarkers

The rapid progression of new therapies for DMD towards clinical testing necessitates an equally fast development of appropriate clinical outcome measures and therapeutic monitoring biomarkers with high predictive power, and that ideally constitute reliable surrogate endpoints. In the specific case of DMD, useful measurements of therapeutic efficacy have lagged behind drug development and this imbalance has led to some controversies regarding the recent approvals for the exon skipping drug Eteplirsen and the stop-codon read-through compound Ataluren by the FDA and EMA respectively. The problem is further highlighted in the case of a phase 3 Drisapersen trial, where the failure to demonstrate a positive treatment effect was likely related to insufficiently restrictive patient inclusion criteria and the choice of the 6MWT as primary endpoint [388]. Evidently, without revisiting outcome measures for clinical testing and improved biomarkers, approval of novel DMD therapeutics may remain elusive. However, it is important to note that, efficient treatments are needed in order to validate therapeutic monitoring biomarkers in DMD patients, highlighting that advances in treatment and biomarker discovery are interdependent on one another. The following paragraphs summarise recent advances in circulating biomarker research and highlight the necessary steps to improve their clinical utility for DMD.

Importantly, only two studies, including the aptamer proteomic study described in this thesis, have demonstrated restoration of circulating protein biomarkers towards wild-type levels after therapeutic intervention, although the findings are limited to DMD animal models [273,306]. Similarly, ex-myomiRs levels in *mdx* mice have shown to be responsive to dystrophin restoring treatment [138,285,286]. However, this finding was not entirely recapitulated in DMD patients treated with Eteplirsen during the first two clinical trials, which only showed a non significant trend towards ex-myomiR restoration [214]. To this end, it is possible that either the number of patients included in the distinct treatment groups was not high enough to detect a significant restoration effect, or the amount of restored dystrophin may have been insufficient to influence ex-myomiR levels [214]. Clearly, additional data regarding the responsiveness of circulating DMD biomarker to

therapy are needed to establish an understanding of the extent to which their predictive power shown in animal models is relevant in DMD patients.

Secondly, for the utility of serum biomarkers in clinical testing, it is of great importance to characterise their relation to patient age and disease progression (including loss of ambulance). Notably, these two factors are difficult to separate since they exhibit a co-linear relationship to each other (i.e. dystrophic pathology generally increases with age). To date, most of the circulating DMD biomarkers identified show a negative correlation with patient age and ambulant status, similar to the reduction of serum myomiR levels observed in the aged *mdx* mice (section 3.3.3). To this end, decreasing levels of miR-1 and miR-133 were also detected in DMD patients older than 10 years [214]. As a consequence, it is likely that ex-myomiR levels are indicative of the remaining muscle mass, at least in older DMD patients that no longer undergo cycles of regeneration and degeneration [214]. In this patient group, serum myomiR levels are unlikely to be suitable biomarkers for monitoring a response to therapy, as a decrease in their level could both indicate successful therapy as well as advanced muscle loss. In contrast, higher serum myomiR levels could suggest an increase in pathology and muscle degeneration, but may also be indicative of muscle growth and differentiation as shown in chapter 3 of this thesis. These limitations underline that ex-myomiR levels must be interpreted in the context of other clinical information and/or additional biomarkers.

With respect to circulating protein biomarkers, no clear correlation was observed between ADAMTS5 (the leading biomarker candidate identified in the aptamer screen in chapter 5) serum levels and DMD patient age. Possible reasons for the lack of correlation include both the small size of each patient cohort, but also the observed high inter-patient variability. Notably, serum abundance of TNNT3, MYL3, FABP3, CKM and CK was higher in ambulant DMD patients without cardiomyopathy [267]. In addition, all of these proteins decreased in abundance in serum with age by approximately 10-19% [267]. Recently, Hathout *et al.* separated a set of 44 putative serum protein biomarkers identified by SOMAscan in DMD patients into four groups, depending on their relation to disease

progression and age [266]. The majority of the identified biomarkers where categorised in the first group. Biomarkers in this group were negatively correlated to DMD patient age and unchanged in healthy controls. This group mainly contained muscle-derived proteins that are released into the circulation due to muscle damage, with serum levels likely to be dependent on the remaining muscle mass and physical activity. Biomarkers with these characteristics are unlikely to be suitable as therapy monitoring/surrogate biomarker as both successful therapy and advanced disease progression may result in decreases in their serum levels. Serum levels of biomarkers in groups 2 and 3 were either consistently higher or consistently lower compared to healthy controls. The four proteins (GDF11, CD55, RELT, WFIKKN1) that were assigned into the last group may be of the highest interest, since their levels were comparable between young patients and controls, but serum abundance changed in opposite direction with age [266]. Nevertheless further validation is needed to confirm whether or not abundance of these four proteins follow disease progression.

Interestingly, there is evidence that MMP9 increases with age and pathology in DMD patients and may consequently be a promising therapeutic monitoring biomarker [272]. However, a recent study questioned the utility of MMP9 as a biomarker, and suggested that MMP9 serum levels are more reflective of a response to corticosteroids treatment and not of disease progression [389]. In contrast, this finding could not be replicated in another cohort of patients [390]. These conflicting observations underline the importance of studying the relation of circulating biomarkers to other therapeutic interventions that are conventionally used to manage DMD symptoms (most importantly corticosteroids). Interestingly, ex-myomiR levels were higher in DMD patients treated with glucocorticoids compared to those not treated with steroids [214]. This finding may also point towards a stronger correlation of ex-myomiR levels to overall muscle mass than to disease progression.

Lastly, establishing reference ranges for new DMD biomarkers that correspond to clinical endpoints and patient benefit is a key step to eventually finding surrogate biomarkers for DMD. However,

efforts to link circulating protein biomarkers to functional outcomes have so far been mostly disappointing. Zaharieva *et al*. found that DMD patients with respiratory muscle weakness (as indicated by low FCV values) had reduced levels of miR-1 and miR-133, although no correlation between ex-myomiR levels and NSAA scores was observed [214].

Furthermore, serum levels of MMP9 and TIMP1 did not correlate with NSAA score in DMD patients [272]. Another recent study showed that TNNT3, CK-MM and FABP3 levels in serum of LGMD2B patients did not correlate with the results from a 10 minute walk test and only a weak correlation with serum MYL3 was observed [267]. Interestingly, the same study showed a positive correlation between these serum protein biomarkers with the FVC in DMD patients [267].

In summary, serum biomarkers for muscular dystrophies have shown potential and clearly fulfil some of the criteria outlined earlier for ideal biomarkers (section 1.5.1): they are minimally invasive, can be easily and cost-efficiently measured throughout the duration of a clinical trial, they sample the pathophysiological state of the whole body and some have shown to be responsive to therapeutic intervention in DMD animal models. However, their predictive power and the relation to functional outcomes need to be further established before they can serve as reliable secondary endpoints in clinical trials. With the progression of clinical testing and increasing numbers of patients enrolled in clinical trials [391], more data should become available in the next few years, which will need to be methodically integrated with current data sets to identify leading candidates [243]. Thorough testing is then required in large patient cohorts to characterise their relationship to age, disease progression, corticosteroids usage and functional outcome/patient benefit. Ideally, placebo groups are needed to understand the behaviour of candidate biomarkers during natural disease progression. Finally, it could be that a panel, rather than a single biomarker, will be identified as most suitable and that this panel may require adjusting for patients at different ages and/or disease stages.

6.4 Concluding remarks

A major challenge in developing novel treatment strategies for human diseases is the identification of suitable disease-associated markers that allow assessment of the therapeutic efficacy of experimental treatments. To this end, the work in my thesis has contributed to a better understanding of the biology and identity of circulating microRNAs and protein biomarkers for muscular wasting diseases, and DMD in particular.

The finding, that muscle-specific miRNAs are selectively released during periods of differentiation, points towards a previously unknown association of ex-myomiRs with myogenesis, and possibly in cellular differentiation in general. This aspect of miRNA biology may be an exciting avenue to be explored in future research. To this end, my studies emphasise that the nature and intracellular location of non-vesicular ex-myomiR carriers need to be investigated in a greater detail in order to understand selective myomiR export and to explain their differential stability observed in the extracellular space. Furthermore, multiple observations from my thesis work are relevant for the usage of ex-myomiRs as biomarkers for DMD, these include: differential stability of ex-myomiRs in serum at 37°C, myomiR release after exercise, correlation of ex-myomiR levels to overall muscle mass and release of myomiRs during muscle growth and myogenic differentiation. All of these factors influence the abundance of serum myomiRs and therefore need to be considered when relating their levels to DMD disease progression or response to a therapeutic intervention.

In the second part of my thesis, I have identified several novel protein serum biomarkers that showed response to dystrophin restoration in a mouse model of DMD, and I demonstrated for one of them a potential utility in DMD patients. Importantly, to our knowledge, this aptamer screen is the first large-scale screening approach undertaken that investigates the restoration of the serum proteome after therapeutic intervention. As such, the biomarkers identified here may contribute towards establishing a set of biomarkers with predictive powers that can be utilised in future clinical trials.

7. References

1. Muntoni F, Wood MJA. Targeting RNA to treat neuromuscular disease. *Nat Rev Drug Discov* 2011; **10**:621–637.

2. Mercuri E, Muntoni F. Muscular dystrophies. *Lancet* 2013; **381**:845–860.

3. Hoffman EP, Brown RH, Kunkel LM. Dystrophin: The protein product of the duchenne muscular dystrophy locus. *Cell* 1987; **51**:919–928.

4. Ranum LPW, Cooper TA. Rna-mediated neuromuscular disorders. *Annu Rev Neurosci* 2006; **29**:259–277.

5. Dixit M, Ansseau E, Tassin A, *et al.* DUX4, a candidate gene of facioscapulohumeral muscular dystrophy, encodes a transcriptional activator of PITX1. *Proc Natl Acad Sci USA* 2007; **104**:18157–18162.

6. Tawil R, van der Maarel SM, Tapscott SJ. Facioscapulohumeral dystrophy: the path to consensus on pathophysiology. *Skeletal Muscle* 2014; **4**:12.

7. Dooley J, Gordon KE, Dodds L, MacSween J. Duchenne muscular dystrophy: a 30-year population-based incidence study. *Clin Pediatr (Phila)* 2010; **49**:177–179.

8. Bushby K, Finkel R, Birnkrant DJ, *et al.* Diagnosis and management of Duchenne muscular dystrophy, part 1: diagnosis, and pharmacological and psychosocial management. *Lancet Neurol* 2010; **9**:77–93.

9. Bresolin N, Castelli E, Comi GP, *et al.* Cognitive impairment in Duchenne muscular dystrophy. *Neuromuscular Disorders* 1994; **4**:359–369.

10. Muntoni F, Torelli S, Ferlini A. Dystrophin and mutations: one gene, several proteins, multiple phenotypes. *Lancet Neurol* 2003; **2**:731–740.

11. Buvoli M, Buvoli A, Leinwand LA. Interplay between Exonic Splicing Enhancers, mRNA Processing, and mRNA Surveillance in the Dystrophic Mdx Mouse. *PLoS ONE* 2007; **2**.

12. Monaco AP, Bertelson CJ, Liechti-Gallati S, Moser H, Kunkel LM. An explanation for the phenotypic differences between patients bearing partial deletions of the DMD locus. *Genomics* 1988; **2**:90–95.

13. Zubrzycka-Gaarn EE, Bulman DE, Karpati G, *et al.* The Duchenne muscular dystrophy gene product is localized in sarcolemma of human skeletal muscle. *Nature* 1988; **333**:466–469.

14. Ervasti JM, Campbell KP. Membrane organization of the dystrophin-glycoprotein complex. *Cell* 1991; **66**:1121–1131.

15. Amann KJ, Renley BA, Ervasti JM. A cluster of basic repeats in the dystrophin rod domain binds F-actin through an electrostatic interaction. *J Biol Chem* 1998; **273**:28419–28423.

16. Lai Y, Thomas GD, Yue Y, *et al.* Dystrophins carrying spectrin-like repeats 16 and 17 anchor nNOS to the sarcolemma and enhance exercise performance in a mouse model of muscular dystrophy. *J Clin Invest* 2009; **119**:624–635.

17. Davies KE, Nowak KJ. Molecular mechanisms of muscular dystrophies: old and new players. *Nat Rev Mol Cell Biol* 2006; **7**:762–773.

18. Ishikawa-Sakurai M, Yoshida M, Imamura M, Davies KE, Ozawa E. ZZ domain is essentially required for the physiological binding of dystrophin and utrophin to beta-dystroglycan. *Hum Mol Genet* 2004; **13**:693–702.

19. Rahimov F, Kunkel LM. Cellular and molecular mechanisms underlying muscular dystrophy. *J Cell Biol* 2013; **201**:499–510.

20. Deconinck N, Dan B. Pathophysiology of duchenne muscular dystrophy: current hypotheses. *Pediatr Neurol* 2007; **36**:1–7.

21. Campbell KP, Kahl SD. Association of dystrophin and an integral membrane glycoprotein. *Nature* 1989; **338**:259–262.

22. Petrof BJ. The molecular basis of activity-induced muscle injury in Duchenne muscular dystrophy. *Mol Cell Biochem* 1998; **179**:111–123.

23. Allen DG, Whitehead NP. Duchenne muscular dystrophy – What causes the increased membrane permeability in skeletal muscle? *The International Journal of Biochemistry & Cell Biology* 2011; **43**:290–294.

24. culligan KG, Ohlendieck K. Abnormal Calcium Handling in Muscular Dystrophy. *Basic Appl Myol* 2002; **12**:147–157.

25. Kumar A, Takada Y, Boriek AM, Aggarwal BB. Nuclear factor-κB: its role in health and disease. *J Mol Med* 2004; **82**:434–448.

26. Sander M, Chavoshan B, Harris SA, *et al.* Functional muscle ischemia in neuronal nitric oxide synthase-deficient skeletal muscle of children with Duchenne muscular dystrophy. *Proc Natl Acad Sci U S A* 2000; **97**:13818–13823.

27. Schmalbruch H. Regenerated muscle fibers in Duchenne muscular dystrophy A serial section study. *Neurology* 1984; **34**:60–60.

28. Heslop L, Morgan JE, Partridge TA. Evidence for a myogenic stem cell that is exhausted in dystrophic muscle. *J Cell Sci* 2000; **113 (Pt 12)**:2299–2308.

29. Boldrin L, Zammit PS, Morgan JE. Satellite cells from dystrophic muscle retain regenerative capacity. *Stem Cell Research* 2015; **14**:20–29.

30. Collins CA, Morgan JE. Duchenne's muscular dystrophy: animal models used to investigate pathogenesis and develop therapeutic strategies. *Int J Exp Pathol* 2003; **84**:165–172.

31. McGreevy JW, Hakim CH, McIntosh MA, Duan D. Animal models of Duchenne muscular dystrophy: from basic mechanisms to gene therapy. *Disease Models & Mechanisms* 2015; **8**:195–213.

32. Lefaucheur JP, Pastoret C, Sebille A. Phenotype of dystrophinopathy in old MDX mice. *Anat Rec* 1995; **242**:70–76.

33. Pastoret C, Sebille A. mdx mice show progressive weakness and muscle deterioration with age. *J Neurol Sci* 1995; **129**:97–105.

34. Biggar WD, Gingras M, Fehlings DL, Harris VA, Steele CA. Deflazacort treatment of Duchenne muscular dystrophy. *J Pediatr* 2001; **138**:45–50.

35. Moxley RT, Pandya S, Ciafaloni E, Fox DJ, Campbell K. Change in natural history of Duchenne muscular dystrophy with long-term corticosteroid treatment: implications for management. *J Child Neurol* 2010; **25**:1116–1129.

36. Aartsma-Rus A, Van Deutekom JCT, Fokkema IF, Van Ommen G-JB, Den Dunnen JT. Entries in the Leiden Duchenne muscular dystrophy mutation database: an overview of mutation types and paradoxical cases that confirm the reading-frame rule. *Muscle Nerve* 2006; **34**:135–144.

37. Haas M, Vlcek V, Balabanov P, *et al.* European Medicines Agency review of ataluren for the treatment of ambulant patients aged 5 years and older with Duchenne muscular dystrophy resulting from a nonsense mutation in the dystrophin gene. *Neuromuscul Disord* 2015; **25**:5–13.

38. McElroy SP, Nomura T, Torrie LS, *et al.* A Lack of Premature Termination Codon Read-Through Efficacy of PTC124 (Ataluren) in a Diverse Array of Reporter Assays. *PLOS Biol* 2013; **11**:e1001593.

39. Bushby K, Kirschner J, Luo X, *et al.* Results of North Star Ambulatory Assessments (NSAA) in the Phase 3 Ataluren Confirmatory Trial in Patients with Nonsense Mutation Duchenne Muscular Dystrophy (ACT DMD) (S28.002). *Neurology* 2016; **86**:S28.002.

40. van Deutekom JCT, van Ommen G-JB. Advances in Duchenne muscular dystrophy gene therapy. *Nat Rev Genet* 2003; **4**:774–783.

41. Sienkiewicz D, Kulak W, Okurowska-Zawada B, Paszko-Patej G, Kawnik K. Duchenne muscular dystrophy: current cell therapies. *Ther Adv Neurol Disord* 2015; **8**:166–177.

42. Tinsley J, Deconinck N, Fisher R, *et al.* Expression of full-length utrophin prevents muscular dystrophy in mdx mice. *Nat Med* 1998; **4**:1441–1444.

43. Anon. PoC Study to Assess Activity and Safety of SMT C1100 (Ezutromid) in Boys With DMD - Full Text View - ClinicalTrials.gov.

44. Li D, Bareja A, Judge L, *et al.* Sarcolemmal nNOS anchoring reveals a qualitative difference between dystrophin and utrophin. *J Cell Sci* 2010; **123**:2008–2013.

45. Guiraud S, Squire SE, Edwards B, *et al.* Second-generation compound for the modulation of utrophin in the therapy of DMD. *Hum Mol Genet* 2015; **24**:4212–4224.

46. Chamberlain JS. Gene therapy of muscular dystrophy. *Hum Mol Genet* 2002; **11**:2355–2362.

47. Bowles DE, McPhee SW, Li C, *et al.* Phase 1 Gene Therapy for Duchenne Muscular Dystrophy Using a Translational Optimized AAV Vector. *Mol Ther* 2012; **20**:443–455.

48. Anon. Press Announcements - FDA grants accelerated approval to first drug for Duchenne muscular dystrophy.

49. Anon. FDA Declines Approval for Drisapersen in DMD. *Medscape*.

50. Jinek M, Chylinski K, Fonfara I, Hauer M, Doudna JA, Charpentier E. A programmable dual-RNA-guided DNA endonuclease in adaptive bacterial immunity. *Science* 2012; **337**:816–821.

51. Tabebordbar M, Zhu K, Cheng JKW, *et al.* In vivo gene editing in dystrophic mouse muscle and muscle stem cells. *Science* 2016; **351**:407–411.

52. Nelson CE, Hakim CH, Ousterout DG, *et al.* In vivo genome editing improves muscle function in a mouse model of Duchenne muscular dystrophy. *Science* 2016; **351**:403–407.

53. Long C, Amoasii L, Mireault AA, *et al.* Postnatal genome editing partially restores dystrophin expression in a mouse model of muscular dystrophy. *Science* 2016; **351**:400–403.

54. National Academies of Sciences E. *International Summit on Human Gene Editing: A Global Discussion*.; 2016.

55. Kleinstiver BP, Pattanayak V, Prew MS, *et al.* High-fidelity CRISPR–Cas9 nucleases with no detectable genome-wide off-target effects. *Nature* 2016; **529**:490–495.

56. Zuris JA, Thompson DB, Shu Y, *et al.* Efficient Delivery of Genome-Editing Proteins In Vitro and In Vivo. *Nat Biotechnol* 2015; **33**:73–80.

57. Marwick C. First “antisense” drug will treat CMV retinitis. *JAMA* 1998; **280**:871.

58. Stephenson ML, Zamecnik PC. Inhibition of Rous sarcoma viral RNA translation by a specific oligodeoxyribonucleotide. *Proc Natl Acad Sci U S A* 1978; **75**:285–288.

59. Kurreck J. Antisense technologies. Improvement through novel chemical modifications. *Eur J Biochem* 2003; **270**:1628–1644.

60. Goyenvalle A, Vulin A, Fougerousse F, *et al.* Rescue of Dystrophic Muscle Through U7 snRNA-Mediated Exon Skipping. *Science* 2004; **306**:1796–1799.

61. Voit T, Topaloglu H, Straub V, *et al.* Safety and efficacy of drisapersen for the treatment of Duchenne muscular dystrophy (DEMAND II): an exploratory, randomised, placebo-controlled phase 2 study. *The Lancet Neurology* 2014; **13**:987–996.

62. Lu Q, Cirak S, Partridge T. What Can We Learn From Clinical Trials of Exon Skipping for DMD? *Mol Ther Nucleic Acids* 2014; **3**:e152.

63. Cirak S, Arechavala-Gomeza V, Guglieri M, *et al.* Exon skipping and dystrophin restoration in patients with Duchenne muscular dystrophy after systemic phosphorodiamidate morpholino oligomer treatment: an open-label, phase 2, dose-escalation study. *Lancet* 2011; **378**:595–605.

64. Ezzat K, Aoki Y, Koo T, *et al.* Self-Assembly into Nanoparticles Is Essential for Receptor Mediated Uptake of Therapeutic Antisense Oligonucleotides. *Nano Lett* 2015; **15**:4364–4373.

65. Jearawiriyapaisarn N, Moulton HM, Buckley B, *et al.* Sustained dystrophin expression induced by peptide-conjugated morpholino oligomers in the muscles of mdx mice. *Mol Ther* 2008; **16**:1624–1629.

66. Yin H, Moulton HM, Betts C, *et al.* Functional rescue of dystrophin-deficient mdx mice by a chimeric peptide-PMO. *Mol Ther* 2010; **18**:1822–1829.

67. Betts C, Saleh AF, Arzumanov AA, *et al.* Pip6-PMO, A New Generation of Peptide-oligonucleotide Conjugates With Improved Cardiac Exon Skipping Activity for DMD Treatment. *Mol Ther Nucleic Acids* 2012; **1**:e38.

68. Goyenvalle A, Griffith G, Babbs A, *et al.* Functional correction in mouse models of muscular dystrophy using exon-skipping tricyclo-DNA oligomers. *Nat Med* 2015; **21**:270–275.

69. Aartsma-Rus A, Fokkema I, Verschuuren J, *et al.* Theoretic applicability of antisense-mediated exon skipping for Duchenne muscular dystrophy mutations. *Hum Mutat* 2009; **30**:293–299.

70. Béroud C, Tuffery-Giraud S, Matsuo M, *et al.* Multiexon skipping leading to an artificial DMD protein lacking amino acids from exons 45 through 55 could rescue up to 63% of patients with Duchenne muscular dystrophy. *Hum Mutat* 2007; **28**:196–202.

71. Miskew Nichols B, Aoki Y, Kuraoka M, Lee JJA, Takeda S 'ichi, Yokota T. Multi-exon Skipping Using Cocktail Antisense Oligonucleotides in the Canine X-linked Muscular Dystrophy. *J Vis Exp* 2016.

72. Filipowicz W, Jaskiewicz L, Kolb FA, Pillai RS. Post-transcriptional gene silencing by siRNAs and miRNAs. *Current Opinion in Structural Biology* 2005; **15**:331–341.

73. Wang Z, Rao D, Senzer N, Nemuaitis J. RNA Interference and Cancer Therapy - Springer. *Pharmaceutical research* 2011; **Dec**:2983–95.

74. Lee RC, Feinbaum RL, Ambros V. The C. elegans heterochronic gene lin-4 encodes small RNAs with antisense complementarity to lin-14. *Cell* 1993; **75**:843–854.

75. Lee RC, Ambros V. An extensive class of small RNAs in Caenorhabditis elegans. *Science* 2001; **294**:862–864.

76. Lagos-Quintana M, Rauhut R, Lendeckel W, Tuschl T. Identification of Novel Genes Coding for Small Expressed RNAs. *Science* 2001; **294**:853–858.

77. Reinhart BJ, Weinstein EG, Rhoades MW, Bartel B, Bartel DP. MicroRNAs in plants. *Genes Dev* 2002; **16**:1616–1626.

78. Friedman RC, Farh KK-H, Burge CB, Bartel DP. Most mammalian mRNAs are conserved targets of microRNAs. *Genome Res* 2009; **19**:92–105.

79. Bartel DP. MicroRNAs: genomics, biogenesis, mechanism, and function. *Cell* 2004; **116**:281–297.

80. Han J, Lee Y, Yeom K-H, *et al.* Molecular Basis for the Recognition of Primary microRNAs by the Drosha-DGCR8 Complex. *Cell* 2006; **125**:887–901.

81. Yi R, Qin Y, Macara IG, Cullen BR. Exportin-5 mediates the nuclear export of pre-microRNAs and short hairpin RNAs. *Genes Dev* 2003; **17**:3011–3016.

82. Ketting RF, Fischer SEJ, Bernstein E, Sijen T, Hannon GJ, Plasterk RHA. Dicer functions in RNA interference and in synthesis of small RNA involved in developmental timing in C. elegans. *Genes Dev* 2001; **15**:2654–2659.

83. Khvorova A, Reynolds A, Jayasena SD. Functional siRNAs and miRNAs Exhibit Strand Bias. *Cell* 2003; **115**:209–216.

84. Schwarz DS, Hutvágner G, Du T, Xu Z, Aronin N, Zamore PD. Asymmetry in the assembly of the RNAi enzyme complex. *Cell* 2003; **115**:199–208.

85. Liu J, Carmell MA, Rivas FV, *et al.* Argonaute2 Is the Catalytic Engine of Mammalian RNAi. *Science* 2004; **305**:1437–1441.

86. Chendrimada TP, Gregory RI, Kumaraswamy E, *et al.* TRBP recruits the Dicer complex to Ago2 for microRNA processing and gene silencing. *Nature* 2005; **436**:740–744.

87. Zeng Y, Yi R, Cullen BR. MicroRNAs and small interfering RNAs can inhibit mRNA expression by similar mechanisms. *PNAS* 2003; **100**:9779–9784.

88. Djuranovic S, Nahvi A, Green R. miRNA-Mediated Gene Silencing by Translational Repression Followed by mRNA Deadenylation and Decay. *Science* 2012; **336**:237–240.

89. Jackson AL, Burchard J, Schelter J, *et al.* Widespread siRNA "off-target" transcript silencing mediated by seed region sequence complementarity. *RNA* 2006; **12**:1179–1187.

90. Mendell JT. MicroRNAs: critical regulators of development, cellular physiology and malignancy. *Cell Cycle* 2005; **4**:1179–1184.

91. Ge Y, Chen J. MicroRNAs in skeletal myogenesis. *Cell Cycle* 2011; **10**:441–448.

92. Mendell JT, Olson EN. MicroRNAs in stress signaling and human disease. *Cell* 2012; **148**:1172–1187.

93. Jiang Q, Wang Y, Hao Y, *et al.* miR2Disease: a manually curated database for microRNA deregulation in human disease. *Nucleic Acids Res* 2009; **37**:D98-104.

94. Li Z, Rana TM. Therapeutic targeting of microRNAs: current status and future challenges. *Nat Rev Drug Discov* 2014; **13**:622–638.

95. Elbashir SM, Harborth J, Lendeckel W, Yalcin A, Weber K, Tuschl T. Duplexes of 21-nucleotide RNAs mediate RNA interference in cultured mammalian cells. *Nature* 2001; **411**:494–498.

96. Buckingham M, Bajard L, Chang T, *et al.* The formation of skeletal muscle: from somite to limb. *J Anat* 2003; **202**:59–68.

97. Relaix F, Zammit PS. Satellite cells are essential for skeletal muscle regeneration: the cell on the edge returns centre stage. *Development* 2012; **139**:2845–2856.

98. Bentzinger CF, Wang YX, Rudnicki MA. Building Muscle: Molecular Regulation of Myogenesis. *Cold Spring Harb Perspect Biol* 2012; **4**:a008342.

99. Zhang Z, O'Rourke JR, McManus MT, Lewandoski M, Harfe BD, Sun X. The microRNA-processing enzyme DICER is dispensable for somite segmentation but essential for limb bud positioning. *Dev Biol* 2011; **351**:254–265.

100. McCarthy JJ. MicroRNA-206: the skeletal muscle-specific myomiR. *Biochim Biophys Acta* 2008; **1779**:682–691.

101. Lagos-Quintana M, Rauhut R, Yalcin A, Meyer J, Lendeckel W, Tuschl T. Identification of tissue-specific microRNAs from mouse. *Curr Biol* 2002; **12**:735–739.

102. Chen J-F, Mandel EM, Thomson JM, *et al.* The role of microRNA-1 and microRNA-133 in skeletal muscle proliferation and differentiation. *Nat Genet* 2006; **38**:228–233.

103. Chen J-F, Tao Y, Li J, *et al.* microRNA-1 and microRNA-206 regulate skeletal muscle satellite cell proliferation and differentiation by repressing Pax7. *J Cell Biol* 2010; **190**:867–879.

104. Liu N, Williams AH, Kim Y, *et al.* An intragenic MEF2-dependent enhancer directs muscle-specific expression of microRNAs 1 and 133. *Proc Natl Acad Sci U S A* 2007; **104**:20844–20849.

105. Kim HK, Lee YS, Sivaprasad U, Malhotra A, Dutta A. Muscle-specific microRNA miR-206 promotes muscle differentiation. *J Cell Biol* 2006; **174**:677–687.

106. Boutz PL, Chawla G, Stoilov P, Black DL. MicroRNAs regulate the expression of the alternative splicing factor nPTB during muscle development. *Genes Dev* 2007; **21**:71–84.

107. Ikeda S, He A, Kong SW, *et al.* MicroRNA-1 negatively regulates expression of the hypertrophy-associated calmodulin and Mef2a genes. *Mol Cell Biol* 2009; **29**:2193–2204.

108. van Rooij E, Quiat D, Johnson BA, *et al.* A family of microRNAs encoded by myosin genes governs myosin expression and muscle performance. *Dev Cell* 2009; **17**:662–673.

109. McCarthy JJ. The MyomiR network in skeletal muscle plasticity. *Exerc Sport Sci Rev* 2011; **39**:150–154.

110. Wang L, Chen X, Zheng Y, *et al.* MiR-23a inhibits myogenic differentiation through down regulation of fast myosin heavy chain isoforms. *Exp Cell Res* 2012; **318**:2324–2334.

111. Sun Q, Zhang Y, Yang G, *et al.* Transforming growth factor-β-regulated miR-24 promotes skeletal muscle differentiation. *Nucl Acids Res* 2008; **36**:2690–2699.

112. Wong CF, Tellam RL. MicroRNA-26a Targets the Histone Methyltransferase Enhancer of Zeste homolog 2 during Myogenesis. *J Biol Chem* 2008; **283**:9836–9843.

113. Dey BK, Gagan J, Yan Z, Dutta A. miR-26a is required for skeletal muscle differentiation and regeneration in mice. *Genes Dev* 2012; **26**:2180–2191.

114. McFarlane C, Vajjala A, Arigela H, *et al.* Negative auto-regulation of myostatin expression is mediated by Smad3 and microRNA-27. *PLoS ONE* 2014; **9**:e87687.

115. Crist CG, Montarras D, Pallafacchina G, *et al.* Muscle stem cell behavior is modified by microRNA-27 regulation of Pax3 expression. *Proc Natl Acad Sci U S A* 2009; **106**:13383–13387.

116. Kriegel AJ, Liu Y, Fang Y, Ding X, Liang M. The miR-29 family: genomics, cell biology, and relevance to renal and cardiovascular injury. *Physiol Genomics* 2012; **44**:237–244.

117. Crist CG, Montarras D, Buckingham M. Muscle satellite cells are primed for myogenesis but maintain quiescence with sequestration of Myf5 mRNA targeted by microRNA-31 in mRNP granules. *Cell Stem Cell* 2012; **11**:118–126.

118. Cacchiarelli D, Incitti T, Martone J, *et al.* miR-31 modulates dystrophin expression: new implications for Duchenne muscular dystrophy therapy. *EMBO Rep* 2011; **12**:136–141.

119. Ge Y, Sun Y, Chen J. IGF-II is regulated by microRNA-125b in skeletal myogenesis. *J Cell Biol* 2011; **192**:69–81.

120. Khanna N, Ge Y, Chen J. MicroRNA-146b Promotes Myogenic Differentiation and Modulates Multiple Gene Targets in Muscle Cells. *PLOS ONE* 2014; **9**:e100657.

121. Naguibneva I, Ameyar-Zazoua M, Polesskaya A, *et al.* The microRNA miR-181 targets the homeobox protein Hox-A11 during mammalian myoblast differentiation. *Nat Cell Biol* 2006; **8**:278–284.

122. Antoniou A, Mastroyiannopoulos NP, Uney JB, Phylactou LA. miR-186 inhibits muscle cell differentiation through myogenin regulation. *J Biol Chem* 2014; **289**:3923–3935.

123. Ma G, Wang Y, Li Y, *et al.* MiR-206, a key modulator of skeletal muscle development and disease. *Int J Biol Sci* 2015; **11**:345–352.

124. Yuasa K, Hagiwara Y, Ando M, Nakamura A, Takeda S 'ichi, Hijikata T. MicroRNA-206 is highly expressed in newly formed muscle fibers: implications regarding potential for muscle regeneration and maturation in muscular dystrophy. *Cell Struct Funct* 2008; **33**:163–169.

125. Cardinali B, Castellani L, Fasanaro P, *et al.* Microrna-221 and Microrna-222 Modulate Differentiation and Maturation of Skeletal Muscle Cells. *PLoS One* 2009; **4**.

126. Arcangelis VD, Serra F, Cogoni C, Vivarelli E, Monaco L, Naro F. β1-Syntrophin Modulation by miR-222 in mdx Mice. *PLOS ONE* 2010; **5**:e12098.

127. Sarkar S, Dey BK, Dutta A. MiR-322/424 and -503 Are Induced during Muscle Differentiation and Promote Cell Cycle Quiescence and Differentiation by Down-Regulation of Cdc25A. *Mol Biol Cell* 2010; **21**:2138–2149.

128. Gagan J, Dey BK, Layer R, Yan Z, Dutta A. MicroRNA-378 targets the myogenic repressor MyoR during myoblast differentiation. *J Biol Chem* 2011; **286**:19431–19438.

129. Alexander MS, Casar JC, Motohashi N, *et al.* Regulation of DMD pathology by an ankyrin-encoded miRNA. *Skeletal Muscle* 2011; **1**:27.

130. Alexander MS, Casar JC, Motohashi N, *et al.* MicroRNA-486-dependent modulation of DOCK3/PTEN/AKT signaling pathways improves muscular dystrophy-associated symptoms. *J Clin Invest* 2014; **124**:2651–2667.

131. Eisenberg I, Eran A, Nishino I, *et al.* Distinctive patterns of microRNA expression in primary muscular disorders. *Proc Natl Acad Sci U S A* 2007; **104**:17016–17021.

132. Greco S, Simone MD, Colussi C, *et al.* Common micro-RNA signature in skeletal muscle damage and regeneration induced by Duchenne muscular dystrophy and acute ischemia. *FASEB J* 2009; **23**:3335–3346.

133. Kovanda A, Režen T, Rogelj B. MicroRNA in skeletal muscle development, growth, atrophy, and disease. *WIREs RNA* 2014; **5**:509–525.

134. Wang XH. MicroRNA in myogenesis and muscle atrophy. *Curr Opin Clin Nutr Metab Care* 2013; **16**:258–266.

135. Goljanek-Whysall K, Sweetman D, Münsterberg AE. microRNAs in skeletal muscle differentiation and disease. *Clinical Science* 2012; **123**:611–625.

136. Simionescu-Bankston A, Kumar A. Noncoding RNAs in the regulation of skeletal muscle biology in health and disease. *J Mol Med* 2016; **94**:853–866.

137. Nie M, Deng Z-L, Liu J, Wang D-Z. Noncoding RNAs, Emerging Regulators of Skeletal Muscle Development and Diseases. *Biomed Res Int* 2015; **2015**.

138. Roberts TC, Blomberg KEM, McClorey G, *et al.* Expression Analysis in Multiple Muscle Groups and Serum Reveals Complexity in the MicroRNA Transcriptome of the mdx Mouse with Implications for Therapy. *Molecular Therapy — Nucleic Acids* 2012; **1**:e39.

139. Cacchiarelli D, Martone J, Girardi E, *et al.* MicroRNAs Involved in Molecular Circuitries Relevant for the Duchenne Muscular Dystrophy Pathogenesis Are Controlled by the Dystrophin/nNOS Pathway. *Cell Metabolism* 2010; **12**:341–351.

140. Wang L, Zhou L, Jiang P, *et al.* Loss of miR-29 in Myoblasts Contributes to Dystrophic Muscle Pathogenesis. *Mol Ther* 2012; **20**:1222–1233.

141. Zanotti S, Gibertini S, Curcio M, *et al.* Opposing roles of miR-21 and miR-29 in the progression of fibrosis in Duchenne muscular dystrophy. *Biochim Biophys Acta* 2015; **1852**:1451–1464.

142. Mandel P., Metais P. Les acides nucléiques du plasma sanguin chez l'homme. 1948; **C. R. Acad. Sci. Paris**:241 – 243.

143. Javillier, M., Fabrykant, M. Recherches experimentales sur le phosphore sanguin et particulierment sur variations de laphosphatemie. *Bull Soc Chim Biol* 1931; **13**:1253.

144. Chim SSC, Shing TKF, Hung ECW, *et al.* Detection and characterization of placental microRNAs in maternal plasma. *Clin Chem* 2008; **54**:482–490.

145. Mitchell PS, Parkin RK, Kroh EM, *et al.* Circulating microRNAs as stable blood-based markers for cancer detection. *Proc Natl Acad Sci USA* 2008; **105**:10513–10518.

146. Chen X, Ba Y, Ma L, *et al.* Characterization of microRNAs in serum: a novel class of biomarkers for diagnosis of cancer and other diseases. *Cell Res* 2008; **18**:997–1006.

147. Lawrie CH, Gal S, Dunlop HM, *et al.* Detection of elevated levels of tumour-associated microRNAs in serum of patients with diffuse large B-cell lymphoma. *Br J Haematol* 2008; **141**:672–675.

148. Weber JA, Baxter DH, Zhang S, *et al.* The microRNA spectrum in 12 body fluids. *Clin Chem* 2010; **56**:1733–1741.

149. Ai J, Zhang R, Li Y, *et al.* Circulating microRNA-1 as a potential novel biomarker for acute myocardial infarction. *Biochem Biophys Res Commun* 2010; **391**:73–77.

150. Mizuno H, Nakamura A, Aoki Y, *et al.* Identification of Muscle-Specific MicroRNAs in Serum of Muscular Dystrophy Animal Models: Promising Novel Blood-Based Markers for Muscular Dystrophy. *PLoS ONE* 2011; **6**:e18388.

151. Laterza OF, Lim L, Garrett-Engele PW, *et al.* Plasma MicroRNAs as sensitive and specific biomarkers of tissue injury. *Clin Chem* 2009; **55**:1977–1983.

152. Turchinovich A, Weiz L, Burwinkel B. Extracellular miRNAs: the mystery of their origin and function. *Trends in Biochemical Sciences* 2012; **37**:460–465.

153. Valadi H, Ekström K, Bossios A, Sjöstrand M, Lee JJ, Lötvall JO. Exosome-mediated transfer of mRNAs and microRNAs is a novel mechanism of genetic exchange between cells. *Nat Cell Biol* 2007; **9**:654–659.

154. Hunter MP, Ismail N, Zhang X, *et al.* Detection of microRNA expression in human peripheral blood microvesicles. *PLoS ONE* 2008; **3**:e3694.

155. Wang K, Zhang S, Weber J, Baxter D, Galas DJ. Export of microRNAs and microRNA-protective protein by mammalian cells. *Nucleic Acids Res* 2010; **38**:7248–7259.

156. Arroyo JD, Chevillet JR, Kroh EM, *et al.* Argonaute2 complexes carry a population of circulating microRNAs independent of vesicles in human plasma. *Proc Natl Acad Sci USA* 2011; **108**:5003–5008.

157. Turchinovich A, Weiz L, Langheinz A, Burwinkel B. Characterization of extracellular circulating microRNA. *Nucleic Acids Res* 2011; **39**:7223–7233.

158. Zernecke A, Bidzhekov K, Noels H, *et al.* Delivery of microRNA-126 by apoptotic bodies induces CXCL12-dependent vascular protection. *Sci Signal* 2009; **2**:ra81.

159. Vickers KC, Palmisano BT, Shoucri BM, Shamburek RD, Remaley AT. MicroRNAs are transported in plasma and delivered to recipient cells by high-density lipoproteins. *Nat Cell Biol* 2011; **13**:423–433.

160. Wagner J, Riwanto M, Besler C, *et al.* Characterization of levels and cellular transfer of circulating lipoprotein-bound microRNAs. *Arterioscler Thromb Vasc Biol* 2013; **33**:1392–1400.

161. Lee Y, El Andaloussi S, Wood MJA. Exosomes and microvesicles: extracellular vesicles for genetic information transfer and gene therapy. *Hum Mol Genet* 2012; **21**:R125-134.

162. EL Andaloussi S, Mäger I, Breakefield XO, Wood MJA. Extracellular vesicles: biology and emerging therapeutic opportunities. *Nat Rev Drug Discov* 2013; **12**:347–357.

163. Mittelbrunn M, Gutiérrez-Vázquez C, Villarroya-Beltri C, *et al.* Unidirectional transfer of microRNA-loaded exosomes from T cells to antigen-presenting cells. *Nat Commun* 2011; **2**:282.

164. Janas T, Janas MM, Sapoń K, Janas T. Mechanisms of RNA loading into exosomes. *FEBS Lett* 2015.

165. Raiborg C, Stenmark H. The ESCRT machinery in endosomal sorting of ubiquitylated membrane proteins. *Nature* 2009; **458**:445–452.

166. Baietti MF, Zhang Z, Mortier E, *et al.* Syndecan-syntenin-ALIX regulates the biogenesis of exosomes. *Nat Cell Biol* 2012; **14**:677–685.

167. Nabhan JF, Hu R, Oh RS, Cohen SN, Lu Q. Formation and release of arrestin domain-containing protein 1-mediated microvesicles (ARMMs) at plasma membrane by recruitment of TSG101 protein. *Proc Natl Acad Sci USA* 2012; **109**:4146–4151.

168. Bobrie A, Colombo M, Raposo G, Théry C. Exosome secretion: molecular mechanisms and roles in immune responses. *Traffic* 2011; **12**:1659–1668.

169. Trajkovic K, Hsu C, Chiantia S, *et al.* Ceramide triggers budding of exosome vesicles into multivesicular endosomes. *Science* 2008; **319**:1244–1247.

170. Zhang Y, Liu D, Chen X, *et al.* Secreted monocytic miR-150 enhances targeted endothelial cell migration. *Mol Cell* 2010; **39**:133–144.

171. Yang J-S, Maurin T, Lai EC. Functional parameters of Dicer-independent microRNA biogenesis. *RNA* 2012; **18**:945–957.

172. Guduric-Fuchs J, O'Connor A, Camp B, O'Neill CL, Medina RJ, Simpson DA. Selective extracellular vesicle-mediated export of an overlapping set of microRNAs from multiple cell types. *BMC Genomics* 2012; **13**:357.

173. Squadrito ML, Baer C, Burdet F, *et al.* Endogenous RNAs Modulate MicroRNA Sorting to Exosomes and Transfer to Acceptor Cells. *Cell Reports* 2014; **8**:1432–1446.

174. Batagov AO, Kurochkin IV. Exosomes secreted by human cells transport largely mRNA fragments that are enriched in the 3'-untranslated regions. *Biol Direct* 2013; **8**:12.

175. Koppers-Lalic D, Hackenberg M, Bijnsdorp IV, *et al.* Nontemplated Nucleotide Additions Distinguish the Small RNA Composition in Cells from Exosomes. *Cell Reports* 2014; **8**:1649–1658.

176. Villarroya-Beltri C, Gutiérrez-Vázquez C, Sánchez-Cabo F, *et al.* Sumoylated hnRNPA2B1 controls the sorting of miRNAs into exosomes through binding to specific motifs. *Nat Commun* 2013; **4**.

177. Pigati L, Yaddanapudi SCS, Iyengar R, *et al.* Selective Release of MicroRNA Species from Normal and Malignant Mammary Epithelial Cells. *PLoS ONE* 2010; **5**:e13515.

178. Tian T, Wang Y, Wang H, Zhu Z, Xiao Z. Visualizing of the cellular uptake and intracellular trafficking of exosomes by live-cell microscopy. *J Cell Biochem* 2010; **111**:488–496.

179. Morelli AE, Larregina AT, Shufesky WJ, *et al.* Endocytosis, intracellular sorting, and processing of exosomes by dendritic cells. *Blood* 2004; **104**:3257–3266.

180. Feng D, Zhao W-L, Ye Y-Y, *et al.* Cellular internalization of exosomes occurs through phagocytosis. *Traffic* 2010; **11**:675–687.

181. Barrès C, Blanc L, Bette-Bobillo P, *et al.* Galectin-5 is bound onto the surface of rat reticulocyte exosomes and modulates vesicle uptake by macrophages. *Blood* 2010; **115**:696–705.

182. Svensson KJ, Christianson HC, Wittrup A, *et al.* Exosome uptake depends on ERK1/2-heat shock protein 27 signaling and lipid Raft-mediated endocytosis negatively regulated by caveolin-1. *J Biol Chem* 2013; **288**:17713–17724.

183. Nanbo A, Kawanishi E, Yoshida R, Yoshiyama H. Exosomes derived from Epstein-Barr virus-infected cells are internalized via caveola-dependent endocytosis and promote phenotypic modulation in target cells. *J Virol* 2013; **87**:10334–10347.

184. Heusermann W, Hean J, Trojer D, *et al.* Exosomes surf on filopodia to enter cells at endocytic hot spots, traffic within endosomes, and are targeted to the ER. *J Cell Biol* 2016; **213**:173–184.

185. Mulcahy LA, Pink RC, Carter DRF. Routes and mechanisms of extracellular vesicle uptake. *J Extracell Vesicles* 2014; **3**.

186. Tian T, Zhu Y-L, Hu F-H, Wang Y-Y, Huang N-P, Xiao Z-D. Dynamics of exosome internalization and trafficking. *J Cell Physiol* 2013; **228**:1487–1495.

187. Kosaka N, Yoshioka Y, Hagiwara K, Tominaga N, Katsuda T, Ochiya T. Trash or Treasure: extracellular microRNAs and cell-to-cell communication. *Front Genet* 2013; **4**:173.

188. Rayner KJ, Hennessy EJ. Extracellular communication via microRNA: lipid particles have a new message. *J Lipid Res* 2013; **54**:1174–1181.

189. Etheridge A, Gomes CPC, Pereira RW, Galas D, Wang K. The complexity, function and applications of RNA in circulation. *Front Genet* 2013; **4**.

190. Sverdlov ED. Amedeo Avogadro's cry: what is 1 μg of exosomes? *Bioessays* 2012; **34**:873–875.

191. Pegtel DM, Cosmopoulos K, Thorley-Lawson DA, *et al.* Functional delivery of viral miRNAs via exosomes. *Proc Natl Acad Sci USA* 2010; **107**:6328–6333.

192. Chevillet JR, Kang Q, Ruf IK, *et al.* Quantitative and stoichiometric analysis of the microRNA content of exosomes. *PNAS* 2014; **111**:14888–14893.

193. Steinman RM, Brodie SE, Cohn ZA. Membrane flow during pinocytosis. A stereologic analysis. *J Cell Biol* 1976; **68**:665–687.

194. Janas T, Janas T, Yarus M. Specific RNA binding to ordered phospholipid bilayers. *Nucleic Acids Res* 2006; **34**:2128–2136.

195. Kim SI, Shin D, Choi TH, *et al.* Systemic and specific delivery of small interfering RNAs to the liver mediated by apolipoprotein A-I. *Mol Ther* 2007; **15**:1145–1152.

196. Süleymanoglu E. Phospholipid-nucleic acid recognition: developing an immobilized liposome chromatography for DNA separation and analysis. *PDA J Pharm Sci Technol* 2006; **60**:232–239.

197. Brown WV. High-density lipoprotein and transport of cholesterol and triglyceride in blood. *J Clin Lipidol* 2007; **1**:7–19.

198. Kosaka N, Iguchi H, Yoshioka Y, Takeshita F, Matsuki Y, Ochiya T. Secretory mechanisms and intercellular transfer of microRNAs in living cells. *J Biol Chem* 2010; **285**:17442–17452.

199. Turchinovich A, Burwinkel B. Distinct AGO1 and AGO2 associated miRNA profiles in human cells and blood plasma. *RNA Biol* 2012; **9**:1066–1075.

200. Yoo B-C, Kragler F, Varkonyi-Gasic E, *et al.* A systemic small RNA signaling system in plants. *Plant Cell* 2004; **16**:1979–2000.

201. Feinberg EH, Hunter CP. Transport of dsRNA into cells by the transmembrane protein SID-1. *Science* 2003; **301**:1545–1547.

202. Jung HJ, Suh Y. Circulating miRNAs in ageing and ageing-related diseases. *J Genet Genomics* 2014; **41**:465–472.

203. Lemoinne S, Thabut D, Housset C, *et al.* The emerging roles of microvesicles in liver diseases. *Nat Rev Gastroenterol Hepatol* 2014; **11**:350–361.

204. Loyer X, Vion A-C, Tedgui A, Boulanger CM. Microvesicles as cell-cell messengers in cardiovascular diseases. *Circ Res* 2014; **114**:345–353.

205. Katsuda T, Kosaka N, Ochiya T. The roles of extracellular vesicles in cancer biology: toward the development of novel cancer biomarkers. *Proteomics* 2014; **14**:412–425.

206. Mi S, Zhang J, Zhang W, Huang RS. Circulating microRNAs as biomarkers for inflammatory diseases. *Microrna* 2013; **2**:63–71.

207. Roberts TC, Godfrey C, McClorey G, *et al.* Extracellular microRNAs are dynamic non-vesicular biomarkers of muscle turnover. *Nucleic Acids Res* 2013; **41**:9500–9513.

208. Witwer KW. Circulating microRNA biomarker studies: pitfalls and potential solutions. *Clin Chem* 2015; **61**:56–63.

209. Moldovan L, Batte KE, Trgovcich J, Wisler J, Marsh CB, Piper M. Methodological challenges in utilizing miRNAs as circulating biomarkers. *J Cell Mol Med* 2014; **18**:371–390.

210. Jia S, Zocco D, Samuels ML, *et al.* Emerging technologies in extracellular vesicle-based molecular diagnostics. *Expert Rev Mol Diagn* 2014; **14**:307–321.

211. Roberts TC, Coenen-Stass AML, Wood MJA. Assessment of RT-qPCR Normalization Strategies for Accurate Quantification of Extracellular microRNAs in Murine Serum. *PLoS ONE* 2014; **9**:e89237.

212. Corsten MF, Dennert R, Jochems S, *et al.* Circulating MicroRNA-208b and MicroRNA-499 reflect myocardial damage in cardiovascular disease. *Circ Cardiovasc Genet* 2010; **3**:499–506.

213. De Rosa S, Fichtlscherer S, Lehmann R, Assmus B, Dimmeler S, Zeiher AM. Transcoronary concentration gradients of circulating microRNAs. *Circulation* 2011; **124**:1936–1944.

214. Zaharieva IT, Calissano M, Scoto M, *et al.* Dystromirs as serum biomarkers for monitoring the disease severity in Duchenne muscular Dystrophy. *PLoS ONE* 2013; **8**:e80263.

215. Cermelli S, Ruggieri A, Marrero JA, Ioannou GN, Beretta L. Circulating microRNAs in patients with chronic hepatitis C and non-alcoholic fatty liver disease. *PLoS ONE* 2011; **6**:e23937.

216. Zampetaki A, Kiechl S, Drozdov I, *et al.* Plasma microRNA profiling reveals loss of endothelial miR-126 and other microRNAs in type 2 diabetes. *Circ Res* 2010; **107**:810–817.

217. Skog J, Würdinger T, van Rijn S, *et al.* Glioblastoma microvesicles transport RNA and proteins that promote tumour growth and provide diagnostic biomarkers. *Nat Cell Biol* 2008; **10**:1470–1476.

218. Nishida-Aoki N, Ochiya T. Interactions between cancer cells and normal cells via miRNAs in extracellular vesicles. *Cell Mol Life Sci* 2015.

219. Biancone L, Bruno S, Deregibus MC, Tetta C, Camussi G. Therapeutic potential of mesenchymal stem cell-derived microvesicles. *Nephrol Dial Transplant* 2012; **27**:3037–3042.

220. Cantaluppi V, Gatti S, Medica D, *et al.* Microvesicles derived from endothelial progenitor cells protect the kidney from ischemia-reperfusion injury by microRNA-dependent reprogramming of resident renal cells. *Kidney Int* 2012; **82**:412–427.

221. Bruno S, Grange C, Deregibus MC, *et al.* Mesenchymal stem cell-derived microvesicles protect against acute tubular injury. *J Am Soc Nephrol* 2009; **20**:1053–1067.

222. Chaput N, Théry C. Exosomes: immune properties and potential clinical implementations. *Semin Immunopathol* 2011; **33**:419–440.

223. Kosaka N, Iguchi H, Yoshioka Y, Hagiwara K, Takeshita F, Ochiya T. Competitive interactions of cancer cells and normal cells via secretory microRNAs. *J Biol Chem* 2012; **287**:1397–1405.

224. Nordin JZ, Lee Y, Vader P, *et al.* Ultrafiltration with size-exclusion liquid chromatography for high yield isolation of extracellular vesicles preserving intact biophysical and functional properties. *Nanomedicine* 2015.

225. Rak J, Guha A. Extracellular vesicles--vehicles that spread cancer genes. *Bioessays* 2012; **34**:489–497.

226. Camussi G, Deregibus M-C, Bruno S, Grange C, Fonsato V, Tetta C. Exosome/microvesicle-mediated epigenetic reprogramming of cells. *Am J Cancer Res* 2011; **1**:98–110.

227. Yang M, Chen J, Su F, *et al.* Microvesicles secreted by macrophages shuttle invasion-potentiating microRNAs into breast cancer cells. *Mol Cancer* 2011; **10**:117.

228. Takamizawa J, Konishi H, Yanagisawa K, *et al.* Reduced expression of the let-7 microRNAs in human lung cancers in association with shortened postoperative survival. *Cancer Res* 2004; **64**:3753–3756.

229. Ohshima K, Inoue K, Fujiwara A, *et al.* Let-7 microRNA family is selectively secreted into the extracellular environment via exosomes in a metastatic gastric cancer cell line. *PLoS ONE* 2010; **5**:e13247.

230. Meng F, Henson R, Wehbe-Janek H, Ghoshal K, Jacob ST, Patel T. MicroRNA-21 regulates expression of the PTEN tumor suppressor gene in human hepatocellular cancer. *Gastroenterology* 2007; **133**:647–658.

231. Fabbri M, Paone A, Calore F, *et al.* MicroRNAs bind to Toll-like receptors to induce prometastatic inflammatory response. *Proc Natl Acad Sci USA* 2012; **109**:E2110-2116.

232. Lehmann SM, Krüger C, Park B, *et al.* An unconventional role for miRNA: let-7 activates Toll-like receptor 7 and causes neurodegeneration. *Nat Neurosci* 2012; **15**:827–835.

233. Marleau AM, Chen C-S, Joyce JA, Tullis RH. Exosome removal as a therapeutic adjuvant in cancer. *J Transl Med* 2012; **10**:134.

234. Alvarez-Erviti L, Seow Y, Yin H, Betts C, Lakhal S, Wood MJA. Delivery of siRNA to the mouse brain by systemic injection of targeted exosomes. *Nature Biotechnology* 2011; **29**:341–345.

235. Lai RC, Arslan F, Lee MM, *et al.* Exosome secreted by MSC reduces myocardial ischemia/reperfusion injury. *Stem Cell Res* 2010; **4**:214–222.

236. Lakhal S, Wood MJA. Exosome nanotechnology: an emerging paradigm shift in drug delivery: exploitation of exosome nanovesicles for systemic in vivo delivery of RNAi heralds new horizons for drug delivery across biological barriers. *Bioessays* 2011; **33**:737–741.

237. Wolfrum C, Shi S, Jayaprakash KN, *et al.* Mechanisms and optimization of in vivo delivery of lipophilic siRNAs. *Nat Biotechnol* 2007; **25**:1149–1157.

238. György B, Hung ME, Breakefield XO, Leonard JN. Therapeutic Applications of Extracellular Vesicles: Clinical Promise and Open Questions. *Annual Review of Pharmacology and Toxicology* 2015; **55**:439–464.

239. Wahlgren J, De L Karlson T, Brisslert M, *et al.* Plasma exosomes can deliver exogenous short interfering RNA to monocytes and lymphocytes. *Nucleic Acids Res* 2012; **40**:e130.

240. Pereira DM, Rodrigues PM, Borralho PM, Rodrigues CMP. Delivering the promise of miRNA cancer therapeutics. *Drug Discov Today* 2013; **18**:282–289.

241. Lamar K-M, McNally EM. Genetic Modifiers for Neuromuscular Diseases. *J Neuromuscul Dis* 2014; **1**:3–13.

242. Lynn S, Aartsma-Rus A, Bushby K, *et al.* Measuring clinical effectiveness of medicinal products for the treatment of Duchenne muscular dystrophy. *Neuromuscul Disord* 2015; **25**:96–105.

243. Aartsma-Rus A, Spitali P. Circulating Biomarkers for Duchenne Muscular Dystrophy. Lochmüller H, ed. *Journal of Neuromuscular Diseases* 2015; **2**:S49–S58.

244. Biomarkers Definitions Working Group. Biomarkers and surrogate endpoints: preferred definitions and conceptual framework. *Clin Pharmacol Ther* 2001; **69**:89–95.

245. Ferlini A, Flanigan KM, Lochmuller H, Muntoni F, 't Hoen PAC, McNally E. 204th ENMC International Workshop on Biomarkers in Duchenne Muscular Dystrophy 24–26 January 2014, Naarden, The Netherlands. *Neuromuscular Disorders* 2015; **25**:184–198.

246. Hathout Y, Seol H, Han MHJ, Zhang A, Brown KJ, Hoffman EP. Clinical utility of serum biomarkers in Duchenne muscular dystrophy. *Clin Proteomics* 2016; **13**.

247. Mazzone ES, Messina S, Vasco G, *et al.* Reliability of the North Star Ambulatory Assessment in a multicentric setting. *Neuromuscul Disord* 2009; **19**:458–461.

248. McDonald CM, Henricson EK, Abresch RT, *et al.* The 6-minute walk test and other endpoints in Duchenne muscular dystrophy: longitudinal natural history observations over 48 weeks from a multicenter study. *Muscle Nerve* 2013; **48**:343–356.

249. Willcocks R, Arpan I, Forbes S, *et al.* Longitudinal measurements of MRI-T2 in boys with Duchenne muscular dystrophy: Effects of age and disease progression. *Neuromuscul Disord* 2014; **24**:393–401.

250. Aartsma-Rus A. Dystrophin Analysis in Clinical Trials. *Journal of Neuromuscular Diseases* 2014; **1**:41–53.

251. Goemans NM, Tulinius M, van den Akker JT, *et al.* Systemic administration of PRO051 in Duchenne's muscular dystrophy. *N Engl J Med* 2011; **364**:1513–1522.

252. Brown KJ, Marathi R, Fiorillo AA, *et al.* Accurate Quantitation of Dystrophin Protein in Human Skeletal Muscle Using Mass Spectrometry. *J Bioanal Biomed* 2012; **Suppl 7**.

253. Godfrey C, Muses S, McClorey G, *et al.* How much dystrophin is enough: the physiological consequences of different levels of dystrophin in the mdx mouse. *Hum Mol Genet* 2015; **24**:4225–4237.

254. Dowling P, Holland A, Ohlendieck K. Mass Spectrometry-Based Identification of Muscle-Associated and Muscle-Derived Proteomic Biomarkers of Dystrophinopathies. *Journal of Neuromuscular Diseases* 2014; **1**:15–40.

255. Rouillon J, Zocevic A, Leger T, *et al.* Proteomics profiling of urine reveals specific titin fragments as biomarkers of Duchenne muscular dystrophy. *Neuromuscular Disorders* 2014; **24**:563–573.

256. Cacchiarelli D, Legnini I, Martone J, *et al.* miRNAs as serum biomarkers for Duchenne muscular dystrophy. *EMBO Mol Med* 2011; **3**:258–265.

257. Vignier N, Amor F, Fogel P, *et al.* Distinctive Serum miRNA Profile in Mouse Models of Striated Muscular Pathologies. *PLoS One* 2013; **8**.

258. Perfetti A, Greco S, Bugiardini E, *et al.* Plasma microRNAs as biomarkers for myotonic dystrophy type 1. *Neuromuscular Disorders* 2014; **24**:509–515.

259. Jeanson-Leh L, Lameth J, Krimi S, *et al.* Serum profiling identifies novel muscle miRNA and cardiomyopathy-related miRNA biomarkers in Golden Retriever muscular dystrophy dogs and Duchenne muscular dystrophy patients. *Am J Pathol* 2014; **184**:2885–2898.

260. Li X, Li Y, Zhao L, *et al.* Circulating Muscle-specific miRNAs in Duchenne Muscular Dystrophy Patients. *Mol Ther Nucleic Acids* 2014; **3**:e177.

261. Zatz M, Rapaport D, Vainzof M, *et al.* Serum creatine-kinase (CK) and pyruvate-kinase (PK) activities in Duchenne (DMD) as compared with Becker (BMD) muscular dystrophy. *J Neurol Sci* 1991; **102**:190–196.

262. Mendell JR, Shilling C, Leslie ND, *et al.* Evidence-based path to newborn screening for Duchenne muscular dystrophy. *Ann Neurol* 2012; **71**:304–313.

263. Baird MF, Graham SM, Baker JS, Bickerstaff GF. Creatine-Kinase- and Exercise-Related Muscle Damage Implications for Muscle Performance and Recovery. *Journal of Nutrition and Metabolism* 2012; **2012**:e960363.

264. Gasper MC, Gilchrist JM. Creatine kinase: a review of its use in the diagnosis of muscle disease. *Med Health R I* 2005; **88**:398, 400–404.

265. Kim HK, Laor T, Horn PS, Racadio JM, Wong B, Dardzinski BJ. T2 mapping in Duchenne muscular dystrophy: distribution of disease activity and correlation with clinical assessments. *Radiology* 2010; **255**:899–908.

266. Hathout Y, Brody E, Clemens PR, *et al.* Large-scale serum protein biomarker discovery in Duchenne muscular dystrophy. *Proc Natl Acad Sci USA* 2015.

267. Burch PM, Pogoryelova O, Goldstein R, *et al.* Muscle-Derived Proteins as Serum Biomarkers for Monitoring Disease Progression in Three Forms of Muscular Dystrophy. *J Neuromuscul Dis* 2015; **2**:241–255.

268. Duguez S, Duddy W, Johnston H, *et al.* Dystrophin deficiency leads to disturbance of LAMP1-vesicle-associated protein secretion. *Cell Mol Life Sci* 2013; **70**:2159–2174.

269. Rouillon J, Poupiot J, Zocevic A, *et al.* Serum proteomic profiling reveals fragments of MYOM3 as potential biomarkers for monitoring the outcome of therapeutic interventions in muscular dystrophies. *Hum Mol Genet* 2015:ddv214.

270. Hathout Y, Marathi RL, Rayavarapu S, *et al.* Discovery of serum protein biomarkers in the mdx mouse model and cross-species comparison to Duchenne muscular dystrophy patients. *Hum Mol Genet* 2014; **23**:6458–6469.

271. Ayoglu B, Chaouch A, Lochmüller H, *et al.* Affinity proteomics within rare diseases: a BIO-NMD study for blood biomarkers of muscular dystrophies. *EMBO Mol Med* 2014.

272. Nadarajah VD, van Putten M, Chaouch A, *et al.* Serum matrix metalloproteinase-9 (MMP-9) as a biomarker for monitoring disease progression in Duchenne muscular dystrophy (DMD). *Neuromuscul Disord* 2011; **21**:569–578.

273. Coenen-Stass AML, McClorey G, Manzano R, *et al.* Identification of novel, therapy-responsive protein biomarkers in a mouse model of Duchenne muscular dystrophy by aptamer-based serum proteomics. *Sci Rep* 2015; **5**:17014.

274. Betts C, Saleh AF, Arzumanov AA, *et al.* Pip6-PMO, A New Generation of Peptide-oligonucleotide Conjugates With Improved Cardiac Exon Skipping Activity for DMD Treatment. *Molecular Therapy — Nucleic Acids* 2012; **1**:e38.

275. Pfaffl MW. A new mathematical model for relative quantification in real-time RT-PCR. *Nucleic Acids Res* 2001; **29**:e45.

276. Nakao R, Yamamoto S, Yasumoto Y, Kadota K, Oishi K. Impact of denervation-induced muscle atrophy on housekeeping gene expression in mice. *Muscle Nerve* 2015; **51**:276–281.

277. Roberts TC, Coenen-Stass AML, Betts CA, Wood MJA. Detection and quantification of extracellular microRNAs in murine biofluids. *Biological Procedures Online* 2014; **16**:5.

278. Balzano F, Deiana M, Dei Giudici S, *et al.* miRNA Stability in Frozen Plasma Samples. *Molecules* 2015; **20**:19030–19040.

279. Ramakers C, Ruijter JM, Deprez RHL, Moorman AFM. Assumption-free analysis of quantitative real-time polymerase chain reaction (PCR) data. *Neurosci Lett* 2003; **339**:62–66.

280. Bustin SA, Benes V, Garson JA, *et al.* The MIQE guidelines: minimum information for publication of quantitative real-time PCR experiments. *Clin Chem* 2009; **55**:611–622.

281. McDermott AM, Kerin MJ, Miller N. Identification and validation of miRNAs as endogenous controls for RQ-PCR in blood specimens for breast cancer studies. *PLoS ONE* 2013; **8**:e83718.

282. Mattie MD, Benz CC, Bowers J, *et al.* Optimized high-throughput microRNA expression profiling provides novel biomarker assessment of clinical prostate and breast cancer biopsies. *Mol Cancer* 2006; **5**:24.

283. Wang L, Liu Y, Du L, *et al.* Identification and validation of reference genes for the detection of serum microRNAs by reverse transcription-quantitative polymerase chain reaction in patients with bladder cancer. *Mol Med Rep* 2015; **12**:615–622.

284. Théry C, Amigorena S, Raposo G, Clayton A. Isolation and characterization of exosomes from cell culture supernatants and biological fluids. *Curr Protoc Cell Biol* 2006; **Chapter 3**:Unit 3.22.

285. Roberts TC, Godfrey C, McClorey G, *et al.* Extracellular microRNAs are dynamic non-vesicular biomarkers of muscle turnover. *Nucl Acids Res* 2013.

286. Cacchiarelli D, Legnini I, Martone J, *et al.* miRNAs as serum biomarkers for Duchenne muscular dystrophy. *EMBO Mol Med* 2011; **3**:258–265.

287. Kirschner MB, Edelman JJB, Kao SC-H, Vallely MP, van Zandwijk N, Reid G. The Impact of Hemolysis on Cell-Free microRNA Biomarkers. *Front Genet* 2013; **4**.

288. Hori SS, Gambhir SS. Mathematical Model Identifies Blood Biomarker–Based Early Cancer Detection Strategies and Limitations. *Science Translational Medicine* 2011; **3**:109ra116-109ra116.

289. Gidlöf O, Andersson P, van der Pals J, Götberg M, Erlinge D. Cardiospecific microRNA plasma levels correlate with troponin and cardiac function in patients with ST elevation myocardial infarction, are selectively dependent on renal elimination, and can be detected in urine samples. *Cardiology* 2011; **118**:217–226.

290. Gokhin DS, Ward SR, Bremner SN, Lieber RL. Quantitative analysis of neonatal skeletal muscle functional improvement in the mouse. *Journal of Experimental Biology* 2008; **211**:837–843.

291. White RB, Biérinx A-S, Gnocchi VF, Zammit PS. Dynamics of muscle fibre growth during postnatal mouse development. *BMC Dev Biol* 2010; **10**:1–11.

292. Neal A, Boldrin L, Morgan JE. The satellite cell in male and female, developing and adult mouse muscle: distinct stem cells for growth and regeneration. *PLoS ONE* 2012; **7**:e37950.

293. Bulfield G, Siller WG, Wight PA, Moore KJ. X chromosome-linked muscular dystrophy (mdx) in the mouse. *Proc Natl Acad Sci U S A* 1984; **81**:1189–1192.

294. Turk R, Sterrenburg E, Meijer E de, Ommen G-J van, Dunnen J den, Hoen P 't. Muscle regeneration in dystrophin-deficient mdx mice studied by gene expression profiling. *BMC Genomics* 2005; **6**:98.

295. Tanabe Y, Esaki K, Nomura T. Skeletal muscle pathology in X chromosome-linked muscular dystrophy (mdx) mouse. *Acta Neuropathol* 1986; **69**:91–95.

296. Goyenvalle A, Babbs A, Wright J, *et al.* Rescue of severely affected dystrophin/utrophin-deficient mice through scAAV-U7snRNA-mediated exon skipping. *Hum Mol Genet* 2012; **21**:2559–2571.

297. Lott JA, Landesman PW. The enzymology of skeletal muscle disorders. *Crit Rev Clin Lab Sci* 1984; **20**:153–190.

298. Bayer PM, Gabl F, Gergely T h, Zazgornik J. [Isoenzymes of creatine kinase in the perinatal period (author's transl)]. *J Clin Chem Clin Biochem* 1977; **15**:349–352.

299. Wang YX, Rudnicki MA. Satellite cells, the engines of muscle repair. *Nat Rev Mol Cell Biol* 2012; **13**:127–133.

300. Järvinen TAH, Järvinen TLN, Kääriäinen M, Kalimo H, Järvinen M. Muscle Injuries Biology and Treatment. *Am J Sports Med* 2005; **33**:745–764.

301. Newham DJ, Mills KR, Quigley BM, Edwards RH. Pain and fatigue after concentric and eccentric muscle contractions. *Clin Sci* 1983; **64**:55–62.

302. Moens P, Baatsen PH, Maréchal G. Increased susceptibility of EDL muscles from mdx mice to damage induced by contractions with stretch. *J Muscle Res Cell Motil* 1993; **14**:446–451.

303. Blaauw B, Agatea L, Toniolo L, *et al.* Eccentric contractions lead to myofibrillar dysfunction in muscular dystrophy. *J Appl Physiol* 2010; **108**:105–111.

304. Dellorusso C, Crawford RW, Chamberlain JS, Brooks SV. Tibialis anterior muscles in mdx mice are highly susceptible to contraction-induced injury. *J Muscle Res Cell Motil* 2001; **22**:467–475.

305. McArdle A, Edwards RH, Jackson MJ. Time course of changes in plasma membrane permeability in the dystrophin-deficient mdx mouse. *Muscle Nerve* 1994; **17**:1378–1384.

306. Rouillon J, Poupiot J, Zocevic A, *et al.* Serum proteomic profiling reveals fragments of MYOM3 as potential biomarkers for monitoring the outcome of therapeutic interventions in muscular dystrophies. *Hum Mol Genet* 2015.

307. Schiaffino S, Rossi AC, Smerdu V, Leinwand LA, Reggiani C. Developmental myosins: expression patterns and functional significance. *Skeletal Muscle* 2015; **5**:22.

308. Kim JY, Park Y-K, Lee K-P, *et al.* Genome-wide profiling of the microRNA-mRNA regulatory network in skeletal muscle with aging. *Aging (Albany NY)* 2014; **6**:524–544.

309. Johnnidis JB, Harris MH, Wheeler RT, *et al.* Regulation of progenitor cell proliferation and granulocyte function by microRNA-223. *Nature* 2008; **451**:1125–1129.

310. Schoneich C, Dremina E, Galeva N, Sharov V. Apoptosis in differentiating C2C12 muscle cells selectively targets Bcl-2-deficient myotubes. *Apoptosis* 2014; **19**:42–57.

311. Bail S, Swerdel M, Liu H, *et al.* Differential regulation of microRNA stability. *RNA* 2010; **16**:1032–1039.

312. Krol J, Loedige I, Filipowicz W. The widespread regulation of microRNA biogenesis, function and decay. *Nat Rev Genet* 2010; **11**:597–610.

313. McDonald JS, Milosevic D, Reddi HV, Grebe SK, Algeciras-Schimnich A. Analysis of circulating microRNA: preanalytical and analytical challenges. *Clin Chem* 2011; **57**:833–840.

314. Köberle V, Pleli T, Schmithals C, *et al.* Differential Stability of Cell-Free Circulating microRNAs: Implications for Their Utilization as Biomarkers. *PLOS ONE* 2013; **8**:e75184.

315. Russell AP, Lamon S, Boon H, *et al.* Regulation of miRNAs in human skeletal muscle following acute endurance exercise and short-term endurance training. *J Physiol (Lond)* 2013; **591**:4637–4653.

316. Nielsen S, Scheele C, Yfanti C, *et al.* Muscle specific microRNAs are regulated by endurance exercise in human skeletal muscle. *J Physiol (Lond)* 2010; **588**:4029–4037.

317. Gomes CPC, Oliveira-Jr GP, Madrid B, Almeida JA, Franco OL, Pereira RW. Circulating miR-1, miR-133a, and miR-206 levels are increased after a half-marathon run. *Biomarkers* 2014; **19**:585–589.

318. Nakasa T, Ishikawa M, Shi M, Shibuya H, Adachi N, Ochi M. Acceleration of muscle regeneration by local injection of muscle-specific microRNAs in rat skeletal muscle injury model. *J Cell Mol Med* 2010; **14**:2495–2505.

319. Liu N, Williams AH, Maxeiner JM, *et al.* microRNA-206 promotes skeletal muscle regeneration and delays progression of Duchenne muscular dystrophy in mice. *J Clin Invest* 2012; **122**:2054–2065.

320. Zatz M, Rapaport D, Vainzof M, *et al.* Serum creatine-kinase (CK) and pyruvate-kinase (PK) activities in Duchenne (DMD) as compared with Becker (BMD) muscular dystrophy. *J Neurol Sci* 1991; **102**:190–196.

321. Blau HM, Cosgrove BD, Ho ATV. The central role of muscle stem cells in regenerative failure with aging. *Nat Med* 2015; **21**:854–862.

322. Willms E, Johansson HJ, Mäger I, *et al.* Cells release subpopulations of exosomes with distinct molecular and biological properties. *Scientific Reports* 2016; **6**:22519.

323. Shenoy A, Blelloch RH. Regulation of microRNA function in somatic stem cell proliferation and differentiation. *Nat Rev Mol Cell Biol* 2014; **15**:565–576.

324. Witwer KW, Buzás EI, Bemis LT, *et al.* Standardization of sample collection, isolation and analysis methods in extracellular vesicle research. *J Extracell Vesicles* 2013; **2**.

325. SZATANEK R, BARAN J, SIEDLAR M, BAJ-KRZYWORZEKA M. Isolation of extracellular vesicles: Determining the correct approach (Review). *Int J Mol Med* 2015; **36**:11–17.

326. Böing AN, van der Pol E, Grootemaat AE, Coumans FAW, Sturk A, Nieuwland R. Single-step isolation of extracellular vesicles by size-exclusion chromatography. *J Extracell Vesicles* 2014; **3**.

327. Muller L, Hong C-S, Stolz DB, Watkins SC, Whiteside TL. Isolation of biologically-active exosomes from human plasma. *J Immunol Methods* 2014; **411**:55–65.

328. Lobb RJ, Becker M, Wen SW, *et al.* Optimized exosome isolation protocol for cell culture supernatant and human plasma. *J Extracell Vesicles* 2015; **4**:27031.

329. Baranyai T, Herczeg K, Onódi Z, *et al.* Isolation of Exosomes from Blood Plasma: Qualitative and Quantitative Comparison of Ultracentrifugation and Size Exclusion Chromatography Methods. *PLOS ONE* 2015; **10**:e0145686.

330. Lin J, Li J, Huang B, *et al.* Exosomes: Novel Biomarkers for Clinical Diagnosis. *ScientificWorldJournal* 2015; **2015**.

331. Ashby J, Flack K, Jimenez LA, *et al.* Distribution profiling of circulating microRNAs in serum. *Anal Chem* 2014; **86**:9343–9349.

332. Havel RJ, Eder HA, Bragdon JH. THE DISTRIBUTION AND CHEMICAL COMPOSITION OF ULTRACENTRIFUGALLY SEPARATED LIPOPROTEINS IN HUMAN SERUM. *J Clin Invest* 1955; **34**:1345–1353.

333. Wood RJ, Volek JS, Liu Y, Shachter NS, Contois JH, Fernandez ML. Carbohydrate Restriction Alters Lipoprotein Metabolism by Modifying VLDL, LDL, and HDL Subfraction Distribution and Size in Overweight Men. *J Nutr* 2006; **136**:384–389.

334. Friedewald WT, Levy RI, Fredrickson DS. Estimation of the Concentration of Low-Density Lipoprotein Cholesterol in Plasma, Without Use of the Preparative Ultracentrifuge. *Clinical Chemistry* 1972; **18**:499–502.

335. De N, Young L, Lau P-W, Meisner N-C, Morrissey DV, MacRae IJ. Highly complementary target RNAs promote release of guide RNAs from human Argonaute2. *Mol Cell* 2013; **50**:344–355.

336. Nishino I, Fu J, Tanji K, *et al.* Primary LAMP-2 deficiency causes X-linked vacuolar cardiomyopathy and myopathy (Danon disease). *Nature* 2000; **406**:906–910.

337. Welton JL, Webber JP, Botos L-A, Jones M, Clayton A. Ready-made chromatography columns for extracellular vesicle isolation from plasma. *Journal of Extracellular Vesicles* 2015; **4**.

338. Branca RMM, Orre LM, Johansson HJ, *et al.* HiRIEF LC-MS enables deep proteome coverage and unbiased proteogenomics. *Nat Methods* 2014; **11**:59–62.

339. Roberts TC, Johansson HJ, McClorey G, *et al.* Multi-level omics analysis in a murine model of dystrophin loss and therapeutic restoration. *Hum Mol Genet* 2015:ddv381.

340. Anderson NL, Anderson NG. The Human Plasma Proteome History, Character, and Diagnostic Prospects. *Mol Cell Proteomics* 2002; **1**:845–867.

341. Ray S, Reddy PJ, Jain R, Gollapalli K, Moiyadi A, Srivastava S. Proteomic technologies for the identification of disease biomarkers in serum: advances and challenges ahead. *Proteomics* 2011; **11**:2139–2161.

342. Yadav AK, Bhardwaj G, Basak T, *et al.* A Systematic Analysis of Eluted Fraction of Plasma Post Immunoaffinity Depletion: Implications in Biomarker Discovery. *PLOS ONE* 2011; **6**:e24442.

343. Gold L, Ayers D, Bertino J, *et al.* Aptamer-Based Multiplexed Proteomic Technology for Biomarker Discovery. *PLoS ONE* 2010; **5**:e15004.

344. Ellington AD, Szostak JW. In vitro selection of RNA molecules that bind specific ligands. *Nature* 1990; **346**:818–822.

345. Tuerk C, Gold L. Systematic evolution of ligands by exponential enrichment: RNA ligands to bacteriophage T4 DNA polymerase. *Science* 1990; **249**:505–510.

346. Saeed AI, Sharov V, White J, *et al.* TM4: a free, open-source system for microarray data management and analysis. *BioTechniques* 2003; **34**:374–378.

347. Ando T, Kato T, Ohsawa M, Fukuyama Y. Myoglobinemia in Duchenne muscular dystrophy carriers. *Brain Dev* 1980; **2**:87–88.

348. Brazeau GA, Mathew M, Entrikin RK. Serum and organ indices of the mdx dystrophic mouse. *Res Commun Chem Pathol Pharmacol* 1992; **77**:179–189.

349. Shin J, Tajrishi MM, Ogura Y, Kumar A. Wasting Mechanisms in Muscular Dystrophy. *Int J Biochem Cell Biol* 2013; **45**:2266–2279.

350. Aartsma-Rus A, Van Deutekom JCT, Fokkema IF, Van Ommen G-JB, Dunnen JT Den. Entries in the Leiden Duchenne muscular dystrophy mutation database: an overview of mutation types and paradoxical cases that confirm the reading-frame rule. *Muscle Nerve* 2006; **34**:135–144.

351. England SB, Nicholson LV, Johnson MA, *et al.* Very mild muscular dystrophy associated with the deletion of 46% of dystrophin. *Nature* 1990; **343**:180–182.

352. Carp SJ, Barr AE, Barbe MF. Serum biomarkers as signals for risk and severity of work-related musculoskeletal injury. *Biomark Med* 2008; **2**:67–79.

353. Brancaccio P, Lippi G, Maffulli N. Biochemical markers of muscular damage. *Clin Chem Lab Med* 2010; **48**:757–767.

354. Zhang J, Yu L, Fu Q, *et al.* Mouse phosphoglycerate mutase M and B isozymes: cDNA cloning, enzyme activity assay and mapping. *Gene* 2001; **264**:273–279.

355. Gardan-Salmon D, Dixon JM, Lonergan SM, Selsby JT. Proteomic assessment of the acute phase of dystrophin deficiency in mdx mice. *Eur J Appl Physiol* 2011; **111**:2763–2773.

356. Hudmon A, Schulman H. Neuronal CA2+/calmodulin-dependent protein kinase II: the role of structure and autoregulation in cellular function. *Annu Rev Biochem* 2002; **71**:473–510.

357. Camors E, Valdivia HH. CaMKII regulation of cardiac ryanodine receptors and inositol triphosphate receptors. *Front Pharmacol* 2014; **5**.

358. Melzer W, Herrmann-Frank A, Lüttgau HC. The role of Ca2+ ions in excitation-contraction coupling of skeletal muscle fibres. *Biochimica et Biophysica Acta (BBA) - Reviews on Biomembranes* 1995; **1241**:59–116.

359. Ather S, Wang W, Wang Q, Li N, Anderson ME, Wehrens XHT. Inhibition of CaMKII phosphorylation of RyR2 prevents inducible ventricular arrhythmias in mice with Duchenne muscular dystrophy. *Heart Rhythm* 2013; **10**:592–599.

360. Dargelos E, Poussard S, Brulé C, Daury L, Cottin P. Calcium-dependent proteolytic system and muscle dysfunctions: A possible role of calpains in sarcopenia. *Biochimie* 2008; **90**:359–368.

361. Bodensteiner JB, Engel AG. Intracellular calcium accumulation in Duchenne dystrophy and other myopathies: a study of 567,000 muscle fibers in 114 biopsies. *Neurology* 1978; **28**:439–446.

362. Spencer MJ, Croall DE, Tidball JG. Calpains are activated in necrotic fibers from mdx dystrophic mice. *J Biol Chem* 1995; **270**:10909–10914.

363. Sorimachi H, Imajoh-Ohmi S, Emori Y, *et al.* Molecular cloning of a novel mammalian calcium-dependent protease distinct from both m- and mu-types. Specific expression of the mRNA in skeletal muscle. *J Biol Chem* 1989; **264**:20106–20111.

364. Hurskainen TL, Hirohata S, Seldin MF, Apte SS. ADAM-TS5, ADAM-TS6, and ADAM-TS7, novel members of a new family of zinc metalloproteases. General features and genomic distribution of the ADAM-TS family. *J Biol Chem* 1999; **274**:25555–25563.

365. Stanton H, Rogerson FM, East CJ, *et al.* ADAMTS5 is the major aggrecanase in mouse cartilage in vivo and in vitro. *Nature* 2005; **434**:648–652.

366. Glasson SS, Askew R, Sheppard B, *et al.* Deletion of active ADAMTS5 prevents cartilage degradation in a murine model of osteoarthritis. *Nature* 2005; **434**:644–648.

367. Marotta M, Ruiz-Roig C, Sarria Y, *et al.* Muscle genome-wide expression profiling during disease evolution in mdx mice. *Physiol Genomics* 2009; **37**:119–132.

368. Kobayashi H, Hirata M, Saito T, Itoh S, Chung U, Kawaguchi H. Transcriptional Induction of ADAMTS5 Protein by Nuclear Factor-κB (NF-κB) Family Member RelA/p65 in Chondrocytes during Osteoarthritis Development. *J Biol Chem* 2013; **288**:28620–28629.

369. Reed P, Porter NC, Strong J, *et al.* Sarcolemmal reorganization in facioscapulohumeral muscular dystrophy. *Ann Neurol* 2006; **59**:289–297.

370. Rahimov F, King OD, Leung DG, *et al.* Transcriptional profiling in facioscapulohumeral muscular dystrophy to identify candidate biomarkers. *Proc Natl Acad Sci U S A* 2012; **109**:16234–16239.

371. Statland J, Donlin-Smith CM, Tapscott SJ, van der Maarel SM, Tawil R. Multiplex Screen of Serum Biomarkers in Facioscapulohumeral Muscular Dystrophy. *Journal of Neuromuscular Diseases* 2014; **1**:181–190.

372. Mustonen E, Aro J, Puhakka J, *et al.* Thrombospondin-4 expression is rapidly upregulated by cardiac overload. *Biochem Biophys Res Commun* 2008; **373**:186–191.

373. Frolova EG, Sopko N, Blech L, *et al.* Thrombospondin-4 regulates fibrosis and remodeling of the myocardium in response to pressure overload. *FASEB J* 2012; **26**:2363–2373.

374. Colussi C, Banfi C, Brioschi M, *et al.* Proteomic profile of differentially expressed plasma proteins from dystrophic mice and following suberoylanilide hydroxamic acid treatment. *Proteomics Clin Appl* 2010; **4**:71–83.

375. Cynthia Martin F, Hiller M, Spitali P, *et al.* Fibronectin is a serum biomarker for Duchenne muscular dystrophy. *Proteomics Clin Appl* 2014; **8**:269–278.

376. Nilsson MI, Nissar AA, Al-Sajee D, *et al.* Xin is a marker of skeletal muscle damage severity in myopathies. *Am J Pathol* 2013; **183**:1703–1709.

377. Alagaratnam S, Mertens BJA, Dalebout JC, *et al.* Serum protein profiling in mice: identification of Factor XIIIa as a potential biomarker for muscular dystrophy. *Proteomics* 2008; **8**:1552–1563.

378. Coenen-Stass AML, Mäger I, Wood MJA. Extracellular microRNAs in Membrane Vesicles and Non-vesicular Carriers. *EXS* 2015; **106**:31–53.

379. Tournadre A, Lenief V, Miossec P. Expression of Toll-like receptor 3 and Toll-like receptor 7 in muscle is characteristic of inflammatory myopathy and is differentially regulated by Th1 and Th17 cytokines. *Arthritis Rheum* 2010; **62**:2144–2151.

380. Forterre A, Jalabert A, Chikh K, *et al.* Myotube-derived exosomal miRNAs downregulate Sirtuin1 in myoblasts during muscle cell differentiation. *Cell Cycle* 2014; **13**:78–89.

381. Nakamura Y, Miyaki S, Ishitobi H, *et al.* Mesenchymal-stem-cell-derived exosomes accelerate skeletal muscle regeneration. *FEBS Lett* 2015; **589**:1257–1265.

382. Landgraf P, Rusu M, Sheridan R, *et al.* A mammalian microRNA expression atlas based on small RNA library sequencing. *Cell* 2007; **129**:1401–1414.

383. Brown BD, Gentner B, Cantore A, *et al.* Endogenous microRNA can be broadly exploited to regulate transgene expression according to tissue, lineage and differentiation state. *Nat Biotechnol* 2007; **25**:1457–1467.

384. Cheung TH, Quach NL, Charville GW, *et al.* Maintenance of muscle stem-cell quiescence by microRNA-489. *Nature* 2012; **482**:524–528.

385. Madison RD, McGee C, Rawson R, Robinson GA. Extracellular vesicles from a muscle cell line (C2C12) enhance cell survival and neurite outgrowth of a motor neuron cell line (NSC-34). *J Extracell Vesicles* 2014; **3**.

386. Korkut C, Li Y, Koles K, *et al.* Regulation of postsynaptic retrograde signaling by presynaptic exosome release. *Neuron* 2013; **77**:1039–1046.

387. Stalder L, Heusermann W, Sokol L, *et al.* The rough endoplasmatic reticulum is a central nucleation site of siRNA-mediated RNA silencing. *EMBO J* 2013; **32**:1115–1127.

388. Wood MJA. To Skip or Not to Skip: That Is the Question for Duchenne Muscular Dystrophy. *Mol Ther* 2013; **21**:2131–2132.

389. Zocevic A, Rouillon J, Wong B, Servais L, Voit T, Svinartchouk F. Evaluation of the serum matrix metalloproteinase-9 as a biomarker for monitoring disease progression in Duchenne muscular dystrophy. *Neuromuscular Disorders* 2015; **25**:444–446.

390. Spitali P, Aartsma-Rus A, Hoen PAC 't. Response to: Evaluation of the serum matrix metalloproteinase-9 as a biomarker for monitoring disease progression in Duchenne muscular dystrophy. *Neuromuscular Disorders* 2015; **25**:446–447.

391. Anon. TREAT-NMD : Current trials in DMD.

8. Appendix

8.1 Manuscripts accepted for publication

First author publications

Coenen-Stass AML, Betts CA, Lee YF, *et al.* Selective release of muscle-specific, extracellular microRNAs during myogenic differentiation. *Human Molecular Genetics* 2016.

Coenen-Stass AM, Graham McClorey, Raquel Manzano, Corinne A. Betts, Alison Blain, Amer F. Saleh, Michael J. Gait, Hanns Lochmüller, Matthew J. A. Wood, Thomas C. Roberts: Identification of novel, therapy-responsive protein biomarkers in a mouse model of Duchenne muscular dystrophy by aptamer-based serum proteomics. *Sci Rep.* 2015 Nov 23;5:17014

Coenen-Stass AM, Mäger I, Wood MJ.: Extracellular microRNAs in Membrane Vesicles and Non-vesicular Carriers. EXS. 2015;106:31-53.

Co-authored publications

Rouillon J, Poupiot J, Zocevic A, Amor F, Léger T, Garcia C, Camadro JM, Wong B, Pinilla R, Cosette J, **Coenen-Stass AM**, Mcclorey G, Roberts TC, Wood MJ, Servais L, Udd B, Voit T, Richard I, Svinartchouk F.: Serum proteomic profiling reveals fragments of MYOM3 as potential biomarkers for monitoring the outcome of therapeutic interventions in muscular dystrophies. *Hum Mol Genet*. 2015 Jun 9.

Ezzat K, Aoki Y, Koo T, McClorey G, Benner L, **Coenen-Stass A**, O'Donovan L, Lehto T, Garcia-Guerra A, Nordin J, Saleh AF, Behlke M, Morris J, Goyenvalle A, Dugovic B, Leumann C, Gordon S, Gait MJ, El Andaloussi S, Wood MJ.: Self-Assembly into Nanoparticles Is Essential for Receptor Mediated Uptake of Therapeutic Antisense Oligonucleotides. *Nano Lett.* 2015 Jun 15.

Betts CA, Saleh AF, Carr CA, Hammond SM, **Coenen-Stass AM**, Godfrey C, McClorey G, Varela MA, Roberts TC, Clarke K, Gait MJ, Wood MJ: Prevention of exercised induced cardiomyopathy following Pip-PMO treatment in dystrophic mdx mice. *Sci Rep*. 2015 Mar 11;5:8986.

Roberts TC, **Coenen-Stass AM**, Betts CA, Wood MJ: Detection and quantification of extracellular microRNAs in murine biofluids. *Biol Proced Online*. 2014 Mar 14;16(1):5.

Roberts TC, **Coenen-Stass AM**, Wood MJ: Assessment of RT-qPCR normalisation strategies for accurate quantification of extracellular microRNAs in murine serum. *PLoS One*. 2014 Feb 19;9(2).

8.2 Attended conferences

Sep 2016 81st Harden Conference: RNA and Disease. Poster flash oral presentation, poster presentation: Selective release of muscle-specific microRNAs during myogenic differentiation, UK

Jan 2016 The Wellcome Trust Sanger Institute AstraZeneca CRISPR Conference

Oct 2015 Oligonucleotide Therapeutics Society Meeting in Leiden, The Netherlands. Poster presentation: Identification of novel, therapy-responsive protein biomarkers in a mouse model of Duchenne muscular dystrophy by aptamer-based serum proteomics.

Sep 2015 Non coding RNAs: Exploring Technologies and Uncover New Functions, Cambridge, UK.

Sep 2015 World Muscle Society Meeting, Brighton, UK. Poster and oral presentation: Identification of novel, therapy-responsive protein biomarkers in a mouse model of Duchenne muscular dystrophy by aptamer-based serum proteomics.

Apr 2015 COST training school on patient communication in Leiden, The Netherlands.

Oct 2014 Oligonucleotide Therapeutics Society Meeting in San Diego, CA, USA. Poster presentation: Extracellular microRNAs: identity and function in relation to muscle regeneration and dystrophic pathology.

Jul 2014 13th International Congress on Neuromuscular Diseases in Nice, France. Poster presentation: Extracellular microRNAs: identity and function in relation to muscle regeneration and dystrophic pathology.

Oct 2013 Oligonucleotide Therapeutics Society Meeting in Naples, Italy.